01 Sep 1976

Non-linear finite element analysis of light gage steel shear diaphragms

Erdal Atrek

Arthur H. Nilson

CCFSS LIBRARY
22 3 * 284
1976

Atrek, E., Nilson, A. H.,
NON-LINEAR FINITE ELEMENT
ANALYSIS OF LIGHT GAGE STEEL
SHEAR DIAPHRAGMS

DATE	ISSUED TO

F/1201-408

Department of Structural Engineering
School of Civil and Environmental Engineering
Cornell University

Report No. 363

NON-LINEAR FINITE ELEMENT ANALYSIS OF LIGHT GAGE STEEL SHEAR DIAPHRAGMS

by
Erdal Atrek
Research Assistant

Arthur H. Nilson
Project Director

A research project sponsored by
The American Iron and Steel Institute
Project No. 1201-408

Ithaca, New York September 1976

ACKNOWLEDGEMENTS

This report was originally presented as a thesis to the Faculty of the Graduate School of Cornell University in partial fulfillment of the requirements for the degree of Doctor of Philosophy, conferred in September 1976.

The research was originally suggested by Professor Arthur H. Nilson and work proceeded under his guidance as Project Director. Acknowledgement is made also of the contributions of Professors Teoman Pekoz, Robert G. Sexsmith, and Subrata Mukherjee.

The report was typed by Diane E. Lounsbury, and figures were prepared by Barbara Boettcher.

The investigation was sponsored by the American Iron and Steel Institute through Research Grant No. 1201-408 to Cornell University.

SUMMARY

Shear diaphragm action of properly designed light gage steel panels used for floors, roofs, and walls in steel buildings increase the stiffness and strength of such buildings. Considerable savings in weight and cost can be realized if full account of this action is taken in design. To make good use of the diaphragm action, detailed knowledge on diaphragm response to loading is essential.

An efficient computer program has been prepared to analyze light gage steel shear diaphragm behavior in the linear and non-linear ranges of response, up to collapse. The program uses figinite element concepts for analysis, and has routines to deal with the beams, purlins, panels, and connections. Beams and purlins are modeled by conventional flexural elements with three degrees of freedom at each node. Panels are represented by rectangular orthotropic plane-stress plate elements. Two different models for corrugated panels are proposed. One model makes use of an average effective shear modulus along the entire panel length, while in the other two different shear moduli are attributed to the end and central regions of the panel. The connections are modeled by spring elements, and, according to location, several different models utilizing these spring elements are used.

The non-linear analysis is based on experimental evidence that, in general, the connections are the only important source of non-linearity up to collapse. For this reason, only the connection behavior is represented by a non-linear function. All

other components of the diaphragm assembly are assumed to remain elastic throughout the loading range.

The connectors can be either welds, used for heavily-stressed shear diaphragms, or screw fasteners, used for more lightly loaded installations. In both cases, the non-linear force-displacement relation used for the connection is a multi-linear approximation of the load-displacement curve obtained from a shear test of the connection and the small region around it.

The program uses a frontal routine for the solution of the stiffness equations. The non-linear analysis is done by the residual force method, which utilizes the original elastic stiffnexx matrix at every stage of the analysis, and which arrives at the correct solution for each load increment through an iterative procedure. A modified Aitken accelerator is used to speed the convergence. In order to reduce the task of preparing input data, a mesh generator has been written. This mesh generator requires only simple basic data for the generation of the complete finite element mesh, for most practical diaphragms.

The computer program has been employed to analyze diaphragms for which test results are available. Both linear analyses up to the elastic limit, and non-linear analyses up to and beyond the elastic limit have been conducted.

For three of the four diaphragms analyzed, very good agreement between numerical and experimental results have been obtained. For a standard corrugated diaphragm, numerical results in the non-linear range show a more flexible behavior than in test. Detailed analysis indicates that this is most probably

due to unavailability of correct connection test data for use in analysis. The force distribution in the diaphragms, overall diaphragm deflections, and seam slips are found at different ranges of response.

As a result of the analyses, it is confirmed that connection non-linearity is the most important factor in the non-linear range of diaphragm response, differences in shear modulus being only of secondary importance. It is concluded that the computer program developed is an efficient and dependable took for research and design.

TABLE OF CONTENTS

LIST OF TABLES

LIST OF FIGURES

CHAPTER 1

INTRODUCTION

1.1 General

Light gage steel cold-formed panels are used in steel framed buildings for floors, roofs, and cladding. Interest in the capacity of assembled systems of panels, with their supporting steel framework, to resist loads causing membrane stresses acting in the plane of the sheeting dates from the early 1950's.

The interaction between panel systems and frames can be exploited in a number of important ways. Initially interest was focussed on the use of steel panel floors and roofs to resist horizontal loads acting on buildings due to wind or seismic forces. The essential features of such a design are shown on Figure 1.1. Horizontal loads applied to the edge of a roof (e.g. from siding subject to wind forces) can be carried by at least three alternate systems. Each rigid frame can be designed to resist sway moments. Alternatively, a diagonal bracing system can be provided. The third possibility, using the membrane shear strength of the decking, is attractive in that sway moments may be reduced or eliminated altogether (if only hinged joints are provided in the interior frames) and unsightly diagonal bracing is avoided. Using the decking as a shear diaphragm utilizes an otherwise wasted capacity of the system, and requires only that some special attention be given to the detailing of the connections in the system. Such

arrangements have been used extensively in highrise structures as well as one-story buildings.

Diaphragm action may also be used to reduce sway moments in the interior frames of shed-type buildings subject to gravity loads. When a gable frame is loaded vertically, there is a tendency for the knee joints to spread outward, as shown in Figure 1.2. It is clear from this sketch that this outward movement can occur only if accompanied by a shear distortion of the cladding. The result is a sharing of the load between the moment-resisting frames and the shear-resisting cladding. Substantial savings in steel results for the interior frames.

The membrane strength of cladding also offers the possibility of stressed-skin construction in folded plate structures. Similar to gable frame structures in outward appearance (see Figure 1.3), the steel folded plate structure requires no interior columns. The cladding serves to collect the surface loads and to deliver them to fold-line members, which are usually light rolled steel angles. Each folded plate element then carries the loads by spanning as a deep plate girder between the end walls of the structure. The fold-line members serve as tension and compression flanges, and the cladding serves as the shear-resistant web. The possibilities of such stressed-skin construction have been used extensively in the U.S..

In order to obtain information on the qualitative and quantitative aspects of shear diaphragm action, systematic research on light gage steel shear diaphragms was started in the nineteen-fifties.

The major portion of this research to date has been in the form of tests conducted on full scale assemblies. While providing the best possible information on the diaphragm being tested, this method has definite disadvantages. Since full scale testing is quite costly and time consuming, it becomes very hard to ascertain the effects of varying certain structural parameters, such as the type and spacing of fasteners, size of perimeter beams, sheet thickness, corrugation geometry, intermediate purlins, etc. Furthermore, due to practical problems with instrumentation, it is not possible to obtain a clear picture of the internal force distribution at various stages of loading.

Related research has centered on arriving at equations defining the overall flexibility of diaphragms by summing up component flexibilities, where these flexibilities are found through semi-empirical means. This research has resulted in the compilation of experimental and analytical data regarding especially the behavior of various fasteners and corrugated sheeting that are used in light gage steel diaphragms, and in a practical design approach. The method depends on knowledge of the internal force distribution and deformation modes. The disadvantage of the method is that it is not informative about the complete response of a diaphragm to increasing load.

With the relatively recent availability of high speed computers and efficient solution algorithms, it has now become possible to treat the complexity of shear diaphragms analytically with a high degree of accuracy and generality, using the

finite element approach. In addition to being considerably more efficient than full scale testing, both in terms of time and cost, finite element analysis can provide extensive information about diaphragm behavior and internal force distribution. Furthermore, the variation of structural parameters, in order to find their relative effects on diaphragm response, does not pose a major problem as this now becomes only a case of changing input data for the relevant computer program. Although some small scale testing will still be necessary in order to provide data on some components (mainly the connections), this is highly preferable to full scale testing.

Once the worthiness of a certain computer program to analyze shear diaphragms has been established, the program can then be considered as a strong alternative to other approaches.

1.2 Scope of the Investigation

Several investigators in the field have already written and used finite element analysis programs to conduct first order (linear) analyses of shear diaphragms, but since it has been seen that light gage steel shear diaphragms exhibit pronounced non-linearity before reaching their ultimate strength, it has been desirable to prepare a program that will analyze this non-linearity up to collapse of the diaphragm, as well as analyzing the initial linear behavior. The investigation reported herein has resulted in a dependable and efficient finite element program which will provide data on diaphragms throughout the linear and non-linear ranges of response.

A clearly defined and workable finite element model of the diaphragm components is established. Modeling difficulties that are inherent to corrugated sheeting which exhibit an essentially non-isotropic behavior, and to diaphragm connections, have been resolved satisfactorily. Results of previous diaphragm tests and recent research on corrugated sheeting have been invaluable as guidelines for this purpose.

Case studies are made for some diaphragms that have already been tested, using the results of the computer analyses that have been conducted, both to compare the experimental and analytical results and to gain more information regarding diaphragm behavior, much of which, for practical reasons, cannot be obtained from tests.

CHAPTER 2

SURVEY OF LITERATURE ON LIGHT GAGE STEEL SHEAR DIAPHRAGMS

Studies on light gage steel shear diaphragms have followed several closely related lines. Full scale experimentation has constituted a major portion of the research done up to present. On the other hand, semi-empirical and analytical methods have been gaining increased importance, these last two being built on the results of experiments that have been performed by previous investigators, and being checked against current experimentation.

According to Nilson (1), the first tests concerning shear diaphragms were conducted by Johnson and Converse in 1947. These were followed by tests on cellular decking by Barnes (2).

A systematic test program was initiated in 1954, at Cornell University by Nilson and Winter. This test program led to improved understanding of the factors involved in diaphragm behavior, especially of the importance of connections. From these studies (1,3) techniques for welding and testing shear diaphragms were developed with a view toward standardization. The "cantilever test" developed for the experimental evaluation of diaphragm shear stiffness gained wide usage and is recommended by AISI (4) (see Figures 2.1a and 2.1b).

Nilson noted that the total deformation of the diaphragm consisted of contributions from individual components. He classified these individual contributions as seam slip, slip between panel and perimeter beams, deflection due to flexure

and deflection due to shear. Simple design modifications suggested by Nilson have resulted in appreciable increase in the strength and stiffness of shear diaphragms. This work was later applied to folded plate structures as well (5).

Luttrell (6,7) and Apparao (8) extended the work by Nilson and investigated the effects of factors such as panel configuration, methods of attachment, length of panel, intermediate purlins and material properties. Both static and pulsating loads were applied to the corrugated diaphragms tested by these investigators. It was found that pulsating loads in the practical design range of the diaphragms (at 30% of the static ultimate load) resulted in an average of 20% reduction in strength. Luttrell developed a semi-empirical formula as a function of the panel length and sheet thickness for the shear rigidity of diaphragms with standard corrugation. He also found that the influence of the diaphragm frame flexibility on the overall diaphragm behavior was minor. Both Luttrell and Apparao concluded that the relationship between sheet thickness and diaphragm stiffness was almost a linear one. Following the above studies, a design brochure was prepared by the AISI (4) in 1967, to establish certain criteria for the testing and design of light gage steel shear diaphragms.

In Britain, work on the stiffening effect of steel sheeting on buildings was started by Bryan, with Godfrey (9). Bryan, with El-Dakhakhni and Bates (10-13) further investigated the same subject and provided experimental results on clad portal frames. A semi-empirical formulation for the treatment of clad pitched portal frames was reached by Bryan and El-Dakhakhni

(12).

Although providing valuable practical data, the studies in the U.S. and Britain were not sufficient to arrive at a general theory to predict the behavior of shear diaphragm installations, because of the difficulty that the distribution of internal forces could not be found.

At the same time, various investigations were under way in Australia (14). A clad model structure with various combinations of sheeting was tested by Koerner (15). Also, Freeman (16) investigated the stiffness and strength of diaphragms both under static and pulsating loading, for variations of sheeting and attachment methods.

In 1967, Bryan and Jackson (17) developed an approach aimed at determining the shear flexibility of diaphragms by theoretical means. The approach consisted of assuming an internal force distribution within the diaphragm and determining the flexibility of each diaphragm component separately due to the resulting deformation. The overall flexibility of the diaphragm was then found by adding up the individual flexibilities. The co-authors classified the contributions as:

1. shear flexibility due to sheet deformation
    a. flexibility due to bending of cross-section
    b. flexibility due to torsion
    c. flexibility due to membrane stresses
    d. flexibility due to shear strain
2. shear flexibility due to slip at fasteners

The formulation was developed for rectangular corrugations with small attachments at every corrugation valley (Figure

2.2a). Values calculated with the method, however, did not agree well with experimental findings, and a discrepancy of 10 to 45% was found. An important reason for this discrepancy has been noted by Libove (32). Bryan and Jackson had assumed that the corrugation generators (lines parallel to the corrugations) undergo inextensional deformation, and tilt and displace while keeping their straightness. Nevertheless, the paper by Bryan and Jackson (17) constitutes a basis for the practical design approach for determining diaphragm flexibility.

Bryan and El-Dakhakhni (18) later revised the method of Reference (17) and also included the flexibility of frame interconnections, the case of attachment spacing greater than one corrugation pitch, and the effect of intermediate purlins. Better agreement with the observed results was obtained, and the discrepancy between tests and theory was less than 20%. The work also involved numerous tests on sheet fasteners and connections between framing members. Equations for diaphragm ultimate strength were formulated for two possible modes of failure, one due to tearing at sheet to perimeter frame fasteners and the other due to tearing at seam fasteners. A test program undertaken by these authors (19) involved 150 experiments to assess the effects of various factors on the behavior of shear diaphragms. This test program yielded important practical data on diaphragm components and provided comparison with the proposed theory.

In the meantime, Rothwell (20) analyzed the stiffness of two types of trapezoidally corrugated sheets (Figure 2.2b)

using the assumption of inextensional deformation of corrugation generators. He also performed tests to check the theory, but did not obtain very satisfactory agreement between the two. It is of interest to note that Rothwell's test specimens were quite short (18") compared to what is used in practice. It is suspected that due to the assumption involving corrugation generators, a higher discrepancy between the theory and observed behavior would exist had longer specimens been tested.

Bryan incorporated his and his co-workers' experimental and analytical findings into a book in 1973 (21). An important volume of design data and considerations was thus assembled. The formulation for determination of diaphragm flexibility by regarding each component separately was improved further and was supplemented by theoretical and experimental data. In this book, Bryan defined the flexibility due to sheet distortion in terms of a dimensionless sheeting constant K, where K depends on the sheet geometry and the spacing of the attachments. Correction factors to be used to account for the effect of intermediate purlins were also proposed. The values of K were computed for various trapezoidally corrugated sheets and attachment spacings. Due to the assumptions involved in the derivation of K, these values were applicable with higher accuracy to sheets of smaller corrugation length.

Davies (22) reviewed Bryan's work and derived an effective shear modulus from Bryan's expressions for flexibilities due to shear distortion and due to shear strain in the sheets for use in finite element analysis, and conducted such analyses.

Although a non-linear analysis program was also described by Davies, only results pertaining to linear analyses are presented in his report. Modifications to Bryan's expressions for connection flexibilities were suggested due to an improved understanding of the assumed force distributions in diaphragms as a result of finite element analyses. Davies also proposed revised equations for computing the ultimate strength of diaphragms.

Other finite element analyses of clad structures and shear diaphragms were under way by this time. Miller (24) analyzed the behavior of clad and bare multi-story frames, and concluded that cladding reduced the side sway of the 26 story frame that was analyzed by about 40% from that of the bare frame.

Ammar (26) used the same program as Miller to make first order analyses of some diaphragms that had been tested by Nilson and Luttrell. He also devised a connection shear test by which the behavior of different types of connections could be easily determined (25). He used the results of these tests as connection data for the finite element analyses he conducted. Due to the essentially non-linear behavior of the analyzed diaphragms, he compared the first order analysis results with the test results at 40% of the experimental ultimate loads. It was found that for cellular type diaphragms finite element analysis results were very satisfactory, although for the non-cellular diaphragm with standard corrugation sheeting (quasi-sinusoidal) the numerical results showed a much more flexible diaphragm than that tested. This was mostly due to the unsatisfactory evaluation

of the effective shear modulus for the sheeting. Ammar's work has been reported in condensed form in Reference (27).

As reported in Reference (14), in Australia Lawrence (28) also developed and employed a finite element analysis program to analyze model shear diaphragms and a model clad shed.

The most accurate theories concerning the shear flexibility of corrugated sheeting have so far been developed by Libove and co-workers (29-36) and by Lawson (23). These theories take into consideration the fact that except for very short diaphragms, the corrugation generators will not only displace as rigid bodies, but will deform and strain as well. As can also be predicted from St. Venant's principle, the appreciable part of this phenomenon will take place in the end regions due to the effect of the discrete attachments.

Libove and co-workers define a dimensionless parameter Ω as the ratio of the shear stiffness of a discretely attached corrugated sheeting to that of the same sheet continuously attached. They have computed and plotted Ω for a high variety of corrugation geometries and dimensions (Figure 2.3), and have developed equations for stiffness and stresses in the sheeting in terms of this parameter. Although they have not considered the case of attachment spacing greater than one corrugation pitch, they have analyzed several different attachment modes within one corrugation pitch (Figure 2.3). They have also noted that the standard corrugation used in practice is closer to sinusoidal in geometry than circular arcs, and have compared both idealizations with the actual shape (36).

Lawson has followed similar theory as Libove in deriving the stiffness expressions for sinusoidally and trapezoidally corrugated sheeting. As his studies are an extension of earlier investigations by Bryan and co-workers, he has defined a dimensionless parameter $\overline{K}$ to take the place of K used by Bryan, and has modified the relevant expression for sheet distortion accordingly. He has computed $\overline{K}$ for a variety of corrugation dimensions and attachment spacings, also including the effect of intermediate purlins.

Both Libove and co-workers and Lawson have derived expressions for an average effective shear modulus for discretely attached corrugated sheeting in terms of the parameters Ω and $\overline{K}$ respectively. The works of these investigators show close agreement. The parts of their work relating to the effective shear modulus and the basic assumptions of the theory are summarized in Section 3.2.1.2.5.

Libove (37) has developed simple asymptotic formulas that can be used to extrapolate the experimental and analytical results obtained for a certain corrugation geometry and attachment configuration to cases of different lengths, other factors being held constant. In comparing the asymptotic formulas with more precise theory, he has found that very good agreement exists.

The stability in shear of light gage sheeting has also been a subject of research. Stability problems exist in this type of construction when the manner of attachment imposes very rigid boundary conditions on the sheeting and does not allow for

appreciable force redistribution. Such rigid attachment is rarely seen in civil engineering diaphragms. Flat sheeting which is more prone to overall instability than corrugated sheeting is almost always stiffened heavily against such phenomenon. The case of flat sheeting without stiffeners is already well documented (38, 39). Most of the research on the stability of corrugated sheeting has been based on the assumption of orthotropy.

Hlavacek (40) has developed formulation for the shear stability of flat sheets with equally spaced stiffeners on both sides. This formulation was also intended to be applied to corrugated sheeting as the basic considerations are similar for the two cases. Earlier, Bergmann and Reissner (41) had also investigated the stability of corrugated sheeting. The formulations derived by both Hlavacek and Bergmann-Reissner were based on the small deflection theory. Easley and McFarland (42) used both small and large deflection theories to derive equations for the critical load. These two investigators defend the orthotropic idealization on the bases that generally the corrugation geometry is small compared to the overall dimensions of the diaphragm, that the interest is on the overall buckling rather than local, and that the buckled shape as observed in tests appears to be independent of corrugation geometry.

In simplified form (43) the small deflection formulas derived by Easley-McFarland and Hlavacek differ by a factor of 1.14, however although being comparable with test results, neither provide totally satisfactory agreement. The reason given for

this is that it is very hard to achieve the assumed boundary conditions in experimentation.

Libove (33) states that the use of the orthotropic plate idealization for the investigation of shear stability may not always be adequate for two main reasons. His reasons are that such an idealization does not reflect the effect of the shear stiffness and that it also neglects the transverse shearing deformations in the plane perpendicular to the corrugations. He then derives total potential energy expressions at the iniation of buckling for corrugated sheeting, based on the actual corrugation geometry. Thus, a trapezoidal corrugation is taken as an assemblage of flat plates, whereas curvilinear sheeting is considered as a shell. It must be noted that all work on the stability of corrugated sheeting is based on the assumption of continuous attachment. The applicability of theories derived in this manner to practical diaphragms is yet unclear.

At the present, the developments in the area of shear diaphragms have given rise to the establishment of certain design and testing criteria. These have been compiled by relevant organizations in the U.S. (4) and Europe (44).

CHAPTER 3

DIAPHRAGM COMPONENTS AND THEIR FINITE ELEMENT REPRESENTATION

3.1 General

A shear diaphragm may be viewed as an assemblage of various structural components put together in such a way as to provide transfer and distribution of applied loads to and from the framing members, making use of the shear carrying capacity of a panel attached to these framing members. Thus the flexural stresses that would have been carried by the frame, had there been no panel, are substantially reduced and the resulting structure is considerably stiffer than that without a shear panel.

In this report, the frame members that are directly attached to the sheets forming the shear panel are included in the term diaphragm as well as the sheets themselves. The diaphragm frame, in general, consists of the framing members at the perimeters of the diaphragm and, in most cases where corrugated sheeting is used, intermediate purlins that span the panel between the perimeter members. To permit unobstructed shear transfer through the sheeting, the connections of the framing members to each other are built as joints that can undergo free rotation.

The shear panel itself consists of one or more light gage steel sheets attached to each other and to the diaphragm frame at discrete locations. The choice of connection depends on the sheeting used for the panel, as do the various stiffeners that

are employed to prevent out-of-plane buckling of the panel.

The sheets that make up the panel fall into two categories. Flat sheets ranging between 12 and 20 gage steel are preferred where high stresses are expected. These are stiffened against instability by cold-formed hat sections or unsymmetrical "ribs" that are spotwelded to the sheets. Other connections involving the sheets are also done by means of welding.

Corrugated sheeting, used for installations where lower loads are expected, is in general manufactured in lighter gage - between 20 and 30 gage. The corrugation geometry may be quasi-sinusoidal, trapezoidal, rectangular or variations and combinations of these (see Figure 2.3). Intermediate purlins are used in many cases to add to the stiffness of the diaphragm and to prevent overall buckling of the panel. Because of the lighter gage of corrugated sheeting, mechanical connectors such as screws, bolts, etc. are preferred over welding for use in such installations.

Unless quite rigid connections are provided at very short intervals, one can rule out the possibility of an instability type of failure for the majority of well designed diaphragms, due to the stiffeners employed against possibility of premature buckling. Since in civil engineering practice rather large spacings are used between connections, stress concentration causes local yielding. As a result, most diaphragms show non-linear behavior with increasing load. Material ductility permits force redistribution, and diaphragms collapse only when a sufficient number of components or connections have reached their

ultimate capacity.

3.2 Diaphragm Components and Their Behavior

This section is dedicated to a qualitative analysis of the diaphragm assemblage and action in terms of the various components.

3.2.1 Panels

The two categories of sheeting (cellular and non-cellular) that are commonly used in the panel show distinct differences in their behavior. Therefore they are studied separately.

3.2.1.1 Flat Sheeting (the isotropic case)

It is assumed that the shear flexibility of the ribs or hat sections spotwelded to the flat sheeting is much greater than that of the sheeting and that they add very little to the shear stiffness although they provide resistance against shear buckling. Thus the behavior of the flat sheeting can be viewed independently of these stiffeners. Then the case simplifies into one of plane isotropy, and the sheet behavior depends directly on the material constants of steel. Such behavior is very well understood and documented, and therefore is not detailed here.

3.2.1.2 Corrugated Sheeting (the orthotropic case)

Although made of an isotropic material, corrugated steel sheeting exhibits an essentially non-isotropic behavior at the macroscopic level, due to the existence of corrugations. Thus,

for example, the apparent modulus of elasticity in the two principal directions will not be the same. The same holds for the apparent Poisson's ratios. Furthermore, the value of the effective shear modulus depends on the end conditions as well as the corrugation geometry.

Since in this report the diaphragm problem is treated in two dimensions, i.e. in the plane of the diaphragm, it becomes necessary to define a flat sheeting which will behave in the same manner as the corrugated sheeting that it represents. In order to adhere to the overall diaphragm dimensions, this flat sheeting must have the projected planar dimensions of the corrugated sheeting. The most conventional approach to such an idealization is to impose a state of orthotropy, and to determine the constants of orthotropy through a comparison of the two sheets. As long as out of plane buckling considerations are not involved, the orthotropic plate idealization of corrugated sheeting is believed to be quite satisfactory for the purposes of this investigation.

For the purpose of finding the elastic constants, two principal directions of orthotropy need to be defined. Thus, the direction along the length of a given corrugation will be L (longitudinal) and the orthogonal direction will be called T (transverse). In the actual installation one of these two will coincide with either of the X or Y axes that will be used to define the directions on the plane of the diaphragm. The apparent constants of elasticity for the orthotropic sheeting have been found satisfactorily by other investigators as functions of the base material constants, corrugation geometry,

and, for the case of the effective shear modulus, the additional factor of the end conditions. Small scale testing may also be used in the determination of the elastic moduli. The following subsections pertain to the determination of the orthotropic elastic constants.

3.2.1.2.1 Effective Elastic Modulus in the Longitudinal Direction

For simplicity, a corrugated sheet of width equal to one corrugation pitch (p), corrugation length L, and thickness t is considered. The developed width of the corrugation is labelled p'. These dimensions are shown on Figure 3.1 along with the proposed orthotropic flat sheet with the same projected dimensions.

The effective elastic modulus E_L of the flat sheet will then depend on the fact that both sheets must undergo the same longitudinal deformation under an applied load P. Therefore, equating the two displacements,

$$\frac{PL}{ptE_L} = \frac{PL}{p'tE_o} \tag{3.1}$$

an expression for E_L is obtained:

$$E_L = \frac{p'}{p} E_o \tag{3.2}$$

3.2.1.2.2 Effective Elastic Modulus in the Transverse Direction

In the transverse direction, the total displacement of a corrugated sheet under a direct load P (P now applied parallel to the transverse direction) will be the sum of the displacements due to the membrane strain and the bending strain (the latter arising due to bending of the corrugation cross-section). Thus, assuming small deflections, the displacement in the transverse direction can be expressed as:

$$\delta_T = \frac{\partial}{\partial P} (U_M + U_B) \tag{3.3}$$

where,

U_M: energy due to membrane strain.

U_B: energy due to bending strain.

On the other hand, the same amount of deflection for the orthotropic flat sheet will be defined by:

$$\delta_T = \frac{Pp}{LtE_T} \tag{3.4}$$

Equating the two displacements one can obtain a general expression for E_T.

Smith (45) has derived such a general equation in an explicit format (see also Figure 3.2):

$$E_T = \frac{I_o}{I} E_o \tag{3.5}$$

where,

$I_o = t^3/12$: Moment of inertia about the corrugation's own plane.

$$I = \frac{1}{p} \left(\int_o^{p'} z^2 \, t \, dp' + \int_o^{p'} I_o \cos^2 \alpha \, dp' \right) \qquad (3.6)$$

I being the moment of inertia about the neutral axis of the corrugation cross-section.

In Equation 3.6,

α: angle of inclination of segment dp' with respect to the neutral axis,

z: distance from the neutral axis of the centroid of segment dp'.

For quasi-senusoidal corrugations, the use of Equation 3.5 is rather complicated. However in Reference (26) an approximate expression considering only bending strain is given for this case. This expression depends on the assumption that the corrugation shape can be expressed as a sinusoidal function (Figure 3.2).

$$F = \frac{h}{2} \sin \left(\frac{2\pi x}{p} \right) \qquad (3.7)$$

Then the expression for the transverse modulus of elasticity is:

$$E_T = \frac{E_o}{6} \left(\frac{2t}{h} \right)^2 \frac{1}{\left[1 + 1.234 \left(\frac{h}{p} \right)^2 \right]} \qquad (3.8)$$

3.2.1.2.3 Principal Poisson's Ratio

μ_{LT} is defined as the absolute value of the ratio of the

apparent strain resulting in the transverse direction due to an imposed strain in the longitudinal direction, to this imposed strain. Therefore,

$$\mu_{LT} \equiv \left|\frac{\varepsilon_T}{\varepsilon_L}\right| \tag{3.9}$$

Since the apparent strain ε_T of a corrugated sheet is that related only to the in plane projection of the deformation, it should be equal to the lateral strain that would result in the orthotropic flat sheet. Thus if a longitudinal strain ε_L is imposed on both sheets, the identity expression for the lateral strains of the sheets will be:

$$\mu_{LT}\,\varepsilon_L = \mu_o \varepsilon_L \tag{3.10}$$

from which,

$$\mu_{LT} = \mu_o \tag{3.11}$$

3.2.1.2.4 Secondary Poisson's Ratio

This ratio is defined as:

$$\mu_{TL} = \left|\frac{\varepsilon_L}{\varepsilon_T}\right| \tag{3.12}$$

where,

ε_T: imposed strain in the transverse direction, and

ε_L: resulting strain in the longitudinal direction.

It should be noted that the expressions on the right hand sides of Equations 3.9 and 3.12 are not numerical reciprocals of each other due to the different definitions of the variables involved.

μ_{TL} can be found easily from the Maxwell-Betti Law of Reciprocity:

$$\mu_{TL}E_L = \mu_{LT}E_T \tag{3.13}$$

which gives:

$$\mu_{TL} = \mu_{LT}\frac{E_T}{E_L} = \mu_o\frac{E_T}{E_L} \tag{3.14}$$

3.2.1.2.5 Effective Shear Modulus

When anisotropy is present, the simple relationship of the shear modulus to the basic Poisson's ratio and Young's modulus ceases to be valid. In the case of corrugated sheets in engineering practice, three factors contributing to the complexity of the problem are the corrugation geometry, the discrete attachments that are typical of such practice, and the length of the corrugations.

Test procedures for the determination of an effective shear modulus for orthotropic materials have been proposed, but difficulties in the introduction of proper boundary conditions in the experiments create questions about the dependability of results obtained in this manner. Furthermore, testing has the important shortcoming that, for a given corrugation geometry,

the effective shear modulus may change drastically with changes in the length of the corrugations. It is easily seen that proper determination of the effective shear modulus for corrugated sheets will require an extraordinary volume of test data even if meticulous care is taken in experimentation. On the other hand, some asymptotic formulas that have been developed by Libove (37) may alleviate the problem of dealing with changes in length.

For the time being, analytical methods of determining the effective shear modulus for a corrugated sheet seem to be the most trouble free, especially for uncomplicated corrugation geometries. Below follows a discussion of the more recent work done by other investigators on this subject. The effective shear moduli used for the corrugated diaphragms analyzed in connection with this report depends on this work.

A corrugated sheet that is sufficiently wide (many corrugations) is assumed, so that the boundary conditions on the two sides cause negligible effect on the sheet behavior. If such a sheet is continuously attached at the corrugation ends such that the corrugation geometry is preserved at the ends, but the warping of the end cross-sections out of their initial cross-section plane is not prohibited, then under a given shear load a uniform shear stress field will be produced in the sheet, (see Figure 3.3a). In this special case, the effective shear modulus is defined simply by:

$$G_{eff} = G_o \frac{p}{p'}, \qquad (3.15)$$

where,

G_o: shear modulus of the parent material.

However, if the attachment is made at discrete locations rather than in a continuous manner, then Equation 3.15 is no longer valid. Discrete attachments at corrugation ends allow the deformation of corrugation geometry under a shear load, especially in the end regions. Therefore, the problem becomes much more difficult than that of continuous attachment.

As the nature of the deformations depend on the initial corrugation shape, the general considerations concerning discretely attached corrugated sheets rather than separate discussions for each corrugation geometry are presented. The detailed treatments can be found in References (23, 29-36).

Up to date the most accurate analyses have been made by Libove and co-workers (29-36) and by Lawson (23). The most important difference between the works of these investigators and those of others (see Chapter 2 and References (17) through (22)) is that the more accurate analyses do not put the restriction that the straight line generators of the corrugations (the lines along the length of a corrugation) should remain straight, (although they would be allowed to move as rigid bodies), but allow these generators to deform and strain as well. Both experimental results and St. Venant's principle bear out the validity of this relaxation, especially for corrugated sheets of practical length, since except for the case of very short sheets, the deformation of the cross-sections will be localized near the ends rather than being distributed

linearly along the corrugation length. Figure 3.3b shows a qualitative comparison of the deformations of a continuously attached corrugated sheet and the same sheet with discrete end attachments.

The analytical approach involves using certain degrees of freedom to represent the assumed cross-sectional and longitudinal deformations while assuming the attachments to be mathematical points and then deriving the strain energy expression for a single corrugation. Then the total potential energy expression obtained by summing the work done by the shear load and the strain energy, is minimized to yield the system of differential equations which, along with the boundary conditions, are solved for the required variables. As the expressions and the algebra are quite lengthy, they are not reproduced herein, but the reader is again referred to References (23, 29-36). In this section, the results pertaining to the effective shear modulus are reviewed.

Libove and co-workers define a dimensionless parameter Ω as the ratio of the shear stiffness of a discretely attached corrugated sheet to that of the same sheet continuously attached. Consequently, the expression for the effective shear modulus of a corrugated sheet can be written as:

$$G_{eff} = G_o \frac{p}{p'} \Omega \qquad (3.16)$$

It will be noted that in the case of a flat sheet $\Omega = 1$, $p = p'$, and therefore $G_{eff} = G_o$.

These investigators have computed and plotted Ω for a great variety of corrugation geometries and dimensions, assuming that attachments have been provided at every corrugation. This type of attachment is preferred in aerospace industry, as opposed to civil engineering practice where larger spacing of attachments is more common. This point is a subject of discussion later in the section. The corrugation geometries and the types of attachments that have been considered by Libove and co-workers are shown on Figure 2.3. Some special cases (numbers aIII, bI, bII, bIII, cI, cIII, and dIII of Figure 2.3) are worth noting. It has been found that for these cases Ω will always equal 1. This is due to the fact that no transverse flexural deformations of the corrugation ends is possible under shear loading.

Although Libove and co-workers have not studied the problem of attachment spacing greater than one corrugation pitch, this does not pose a major obstruction for the analysis of civil engineering diaphragms. The added type of deformation for greater attachment spacings than one corrugation pitch is the accordion like action of the corrugations and sometimes the lifting of corrugation ends intermediate to the attachments. Use of the smaller modulus of elasticity in the direction perpendicular to the length of the corrugations will account for the accordion like deformations in a finite element analysis. Thus the major portion of the behavior due to such attachment will be modeled.

Lawson (23) in furthering the work done by Bryan and others

has derived flexibility expressions for trapezoidally and sinusoidally corrugated sheets. He estimates the total flexibility of a diaphragm by adding up the flexibility terms for each of the components in the diaphragm. The flexibility term for the corrugated sheets is given in terms of a dimensionless parameter $\overline{K}$. In cases where attachment spacing is greater than one corrugation pitch, $\overline{K}$ is calculated to reflect the effect of the accordion like behavior. Thus the lack of using the smaller modulus of elasticity is accounted for in this manner.

Lawson has derived the following expression for the effective shear modulus:

$$G_{eff} = \frac{G_o}{\frac{p'}{p} + \frac{p^{2.5} K\, G_o}{t^{1.5} L\, E_o}} \tag{3.17}$$

Writing this in the form of Equation 3.16 gives:

$$G_{eff} = G_o \frac{p}{p'} \left[1 + \frac{p^{3.5}\, \overline{K}}{2\, p'\, t^{1.5}\, L(1+\mu)} \right]^{-1} \tag{3.18}$$

Lawson has tabulated values of $\overline{K}$ for trapezoidally and sinusoidally corrugated sheets for various attachment spacings, and different number of intermediate purlins. However, due to the finite element approach taken herein, the values of $\overline{K}$ that are of interest are those for no intermediate purlins and for an attachment spacing of one corrugation pitch. The other factors are taken care of directly by the method.

The use of G_{eff} as obtained from Equations 3.16 and 3.18

in a finite element analysis is not strictly correct even in view of the assumptions made up to this point, as the end regions of the corrugated sheets will show a markedly less stiff behavior against shear than the central region. In other words, since G_{eff} is the average effective shear modulus for the entire length of the sheet, the actual average shear modulus for the end regions (G_{ae}) will be smaller than G_{eff}, and that for the central region will be greater than G_{eff}. This is derived from St. Venant's principle which states that the end effects - here those due to the discrete attachments - will decay in some asymptotic manner as one gets farther away from the ends. Assuming that the effect of the discrete attachments is negligible after a distance a from the ends, there will be a central region (L-2a) that will strain in shear similar to a diaphragm with continuous end attachment (37). Although the value of the distance a is not known, it will be independent of L, but will depend on the corrugation geometry and perhaps the spacing of the end attachments. Available photographs of some experimental results (6) indicate that the value of a is somewhere between the corrugation pitch (p) and the spacing of the attachments.

Figure 3.3c compares the following three cases under shear loading:

a. deformation of corrugated sheet with continuous end attachment.

b. deformation of same sheet with discrete end attachments, but using G_{eff} for entire length of sheet.

c. deformation of same sheet with discrete end attach-

ments, but using different shear moduli for the end regions (G_{ae}), and for the central region (G_{L-2a}).

Thus, when the surrounding diaphragm components - attachments, other sheets, beams - and the forces acting on these are taken into consideration, the use of case (c) above is seen to be the one that will produce the most accurate results in a finite element analysis. As this will require a more refined mesh than the use of G_{eff} for the entire length would, solution speed will be lowered. Whether and when the use of case (c) is warranted is discussed in Chapter 5 along with the computer analyses conducted and the results obtained.

Finding the shear moduli for case (c) is a straightforward process. For the central region, since the effects of the discrete end attachments are assumed to be negligible after a distance a, the effective shear modulus for this region will be simply:

$$G_{L-2a} = G_o \frac{p}{p'}, \tag{3.19}$$

i.e., the same as that for a sheet with continuous end attachment.

For the end regions of length a, Figure 3.3c provides the necessary geometric condition. From this figure it is seen that the ratio of the total deflections for the above two cases (b) and (c) is equal to 1. This ratio can be written in simplified form as:

$$\left(\frac{L - 2a}{G_{L-2a}} + \frac{2a}{G_{ae}}\right) \left(\frac{L}{G_{eff}}\right)^{-1} = 1 \qquad (3.20)$$

where the variables are as defined before. Substituting for G_{eff} and for G_{L-2a} from Equations 3.16 and 3.19 respectively, G_{ae} (the average effective shear modulus for the end regions) is found to be:

$$G_{ae} = G_o \frac{p}{p'} \left[\left(\frac{1}{\Omega} - 1\right) \frac{L}{2a} + 1\right]^{-1} \qquad (3.21)$$

If Lawson's work is to be used, then Ω corresponds to the reciprocal of the term in brackets in Equation 3.18.

3.2.2 Framing Members

The diaphragm frame used for typical tests consists of the perimeter beams in the two planar directions and the intermediate purlins. In order to accomplish shear transfer through the diaphragm panel, frame interconnections are usually built to be relatively free of moment resistance. Thus, in tests, the bare frame offers very little (negligible) resistance against shear distortion. The details of several such connections are shown on Figure 3.4.

The choice of the frame members depends on the loads they are expected to be exposed to. Both hot-rolled and cold-formed sections are used in practice and in tests. Mostly due to the need for load distribution, the perimeter sections are chosen to be stiffer than those for the intermediate purlins.

3.2.3 Connections

In this report, the term "connection" is employed to mean the combination of the connector - weld, screw, etc. - that is used to attach the panel sheets to each other or to the diaphragm frame, and the small regions of attached material in the immediate vicinity of the connector. This definition is deemed necessary because connection non-linearity in light gage steel shear diaphragms is quite often due to excessive deformation or tearing of the sheet material around the connector as well as being caused by tilting of screws or yielding of welds.

The connections are generally the weakest components of a diaphragm. Experimental results indicate that in the majority of cases the non-linearity of diaphragm behavior is completely due to connection non-linearity. The other components of the diaphragm seldom get stressed beyond their elastic limit. Therefore for an assessment of the non-linear behavior of diaphragms, knowledge of connection behavior is essential. For this purpose connection shear tests have been devised and conducted by several investigators (17, 25) on the types of connections used in shear diaphragms. The apparatus and the procedure for such tests are quite simple and valuable information regarding connection behavior in shear can be obtained.

For the purposes of this report, connections are separated into several categories. The following categories are similar to those used in References (6, 26).

1. End connections: These are the connections that are made to attach the two ends of a given sheet to the

perimeter members, (Figure 3.5a).

2. Seam connections: These are provided to accomplish attachment of two adjacent sheets to each other along their sides so that the full panel width can be developed, (Figure 3.5b).
3. Edge connections: These connect the outer sides of the first and the last sheets of the panel to the perimeter frame members, (Figure 3.5c).
4. Sheet to purlin connections: These are the connections between the sheets and the intermediate purlins, (Figure 3.5d).
5. In some cases two or more sheets may be connected to each other end to end to build up the length of the diaphragm, (Figure 3.5e). Such connections will behave like those of the first category above except that now the restriction of the rigid flange of the perimeter beam against downward movement at the connection is non-existant unless an intermediate purlin has been provided along the sheet ends being connected.

3.3 Finite Element Representation

Although a light gage steel shear diaphragm is a three dimensional structure, it can satisfactorily be modeled in two dimensions, these dimensions being those on the plane of the diaphragm, since the structural action that is of interest takes place on this plane (Figure 5.10). Therefore for modeling purposes a set of Cartesian coordinates X and Y are used to define the two orthogonal directions on the plane.

There are several basic considerations that need to be followed for a satisfactory finite element representation of a structure:

1. Each basic component of the structure (here the beams, sheets, connections) should be modeled by finite elements that reflect the particular behavior of the components in question.
2. The fineness of the mesh - the number of finite elements used to model the structure - should be optimized. Due to the energy considerations utilized to derive the stiffness matrices for the finite elements, too coarse a mesh will result in the structure acting appreciably stiffer than it actually is. On the other hand, computer time and therefore solution cost is increased to impractical levels if too fine a mesh is used.
3. When the number of finite elements and the degrees of freedom are high, the assemblage of the finite elements into substructures (subassemblies) should be considered as this will increase the efficiency of the use of auxiliary storage devices.

The computer program described in Chapter 4 and detailed in the appendices has been prepared to work with subassemblies, although if necessary a single finite element is also accepted as one subassembly. However, there are two restrictions as the program has been prepared. A subassembly may only contain finite elements that are exact replicas of each other (except for support and load conditions) and the total degrees of freedom

per subassembly may not exceed 40. Typical subassemblies are shown on Figures 5.4, 5.12, A.1.3 and A.1.4. Of these, the "split" subassemblies can only be used when the long form of input (see Appendix 1) has been chosen. In some instances such a choice of subassembly will be helpful in decreasing the total number of subassemblies without considerable increase in computation time. An example of what the author believes is an efficient use of "split" subassemblies is shown in their use in the finite element representation of the 10' x 12' box rib diaphragm of Section 5.5, (Figures 5.29, 5.30).

The rest of this section is devoted to the discussion of the finite elements and the mesh size used for each of the basic components of a shear diaphragm.

3.3.1 Panels

The sheets are modeled by rectangular orthotropic plane stress plate elements with four nodes and two degrees of freedom at each node (Figure 3.6). The two degrees of freedom at each node correspond to the translations in the X and Y directions. The material constants are chosen in accordance with Sections 3.2.1.1 (flat sheeting) and 3.2.1.2 (corrugated sheeting). When the sheeting is flat, the use of the same constants in the two principal directions automatically reduces the plate element into an isotropic one. The stiffness matrix for the orthotropic plate element of Figure 3.6 is given on Table 3.1. The derivation of this matrix can be found in References (24, 26).

According to Ammar (26), if the size of the plate elements is chosen to be on the order of 1/10 to 1/20 of the overall

dimensions of the diaphragm, acceptable results should be obtained for the case of flat sheet diaphragms. The same reference indicates that for this isotropic case, the practical range of the aspect ratio for the plate element dimensions should be between 1.5 and 2, with a maximum advisable value of 3.

In the orthotropic case (corrugated sheeting) however, the choice of aspect ratio is affected by the elastic moduli in the two principal directions. The reason for this is that in the main diagonal of the element stiffness matrix the elastic modulus in the X direction is multiplied by the length in the Y direction, and the elastic modulus in the Y direction is multiplied by the length in the X direction. Thus it is seen that a rectangular plate element with a longer dimension in the direction of the higher elastic modulus, and a comparatively much shorter second dimension will result in better conditioning of the element stiffness matrix.

3.3.2 Framing Members

All framing members are represented by conventional flexural elements with two nodes and three degrees of freedom at each node. Two of these degrees of freedom correspond to translations in the X and Y directions and the third one to rotation around an axis perpendicular to the plane of the diaphragm.

For input purposes, two types of flexural elements are considered. One is the "beam" element spanning parallel to the X-axis (Figure 3.7a), and the other is the "column" element spanning parallel to the Y-axis (Figure 3.7b). The two basic

elements differ only by a factor of the coordinate transformation required to account for the orthogonality.

When dealing with frame members it should be quite sufficient to allow for only one flexural element between two sheet to frame connections, unless other considerations are involved. For example, if the connections are unevenly spaced, a higher number of flexural elements between some connections will help to keep all flexural elements at the same length and therefore a lower number of subassemblies will be necessary. This will decrease input data and the use of auxiliary storage devices. On the other hand, the total number of degrees of freedom will increase.

Since the connections of the frame members to each other are built to be freely rotating joints, these can be considered as internal hinges. The treatment of this is very simple with the given input format and the solution routine. Assigning different numbers at the hinge to the rotational degrees of freedom of the two flexural elements meeting at that point is sufficient (see Section A.1.2. for more detailed discussion of numbering of degrees of freedom).

3.3.3 Connections

The variety and the complexity of the shapes and types of connections make it practically impossible to develop a representative finite element on the basis of geometry. On the other hand, if the connections are treated as discrete elements with experimentally derived input and output characteristics,

sophisticated representation will be unnecessary. In current practice (22, 24, 26), the connections are modeled by simple spring elements in the two orthogonal directions (Figure 3.8a).

In a first order analysis it is sufficient to define a spring constant for these spring elements. Since the results of connection shear tests are generally far from being linear, previous investigators have chosen the spring constants as the tangent of the angle made by a line drawn from the origin to a point on the test curve at a certain percentage of the ultimate load. This percentage has been recommended as 40 (see Figure 3.9) by the AISI (4). Such a simplification is not made for a non-linear analysis because it is necessary to follow the connection behavior continuously with increasing load.

Connection behavior is not necessarily the same in the two principal directions, neither may it be expected to be the same in any given two directions. For a first order analysis, this fact can be remedied substantially by obtaining results from two separate connection tests in the two principal directions. Thus different spring constants can be assigned to the two springs representing the connection. However, for non-linear analysis purposes, the interaction of the two springs needs to be known for the best estimate of the stage the connection is in during a loading. At the present, there is no data available on the interaction of connection behavior in the two principal directions and it is also believed by the author that, within the limits of practicality, obtaining such data will be quite difficult if not impossible. The main reason for this is that, in the case of connections, one cannot readily speak in

terms of a simple material non-linearity (the material being assumed as that the connector is made of) since the non-linearity may be due to several different phenomena (see Section 3.2.3). Therefore, it is not possible to formulate a yield function involving two different behaviors in the two principal directions. For this reason, in this research, a connection is assumed to behave similarly in all directions and that this behavior will be the same as that obtained through a shear test of the connection. There are two exceptions to this assumption. The first one has already appeared above and is the case of first order analysis. Within the limits of the computer program detailed in this report, it is possible to assign different spring constants in the two directions for a first order analysis by arranging the input accordingly (see Section A.1.4). The other exception is in the case of the sheet to sheet seam connections as will be seen below.

The types of connections that are considered have been defined and labelled in Section 3.2.3. Representation of these connections by spring elements also involve considerations regarding their locations. Below is a description of how each type of connection has been modeled for this research. The computer program has been prepared to take full advantage of this description.

1. End connections: In general, two springs in the X and Y directions represent each of these connections. The only exception is the case where a mechanical end connector exists at the end of a seam line. In such a

case, the two sheet corners at that location are attached to the flange of the perimeter beam by a screw or other mechanical connector passing through both sheets, since an overlap exists (Figure 3.8c). As the attachment to a relatively rigid flange will not permit the tilting of the connector it is possible to view the connector as an extension of the flange (Figure 3.8d). This assumption is supported by experimental results which show that at sheet ends the connection non-linearity is due to tearing or piling up of the sheet material around the connection (6, 21). Therefore a reasonable model will involve independent connections of the flange to each of the two sheets at that point. Then the representation of the connection is done by four spring elements, two for each independent connection (Figure 3.8e). In the case where welding is the manner of attachment, the two sheets are generally welded to the flange independently, thus eliminating the need for the above assumption.

2. Seam connections: Experimental results indicate that there is virtually no separation of adjacent sheets in the direction orthogonal to a seam line. This has led Ammar (26) to use a very high spring constant in this direction for the first order analyses he has conducted on shear diaphragms. Since such an arrangement would create difficulties in a non-linear analysis, the

spring in the direction orthogonal to the seam line has been discarded altogether in this research, and has been replaced by a rigid link between the two sheets where a seam connection exists. Thus, for sheet to sheet seam connections only one spring - parallel to the seam line - is sufficient to model the connection, (Figure 3.8b). The case of sheet to intermediate purlin connections which are made at seams is discussed under (4) below.

3. Edge connections: These connections are modeled by two springs in the two directions without exception.
4. Sheet to intermediate purlin connections: All of these connections with the exception of those made at seams are modeled as (3) above. At the seams the connection is modeled by four springs making up the two independent connections between the purlin and the two adjacent sheets (see (1) above). Furthermore, the two sheets share the same degree of freedom in the direction perpendicular to the seam line (rigid link - see (2) above). This representation of the connection is shown on Figure 3.8f.

For all of the above types of connections, the spring behavior is obtained through shear tests and is represented by a multi-linear approximation of the test curve. Further discussion of the treatment of connections in the non-linear analysis is given in Chapter 4 along with the theory of the computer program.

CHAPTER 4

THE COMPUTER PROGRAM

4.1 General

The computer program documented in this report has been prepared for the purpose of analyzing the behavior of cantilevered light gage steel shear diaphragms loaded in the linear and non-linear ranges up to collapse.

The program originates from a frontal solution routine written by Irons (46), and a computer program utilizing this solution routine, written by Miller (24) for the elastic analysis of multi-story frames with light gage steel panel infills. This computer program was also used by Ammar (26) for the first order analysis of light gage steel shear diaphragms of the type discussed herein.

Due to the specialized nature of the documented program, some parts of the solution routine written by Irons are either left out of simplified. In addition, some subroutines used by Miller for his work are either omitted or have undergone major simplification. These omissions or changes noted above were seen to be necessary in order to cut down on the core usage, so as to fit the program in smaller computers, and to cut down on the time and therefore the cost of the elastic solution. As a side benefit, this reduces the logic circuitry that is encountered during every iteration for the non-linear analysis.

For reasons that are detailed in Sections 4.3 and 4.4, it was decided that, given the solution routine mentioned above,

the most suitable approach for analysis of a structure in the non-linear range would be the residual force (initial stress) method in which an elastic solution is made at every load increment and the residual forces due to elements which show material non-linearity are redistributed elastically through the structure. The method is documented by Zienkiewicz and coworkers (47, 48). In Section 4.4.2 the theory behind the method is reviewed, and the application to the special case at hand is detailed in conjunction with the computational steps.

To speed up the convergence of iterations during any given load increment, an acceleration technique proposed by Boyle and Jennings (49, 50) was employed with very satisfactory results. This is discussed in Section 4.5.

It was shown in earlier experimental investigations that the only important source of material non-linearity in most civil engineering diaphragms is the connections. The steel sheeting and the perimeter beams as well as the intermediate purlins remain elastic throughout the loading range. For this reason, the only type of material non-linearity sought in the analysis is that of the connections. The curves for connection behavior under loading, as provided by Ammar (25), or interpolations derived from these curves are approximated by a series of straight lines for use in the analysis.

The input specifications for the computer program are given in Appendix 1. The rest of the documentation for the program can be found in Appendices 2 through 4.

4.2 Frontal Solution

The finite element analysis of a structure by the stiffness method comprises the solution of the symmetric positive definite matrix equation

$$[K]\{\delta\} = \{P\} \tag{4.1}$$

where,

[K]: the structural stiffness matrix in global coordinates,

{δ}: the vector of nodal degrees of freedom (the deflections, also called the variables later in the text)

{P}: the vector of external forces and reactions.

When [K] is of rather large dimensions, the direct inversion of [K] to solve for {δ} is very impractical. Numerical methods have successfully been used to reduce [K] into an upper triangle matrix, after which a back-substitution process determines the variables {δ}. A very common such method is the Gaussian Elimination.

Special solution routines that deserve serious attention make use of the fact that [K] is in general sparsely populated. If the order of the variables has been chosen sufficiently well such that [K] is a tightly banded matrix, a band solution technique can be employed. In this case the core usage and the computation speed depends on the bandwidth.

Frontal solution is a variation of the Gaussian Elimination in that it does not depend on the numbering of the variables.

In the frontal solution, the variables are eliminated right after their last appearance - that is, as soon as the accumulation of the element coefficients for the relevant stiffness equation is finished. Therefore elimination of the variables proceeds alternately with the coefficient assembly process. This means that only the variables that have not been eliminated yet, but that have appeared for assembly need to be kept in core.

The appearance of the variables is dictated by the order of the elements to which they belong. The so called front advances as each element is introduced, the variables from previous elements - those variables that have not yet been eliminated - plus the variables that have been introduced with the new element being kept in core, then the variables that have appeared for the last time being eliminated, and finally those variables that are left in core comprising a boundary between the elements that have been introduced and those that have not been. Therefore it is seen that ordering of the elements, not of the variables, is essential to the efficiency of the frontal solution. It is stressed that ordering of the elements efficiently is a much easier and more natural task than doing the same for the variables. Furthermore, since the maximum possible size of the front will be dictated by the dimensioning statements in the program, care need only be taken to keep the front smaller than the prescribed dimension.

Further discussion of the frontal solution can be found in the next section and in Reference (46).

4.3 The Solution Routine and Miller's Program

Several features made the frontal solution routine written by Irons (46) desirable for use in the computer program documented in this report. One of the most important of these is the re-solution facility already incorporated into the solution package. This is discussed later in this section.

Another very important feature has already been discussed in the previous section. The numbering order of the variables is irrelevant to the frontal technique, both in terms of solution speed and core usage. This is most advantageous in giving the programmer an opportunity to provide for automatic numbering of the degrees of freedom, especially if the program is intended to solve only a certain type of structure with prescribed standard features. Moreover, in case of changes in the finite element mesh, the extensive renumbering required to preserve a small bandwidth for band solutions is unnecessary for the frontal solution.

Internal hinges in a structure can be treated with extreme ease, given the solution routine discussed herein. It is sufficient to assign different numbers to the rotational degrees of freedom of the different element nodes converging at the hinge. With many other solution routines, the use of Lagrange multipliers is necessitated to treat the same case.

Iron's routine has been written so as to provide for re-solutions without having to reassemble and reduce the structural stiffness matrix. Only the right hand sides ({P}) of the stiffness equations need to be modified for a re-solution. This

facility suggested the use of a technique different than the Newton-Raphson method, since the Newton-Raphson method requires that the stiffness matrix be modified and therefore reduced at every load increment. The residual force method - also called the initial stress method - was found to be the best suitable for use with the solution routine. This method has other important advantages which are discussed in Section 4.4.

The original solution routine as fully documented in Reference (46) also provides for the use of fragmented elements (essentially, elements with data too long to fit on one tape record) and for the processing of more than one load condition at a time during a re-solution. However, these two features have been removed from the routine since they are not required for the program that has been developed.

A computer program for the first order analysis of multi-story frames with infills was written by Miller (24) utilizing the above mentioned solution routine. This program became the starting point for the computer program documented in this report. Miller's program has also been used by Ammar (26) for first order analyses of light gage steel diaphragms.

Miller's program being too versatile to serve efficiently for the purposes of the research presented herein, it was decided to condense the program such that anything unrelated to the analysis of light gage steel diaphragms was left out. This resulted in large savings on core usage and computation time for first order analysis. However, one major contribution by Miller has been kept with some modifications. This is the

routine for the formation of subassemblies, the use of which greatly increases the efficiency of auxiliary storage utilization.

The non-linear analysis algorithm that is detailed in subsequent sections and in the appendices, and a mesh generator routine that greatly simplifies and reduces the input data were then merged with the condensed program.

4.4 Non-linear Analysis

4.4.1 General

It has already been observed that in most civil engineering shear diaphragms, the connections are the only important source of non-linearity, all other components of the diaphragm remaining elastic or nearly so until the initiation of collapse. For this reason, the computer program has been set up such that only the connections are given non-linear properties.

There are several methods for non-linear analysis. One of the best known is the Newton-Raphson procedure where the structural stiffness matrix undergoes modification to account for the material non-linearity encountered at each load increment, therefore necessitating the re-solution of Equation 4.1 by a new reduction of [K] at every load increment. This method is in general time consuming and special precautions must be taken to insure elastic unloading. The residual force method, which makes use of the initial stiffness matrix throughout the analysis, however, requires only the modification of the right hand sides of the stiffness equations, and requires no special

treatment to insure elastic unloading. This method is discussed below.

4.4.2 Residual Force Method

The residual force method depends on the fact that in material non-linearity, a given increment of deflections will uniquely describe the internal force distribution, while the opposite is not necessarily true. Therefore, any residual forces can be redistributed elastically in the structure to adjust towards the correct equilibrium condition. This method has the definite advantage of making use of the initial stiffness matrix throughout, therefore requiring no more than one reduction of this matrix. The elastic redistribution of residual forces is done through iterations which will converge when new iterations will bring no appreciable changes in the structural response. Although convergence may be slow when plasticity is extensive, the method yields itself very easily to the use of accelerators (see Section 4.6) resulting in fast rates of convergence.

The method is detailed thoroughly in References (47) and (48) for use in even quite sophisticated problems. The use of the method in connection with this report, however, is a rather simple special case, especially so since the connections which are investigated for non-linear behavior are idealized as spring elements (Chapter 3). The spring elements undergo the same treatment as axial members and so are relatively easy to deal with in the context of the residual force method.

The basic outline of the residual force method is given herein, followed by a detailed presentation of the actual steps followed in the computer analysis.

A typical cycle in the residual force process starts with the application of a load increment on a given structure. An elastic solution is performed, finding the deflections and forces corresponding to the load increment. If, however, one or more of the elements describing the structure have gone into the plastic range with the application of the load increment, then the forces allocated to these elements through the elastic solution will in general be in excess of those forces that would actually correspond to the deflection increment. This can be best illustrated with the aid of a figure. On Figure 4.1a, an axial element, which is part of a structure, is shown in free body state. Figure 4.1b gives the tension test behavior of this particular element. It is assumed that some load has been applied on the structure, and it is further assumed that if an elastic solution is performed, the axial force in the member of Figure 4.1a will be found to be F corresponding to the elastic member stretch Δ. It is seen that the point defined by F and Δ does not fall on the curve of Figure 4.1b since these values were obtained by using the initial stiffnesses of the elements comprising the structure. The correct force defined by the curve would rather be F* as shown on the figure. Hence, the residual force due to this element will be the difference F-F*. When the residual forces have been computed for all elements (of the structure) that have entered the plastic range,

these forces are applied on the structure as additional loads, and the structure is again analyzed elastically, this new solution producing further deformation of the structure. In general, the improved results will again not be correct, maybe necessitating further redistributions, depending on the criteria for convergence. (Two more cycles regarding the axial element are shown on Figure 4.1b). As a result, the total deformation of the structure will be the sum of the original deformation and those found through the iterations.

Unless the structure is at collapse condition, the iterations will be convergent, that is at one point further iterations will bring no appreciable improvement to the results. This point determines with sufficient accuracy the deflections and forces in the structure and the acceptable equilibrium configuration.

It is seen from the above that it is rather easy to determine the residual forces in the case of axial elements. In the case of elements with more than one degree of freedom per node and/or with more than two nodes, the best approach to find the residual forces is to use the elasto-plastic matrix. The elasto-plastic matrix takes the place of the element stiffness matrix in incremental analysis, and it is used to find the correct force increment in the element corresponding to the imposed deflection increment. This matrix is derived by making use of the total stress-strain relationships, the relevant yield criterion, and the normality rule. The derivation and the use of the elasto-plastic matrix in the residual force

method can be found in References (47) and (48), and will not be discussed further herein.

4.4.3 Application of the Residual Force Method in Diaphragm Analysis

A. Pre-solution

1. The diaphragm assembly is modeled with finite elements (Section 3.3 and Appendix 1).
2. The finite element mesh is divided into subassemblies.
3. The input data is formulated (Appendix 1) and is fed into the program along with the initial load and the desired incremental load.

B. First Order Solution and the Elastic Limit

4. The computer program analyzes the structure elastically for the given initial load, by using the frontal solution routine.
5. As the deflections for each subassembly appear during the back-substitution process, the subassembly is checked as to whether it is a connection subassembly or otherwise.
6. If a connection subassembly, the resultant force in each connection is found, and is compared to the elastic limit of the connection as found from connection test. This comparison yields for each connection a factor that can resize the connection force to the elastic limit of the connection.
7. If not a connection subassembly, step 6 is bypassed.
8. As each subassembly appears, the deflections are also

placed in the appropriate locations of the global deflections vector {δ} for display purposes.

9. After the last connection subassembly appears during the back-substitution, all factors to the elastic limit are compared, and the factor for the connection that would reach this limit first is chosen to be the factor that will bring the structure to its elastic limit.
10. The subroutine for the residual force analysis (PLAST) is called.
11. The connection subassemblies again appear one by one. All forces are multiplied by the factor computed in step 9 and are displayed.
12. The first load increment beyond the elastic limit is applied. No new solution is needed for the application of a load increment since a simple proportioning of the results obtained for the initial load is sufficient.
13. In the first cycle after the elastic limit, every connection is checked for non-linearity in the following manner. The absolute value of the elastically computed deflection $\bar{S}$ ($\bar{S}$ being the resultant deflection $(S_x^2 + S_y^2)^{0.5}$ if the connection is idealized by two spring elements as for edge or end connections) is compared to the slip at the elastic limit of the connection as obtained from the connection curve.
14. If $\bar{S}$ is less than the connection elastic limit ("yield") slip, no non-linearity is present, therefore the residual forces for that connection are set equal to zero.

15. If $\overline{S}$ is greater than the yield deflection, the new yield point F* (CYP in the computer program) is found from the connection curve using $\overline{S}$. Then F* is subtracted from the elastic resultant force $\overline{P}$ to give the resultant residual force $\overline{R}$.
16. If the connection is a sheet to sheet seam connection - idealized by only one spring element - the residual force at each node of the element is equal in magnitude to $\overline{R}$. Then the correct directions of the residual forces at each node is found by referring to the directions of the components of $\overline{P}$.
17. If the connection has been idealized as two spring elements the components of $\overline{R}$ in the X and Y directions are found with the correct signs.
18. The connection forces corresponding to the deflection increment are found by subtracting the residual forces from the elastically computed forces.
19. After each connection is dealt with, the subroutine for check on convergence (CONV) is called to determine the contributions to the residual force norm (see Section 4.5).
20. When all the connections in a certain number of subassemblies have been dealt with, the connection forces, deflections and the new yield points are stored on tape. The residual forces are stored in a long vector (STORE) as data for the re-solution phase.
21. After the last connection subassembly is analyzed,

possibility of convergence is checked against the convergence criterion in subroutine CONV.

22. If convergence has been attained, only one more iteration will be allowed.
23. Return to main program is affected and any other subassemblies that are left, go through the back-substitution phase.
24. The global deflection vector is multiplied by the factor of step 9, and the deflections at the elastic limit are displayed, then stored in the vector STORE.
25. The incremental deflection vector corresponding to the standard load increment is computed and is written on tape.
26. Control goes back to the beginning of the solution routine, for the first re-solution after the elastic limit.

C. Later Iterations (re-solutions)

All iterations between any two load increments are conducted for the purpose of elastically redistributing the residual forces. Therefore, now, the residual forces make up the right hand sides of the stiffness equations. Since the global stiffness matrix has already undergone reduction during the first solution, only the right hand sides need to be modified. As a result, a re-solution takes only a fraction of the time necessary for the initial solution.

The resulting deflections after each re-solution are the incremental elastic deflections due to the residual forces

redistributed during that iteration. During the non-linear analysis of the connections in subroutine PLAST, the force increment corresponding to these deflections is computed for each connection and is added to the previous connection force as read from tape. Then the status of the connection is again compared to its behavior range as defined by the connection curve, and the residual forces are calculated.

Except after an acceleration attempt (see Section 4.5), subroutine PLAST is called once for each connection subassembly, as opposed to only once in the first solution. This has the advantage of reducing vector arithmetic and keeping vector dimensions at a minimum in addition to providing a somewhat more organized use of auxiliary storage devices by enabling the direct recording of the residual forces on tape.

After every third iteration - if convergence has not been attained after the second iteration in the triplet - the rate of convergence is increased by an accelerator as discussed in Section 4.5.

4.5 Convergence

It is felt that since the diaphragm behavior is governed by the magnitude of the residual forces, then these forces should be the true measure of convergence. Nayak and Zienkiewicz (48) suggest a convergence criterion, along with other criteria, whereby the residual force norm defined as

$$||R|| = \{R\}^T \{R\} \qquad (4.2)$$

where {R} is the vector of residual forces for the whole structure, is calculated and is compared to a fraction of the externally applied load norm which is defined similarly. They also suggest that this fraction be between 10^{-4} and 10^{-5}. It was seen during computer analyses that the effect of residual forces when they are small is rather negligible, therefore the value of the fraction for this computer program has been chosen as 10^{-4}. Although this may look less conservative than 10^{-5}, the effect of the difference is minute, and the use of 10^{-4} avoids excessive iterations.

When $||R||$ is less than 10^{-4} times the applied load norm, convergence is deemed to have been achieved. One more iteration is done after this point, however, in order to properly update the records with the knowledge of convergence and to apply the next load increment after this last iteration. This also has the effect of decreasing the residual forces further. The results of this last iteration are added to the next load increment that ensues so that errors will not accumulate with each load increment.

4.6 Acceleration of Convergence

4.6.1 Theory

Even though the residual force method avoids the modification and the reduction of the stiffness matrix at every iteration, it does pose the difficulty that when the degree of nonlinearity is high, convergence tends to be rather slow. Obviously, to compensate for the difference between the correct

equilibrium condition and the elastic solution done at each load increment, more elastic redistributions are needed as non-linearity progresses. Therefore, some method of speeding up the convergence rate was sought in order to avoid excessive computer times.

After a review of the current literature on acceleration techniques, it was decided that a modification of the Aitken accelerator, proposed by Boyle and Jennings (50), would be the most suitable for both the problem at hand and the set-up of the computer program.

Aitken's δ^2 process (51) depends on the assumption that the rate of convergence of an iteration sequence is geometrical. Working with this assumption, it can be shown that the error e_i in a given iteration (i^{th}) is proportional to the error e_{i-1} of the previous iteration, the proportionality constant C being independent of the number of the iteration. This can be written as

$$e_i = Ce_{i-1} \tag{4.3}$$

Recursive application of Equation 4.3 gives

$$e_i = C^i e_o = x_i - \xi \tag{4.4}$$

where,

e_o : the initial error,

x_i : value of the variable at the i^{th} iteration,

ξ : actual value of the variable - i.e. the value to be attained on convergence.

If x_i, x_{i+1} and x_{i+2} are three successive iterates, it can be shown that (52):

$$\xi = \frac{x_i\, x_{i+2} - x^2_{i+1}}{x_{i+2} - 2x_{i+1} + x_i} \tag{4.5}$$

Even if the iteration sequence x_i converges in a different manner than assumed, it can still be proven that the sequence defined by

$$x_i^* = \frac{x_i\, x_{i+2} - x^2_{i+1}}{x_{i+2} - 2x_{i+1} + x_i} \tag{4.6}$$

will lead to faster convergence than the sequence x_i.

Aitken's δ^2 process is expressed in the more convenient form (52)

$$x_i^* = x_i - \frac{(\Delta x_i)^2}{\Delta^2 x_i} \tag{4.7}$$

where,

$$\Delta x_i = x_{i+1} - x_i$$

$$\Delta^2 x_i = x_{i+2} - 2x_{i+1} + x_i$$

or as (49)

$$x_i^* = x_{i+2} + S_i^* (x_{i+2} - x_{i+1}) \tag{4.7a}$$

where S_i^* is the acceleration factor - the overstep value - defined by

$$S_i^* = \frac{x_{i+1} - x_{i+2}}{x_i - 2x_{i+1} + x_{i+2}} \qquad (4.7b)$$

Aitken's process has the important shortcoming that the user might encounter zero or very small denominator in Equation 4.7b in a computer application, this in turn resulting in gross estimates for acceleration.

The above difficulty can be avoided when a vector of variables is considered for acceleration. Jennings (49) has proposed a modification to Aitken's process, using a common overstep value for all the variables in the accelerated vector. The overstep value is found in a manner similar to Equation 4.7b, except that now it is determined from the weighted mean of differences:

$$S = \frac{\{W\}^T(\{X\}_{i+1} - \{X\}_{i+2})}{\{W\}^T(\{X\}_i - 2\{X\}_{i+1} + \{X\}_{i+2})} \qquad (4.8)$$

where $\{X\}$ is the vector of variables and $\{W\}$ is a vector of relative weights.

For the use of Equation 4.8 in residual force analysis, Boyle and Jennings recommend (50):

$$\{W\} = \{X\}_i - 2\{X\}_{i+1} + \{X\}_{i+2} \qquad (4.9)$$

Therefore, the acceleration sequence is defined by:

$$\{X\}^* = \{X\}_{i+2} + S(\{X\}_{i+2} - \{X\}_{i+1}) \qquad (4.10a)$$

where,

$\{X\}^*$: the modified variables vector, and

$$S = \frac{(\{X\}_i - 2\{X\}_{i+1} + \{X\}_{i+2})^T (\{X\}_{i+1} - \{X\}_{i+2})}{(\{X\}_i - 2\{X\}_{i+1} + \{X\}_{i+2})^T (\{X\}_i - 2\{X\}_{i+1} + \{X\}_{i+2})} \qquad (4.10b)$$

the subscripts indicating the number of the iteration.

4.6.2 Application to the Present Problem

It has already been mentioned that in the residual force method, every iteration is used to redistribute the residual forces elastically through the structure. Therefore the result of a given iteration is not the total deflection vector, but the difference in deflections between the beginning and the end of the iteration. In the present computer program, after each iteration these deflection changes are added to the previous deflections to obtain the vector of total deflections.

Considering a group of any three iterations during a given load increment, it can be seen that the vector of the difference in deflections at the end of the third iteration is equal to the term $(\{X\}_{i+2} - \{X\}_{i+1})$ of Equation 4.10a. The same term is seen in Equation 4.10b with the sign reversed. Furthermore, the vector common to the numerator and the denominator of Equation 4.10b can be broken into $(\{X\}_i - \{X\}_{i+1}) + (\{X\}_{i+2} - \{X\}_{i+1})$. The first term in this summation is the negative of the deflection changes between the results of the first and second

iterations of the triplet of iterations.

Therefore, letting

$$\{\Delta\}_1 = (\{X\}_{i+1} - \{X\}_i)$$

and

$$\{\Delta\}_2 = (\{X\}_{i+2} - \{X\}_{i+1}) \tag{4.11}$$

Equations 4.10a and 4.10b can be written as:

$$\{X\}^* = \{X\}_{i+2} + S\{\Delta\}_2 \tag{4.12a}$$

and

$$S = \frac{(\{\Delta\}_2 - \{\Delta\}_1)^T (-\{\Delta\}_2)}{(\{\Delta\}_2 - \{\Delta\}_1)^T (\{\Delta\}_2 - \{\Delta\}_1)} \tag{4.12b}$$

When the time for acceleration arrives, i.e. after the third iteration, $\{\Delta\}_2$ and $\{X\}_{i+2}$ are already in high-speed storage. Therefore extra storage need to be set up only for $\{\Delta\}_1$.

It should be noted at this point, that the acceleration factor S may sometimes turn out to be negative, which is unacceptable. This occurs when $\{\Delta\}_2^T\{\Delta\}_2 > \{\Delta\}_1^T\{\Delta\}_2$. If a significant number of connections enter the non-linear range during a load increment and this becomes evident through the results of the second iteration of a triplet of iterations in that load increment, then the pattern of decay followed in the previous iterations will be lost. In other words, the deflections that will be computed at the end of the third iteration will be higher than that would have been expected from the earlier trend.

This fact is illustrated in Figure 4.2 for one variable. It can be seen that the convergence, defined by zero slope of the deflection curve, assumes different meanings for the two curves. Obviously to employ the negative acceleration factor would cause the structure to unload elastically and would produce erroneous results. The actual expected behavior of the structure (for the case of the single variable, that of the variable) is shown by the dotted line on Figure 4.2. Therefore, it is seen that new iterations are needed before acceleration can be employed. This is the way the negative acceleration factor is treated in the documented program. When a negative S is encountered, the acceleration stage is bypassed and three more iterations are performed before another attempt is made to accelerate.

Equations 4.12a and 4.12b depend on the extension of 4.3 to matrix notation:

$$\{e\}_i = [M]\{e\}_{i-1} \tag{4.13}$$

where, [M] is an iteration matrix independent of the number of iteration and not necessarily symmetric (50).

If Equation 4.13 were strictly the case, then the modified variables $\{X\}^*$ obtained from 4.12a would be the correct ones and no more iterations would be necessary. However, in general, Equation 4.13 will not be correct, although the error decay may behave very nearly so. Boyle and Jennings point out that the variables will behave as though the iteration process is governed by an iteration matrix if a limited number of iterations are

considered (50) - refer to last paragraph of the previous section for the case when this is not so. In any case, it is seen that there is, in general, still an error present after the acceleration has been done. Therefore, unless the error is within acceptable limits, more iterations will be needed after an acceleration. To perform these iterations, the residual forces that need to be redistributed after $\{X\}^*$ has been found need to be known. Detailed below is the description of this process for the given computer program.

At the end of a triplet of iterations, the calculation of residual forces due to the effect of $\{\Delta\}_2$ is bypassed, unless the acceleration proves unsuccessful - i.e. negative acceleration factor. $\{X\}^*$ need only be found for the degrees of freedom associated with the connections if it is not required for display. Then the new change in the deflections of these degrees of freedom is:

$$\{\Delta\}^* = \{X\}^* - \{X\}_{i+1} \tag{4.14}$$

When the connection forces are updated to reflect the change $\{\Delta\}^*$, the corresponding residual forces $\{R\}^*$ are calculated. Now:

$$\{R\}^* = \{R\}_A + \{R\}_\varepsilon \tag{4.15}$$

where,

$\{R\}_A$: the total of all the residual force vectors that

would have created a total deflection difference of $\{\Delta\}^*$, had no acceleration been employed, assuming that then say n iterations would have been needed to reach $\{X\}^*$.

$\{R\}_\varepsilon$: Since convergence is, in general, not strictly governed by Equation 4.13, the difference between the deflections at the end of the $(n-1)^{th}$ iteration and $\{X\}^*$ would have created new residual forces that would in turn cause additional deflections beyond $\{X\}^*$, if no acceleration had been done. $\{R\}_\varepsilon$ are these residual forces. In other words, $\{R\}_\varepsilon$ exist because of the error in the assumption that convergence is strictly governed by Equation 4.13.

It is seen that, in the case of no acceleration, $\{R\}_\varepsilon$ would have been the residual forces to continue with, after the deflections $\{X\}^*$ were attained. The same holds true also when an acceleration has been done. However, instead of calculating $\{R\}_A$ or $\{R\}_\varepsilon$, a redistribution of the residual forces $\{R\}^*$ can be made - keeping the structural deflection vector at $\{X\}_{i+2}$ and the vector for the d.o.f. associated with the connections at $S\{\Delta\}_2$ - and progress can thus be made to $[\{X\}^* + \{\Delta\}_\varepsilon]$, where $\{\Delta\}_\varepsilon$ is the additional deflections due to $\{R\}_\varepsilon$. Although $\{\Delta\}_\varepsilon$ is not explicitly calculated, it can be computed for the d.o.f. associated with the connections from:

$$\{\Delta\}_\varepsilon = \{\Delta\} - S\{\Delta\}_2 \qquad (4.16)$$

where, $\{\Delta\}$ is the deflection difference between $[\{X\}^* + \{\Delta\}_\varepsilon]$ and $\{X\}_{i+2}$, and where the three vectors correspond only to d.o.f. associated with the connections. Thus after $\{\Delta\}_\varepsilon$ has been computed by Equation 4.16, corresponding residual forces can be found to proceed on to the second iteration beyond the acceleration.

The use of the accelerator has proven very beneficial. For example, when the 24" x 28" shear diaphragm of Section 5.2 was analyzed without an accelerator, convergence was reached in 7 iterations in the first load increment beyond the elastic limit, and no convergence was attained in 20 iterations in the second increment. When the accelerator was employed, 4 and 5 iterations, respectively, were sufficient to reach convergence in these two load increments, one acceleration per increment being sufficient.

CHAPTER 5

APPLICATIONS

5.1 General

A total of four cantilevered shear diaphragms have been analyzed for non-linear behavior, using the computer program documented in this report. These are, in the order they are discussed in the subsequent sections:

(a) 24" x 28" standard corrugated diaphragm,

(b) 10' x 12' welded cellular metal deck,

(c) 10' x 12' standard corrugated diaphragm,

(d) 10' x 12' trapezoidally corrugated diaphragm.

All four of these diaphragms were tested by earlier investigators in previous research at Cornell University. Therefore, test results are available for comparison with computer results.

5.2 24" x 28" Standard Corrugated Diaphragm

This diaphragm was tested by Luttrell (6) in his small diaphragm test series and was labelled Test no. 3C1-1. The diaphragm was later analyzed by Ammar (26) for elastic behavior.

5.2.1 Description of the Test Installation

The test arrangement for the diaphragm is shown on Figure 5.1.

The panel of the diaphragm was cut from a 26 gage standard corrugated sheet of 2' width, the dimension of the panel along the length of the corrugations being 2'4". This was connected

to L 1 1/2" x 1 1/2" x 1/4" perimeter members by no. 14 self tapping screws, these screws being placed in the valleys of the corrugations at the two ends of the sheet with a spacing of three corrugation pitches, and at the edges, one screw to an edge, halfway along the length of the sheet. All four perimeter members were hinge-connected to each other at their ends. The support conditions and the location of the load were as shown on Figure 5.1.

5.2.2 The Finite Element Model

The finite element model which is shown on Figures 5.2 through 5.4, is somewhat different than that used by Ammar in Reference (26). With the new model, a smaller number of sub-assemblies provide improved computational speed. Also the better idealization of some of the connections that were modeled differently by Ammar make non-linear analysis possible.

Since the non-linear analyses on this small diaphragm were conducted during the initial stages of the research and early in the development of the computer program, to check the program for improvements and new computational devices, no need was seen to improve on the geometrical and material data provided by Ammar (26). (Later research showed that better predictions of the shear modulus can be obtained from more current literature). In addition, in the modeling of this diaphragm, instead of the multi-linear idealization of the connection behavior - as has been done for the later analyses - an elastic-perfectly plastic simplification was made. Therefore, the results obtained for

this diaphragm are not meant to be strict guidelines for the understanding of diaphragm behavior, but are nevertheless satisfactory and are of some academic interest.

The panel is modeled into three subassemblies, each subassembly being composed of 12 orthotropic plate elements. Each plate element is one corrugation pitch wide (2.667") and 7" long, with a thickness of 0.018". The material properties, as obtained from Ammar's work (26), are:

E_x: 33000 ksi E_y: 33 ksi G_{eff}: 500 ksi

μ_{xy}: 0.3 μ_{yx}: 0.0003

The two perimeter members spanning parallel to the y-axis were taken as one subassembly each, with three 8" long column elements to each subassembly. The other two perimeter members were likewise considered as one subassembly each, with two 14" long beam elements making up one subassembly. The geometric and material properties are:

Area = 0.69 $in.^2$, Mom. of inertia = 0.14 $in.^4$, E = 29500 ksi

The four end connections on each side make up one subassembly. Each connection is idealized as two spring elements in orthogonal directions, but with same material properties. The connection on each edge is considered a subassembly by itself and is modeled like the end connections. The spring behavior is idealized to be elastic-perfectly plastic, this behavior being approximated from the shear test results provided by Ammar (26) on the no. 14 self tapping screw used in edge connections of 26 gage material. The actual screw shear test behavior, and the idealization, are shown on Figure 5.5.

5.2.3 Analyses and Results

Two non-linear analyses were conducted on the 24" x 28" diaphragm, with only one varying analysis parameter. No accelerator was used in the first analysis and the results indicated a need for one. Therefore, after the modified Aitken accelerator (see Section 4.6) was implemented in the program, a second run was conducted.

In both cases, an initial load of 1 kip was applied on the diaphragm and the elastic limit was found after a linear analysis with this load. Then the load was increased in increments of 0.05 kip beyond the elastic limit.

Without the accelerator, convergence to equilibrium was reached in 7 iterations in the first increment beyond the elastic limit, but 20 iterations were not sufficient for convergence in the second one although it was seen from the results that collapse would not be reached in this increment.

With the accelerator, 4 and 5 iterations respectively for each of these two increments, were sufficient for convergence, only one acceleration being necessary in each case. Convergence required 16 iterations and 5 accelerations in the third load increment since at this stage the non-linearity was extensive. In the fourth increment beyond the elastic limit, an unexpected negative acceleration factor caused elastic unloading. As a result zero residual forces were computed and the rest of the iterations did not have any meaning. However, a check of the connection forces before this acceleration revealed that all connections had reached their ultimate capacity as modeled,

therefore preventing any further shear transfer between the perimeter members and the panel. At this time, it was thought that the negative acceleration factor is totally due to collapse condition (which is indeed the case for this diaphragm), therefore no counter measures were taken.

The computer results for the deflection of a representative degree of freedom (d.o.f. no. 110 on Figure 5.3) are shown on Figure 5.6. It is seen that the ultimate load as found by computer analysis compares well with that reported for the test. Since the only other test result that has been reported for this diaphragm is the effective shear modulus, found as the slope of a line drawn from the origin to the test curve at 40% of the ultimate load, as recommended by the AISI (4), the computer output can only be compared to this line. The initial linear portion of the test curve is expected to have had a higher slope than this line since at 40% of the ultimate load some non-linearity in diaphragm behavior would be present. This early non-linearity does not show on the computer results due to the idealization of the connector behavior (see Figure 5.5). This idealization is for the most part responsible for the slightly higher ultimate load that was computed, since if a multi-linear idealization had been chosen the elastic limit would have been lower and the redistribution of residual forces due to extended non-linearity would have tended to bring the ultimate load down. On the other hand the difference between

the ultimate points of the two curves on Figure 5.5 would have tended to do the opposite.

Figures 5.7 and 5.8 indicate the forces acting on the perimeter members at the elastic limit of the diaphragm. Computer analysis statistics are not given for this diaphragm since the program has undergone extensive modification at later stages.

5.3 10' x 12' Welded Cellular Metal Deck

This diaphragm was tested by Nilson (53) as part of a series for Fenestra Inc. and is labelled Test no. 57.2. Ammar (26) later analyzed the diaphragm for elastic behavior.

5.3.1 Description of the Test Installation

The test arrangement of the diaphragm is shown on Figure 5.9.

The panel of the diaphragm consisted of six 16 gage flat sheets, each sheet 2' x 10' and stiffened by two hat sections that were spotwelded to the sheet. The sheets were connected to each other at the seams by 1 1/2" long burn-through welds 18" center to center. The outer edges of the first and the sixth sheets were connected to the x-direction perimeter members by 1" diameter puddle welds 24" o.c. The end connections consisted of three 1" diameter puddle welds with a spacing of 12" o.c. per sheet end. The panel was installed flat plate down.

The perimeter members were hot-rolled sections hinged to

each other at their ends. The properties of the perimeter members were as follows:

Both beams in the x-direction

Section: W 12 x 27 , Length: 120"

Area: 7.97 $in.^2$, Mom. of inertia: 16.6 $in.^4$

Left Beam in the y-direction

Section: W 10 x 21 , Length: 144"

Area: 6.19 $in.^2$, Mom. of inertia: 9.7 $in.^4$

Right beam in the y-direction

Section: W 10 x 33 , Length: 144"

Area: 9.71 $in.^2$, Mom. of inertia: 36.5 $in.^4$

The support conditions and the location of the load were as shown on Figure 5.9.

5.3.2 The Finite Element Model

Figures 5.10 through 5.12 show the finite element model of the diaphragm.

Each of the six sheets is modeled into four plate subassemblies with ten isotropic plate elements (5 in the x-direction and 2 in the y-direction) to a subassembly. Each plate element is 6" wide (in the x-direction) and 12" long, with a thickness of 0.06". The material properties are:

$$E_x = E_y = E_o = 29500 \text{ ksi} , \mu_{xy} = \mu_{yx} = \mu_o = 0.3$$

$$G_{eff} = G_o = E_o/2(1+\mu_o) = 11346 \text{ ksi}$$

The two perimeter members spanning parallel to the x-axis are modeled by one subassembly each with five 24" long beam

elements making up each subassembly.

The y-direction perimeter members are modeled by three subassemblies each with four 12" long column elements to a subassembly.

The Young's modulus of elasticity is taken to be 29500 ksi for all perimeter members, the other properties being those given in Section 5.3.1.

The connections were modeled as follows:

End connections: Six connection subassemblies for each side of the diaphragm, each subassembly consisting of the three connections at one end of a sheet. The connections themselves are modeled by two springs in orthogonal directions, with identical properties. The idealization of the spring behavior consists of a multi-linear representation of the connection behavior in shear. Since there were no shear test results available on end connections of 16 gage material with 1" diameter puddle weld, such a curve was derived by extrapolation from the shear test results given in Reference (25) for 1" diameter puddle weld end connection of 14 gage material. This curve is shown on Figure 5.13. The multi-linear representation was arrived at by connecting the points shown on the curve, by straight lines.

Edge connections: One subassembly for each side of the diaphragm, each subassembly consisting of the four connections at an edge. The connections themselves are modeled exactly the same as the end connections.

Seam connections: One subassembly per seam line, each

subassembly being made up of the seven seam connections on that seam line. Each seam connection is modeled as a one-dimensional spring element in the x-direction, the plate elements sharing the same degree of freedom in the y-direction at the nodes that are connected together by this seam connector. Since no shear test results were available for 1 1/2" long welds used in side-lap connections of 16 gage sheets either, a curve was derived by interpolation from test results provided in Reference (25) for 1", 2", and 3" long welds. This curve is shown also on Figure 5.13. Again the points on the curve define the multi-linear idealization.

5.3.3 Analysis and Results

An initial load of 10 kips was applied to the diaphragm for the elastic solution and the factor to the elastic limit was found. After the elastic analysis results and the load were brought to the elastic limit, the load was increased in increments of 5 kips. Six such increments were applied beyond the elastic limit of the diaphragm. During the sixth increment, a negative acceleration factor, against which no protection had yet been built in, was encountered. The resulting acceleration caused elastic unloading of the structure, therefore throwing the rest of the iterations off course. However, a subsequent check of the results showed that the structure would nevertheless collapse in this load increment.

The deflection with respect to load of the representative degree of freedom (d.o.f. 738 of Figure 5.11) is compared with

the test results on Figure 5.14. It is seen that at the end of the fifth load increment beyond the elastic limit, the two results agree almost exactly and that both curves flatten out after this point. In general the two curves show very good agreement all the way.

Since it was found that collapse would have occurred in the sixth increment in any case, a new analysis of this diaphragm with preventive measures against a negative acceleration factor was not warranted. However, the reason behind this phenomenon was investigated and necessary measures were taken (see Section 4.6.2).

The seam slips at the locations where dial gages were used in the test (see Figure 5.9) are compared on Table 5.1. The good agreement between the test results and the computer results leaves little room for discussion. There is only one point that may need consideration. In the actual test, the least seam slip was noted under gage H, however, with the computer analysis, the least seam slip is found under gage G. This is most probably due to the slight differences in the welds of the test specimen.

Figures 5.15 through 5.17 show and compare the forces transferred through connections at a seam line, and to the perimeter members, both at the elastic limit of the diaphragm and at the fifth load increment beyond the elastic limit.

On Figure 5.15, the forces in the connections of the middle seam line are displayed. It is seen that at the elastic limit, a uniform transfer of shear is not present, with the forces near the ends of the seam line only about 50% of the force carried by

the connection at the middle of the seam line. However, at the fifth load increment beyond the elastic limit, the difference drops down to about 10% and a much more uniform transfer of shear is obtained. Therefore, with increased non-linearity in diaphragm behavior, the somewhat parabolic variation of shear transfer at the seams changes into a uniform one, due to the redistribution of internal forces. Each seam line carries an equal magnitude of shear. The sum of the shear forces carried by a seam line and the forces in the end connections at the corners of the relevant sheets, is equal to the reaction in the direction parallel to the seam lines.

Figure 5.16 shows the longitudinal (parallel to member) forces acting on the perimeter members. It is seen that the sum of the longitudinal forces on any member is equal to the reaction parallel to that member as expected. In the case of the y-direction perimeter beams at the elastic limit, the forces opposite the corners of one end of a sheet are seen to be nearly equal, and the force due to the center connection for each sheet end is seen to be somewhat less. This difference is small at the very corners of the diaphragm, but away from the corners, starting from the side nearest the jack, the ratios of the two forces start from 74% and drop to 63% near the roller support for the left beam, and stay at a constant 65% for the right beam. An interesting change is seen in the fifth increment loading as the center connection forces rise above the forces opposite the sheet corners. The forces at the two ends do not show appreciable change from those at the elastic limit. Except

for the forces at the two ends of the member, the longitudinal forces acting on the right beam are seen to be quite uniformly distributed at the fifth load increment beyond the elastic limit. Less uniformity is seen for the left beam, as before. As for the edge beams, the two observations that can be made are that there is some force redistribution in the higher load range, although this is not as pronounced as in the above cases, and that the forces at the two ends of the members do not remain close to those at the elastic limit, but increase with increasing load.

Figure 5.17 gives the lateral forces acting on the perimeter members at the two load levels discussed above. As expected, the resultant magnitude of the lateral forces are comparatively small. The forces on a corner weld from the two adjacent sheets are of opposite signs and of nearly equal magnitude such that they practically cancel out. Only the resultant forces acting on the perimeter beams have been shown in the figure.

Table 5.2 gives iteration and analysis statistics. Since the analysis of this diaphragm was conducted before the mesh generator was written, less computer core and compilation time was required at that time. However, it is expected that due to some other changes made, the execution time should be less for the same number of load increments and iterations, with the present shape of the program.

5.4 10' x 12' Standard Corrugated Diaphragm

This diaphragm was tested by Luttrell (6) in his series of

light frame tests on 26 gage standard corrugated diaphragms. The test was designated no. 5P. Ammar (26) later conducted a first order analysis of the diaphragm.

5.4.1 Description of the Test Installation

A sketch of the test installation is shown on Figure 5.18.

The panel of the diaphragm consisted of five 26 gage corrugated sheets of the same type that the 24" x 28" diaphragm panel described earlier was cut from. Each sheet was 2' wide, and was 12' long along the length of the corrugations. The measured ungalvanized thickness of the sheet material was 0.01875".

The sheets were connected to each other along the seams by no. 10 sheet metal screws, 36" o.c., the two outside screws being 18" away from the sheet ends.

Three symmetrically placed intermediate purlins crossed the sheets perpendicular to the longer direction of the sheets. The purlins consisted of 16 gage 6" x 1 1/2" cold-formed channels. The spacing between the purlins was 36". Connections of the purlins to the sheets were made by no. 14 self tapping screws with aluminum backed neoprene washers, at every third corrugation. At the seams, these screws passed through both sheets common to the seam. The ends of the three purlins were connected to the x-direction perimeter members by light clip angles which provided very little resistance against rotation.

All perimeter members were 14 gage 6" x 1 1/2" channels. The two x-direction channels were 144" long and the y-direction

ones were 120" long. All four were hinged to each other at their ends.

The sheet ends were connected to the y-direction beams by no. 14 self tapping screws of the same type as used in the sheet to intermediate purlin connections. The connection was done at every third corrugation. At the ends of the seam lines, the screws passed through both sheets common to the seam. The outside edges of the first and the fifth sheets were connected to the x-direction perimeter members again by no. 14 screws, this time 18" o.c.

The support conditions and the location of the load were as shown on Figure 5.18.

5.4.2 The Finite Element Model

Several analyses were conducted on the 10' x 12' standard corrugated diaphragm, both linear and non-linear, with varying finite element models and effective shear moduli. The simplest of these models is shown on Figure 5.19.

5.4.2.1 Model of Figure 5.19

This model was adopted to analyze the diaphragm based on the use of an average effective shear modulus along the whole length of the diaphragm, and is labelled Model A for future reference.

Each sheet is modeled into two subassemblies, 4 orthotropic plate elements in the x-direction and 3 in the y-direction (therefore, a total of 12 plate elements) per plate subassembly.

The dimensions of the plate elements are 18" in the x-direction and 8" in the y-direction.

The moduli of elasticity and the associated Poisson's ratios were found by the methods explained in Section 3.2.1.2. These are:

E_x: 32100 ksi $\qquad$ E_y = 6.955 ksi

μ_{xy}: 0.3 $\qquad$ μ_{yx}: 0.000065

Three different values of the effective shear modulus were used with Model A, for reasons explained in Section 5.4.3. These involved variations on the possible effects of the connections and their geometry on the behavior of the diaphragm. The three values used were:

$G_{eff} = G_o \frac{p}{p'}$, Ω_1 = 7343 ksi, with Ω_1 found from Reference (36) for quasi-sinusoidal corrugations with point attachments in the valleys.

$G_{eff} = G_o \frac{p}{p'}$, Ω_2 = 10000 ksi, with Ω_2 found again from Reference (36) for quasi-sinusoidal corrugations with point attachments at mid-height of corrugations, and

$G_{eff} = G_o \frac{p}{p'}$, = 10450 ksi

(See Section 3.2.1.2 for definitions of the variables).

The connections are modeled as follows:

End connections: The end connections are modeled into five subassemblies of four connections each, on each side of the diaphragm. The connections themselves are again modeled by two spring finite elements in orthogonal directions, but with

identical material properties. The spring behavior is a multi-linear idealization of the connection shear test results provided by Ammar (25) for edge connections of 26 gage material by no. 14 self tapping screws. The shear test curve and the points chosen for multi-linear idealization are shown on Figure 5.20.

Edge connections: The connections on each edge are modeled into one subassembly, therefore with 7 connections to a subassembly. The connections themselves are modeled exactly the same as the end connections.

Sheet to sheet seam connections: The four sheet to sheet seam connections in each seam line are modeled as one subassembly. A one-dimensional spring in the x-direction is used to model the individual connections. The y-direction degree of freedom at each of these connections is shared by the plate elements being connected. The shear test results provided by Ammar (25) for sidelap connections of 26 gage material by no. 10 sheet metal screws, and its idealization are shown on Figure 5.21.

Sheet to intermediate purlin connections: These are modeled in almost exactly the same way as the end connections. The only difference is that, since in this diaphragm there are no sheet to purlin connections at the ends of the intermediate purlins, the two outermost connection subassemblies of each purlin have only three connections each.

It should be noted that where a sheet to frame (perimeter member or intermediate purlin) connection has been provided at a seam line or at its ends, this connection is modeled by two

connections - one sheet to frame and the other sheet to frame - in accordance with Section 3.3.3.

The y-direction perimeter members and the intermediate purlins are each modeled into five subassemblies with three column elements to the subassembly. The properties of these column elements are as follows:

	Area ($in.^2$)	Mom. of inertia ($in.^4$)	Length (in.)	E (ksi)
y-direction perimeter members	0.655	0.117	8.	29500.
intermediate purlins	0.526	0.0951	8.	29500.

Each x-direction perimeter beam is modeled as one subassembly with 8 beam elements. For each beam element: Area = 0.655 $in.^2$, Mom. of inertia = 0.117 $in.^4$, Length = 18 in.

5.4.2.2 More Refined Models

Since the effects of the connections at sheet ends decay some distance away from the ends, it was decided to devise models that would reflect this beahvior to some extent. As was discussed in Section 3.2.1.2, this can be done by assigning a smaller shear modulus near the ends and using $G_{eff} = G_o \frac{p}{p'}$, for the middle region of each sheet. Two such models were developed and investigated. They are labelled Model B and Model C for future reference.

Model B: This model was based on the assumption that the

effect of the end attachments in reduction of the shear modulus will become negligible after a distance equal to the spacing of the attachments. The model is shown on Figure 5.22.

Each sheet is modeled by six plate subassemblies. The one subassembly at each end of a sheet is composed of six orthotropic plate elements (two in the x-direction and three in the y-direction). The dimensions of each of these plate elements is 4" (x-dir.) by 8" (y-dir.), the thickness and other properties except the shear modulus being the same as those for Model A. The shear modulus of 841 ksi is found by substituting (p) for (a) in Equation 3.21 of Section 3.2.1.5. The second and fifth subassemblies of each sheet are composed of three plate elements in the y-direction. The dimensions of these plate elements are 10" (x-dir.) by 8" (y-dir.). Thickness and other properties are again the same as those for Model A, except for the shear modulus which is $G = G_o \frac{p}{p'} = 10450$ ksi. The middle two subassemblies in each sheet are modeled by nine orthotropic plate elements (three in the x-dir. and three in the y-dir.) each. The plate dimensions are 18" (x-dir.) by 8" (y-dir.). Other properties are exactly the same as the second and fifth subassemblies of the sheet.

The rest of the diaphragm for Model B is modeled the same way as for Model A.

Model C: This second model with the smaller shear modulus near the ends was based on the assumption that the end effects would become negligible after a distance equal to the pitch of the corrugations. This model is similar to Model B, except for

three differences:

__The plate elements of the first and sixth subassemblies of each sheet are 1.33" (x-dir.) by 8".

__The shear modulus for the plate elements of the above two subassemblies is again 841 ksi, but now this value is used only in a region of length 2.67" at each end.

__The plate elements of the second and fifth subassemblies of each sheet are 15.33" in the x-direction instead of 10".

5.4.3 Analyses and Results

The analyses centered around two main objectives:

__To learn more about the effective shear modulus for corrugated sections.

__To find the most suitable model for satisfactory and efficient analysis of a corrugated diaphragm.

Both linear (only up to the elastic limit of the diaphragm) and non-linear (up to and beyond the elastic limit) analyses were conducted to reach the above two objectives.

5.4.3.1 Linear Analyses on the 10' x 12' Standard Corrugated Diaphragm

Linear analyses were conducted for the following cases:

1. Model A with G_{eff}: 7343 ksi
2. Model A with G_{eff}: 10000 ksi
3. Model A with G_{eff}: 10450 ksi
4. Model B
5. Model C

The elastic limit load, the deflection of the representative degree of freedom at this load and the elastic slope for the above five cases are given on Table 5.3 along with the test results.

The linear analyses were first done for the first, fourth and the fifth cases. It was found (as can be seen from Table 5.3) that case 4 (Model B) gave results that are markedly more flexible than the other two when compared against the test results. Therefore it was assumed that the end effects do not stretch as far into the diaphragm as the spacing of the connectors (when this spacing is greater than the corrugation pitch). This case was discarded from further analysis. Cases 1 and 5 gave almost identical results, both close to those of the test elastic curve, with case 1 being somewhat stiffer and closer to the test results than case 5.

Cases 2 and 3 were analyzed after it was found (as discussed in the next Section 5.4.3.2) that in the non-linear range, the models of cases 1 and 5 show increasing divergence from the test results as the load is increased, the test results indicating a stronger diaphragm. This phenomenon necessitated a review of the details of the connections.

Since the valleys of a sinusoidally corrugated diaphragm are of practically zero width, the clamping effect of the screw will tend to distort and flatten the corrugation near the valleys, the magnitude of this effect depending on the washer size among other factors. Photographs of small diaphragm tests in Reference (6) do indeed show such a distortion of corrugation

geometry. No details of the screws are available in References (6) and (25), however a consultation with the laboratory technician, who was present during both Luttrell's diaphragm tests and the shear tests done by Ammar, revealed that the screws in the two cases came from different manufacturers. Also a number 14 screw, for example, may come in with a wide range of washer sizes, an intermediate washer diameter being 5/8". The relative sizes of such a screw and the corrugation are shown in Figure 5.23a. It is obvious that the effect of such a connection will be more pronounced than a point attachment (such as spotwelding), in the case when the width of the corrugation valley is small. Furthermore, when the attachment is made to a rigid flange - for which there are no results in Reference (36) - there will be more increase in the strength of the connection. It can be seen from Figure 5.23a, that during loading, the inclines of the corrugation will bear on the sides of the washer. This may be compared to the case of point attachments at mid-height (Figure 5.23b) for which results are available in Reference (36). An effective shear modulus of 10000 ksi was found with this assumption. This and the theoretical upper limit for the effective shear modulus ($G_{eff} = G_o \frac{p}{p'}$ = 10450 ksi) were used in two more elastic analyses of Model A. As expected, the two results were very close to each other and the use of G_{eff} = 10450 ksi almost duplicated the elastic slope of the test curve. Therefore, it was decided to conduct another non-linear analysis, with case 3, since it was seen that the refined mesh of Model C did not give appreciably different results (maximum difference on the order of 3%), but resulted in

noticeably higher solution times due to a higher number of sub-assemblies and degrees of freedom.

5.4.3.2 Non-linear Analyses on the 10' x 12' Standard Corrugated Diaphragm

The first two non-linear analyses consisted of the application of one load increment beyond the elastic limit, for the cases 1 and 5 of Section 5.4.3.1. An initial load of 1 kip was applied to the diaphragm, and after the elastic limit was found, an increment of 2 kips was added. The results are shown on Figure 5.24. It is seen that there is increased divergence from the test results in the non-linear range even though this divergence is not to pronounced at this initial stage. Therefore, case 1 was chosen for further loading, since case 5 gave results very close to case 1, but required substantially more solution time.

This time four load increments of 1 kip each were applied to the diaphragm and it was seen that with each load increment, the percent divergence from the test results increased. The results are compared with the test results on Figure 5.25.

After the results of the elastic analysis for case 3 were found to be promising, it was decided to run a full non-linear analysis for this case with the maximum allowable number of iterations per load increment increased from 20 to 25. The results showed that even though this case is stiffer than case 1, the divergence from the test results is reduced by only a small amount. These results are also shown on Figure 5.25.

Only four load increments beyond the elastic limit could be applied because no convergence could be reached in 25 iterations in the fifth load increment. It is difficult to decide from the output whether collapse was reached in this increment, however, the magnitude of residual forces indicate that the load at the fifth increment is very close to the collapse load. This can also be seen from the trend of the curve on Figure 5.25.

The disagreement of the test and computer results in the non-linear range, even for case 3, can point to only one conclusion; that the connections in the test assembly behaved stronger and stiffer than found by the shear tests of Reference (25). Several possible reasons as to why may immediately be listed:

1. The screws in the two tests were obtained from different manufacturers and therefore showed some difference in geometry.

2. The washer diameters were different.

3. The shear tests were conducted on flat sheets where the bearing of the sheets were on the shaft of the screw, as compared to the full scale test where there would be substantial bearing on the sides of the washers by the inclines of the corrugations.

4. Since the clamping effect of the washers will increase the elastic stiffness of the diaphragm by its indirect effect on the effective shear modulus, it is natural to assume that the strength of the connection and its non-linear behavior will also be affected.

5. References (18, 25) indicate that there is a spread of 15% to 70% on results of connection shear tests.

The magnitude of the stiffening of connections due to the clamping effect can be estimated from the computer results by computing the rate of increase of divergence from the test results. From Figure 5.25, this rate can be seen to be around 20% on the average, between each load increment. Therefore it may be said that if the connection curves of Figures 5.20 and 5.21 were modified such that the resulting curves were for 20% stronger and stiffer connections, much better agreement with the test results could have been obtained, for this diaphragm. However, this was not done since the justification behind it is rather empirical and depends only on the results for one corrugated diaphragm. In addition the value of the percent difference in behavior may not be the same for both sheet to sheet connections and sheet to frame connections.

The seam slip values at midpoints of each seam line are given on Table 5.4, for case 3, starting with the seam line closest to the x-axis. Since test results on seam slip are not available, no comparison can be made. The seam slip computed at the ends of the seam lines is about 15-25% less than the values shown on Table 5.4.

Unfortunately, due to an error made in one of the changes in the program, the output for the connection forces was not printed from the correct place in the program (except at the elastic limit) when convergence was reached. Therefore only the forces in the sheet to sheet seam connections are compared

at two different load levels on Figure 5.26. It is possible to obtain the forces in these connections from the output for deflections since these are one dimensional, but with the perimeter connections and sheet to intermediate purlin connections it is quite difficult to find the forces in the two separate directions from the output for deflections in the non-linear range of the connection, due to the yield condition that is defined in Chapter 4. The connection forces shown on Figure 5.26 follow the same trend as seen for the 10' x 12' welded diaphragm. At the end of the 4th load increment, the sheet to sheet seam connections are seen to be very close to their ultimate load. However, a coarse survey of the other connection forces showed that these connections still have some reserve strength at this stage.

Iteration and other computer analysis statistics for this diaphragm are given on Table 5.5.

5.5 10' x 12' Trapezoidally Corrugated Diaphragm (Box Rib)

This diaphragm was tested by Luttrell (6) in his heavy frame series and is labelled Test no. 10. It has not been subject to finite element analysis previous to this report. This diaphragm was chosen for analysis here, in order to compare the cases of corrugations with narrow valleys (as in the case of the standard corrugated diaphragm of Section 5.4) and corrugations with wide valleys, in terms of the magnitude of the end effects due to the end connections. Another subject of comparison is that of modeling with an effective shear modulus along

the whole length of the corrugations versus modeling with different shear moduli at the end regions and the middle region, when some seam connections are within a reasonable range (namely the length of a corrugation pitch) of the ends.

5.5.1 Description of the Test Installation

A sketch of the test installation is shown on Figure 5.27.

The panel of the diaphragm was made up of six 26 gage trapezoidally corrugated sheets, each 2' x 10'. The perimeter members were W 10 x 21 sections, hinged to each other at the ends. Only one intermediate purlin - C 4 x 7.25 - was used. This purlin ran perpendicular to the seam lines and was attached to the x-direction perimeter members by light clip angles.

The other connections were made as follows:

End connections: These were made by no. 14 screws at corrugations valleys with a spacing of one corrugation pitch for each sheet, three screws being used at each sheet end. Contrary to prior cases, no attachment was provided at sheet corners (this necessitated the use of the longer type of input for the computer analysis), but the outside screws of each sheet end were half a corrugation pitch away from the sheet corners.

Edge connections: Again no. 14 screws were used for these connections. Three were provided at each of the two edges, with the unsymmetrical spacing shown on Figure 5.27.

Sheet to sheet seam connections: These connections were made by no. 10 screws spaced in the same manner as the edge connections except that at the extreme right end of each seam line

a fourth connector was provided. This last connection cannot be considered an end connection, since due to the geometry (refer to cross-section of corrugation on Figure 5.27) the screw passed only through the two sheets at that point, but not through the perimeter member.

Sheet to intermediate purlin connections: These were what are termed "special connections" in Luttrell's report (6). They were used to prevent shear transfer into the purlins, thereby to eliminate purlin restraints, but to preserve the restraint against out-of-plane buckling of the panel. Figure 5.28 shows this type of a connection. A bolt is passed through an oversized hole in the sheet and not allowed to touch the sheet. To back up the bolts, greased cover plates were used. The spacing of these connections were the same as that for the end connections. On Figure 5.27 these are labelled as "non-load resisting connection" in keeping with the terminology of Reference (6). Whether this is strictly true in reality is discussed in Section 5.5.3 along with the results of analyses.

The supports and the location of the loading are also shown on Figure 5.27.

5.5.2 The Finite Element Models

Two different finite element models were prepared following similar logic as for the models A and C of Section 5.4.2. The two models are shown on Figures 5.29 and 5.30 (partially shown), and are labelled Model AT and Model BT respectively, the T standing for trapezoidal corrugation.

The simpler model AT is based on the usage of one effective shear modulus throughout the entire length of the corrugations. Each sheet is modeled into three continuous and two split subassemblies. The letters "a" and "b" following the subassembly numbers on Figure 5.29 indicate the two parts of a split subassembly. These split subassemblies were used to save on auxiliary storage device use, and it is believed that their use as on Figure 5.29 does not cause any significant increase in computation time with the Frontal technique. (It should be kept in mind that a subassemblage of finite elements depends on the geometric and material characteristics of the elements as per definition of a subassembly in Section 3.3). Each sheet is modeled in exactly the same way, therefore, even though the below description of the modeling will be made for only the lowest sheet on Figure 5.29 for ease of explanation, it holds true for all.

Every plate element on this sheet is modeled with the same material properties and thickness, which are:

E_x = 37022 ksi , E_y = 2 ksi , G_{eff} = 1153 ksi

μ_{xy} = 0.3 , μ_{yx} = 0.0000162 , t = 0.0179 in.

where G_{eff} has been found from Reference (35) for trapezoidal corrugation attached to a rigid flange at midpoints of the valleys, and E_x and E_y have been found by the methods of Section 3.2.1.2.

Subassembly 6 is composed of two orthotropic plate elements, one on each side of the sheet, with the dimensions 12" in the x-direction and 4" in the y-direction. In the below descriptions

of the plate elements of the other subassemblies, the first dimension given will always be in the x-direction.

Subassembly 7 is a continuous subassembly with two orthotropic plate elements, each 12" x 8".

Subassembly 8 consists of six orthotropic plate elements, three on each side of the sheet, each plate element 36" x 4".

There are also six plate elements in subassembly 9, and each is 36" x 8".

The two x-direction perimeter members are modeled as one beam subassembly, each with ten 12" beam elements to a subassembly.

Each of the two y-direction perimeter members is composed of three continuous subassemblies plus one part of each of two subassemblies that are split between the left and right y-directions members. The split subassemblies each have two 4" column elements, one on either side. The first continuous subassembly on either side (nos. 4 and 11) is made up of five 8" column elements, and the next two subassemblies, of six 8" column elements.

Since the sheet to intermediate purlin connections were assumed not to resist any load, these are left out from the model, and the purlin is modeled only by two 72" column elements, with its only connections being those made with light clip angles to the x-direction marginal beams at the ends of the purlin.

The other connections are modeled as follows:

End connections: These are idealized as three subassemblies to each side with six connections (therefore 12 spring elements)

to every subassembly.

Edge connections: The three edge connections (6 spring elements) on either side make up one subassembly.

Both the end and edge connections are modeled exactly the same way as the connections of the 10' x 12' standard corrugated diaphragm (Section 5.4) and their behavior is defined by the shear test curve of Figure 5.20.

Sheet to sheet seam connections: The four connections at a seam line constitute a subassembly. These seam connections are modeled the same as the seam connections of the 10' x 12' standard corrugated diaphragm and present the same behavior (Figure 5.21).

Model BT differs from Model AT in that the sheets are modeled such that two different shear moduli can be used for the end and middle regions. Figure 5.30 shows one sheet for which the necessary changes have been made. For ease of discussion, the subassemblies on this sheet have been numbered internally from 1 to 10. This numbering also shows the sequence that was used for each sheet for the solution.

Material properties (except for the shear modulus) and the thickness for the plate elements are the same as those for Model AT.

For subassemblies 1, 2, 9 and 10 of Figure 5.30,

G_{eff} = 172.7 ksi

as found by Equation 3.21 of Section 3.2.1.2.5. For the other subassemblies:

$$G_{eff} = G_o \frac{p}{p'} = 9040.8 \text{ ksi}$$

The number of plate elements in each of the subassemblies and the dimensions of the plate elements are as follows:

Subassembly	No. of plate elements	Dimensions (in.) (x-dir. x y-dir.)
1 and 9	2	8 x 4
2 and 10	2	8 x 8
3	2	4 x 4
4	2	4 x 8
5	4	36 x 4
6	4	36 x 8
7	2	28 x 4
8	2	28 x 8

A point of interest is the ease of numbering the new degrees of freedom due to the refined mesh. The degrees of freedom on the sheet of Figure 5.30 have been numbered assuming that this is the sheet closet to the x-axis. It is seen that the old numbers do not change at all, and the new d.o.f. are numbered starting from the last number of Figure 5.29. With the Frontal technique, this numbering is totally irrelevant to solution speed. If the mesh generator could have been used for this diaphragm, it would have generated a whole new set of numbers for the d.o.f., but this also would not have placed any additional burden on the user.

5.5.3 Analyses and Results

5.5.3.1 Linear Analyses

These consisted of one analysis up to the elastic limit for each of the two models AT and BT, in order to compare the relative merits of these two. The following results were obtained:

	Test	Model AT	Model BT
Elastic slope (k/in.)	13.9	14.13	14.0
Elastic limit (kip)	0.336	0.3434	0.3394

It is seen that in terms of the above parameters, the two models give results within 1% of each other and very close to those of the test. The difference between the two models is more pronounced when the force distribution through the connections is considered. There is a maximum difference of about 20% between the two cases in terms of resultant connection forces. Figure 5.31 compares the force distributions at significant locations for the Models AT and BT.

Thus, although the overall stiffness of the diaphragm is almost the same for the two cases in the elastic range, the order and the loads at which the various connections will enter non-linear behavior will be different at loads beyond the elastic limit. It can be expected with a reasonable justification that Model BT will become more than 1% more flexible than Model AT as the load on the diaphragm is increased, the difference between the two models perhaps increasing up to 5-15%. Even though this is the case, Model AT was chosen for a complete non-linear analysis of this diaphragm since the difference in

the results for the two models does not warrant the use of Model BT which would require substantially more solution time.

It will be recalled that in the case of the 10' x 12' standard corrugated diaphragm, the maximum difference between the two models was only 3%. The reason why this difference is more like 20% for the trapezoidally corrugated diaphragm, can be seen from a visual comparison of the two diaphragms. The pitch of the trapezoidal corrugations (8") is about three times greater than that of the quasi-sinusoidal corrugation (2.67"). Since the refined model has the lower shear modulus in end regions of length equal to one corrugation pitch, the increased effect of modeling the trapezoidally corrugated diaphragm as such is obvious. Furthermore, the two outer connections at each seam line of the trapezoidally corrugated diaphragm fall close to the range of this end effect.

5.5.3.2 Non-Linear Analysis

The non-linear analysis consisted of the application of five load increments of 0.5 kip each on Model AT, beyond the elastic limit.*

Collapse of the diaphragm in the fifth load increment was noted due to non-convergence in the very generous limit of 75 iterations. A check of the residual force norms at each

*This diaphragm was actually analyzed twice. The first analysis did not include the last two points on Figure 5.32. Some small changes were made in the program before the second analysis. Due to a slight error made at this stage, the second analysis results do not actually match those of the first, although the difference is negligible. Thus some caution may be exercised regarding the deflections in the last two load increments. More precise results for these increments would be slightly in the direction of increased flexibility, but the difference would probably not be obvious on the scale of Figure 5.32.

iteration showed that the residual forces showed no tendency to fall below a certain magnitude, confirming the conclusion that collapse had occurred.

The deflection of degree of freedom 312 of Figure 5.29 is plotted against the test results on Figure 5.32. The last point on the plot is that obtained at the end of 76 iterations in the 5th load increment beyond elastic limit, and represents only a lower bound for deflections and an upper bound for diaphragm strength. Therefore, the broken line is used to connect this point and the previous one.

Figure 5.32 presents three main points of interest which are discussed below.

First, it is seen that much better agreement with the test results is obtained than in the case of the standard corrugated diaphragm of Section 5.4. Evidently, when the corrugation valley is wide, the effect of different size screws, washers and so forth is quite negligible, since the clamped width of the sheet will be small compared to the valley width.

The second point of interest is that in the first half of the non-linear range, the computer results show a stiffer diaphragm than that of the test. It will be recalled that in the comparison of Models AT and BT in the elastic range, it was found that although there is only 1% difference in the elastic slopes obtained for the two models, the connection forces differed by up to 20%. This latter difference is the deciding factor in differentiating between the behaviors of the two models in the non-linear range. Although equilibrium is always

satisfied in the two directions for both models, the connection force resultants will decide the order and the loads at which the connections of the two models will enter non-linear behavior. Furthermore, the residual forces that may arise earlier in one model than the other will contribute to yielding of other connections again earlier in that model. As a result, the difference in the behaviors of the two models will grow as the load is increased beyond the elastic limit. The first order analyses of Section 5.4.3.1 show that Model AT is the stiffer model. Therefore it is reasonable to assume that if Model BT were used in the non-linear analysis, better agreement with the test results would be obtained in this region of the curve under consideration.

The last portion of the curve of computer results on Figure 5.32 indicates that at high loads the finite element model is more flexible than the test specimen. The reason for this can be better understood with the aid of some data on deflection and referral to Figure 5.28 ("non-load resisting connection"). From Figure 5.28 it is seen that at these connections, the maximum theoretical tolerance between the sheet and the bolt is:

$$1/2\ (\frac{3}{4} - \frac{3}{16}) = 0.28125 \text{ in.}$$

Therefore, after a deflection of about this much, the bolt and the sheet would come in contact and shear forces would be transferred through the purlin also, thus increasing the overall

stiffness of the diaphragm at this stage. A check of the computed deflections at the 4th load increment beyond the elastic limit was done for degrees of freedom 16, 26, 36, 62, 72, 82, 108, 118, etc. (refer to Figure 5.29) which are reasonably close (8") to the sheet to intermediate purlin connections. The average deflection at these points was found to be 0.23 in. with a maximum value of 0.236 in., both of which practically take up all the tolerance even with this stiffer Model AT. Considering that the test installation would not be expected to be accurate up to 0.05" in the exact distance between the bolts and the rims of the holes, it is perfectly reasonable to assume that by this point the plates would be bearing on the bolts of these connections. Thus, since the computer program cannot account for this increase in stiffness, the computer results indicate a more flexible behavior in this region than the actual case.

The forces on the marginal members and in the seam connections at the elastic limit of the diaphragm are compared with those at the 4th load increment beyond this limit on Figures 5.33 through 5.35. In general the behavior is similar to that of the 10' x 12' welded diaphragm. However, there are some aspects worth consideration.

Since there are no connections at sheet corners, but rather 4" away from these, the longitudinal forces transferred to and from the y-direction perimeter members by the two outer connections at each sheet end always remain less than those transferred by the interior connection. This creates a relative stability

in the ratio of the forces transferred by these connections as the load is increased, excepting loads very close to the collapse load. Another point of interest is that the longitudinal forces transferred to a perimeter member from the connections along its length do not add up to the reaction in that direction unless the lateral forces acting on the perimeter members orthogonal to the member in question are included in the sum. This is again attributed to the lack of attachments at sheet corners. A third aspect is that since the total stiffness and - for high loads - the ultimate capacity of the edge or seam connections in one line is rather small, a high concentration of lateral forces (x-direction) is seen at sheet ends. Addition of active purlin restraints would tend to redistribute these concentrated forces as well as increase the stiffness and strength of the diaphragm.

The seam slip values at midpoints of each seam (found by interpolation) are given on Table 5.6. There are no test results available for these, so no comparison can be made.

Lastly, Table 5.7 provides the computer analysis statistics for the diaphragm.

5.6 Further Discussion

It has been seen that as long as a diaphragm is properly modeled, within the framework of the given capabilities, a non-linear finite element analysis will provide very satisfactory results. In cases where doubts may be raised about the accuracy of a given model, it is easy to determine whether the solution will be a lower or an upper bound through simple consideration of how the diaphragm is supposed to act as opposed to the finite

element model. Furthermore, it may be quite possible to determine the margin of error in such cases within reasonable limits.

The limit of linear behavior for most diaphragms will depend on the characteristics of the sheet to sheet connections, since, in general, these are the weakest components of a diaphragm assembly. All three full sized diaphragms analyzed in connection with this report entered the non-linear range of behavior due to a sheet to sheet connection reaching its limit of linear behavior. Since the sheet to frame connections are in most cases stronger than the sheet to sheet connections, they generally exhibit linear behavior until all the sheet to sheet connections are either well in the non-linear behavior range or have reached ultimate capacity.

In previous investigations of diaphragms by the finite element method (22, 26) only linear behavior has been considered. Ammar (26) has compared the results obtained this way with the test results at 40% of the diaphragm ultimate strength. However, it is seen that at 40% of its ultimate strength, a diaphragm may well be past the limit of its linear behavior. Therefore, estimation of diaphragm behavior purely by a first order analysis may not always be satisfactory. Furthermore, to match test results at 40% of ultimate strength would require that the finite element model of the diaphragm have a lower initial stiffness than would actually be the case. Although some empirical data does exist on the possible relative magnitude of such a reduction in stiffness, it is believed that an analysis that follows the diaphragm behavior step by step is much more accurate and more instructional.

In practice it is helpful to have an idea about the elastic

limit and the ultimate capacity of a diaphragm before attempting a full scale non-linear analysis. The first of these can easily be found by employing the documented program to run a first degree analysis up to the point of first yield. Then the number and the size of the load increments between this point and the expected ultimate strength can be determined. It is perfectly safe to ask for a higher number of load increments than deemed sufficient, since the collapse condition is determined through either the attainment of ultimate capacity in all perimeter connections or non-convergence in a specified number of iterations. The first condition may be hard to establish in many cases since it may require an unreasonable number of iterations to pinpoint the failure of the last perimeter connection, especially when the applied load is rather close to the ultimate load - as opposed to being appreciably higher so that application of the last increment leading to this load will bring about the instant failure of all remaining connections. Therefore, in many practical cases, the number of specified iterations may be the deciding factor. Experience with the analyzed diaphragms shows that specifying a maximum of 40 to 45 iterations per load increment should prove satisfactory in recognizing collapse, although it is very hard to set a rigid limit since many factors are involved. Regarding the recognition of collapse through failure of perimeter connections, it should be pointed out that in the analyses described in this chapter, all connections were assumed to show perfectly plastic behavior after reaching ultimate strength. It is plausible that if the breaking points of the

connections are known (which can be accounted for by the computer program) recognition of collapse by this method will take place before the specified number of iterations are performed.

CHAPTER 6

SUMMARY, CONCLUSIONS AND RECOMMENDATIONS FOR FURTHER RESEARCH

6.1 Summary

The research that has been reported herein is a continuation of earlier work done by Miller (24), Ammar, and Nilson (25, 26) who applied the finite element method to predict diaphragm behavior through first order analysis. It was desirable to extend the finite element analyses into the non-linear range in order to predict such behavior more completely and accurately, to permit a more accurate appraisal of failure load, and to study the internal force redistribution that takes place before failure.

Such analysis has been made possible by the computer program that was developed as a part of this research. The program makes use of the residual force method. Since it is known that the connections are the main source of non-linearity, a specialized routine to deal only with connection non-linearity has been included. The connections, which are modeled by spring elements, have been classified for modeling according to their locations, and several improved models, varying in degree of outward complexity, but easy to use, have been developed. The spring behavior is defined by multi-linear approximations of connection shear test results.

In the case of corrugated sheeting, which is represented by orthotropic flat plates, previous investigators had experienced difficulties determining the correct effective shear modulus for

the sheeting. Recent research on the stiffness of corrugated sheeting with discrete end attachments has clarified this issue, and improved representations have been included in the present work. Two different models are proposed for this representation. One model involves the use of an average effective shear modulus throughout the entire length of the corrugations, while the other model makes use of different shear moduli in the end and central regions.

Four diaphragms, for which test results are available, have been analyzed. These are:

1. a welded cellular metal deck diaphragm
2. a small size standard corrugated diaphragm
3. a full size standard corrugated diaphragm
4. a trapezoidally corrugated diaphragm.

It has been found that the proposed analysis is feasible, inexpensive and accurate. Extremely satisfactory correlation with the test results have been obtained for all cases above except for case 3. The results for this case agree well with the test results in the linear range of the diaphragm, but, due to reasons detailed in Section 5.4.3.2, do not agree so well in the non-linear range. However, the results show marked improvement over those reported in Reference (26) for first order analysis.

It has been found possible to analyze the diaphragms for much less cost than for full scale testing. Added advantages of computer analysis are the great savings in time compared with testing, and the much more complete information on internal forces. In order to reduce the task of preparing input

data, a mesh generator routine that requires only a minimum of information has been written.

6.2 Conclusions

The following conclusions have been reached as a result of this research:

1. Connection tests are essential to provide necessary input data for the computer analysis.

2. Both cellular metal decks and trapezoidally corrugated diaphragms can be modeled to yield accurate predictions of behavior and strength in a non-linear analysis.

3. Within the limits of this study, it appears that the accuracy of the analysis for corrugated diaphragms can be increased by using different shear moduli in the end and central regions (see Section 3.2.1.2.5) for cases where the corrugation pitch is large, and if some seam connections are within range of the end effects. Otherwise, the added expense which accompanies such refinement is not warranted.

4. For the standard corrugated diaphragm, the clamping and the distortion of the sheeting due to the tightening of the screws in the narrow corrugation valleys (see Section 5.4.3.2) is thought to be the main cause of the less satisfactory results obtained. However, the numerical results were a lower bound for strength and stiffness, and therefore were conservative.

5. The assumption that the connections are the only source of non-linearity has proved to be satisfactory for the diaphragms

analyzed. For most civil engineering diaphragms it does not seem necessary or practical to search for material or geometric non-linearity elsewhere.

6. From the numerical evidence, in practical diaphragms, collapse of the diaphragm is initiated when all perimeter connections reach their ultimate strength. However, this will not happen before the seam connections either have reached their ultimate strength or are very close to it.

7. The initiation of non-linear behavior was seen to take place when the first seam connection reaches the limit of its linear range in typical cases. In all the cases analyzed, the seam connections near the middle of a seam line were the highest stressed seam connections in the linear range, and therefore reached their elastic limits before other connections.

8. As seen from the results for the standard corrugated diaphragm (Section 5.4.3.2), diaphragm response in the non-linear range is not drastically affected by changes in the effective shear modulus, but is highly dependent on connection behavior. As only one cellular metal deck has been analyzed in this research, there is not enough evidence to show whether this holds true also for cellular diaphragms, although it probably does.

9. The effective shear modulus of corrugated sheeting with discrete end attachments has been formulated by other investigators, and has been satisfactorily used as data in this research. Where closed form solutions do not exist yet for some practical corrugation geometry or manner of attachment, educated guesses can be made in view of other results without much loss

of accuracy (see 8 above).

10. Using identical spring stiffness in the two orthogonal directions, where the connections are modeled by two orthogonal interacting springs, is seen to be adequate and practical. However, further studies may perhaps reveal that an orthotropic connection model is also feasible. Modeling the sheet to sheet seam connections by a single spring element in the direction of the seam and by a rigid link in the other direction is believed to be totally satisfactory.

6.3 Recommendations for Further Research

Although the proposed method of analysis is powerful, it requires correct data to be effective. Therefore:

1. Connection tests should be performed before analyzing a diaphragm if results of such tests are not already available. The results should include the point at which rupture of the connection occurs.

2. The possibility, though remote, of modeling the connections (those other than sheet to sheet seam connections) by two interacting springs with different spring stiffnesses (i.e. orthotropic connection) for non-linear analysis may be worthy of investigation. Such investigation will have to determine the correct interaction between the two directions.

3. Analytical results on the effective shear modulus for corrugated sheeting are available for many practical corrugation geometries and manners of attachment. However, studies on quasi-sinusoidal corrugation with narrow corrugation pitch and

comparatively wide attachment are needed.

Other recommendations are as follows:

4. As only a limited number of diaphragms have been analyzed by the computer program, it is suggested that further analyses be made for diaphragms for which test results are available.

5. The changes required in the program for the treatment of cyclic loading are not extensive. This feature could be added with relative ease.

6. Incorporation of a stability analysis into the existing program was originally planned, but, during the development of the program, time limits and the impracticality of too large a program prevented this, and the idea was abandoned. For practical reasons, a separate program is thought to be more logical if a numerical stability analysis is desired. It is not completely clear whether such a program is warranted at the present time.

REFERENCES

1. Nilson, A.H., "Shear Diaphragms of Light Gage Steel", Journal of the Structural Division, ASCE, Vol. 86, No. ST11, Proc. Paper 2650, Nov., 1960, pp. 111-140.

2. Barnes, S.B., "Report on Test Program of 4 1/2" D Fenestra Decking Acting as a Diaphragm", 1950, as reported in Ref. 1.

3. Nilson, A.H., Deflection of Light Gage Steel Floor Systems Under The Action of Horizontal Loads, M.S. Thesis, Cornell University, Ithaca, New York, 1956.

4. _____, Design of Light Gage Steel Diaphragms, American Iron and Steel Institute (AISI), New York, New York, 1967.

5. Nilson, A.H., "Folded Plate Structures of Light Gage Steel", Journal of the Structural Division, ASCE, Vol. 87, No. ST7, Proc. Paper 2970, Oct. 1961, pp. 215-240.

6. Luttrell, L.D., Winter, G., Structural Performance of Light Gage Steel Diaphragms, Research Report No. 319, Dept. of Structural Engineering, Cornell University, Ithaca, New York, Aug., 1965.

7. Luttrell, L.D., "Strength and Behavior of Light Gage Steel Shear Diaphragms", Cornell University Engineering Research Bulletin No. 67-1, Dept. of Structural Engineering, Cornell University, Ithaca, New York, 1967.

8. Apparao, T.V.S.R., Winter, G., Tests on Light Gage Steel Diaphragms, Research Report No. 328, Dept. of Structural Engineering, Cornell University, Ithaca, New York, Dec. 1966.

9. Godfrey, D.A., Bryan, E.R., "The Calculated and Observed Effects of Dead Loads and Dynamic Crane Loads on the Framework of a Workshops Building", Proc. of the Inst. of Civil Engineers, London, Vol. 13, June, 1959, pp. 197-214.

10. El-Dakhakhni, W.M., Effect of Membranes in Stiffening Pitched Roof Portal Frame Sheds, Ph.D. Thesis, University of Manchester, 1963.

11. Bryan, E.R., El-Dakhakhni, W.M., "Shear of Thin Plates with Flexible Edge Members", Journal of the Structural Division, ASCE, Vol. 90, No. ST4, Proc. Paper 3991, Aug., 1964, pp. 1-14.

12. Bryan, E.R., El-Dakhakhni, W.M., "Behavior of Sheeted Portal Frame Sheds: Theory and Experiments", Proc. of the

Inst. of Civil Engineers, London, Vol. 29, Dec., 1964, pp. 743-778.

13. Bates, W., Bryan, E.R., El-Dakhakhni, W.M., "Full Scale Tests on a Portal Frame Shed", The Structural Engineer, Vol. 43, No. 6, June, 1965, pp. 199-208.

14. Beck, V.R., "Stressed Skin Design of Steel Claddings", Australia Institute of Steel Construction (AISC), Conference on Steel Developments, Newcastle, 21-25, May, 1973, pp. 37-44.

15. Koerner, R.J., The Interaction Between Rigidly Jointed Frames and Light Cladding, M.E. Sc. Thesis, University of Melbourne, June, 1961.

16. Freeman, D.J., The Structural Action of Light Cladding, M.E. Sc. Thesis, University of Melbourne, June, 1964.

17. Bryan, E.R., Jackson, P., "The Shear Behavior of Corrugated Steel Sheeting", Thin Walled Steel Structures: Their Design and Uses in Building, Editors: Rockey, K.C., Hill, H.V., Crosby-Lockwood, London, 1969, pp. 258-274.

18. Bryan, E.R., El-Dakhakhni, W.M., "Shear Flexibility and Strength of Corrugated Decks", Journal of the Structural Division, ASCE, Vol. 94, No. ST11, Proc. Paper 6218, Nov., 1968, pp. 2549-2580.

19. Bryan, E.R., El-Dakhakhni, W.M., "Shear of Corrugated Decks: Calculated and Observed Behavior", Proc. of the Inst. of Civil Engineers, London, Vol. 41, Nov., 1968, pp. 523-540.

20. Rothwell, A., "The Shear Stiffness of Flat-Sided Corrugated Webs", Aeronautical Quarterly, Vol. 19, Aug., 1968, pp. 224-234.

21. Bryan, E.R., Stressed Skin Design of Steel Buildings, Crosby Lockwood Staples, London, England, 1973.

22. Davies, J.M., The Design of Shear Diaphragms of Corrugated Steel Sheeting, Report No. 74/50, Dept. of Civil Engineering, University of Salford, Sept., 1974.

23. Lawson, R.M., The Flexibility of Practical Shear Diaphragms, Report No. 75/69, Dept. of Civil Engineering, University of Salford, Oct., 1975.

24. Miller, C.J., Sexsmith, R.G., Analysis of Multistory Frames with Light Gauge Steel Panel Infills, Research Report No. 349, Dept. of Structural Engineering, Cornell University, Ithaca, New York, Aug., 1972.

25. Ammar, A.R., Nilson, A.H., Analysis of Light Gage Steel Shear Diaphragms, Part I, Research Report No. 350, Dept. of Structural Engineering, Cornell University, Ithaca, New York, Aug., 1972.

26. Ammar, A.R., Nilson, A.H., Analysis of Light Gage Steel Shear Diaphragms, Part II, Research Report No. 351, Dept. of Structural Engineering, Cornell University, Ithaca, New York, July, 1973.

27. Nilson, A.H., Ammar, A.R., "Finite Element Analysis of Metal Deck Shear Diaphragms", Journal of the Structural Division, ASCE, Vol. 100, No. ST4, Proc. Paper 10467, April, 1974, pp. 711-726.

28. Lawrence, S.J., Sved, G., "A Finite Element Analysis of Clad Structures", Conference on Metal Structures Research and Its Applications, Sydney, Nov., 1972.

29. Lin, C., Libove, C., Theoretical Study of Corrugated Plates: Shearing of a Trapezoidally Corrugated Plate with Trough Lines Permitted to Curve, Report No. MAE 1833-T2, Syracuse University, Research Institute, June, 1970.

30. Hsiao, C., Libove, C., Theoretical Study of Corrugated Plates: Shear Stiffness of a Trapezoidally Corrugated Plate with Discrete Attachments to a Rigid Flange at the Ends of the Corrugations, Report No. MAE 1833-T3, Dept. of Mechanical and Aerospace Engineering, Syracuse University, July, 1971.

31. Wu, L-H., Libove, C., Theoretical Study of Corrugated Plates: Shearing of a Corrugated Plate with Curvilinear Corrugations, Report No. MAE 1833-T4, Dept. of Mechanical and Aerospace Engineering, Syracuse University, Jan., 1972.

32. Libove, C., "Survey of Recent Work on the Analysis of Discretely Attached Corrugated Shear Webs", AIAA Paper No. 72-351, AIAA/ASME/SAE 13th Structures, Structural Dynamics, and Materials Conference, San Antonio, Texas, April 10-12, 1972.

33. Libove, C., "On the Stiffness, Stresses and Buckling Analysis of Corrugated Shear Webs", Report of the Dept. of Mechanical and Aerospace Engineering, Syracuse University, Syracuse, New York, March, 1973. Also, under same title in Current Research and Design Trends, Proc. of the Second Specialty Conference on Cold-Formed Steel Structures, Dept. of Civil Engineering, University of Missouri, Rolla, Oct. 22-24, 1973, pp. 259-301.

34. Wu, L-H., Libove, C., Theoretical Stress and Stiffness Data for Discretely Attached Corrugated Shear Webs with Curvi-

linear Corrugations, Report No. MAE 5170-T2, Dept. of Mechanical and Aerospace Engineering, Syracuse University, May, 1974.

35. Hussain, M.I., Libove, C., Stress and Stiffness Data for Discretely Attached Corrugated Shear Webs with Trapezoidal Corrugations, Report No. MAE 5170-T3, Dept. of Mechanical and Aerospace Engineering, Syracuse University, Dec., 1974.

36. Wu, L-H., Libove, C., Stiffness and Stress Analysis of Discretely Attached Corrugated Shear Webs with Quasi-Sinusoidal Corrugations, Report No. MAE 5170-T5, Dept. of Mechanical and Aerospace Engineering, Syracuse University, July, 1975.

37. Libove, C., Asymptotic Behavior of Discretely Attached Corrugated Shear Webs, Report No. MAE 5170-T4, Dept. of Mechanical and Aerospace Engineering, Syracuse University, March, 1975.

38. Timoshenko S., Gere, J.M., Theory of Elastic Stability, McGraw-Hill, New York, Second Edition, 1961.

39. Timoshenko, S., Woinowsky-Krieger, S., Theory of Plates and Shells, McGraw-Hill, New York, Second Edition, 1959.

40. Hlavacek, V., "Shear Instability of Orthotropic Panels", Acta Technica, CSAV, Prague, No. 1, 1968, pp. 134-158.

41. Bergmann, V.S., Reissner, H., "Neuere Probleme aus der Flugzeugstatik", Zeitschrift Flugtech und Motorluftsch, Vol. 20, 1929.

42. Easley, J.T., McFarland, D.E., "Buckling of Light-Gage Corrugated Metal Shear Diaphragms", Journal of the Structural Division, ASCE, Vol. 95, No. ST7, Proc. Paper 6683, July, 1969, pp. 1497-1516.

43. Easley, J.T., "Buckling Formulas for Corrugated Metal Shear Diaphragms", Journal of the Structural Division, ASCE, Vol. 101, No. ST7, Proc. Paper 11429, July, 1975, pp. 1403-1417.

44. _____, Stressed Skin Design, Draft of European Recommendations, European Convention for Constructional Steelwork, Committee 17 - Cold-formed Thin-Walled Sheet Steel in Building, May, 1975.

45. Smith, G.E., Elastic Buckling in Shear of Infinitely Long Corrugated Plates with Clamped Parallel Edges, M.S. Thesis, School of Aeronautical Engineering, Cornell University, Ithaca, New York, Sept., 1957.

46. Irons, B.M., "A Frontal Solution Program for Finite Element Analysis", International Journal for Numerical Methods in Engineering, Vol. 2, 1970, pp. 5-32.

47. Zienkiewicz, O.C., Valliappan, S., King, I.P., "Elasto-Plastic Solutions of Engineering Problems, 'Initial Stress' Finite Element Approach", International Journal for Numerical Methods in Engineering, Vol. 1, 1969, pp. 75-100.

48. Nayak, G.C., Zienkiewicz, O.C., "Elasto-Plastic Stress Analysis. A Generalization for Various Constitutive Relations Including Strain Softening", International Journal for Numerical Methods in Engineering, Vol. 5, 1972, pp. 113-135.

49. Jennings, A., "Accelerating the Convergence of Matrix Iterative Processes", Journal of the Institute of Mathematics and Its Applications, Vol. 8, 1971, pp. 99-110.

50. Boyle, E.F., Jennings, A., "Accelerating the Convergence of Elasto-Plastic Stress Analysis", International Journal for Numerical Methods in Engineering, Vol. 7, 1973, pp. 232-235.

51. Aitken, A.C., Proc. R. Soc. Edinb., Vol. 46, 1926, pp. 289-305.

52. Conte, S.D., Elementary Numerical Analysis, McGraw-Hill, Kōgakusha, Tokyo, 1965.

53. Nilson, A.H., "Report on Tests of Light Gage Steel Floor Diaphragms, 1957 Series", Research Report, Dept. of Structural Engineering, Cornell University, Ithaca, New York, 1957.

APPENDIX 1

INPUT SPECIFICATIONS FOR THE COMPUTER PROGRAM

A.1.1 General

The computer program has been prepared to accept two different types of input. For most practical cantilevered diaphragms, a quite versatile mesh generator requiring a minimum of input can be used for the generation of the complete finite element mesh. If a diaphragm does not fall within the limitations imposed by the mesh generator, input data should be prepared in a longer form. Both types of input must conform to the definitions and limitations set forth in Section 3.3.

Figures A.1.1 through A.1.6 will be used as guides to the input specifications given in this section. The data for the example cantilevered diaphragm shown on Figure A.1.1 can be prepared in either of two ways. In both cases, the user should first draw the finite element mesh and decide in which order the subassemblies must be presented for maximum efficiency without exceeding the wavefront during assembly and reduction of the stiffness equations. The tentative numbering of the subassemblies on Figure A.1.1 is given as an example of this.

A.1.2 Manual Input

Since this longer type of input is more general and since it will provide the basis for better understanding of how the automatic mesh generator can be used, it will be detailed first. The input data for the simple diaphragm of Section 5.2 is given

as an additional guide for this case (Table A.1.1).

If the user has been compelled to choose the manual input, then all degrees of freedom at each node should be numbered, either according to the definitions of Section 3.3, or according to the user's understanding of the behavior of the diaphragm components. For example, if it has been decided that two finite elements should share a common degree of freedom at a given node, then the number for this degree of freedom will be the same for both finite elements. A more explicit example is that of an internal hinge. Two beam elements meeting at this hinge would share the same translational degrees of freedom at the hinge, but would have different rotational degrees of freedom.

Figure A.1.2 shows a tentative numbering of degrees of freedom for the example diaphragm. In numbering this diaphragm, it was assumed that all frame interconnections are hinged and that two individual sheets connected at seams share the same degrees of freedom in the direction perpendicular to the seam line at nodes where seam connectors exist. It is noted at this point that this numbering also coincides with numbering by the mesh generator (Section A.1.3) although this is not necessary.

Card Input

Title Cards

There are two mandatory title cards on which the user may punch information regarding the problem that is to be solved, using all 80 columns of each card if necessary. FORMAT (20A4)

Basic Control Card

This card provides information about what the program is requested to do. The variables are:

NOPT1, NOPT2, NOPT3, MITER, NSU, NOOS, NOOM, PINF

FORMAT (7I5,5X,F10.6)

NOPT1: 0 if only a linear analysis up to the elastic limit is requested.

If a non-linear analysis is desired, NOPT1 should be equal to the maximum number of load increments beyond the elastic limit, up to which analysis is requested.

NOPT2: 0 if the longer type of input is going to be used.

1 if the automatic mesh generator is going to be utilized.

NOPT3: 0 if output is required only at end of each load increment.

1 if output for every iteration and acceleration is required in addition. Since NOPT3 = 1 would produce a very large volume of output, practically NOPT3 would be chosen as 0, except for academic interest.

MITER: Maximum number of iterations specified per load increment.

NSU: The total number of subassemblies in the structure.

NOOS: All subassemblies that have exactly the same geometric, material, and element properties fall into one group. NOOS (no. of original

subassemblies) is the total number of all such groups.

NOOM: All subassemblies whose basic finite elements have the same geometric and material properties fall into one group, regardless of the number of finite elements making up the subassembly. NOOM (no. of original materials) is the total number of all such groups.

The values of NOOS and NOOM are immaterial if the longer type of input has been chosen.

PINF: This is the ratio of the incremental load to the originally applied load, and is a positive non-integer variable. Value is immaterial if NOPT1 = 0.

Subassembly Information Cards

When the manual input is chosen, at least two cards are needed for each subassembly in the structure. These groups of two or more cards are fed in the same order as the subassemblies have been numbered (such as on Figure A.1.1).

The first card of each group contains the following variables:

KUREL, KL1, NTYPE, NRE, KL2, LIKE, KE, NX

where KL1 through NX are read directly into a long array NIX. FORMAT (16I5)

KUREL: The total number of degrees of freedom in the subassembly. For connection subassemblies only, if a d.o.f. is associated with more than one

spring element in the subassembly, then it should be counted as many times as it is repeated.

KL1: (see also definition of an original subassembly, NOOS, on basic control card).
0 if the subassembly is one of a kind or if saving the relevant stiffness matrix would lead to exceeding the limit of vector STORE that is set aside for this purpose in the pre-program (see also Appendices 2 and 3).
n if this is the first appearance of a subassembly of this kind.
-n if this is a subsequent appearance of a subassembly of kind n.
n should start from 1, and increase one by one every time for the first appearance of a new type of subassembly.

NTYPE: -3 if sheet to intermediate purlin connection (two springs in orthogonal directions).
-2 if end or edge connection (similar to above, the difference in NTYPE being due to considerations of the check of collapse condition).
-1 if one dimensional connection spring element (as for sheet to sheet seam connections).
1 if beam element (in x-direction)
2 if column element (in y-direction)
3 if plate element.

The values of KUREL, KL1, and NTYPE must always be entered.

NRE: Total number of supported degrees of freedom in

the subassembly. If two or more subassemblies share the same supported degree of freedom, the support may be related to only one of them, the choice being left to the user.

KL2: Total number of loaded degrees of freedom in the subassembly. If two or more subassemblies share the same loaded d.o.f., the same rule as for NRE applies.

The next three variables need not be entered if KL1 is negative.

LIKE: (see also definition of original material, NOOM, on basic control card).
0 if the subassembly is made up of only one finite element and is the only subassembly that uses this finite element.
n if first appearance of the group of subassemblies composed of the same basic finite element n.
-n for subsequent appearances of subassemblies with basic finite element n.
For the case of LIKE, n need not start from 1, neither need it increase in order.

KE: Total number of finite elements in the subassembly. KE should be negative if this is a split subassembly (see Section 3.3 and the next group of cards).

NX: (Necessary only for plate subassemblies which are not split subassemblies).

Total number of plate elements in the direction parallel to the seams in the subassembly, counted for only one row of plate elements.

The second and subsequent cards of the group contain the elements of the vector LVABL, where LVABL (I), I = 1, KUREL, is the list of the degrees of freedom in the subassembly as these d.o.f.s have been numbered in the structural numbering system (as on Figure A.1.2). Examples below are for subassemblies 1, 4, and 5 respectively of Figure A.1.1. Note repeating d.o.f.s 271 and 272 for subassembly 4 (see also above definition of KUREL).

FORMAT (16I5)

Example: Subassembly 1

Vector LVABL:

225 226 227 228 229 230 231 232 233 234 235 236 237 238 239 24

241 242 243 244 245

Example: Subassembly 4

Vector LVABL:

1 225 2 226 27 268 28 269 53 271 54 272 79 271 80 272

100 274 101 275

Example: Subassembly 5

Vector LVABL:

1 2 3 4 5 6 7 8 9 10 27 28 29 30 31 32

33 34 35 36 53 54 55 56 57 58 59 60 61 62

The total number of the groups of cards for the subassembly information should be equal to NSU.

Element, Load, and Support Data

This group is reviewed in three parts:

- Element Information Cards
- Load Information Cards
- Support Information Cards

Element Information Cards:

These consist of card(s) that give the geometric and material properties of the basic finite element of a subassembly for which LIKE is zero or positive, except for the case of a split subassembly (negative KE) for which element degree of freedom numbers in the subassembly numbering system should also be provided for each element in the subassembly unless KL1 is negative. This numbering is done internally when the subassembly is continuous, however a knowledge of how this is done is necessary in order to properly furnish data for loaded and supported degrees of freedom.

Subassembly numbering system:

Since a subassembly is composed of a number of finite elements, it is necessary to establish the order in which these elements are located in the subassembly, and thereby to relate this location to the structural degrees of freedom. This is done by what here is called a subassembly numbering system, as opposed to the structural numbering system shown on Figure A.1.2. The degrees of freedom in each subassembly are numbered from 1 to the maximum number of degrees of freedom in the subassembly, this order being the same as the order of the structural

degrees of freedom in the vector LVABL. Figure A.1.3 gives examples of this numbering for each basic component of the example diaphragm of Figure A.1.1. The reader will also note that each finite element has been numbered from 1 to KE. Thus each element can be identified with the numbers associated with its nodes.

For each of the beam, column or connection elements, the numbers associated with the element will follow the sequence in which the subassembly has been numbered. However, for plate elements, the numbers are read in a counter-clockwise order. For example, for plate element number 6 of Figure A.1.3, the numbers would be: 13 14 15 16 25 26 23 24.

As noted earlier, this information is not required for continuous subassemblies, however, when split subassemblies are utilized, relevant cards must be provided for each element in a split subassembly. The reason why the numbers cannot be generated by the program in this case can clearly be seen from a comparison of Figures A.1.3 and A.1.4.

The cards are presented in the order that the elements have been numbered in the subassembly, except that if at the same time LIKE is positive for the subassembly, then the card relating to the geometric and material properties of the basic finite element should be placed after the numbering card for the first element.

The numbers are read into a vector NVABL.

FORMAT (16I5)

Geometric and Material Properties Data:

This is to be provided when LIKE is zero or positive for the subassembly. The input depends on NTYPE.

NTYPE = -3 or -2 or -1 (spring connection)

The variables associated with this case are NCDAT and the vectors X and Y, where these vectors correspond to the deflection and load coordinates respectively of the multi-linear representation of the connection behavior as found from a shear test. The order of the data is:

NCDAT X_1 Y_1 X_2 Y_2 ..... X_{NCDAT} Y_{NCDAT}

FORMAT (I5,5X,7F10.6,10(/,8F10.6))

(X_1 , Y_1) should be the elastic limit of the connection test. If the point at which the connection actually breaks has been noted, then this point should be given as ($X_{NCDAT-1}$, $Y_{NCDAT-1}$), and (X_{NCDAT} , Y_{NCDAT}) will be any negative numbers. If (X_{NCDAT} , Y_{NCDAT}) are positive, then any deflections greater than X_{NCDAT} will be assumed to correspond to perfectly plastic behavior. This device is provided for ease of avoiding infinite negative slopes in the multi-linear representation.

NTYPE = 1 or 2 (beam or column element)

The variables are:

ALEN, ZI, AX, YM

FORMAT (8F10.6)

ALEN: Length of beam or column element

ZI: Moment of inertia around an axis perpendicular to the plane of the diaphragm

AX: Cross-sectional area of the element

YM: Young's modulus of elasticity of the base material.

NTYPE = 3 (plate element)

The variables are:

UXY, UYX, YL, XL, EX, EY, T, G

FORMAT (8F10.6)

UXY: Poisson's ratio that relates strains in the y-direction to stresses in the x-direction

UYX: Poisson's ratio that relates strains in the x-direction to stresses in the y-direction.

YL: Length of the side of the plate element in the y-direction

XL: Length of the side of the plate element in the x-direction

EX: Elastic modulus in the x-direction

EY: Elastic modulus in the y-direction

T: Thickness of the plate material

G: Effective shear modulus of the plate element

If an isotropic plate element is used, then EX = EY and UXY = UYX.

If an orthotropic plate element is used, a simple rule of thumb is that when EX is the smaller modulus of elasticity, then UXY will be the smaller Poisson's ratio and vice versa.

Load Information Cards:

These should be provided only if the variable KL2 is non-

zero for a subassembly. If element information cards exist for that subassembly, the load data follows these cards.

Variables associated are the vectors NDOF and PP, and the input order is:

$NDOF_1$ PP_1 $NDOF_2$ PP_2 ..... $NDOF_{KL2}$ PP_{KL2}

FORMAT (4(I5,5X,F10.6))

NDOF: Vector whose elements are the numbers of the loaded degrees of freedom in the subassembly numbering system.

PP: Vector whose elements are the loads applied on the above degrees of freedom, with the correct sign with respect to the global coordinates.

Support Information Cards:

These are necessary only when NRE is non-zero for the subassembly in question, and come after material and load data (if such exist) for the subassembly.

Variables associated are the elements of the vector NR.

FORMAT (16I5)

NR: Supported degrees of freedom in the subassembly numbering system.

A.1.3 Input with Mesh Generator

Input is greatly simplified when the diaphragm to be analyzed conforms to the restrictions below.

a. The layout of the diaphragm is similar to that of the cantilever test recommended by the AISI (4).

b. At most two subassemblies have supported degrees of

freedom.

c. Loads are applied on only one subassembly.

d. Intermediate purlins (if any) run perpendicular to the seam lines.

e. There are end fasteners at least at the corners of each sheet.

f. There are sheet to sheet seam connectors except when the panel is made up of only one sheet.

g. There are edge connectors.

h. There are no split subassemblies.

i. The number of the end connection subassemblies equals the number of the perimeter column element subassemblies.

j. All sheets are modeled in exactly the same way.

In this case, all structural numbering for the subassemblies is done by a mesh generator subroutine (SUBROUTINE GMESH).

Figures A.1.1 through A.1.3 will again be used as a guide to the input specifications along with Figure A.1.5. Furthermore, the input data for the example diaphragm of Figure A.1.5 is given in Table A.1.2 for reference.

For the proper use of the mesh generator, it is necessary to understand how the structural numbering is done by SUBROUTINE GMESH for each component of the diaphragm and the relevant subassemblies. It is also necessary that the global x-axis of the diaphragm be defined as being parallel to the seam lines, when there is more than one sheet making up the diaphragm panel, as on Figure A.1.1.

A.1.3.1 Numbering of Subassemblies by the Mesh Generator

The mesh generation is started from the panel sheets, the first sheet to be numbered being the one closest to the x-axis. Once all the degrees of freedom on this sheet have been numbered, the numbers associated with each subassembly of the sheet are picked and stored according to an order that is defined later. When the first sheet has been numbered, the mesh generator moves on to the seam connections between this sheet and the next. After the process is repeated for the seam connections, the degrees of freedom of the next sheet are numbered and so on until the numbering for the last sheet is completed.

There may be one or more rows of plate element subassemblies in a given sheet (a row being defined in the x-direction). These subassemblies are associated with the structural degrees of freedom numbers row by row, starting with the row closet to the x-axis, and within each row, starting with the leftmost (closest to the y-axis) subassembly. The seam connection subassemblies (if there is more than one in a given seam line) are treated the same way starting with the leftmost seam connection subassembly. It is helpful to the reader to refer to Figure A.1.5 where the numbers in parentheses indicate the order of this procedure for the whole diaphragm.

After all the sheets and the seam connections have been numbered, the mesh generator then numbers the subassemblies of the beam (x-dir.) closest to the x-axis, starting again with the leftmost subassembly. Then the degrees of freedom

of the edge connection subassemblies between this beam and the first sheet are numbered, The process is then repeated for the beam farthest away from the x-axis and the associated edge connections, in this order.

The numbering of the degrees of freedom for the perimeter column subassemblies and the end connection subassemblies follows a similar order, this time starting with those subassemblies closest to the x-axis.

The last components to be numbered are the sheet to intermediate purlin connections and the intermediate purlins, in the case that these exist. There is one restriction in the formation of subassemblies of these last two diaphragm components: The subassembly will be defined as being on only one sheet, i.e. a sheet to intermediate purlin connection subassembly or an intermediate purlin subassembly cannot span more than one sheet width. This restriction can be seen clearer on Figure A.1.5. The last two components, therefore, are numbered sheet by sheet for each purlin, starting with the leftmost connection subassembly on the sheet closest to the x-axis, then going on to the purlin subassembly associated with the above connections, and continuing with the next connection subassembly on the next sheet, etc.

The order in which the subassemblies are numbered by the mesh generator should not be confused with the order in which the user wants the subassemblies to be ordered for solution. It is the responsibility of the user to match the two different sequences. This is done, as later explained in the card input

specifications, through the use of a vector MSUB. On Figure A.1.5, the subassembly numbers not in parentheses indicate a user's possible choice of subassembly ordering for solution.

A.1.3.2 Actual Card Input

Title Cards

These two cards are the same as for the longer type of input.

Basic Control Card

The variables on this card are the same as for the longer type of input. However, it should be noted that the value of NOPT2 will now be 1, and the values of NOOS and NOOM are important.

Mesh Data

This data is fed into the program through several READ statements. The READ statements and the associated variables are given below in the order the relevant data has to be provided. Input format is the same for all the READ statements associated with mesh data: FORMAT (16I5).

```
READ (5,200) NA, NB, NC, ND, NE, NF1, NFB, NFB1, NFBB, NFBB1,
             NG, NGB, NGBB, NGB1, NGB2, NH, NHB, NBX, NBY,
             NPUR, (NS(I),I=1,NF1), (NEV(I),I=1,NG), (NXV(I),
             I=1,NBX), (NYV(I),I=1,NBY), (NCY(I),I=1,NBY)
```

This data is continuous and is given in as many cards as necessary

in order to fit in the above vectors.

NA: The number of sheets making up the diaphragm panel.

NB: The number of plate subassemblies in the x-direction per sheet.

NC: The number of plate subassemblies in the y-direction per sheet.

ND: If all plate subassemblies are alike, ND will be the number of plate elements in the x-direction per plate subassembly. If not, any integer may be used.

NE: All plate subassemblies are required to have the same number of plate elements in the y-direction. NE is this number.

NF1: The number of sheet to sheet (sheet to purlin not included) seam connection subassemblies in any given seam line. If the panel is made up of only one sheet so that there are no seam connectors, then NF1 should be 1, not zero.

NF_B: The number of plate elements counted from the left end (nearest to the y-axis) of a seam line before the first seam connector (sheet to sheet or sheet to purlin) appears.

NF_{B1}: The number of plate elements counted from the left end of a seam line before the first sheet to sheet seam connector appears.

NF_{BB}: The number of plate elements between two seam

connectors, (sheet to sheet or sheet to purlin).

NFBB1: The number of plate elements between two sheet to sheet seam connectors.

NG: The number of edge connection subassemblies on either of the two edges.

NGB: The number of plate elements counted from the left end of an edge before the first edge connector appears.

NGBB: The number of plate elements between two edge connectors.

NGB1: The number of beam elements counted from the left end of an edge before the first edge connector appears.

NGB2: The number of beam elements between two edge connectors.

NH: The number of end connectors on one end of any sheet.

NHB: The number of plate elements between the connectors on one end of any sheet.

NBX: The number of beam (x-dir.) subassemblies on any one of the two perimeter beams.

NBY: The number of column (y-dir.) subassemblies on any one of the two perimeter columns.

NPUR: The number of intermediate purlins.

(NS(I),I=1,NF1): Integer vector of effective length NF1. The data is the number of sheet to sheet seam connections in each of the NF1 subassemblies, these subassemblies being ordered in the positive x-direction. If there are no seam connection subassemblies (allowed only for the case of one sheet making up the panel) then a zero should be punched recalling that NF1 is still given as 1 for this case.

(NEV(I),I=1,NG): Integer vector of effective length NG. The data is the number of edge connections (not the number of spring finite elements) in each of the NG subassemblies, the subassemblies being ordered in the positive x-direction.

(NXV(I),I=1,NBX): Integer vector of effective length NBX. The data is the number of beam elements in each of the NBX subassemblies (order same as above).

(NYV(I),I=1,NBY): Integer vector of effective length NBY.

The data is the number of column elements in each of the NBY subassemblies, these subassemblies being ordered in the positive y-direction.

(NCY(I),I=1,NBY): Integer vector of effective length NBY. The data is the number of end connections (not the number of spring finite elements) in each of the NBY subassemblies (order same as for NYV).

The next READ statement is activated only when NPUR is non-zero.

READ (5,200) NPUR1, NPUR2, NPUR3, NPUR4, NPURB1, NPURB2, NSE, (MPURC(I), I=1, NA), (MPURL(I), I=1, NA)

This data is also continuous and is given in as many cards as necessary.

NPUR1: The number of plate elements (in the x-direction) counted from the left before the first intermediate purlin appears.

NPUR2: The number of plate elements between two intermediate purlins.

NPUR3: The number of plate elements in the y-direction between any two sheet to purlin connectors, for a purlin in a given sheet.

NPUR4: The number of plate elements in the y-direction, counted from either end of a purlin before the first sheet to purlin connector appears.

NPURB1: The number of perimeter beam elements (x-dir.) counted from the left side before the first intermediate purlin appears.

NPURB2: The number of perimeter beam elements between two intermediate purlins.

NSE: 0 if the intermediate purlins are not connected to the sheets at seams,
1 if the intermediate purlins are connected to the sheets at seams.

(MPURC(I),I=1,NA): Integer vector of effective length NA. The data is the number, as modeled, of sheet to purlin connections (not the number of spring finite elements) on each of the NA sheets for one intermediate purlin (since there will be NA such subassemblies for each purlin).

(MPURL(I),I=1,NA): Integer vector of effective length NA. The data is the number of purlin elements (treated the same as column elements) in each of the NA sheets, for one intermediate purlin.

Data for the following READ statement is mandatory.

READ (5,200) NCORR, (MSUB(I), I=1, NSU)

The data is again continuous and is given on as many cards as are necessary.

NCORR: 0 if all plate subassemblies have the same number of plate elements in the x-direction.

1 if the number of the plate elements in the x-direction is not the same for all NB subassemblies (see previous definition of NB) of a row on a given sheet.

(MSUB(I),I=1,NSU): Integer vector of effective length NSU. This vector is used to match the subassembly order of the mesh generator with the user defined order (refer back to Section A.1.3.1 and Figure A.1.5). For the example problem, the subscripts I of the vector MSUB(I) are the numbers in parentheses on Figure A.1.5, and the values of MSUB(I) are the numbers not in parentheses, (user defined order). Thus for example: MSUB(1) = 7 , MSUB(2) = 10, ... , MSUB(8) = 24 , etc.

Data for the next READ statement is to be provided only if NCORR = 1.

READ (5,200) (NDV(I), I=1, NB)

(NDV(I),I=1,NB): Integer vector of effective length NB. The data is the number of plate elements in the x-direction in each of the NB plate subassemblies of a row of a sheet.

The next READ statement is activated a total of (NOOS+NOOM) times as shown below in the double DO loops. In the first cycle

data associated with the variable NOOS is read. Then a similar cycle is affected for NOOM.

```
      DO 84 I=1,2
      DO 172 J=1,NOOS
      READ (5,200) NOS, (MSUB(K), K=1, NOS)
      .......
      .......
      .......
  172 CONTINUE
   84 NOOS = NOOM
```

Data associated with NOOS:

Each card defines the subassemblies that fall into one group because they are exact replicas of each other.

Data associated with NOOM:

Each card defines the subassemblies that fall into one group due to the exactly same basic finite element that each subassembly in the group is composed of.

NOS: The total number of subassemblies in a given group.

(MSUB(K),K=1,NOS): Integer vector of effective length NOS. The data is the user defined numbers (see Figure A.1.5) of each of the subassemblies in the group.

It should be noted that ordering of these groups for both cases depends on the user defined order in which the first subassembly of each group is going to be considered for the solution phase, since for the case of NOOS the data is used to generate

KL1, which has been defined in the input specifications for the longer type of input, and for the case of NOOM the data is used to generate LIKE.

The next input card contains the data associated with the supports and the loads on the structure.

READ (5,200) NRE1, NRE11, NRE2, NRE22, KLS, KL2

NRE1: User defined number of one of the two possible subassemblies on which some degrees of freedom are supported.

NRE11: Total number of supported degrees of freedom on subassembly NRE1.

NRE2: If there are supports on a second subassembly, then NRE2 is the number of this subassembly. NRE2 is always greater than NRE1 except when all supports are on subassembly NRE1, in which case NRE2 should be any integer less than NRE1.

NRE22: Total number of supported degrees of freedom on subassembly NRE2.

KLS: The user defined number of the subassembly on which loads are applied.

KL2: The total number of loaded degrees of freedom on subassembly KLS.

Element, Load, and Support Data

This data is furnished in the same manner as for the longer type of input except that no split subassemblies are allowed. The ordering of the data also follows similar considerations.

A.1.4 Other Considerations

It may have been noted that the diaphragm shown on Figure A.1.5 is probably not a good example of a well designed diaphragm. It has been given in order to show that absolute symmetry is not essential to use the mesh generator provided that the restrictions set forth in the beginning of Section A.1.3 and the below consideration are kept in mind. When the input instructions read "as counted from the left", this means that a count from the right does not have to give the same arithmetic result. However, the intermediate spacings which are given as supplementary data, should not alter for the component in question.

It is quite possible to extend the range of the mesh generator by making small changes and additions in Subroutine GMESH. For example, within certain limits, the case where the seam connectors are at the crests rather than the valleys of the corrugations (case of no end connectors at sheet corners) can be treated with minor changes in the program. This case was not implemented because with the longer type of input more efficient solution times can be attained, for this, even though it is necessary to provide a larger volume of data. In such cases the longer type of input provides more flexibility in decreasing the total number of subassemblies.

Similarly, the case of no edge or end connectors was not implemented since a well designed diaphragm will most likely have these components.

This trade-off between a more general mesh generator and

practical situations is therefore justified since a more general mesh generator would either result in less efficient solution times or would have to require more data and become quite lengthy.

When the mesh generator is used, the incidences of the spring elements that make up the connections are invariably taken as sheet to frame for sheet to frame connections, and lower sheet (closer to the x-axis) to upper sheet for the sheet to sheet connections, by the mesh generator. When the manual input is chosen, the user is free to make a different choice of spring incidences. In either case, the directions of the resulting forces should be evaluated depending on the incidence of the respective element.

If it is desired to conduct a first order analysis by using two different spring constants in the two directions for a given connection, it is sufficient to group the spring elements in one direction under one subassembly and those in the other direction under another subassembly. However, there are two drawbacks to this. One is that the longer type of input will be necessary. The other drawback is that the elastic limit will not be computed correctly due to the considerations involved in the algorithm, although the correct deflections at the given initial load can be found correctly by simple proportioning from the results printed at the elastic limit.

Input data for the 10' x 12' welded cellular diaphragm and the 10' x 12' standard corrugated diaphragm are given on Tables A.1.3 and A.1.4.

APPENDIX 2

LIMITATIONS ON PROBLEM SIZE

This appendix gives the limits imposed by the program on the sizes of problems to be solved. In case the below limits are not sufficient, the three other appendices should be reviewed carefully in order to make the necessary changes in the program. In many cases the required changes will be minimal.

Maximum number of d.o.f.	: 1500
Maximum number of connection subassemblies	: 50
Maximum number of d.o.f. per subassembly	: 40
Maximum number of d.o.f. in the wavefront	: 80
Different type and/or size finite elements	: 15
Different type and/or size subassemblies	: 16
D.o.f. associated with connections	: 750
Connection types with different test curves	: 5
Maximum number of data points for a connection curve	: 10
Maximum number of supported d.o.f. in the structure	: 10
Maximum number of supported d.o.f. in a subassembly	: 10
Maximum number of loaded d.o.f. in a subassembly	: 10
$\sum_{i=1}^{n} (N_i + 1) \times N_i/2$	: 2250

where,

n : number of original subassemblies that appear more than once,

N_i : total number of d.o.f. associated with subassembly i.

This limitation is imposed so that for similar subassemblies, the stiffness matrix need be generated only once, the stiffness coefficients then being kept in array STORE to be used for the next such subassembly (see KL1 in input). For KL1 = 0, the stiffness matrix is not kept. Thus if the above limitation is troublesome, it is sufficient to manipulate the value of KL1.

The following additional limits are imposed by the mesh generator only. They can be ignored if the longer type of input is going to be used.

Maximum number of subassemblies	: 100
Maximum number of sheet to sheet seam connections on one seam line	: 20
Maximum number of nodal points on a given sheet	: 100
Maximum number of beam finite elements for a frame member	: 65
Maximum number of edge connections on one edge	: 25
Maximum number of intermediate purlins	: 8
Maximum number of subassemblies that have supported d.o.f.	: 2
Maximum number of subassemblies on which there are loads	: 1

APPENDIX 3

ARRAYS AND VARIABLES USED IN THE PROGRAM

This appendix gives a listing of the arrays and major variables that are used in the program, other than those already defined in Appendix 1.

A.3.1 Arrays

BMK: Beam element stiffness matrix.

CLK: Column element stiffness matrix.

CY: Corrected resultant connection forces as obtained from connection test curves. CY accommodates JPASS (here 5) number of connection subassemblies at a time, to be stored on tape after every iteration. (see also Figure A.3.1).

EL: Initially used to store subassembly coefficients to be written on tape, EL also accommodates other vectors in routines GMESH and PLAST. For a complete map of EL see Figure A.3.1.

ELPA: This is the main working area in the program. See Figure A.3.2 for a complete map.

EQVEC: Raw yield functions for connections while checking for diaphragm elastic limit. One connection subassembly at a time.

JJ: -Pre-solution: 1. Alphanumeric vector to print out program label.

2. Later used to store values of LIKE.

-Mesh generator: Alias NSEAM (see NSEAM).

KCONN: Coded connection subassembly ordering and number of test data points.

LCONN: -Temporary KCONN during pre-program.

-Permanent storage for KUREL and LIKE for connection subassemblies.

LDEST: Coded d.o.f. destinations for each subassembly.

LND: Vector to pick connection stiffness coefficients from beam stiffness matrix.

LOC: Addresses of start of subassembly stiffness coefficients in vector STORE. (see Figure A.3.3).

LVABL: -Mesh generator: Temporarily used to store d.o.f. numbers for plate subassemblies.

-Main program: Stores d.o.f. numbers (in structural numbering system) for each subassembly (see also input).

MVABL: -List of active variables (variables in the wavefront.

-Alias NS (see input) in the mesh generator.

NCEDGE: Edge connection d.o.f.s are collected in this vector during mesh generation.

NCEND: End connection d.o.f.s are collected in this vector during mesh generation (see also Figure A.3.2).

NCONVE: Description of whether or which type of connection, for each subassembly in the structure.

NCOMP: Vector in mesh generator, where the diaphragm component d.o.f.s are collected before more detailed breakdown.

NIX: Integer vector located in ELPA (see Figure A.3.2). It is used in the pre-program to store variable numbers, addresses and basic subassembly information,

NRA: Supported d.o.f.s in the structural numbering system.

NSEAM: Seam connection d.o.f.s are collected in this vector during mesh generation. (see also JJ).

NSHARE: D.o.f.s that are shared between two components of the diaphragm are stored in this vector during mesh generation.

NTO: Number of pairs of spring finite elements in each connection subassembly. If odd number (n) of springs, as could be for seam connections, then the number of pairs is taken as (n+1)/2. Later, keeps actual subassembly numbers for connection subassemblies (NELEM)

NVABL: Vector where the element d.o.f.s in the subassembly numbering system are kept (see also input).

OL: Connection spring elements cumulative internal forces, JPASS subassemblies at a time. (see also Figure A.3.2). Also first order incremental forces.

OLD: Connection spring elements cumulative deformations, JPASS subassemblies at a time. (see also Figure A.3.2).

OU: Corrected, connection spring elements cumulative internal forces ready for output, one subassembly at a time. (see also Figure A.3.2).

RES: Residual forces due to connections showing non-linear behavior. One subassembly at a time.

S: Plate element stiffness matrix.

SK: Each element stiffness matrix assumes the alias SK in subroutine SUBK.

SSK: Three dimensional matrix where the stiffness matrices for original finite elements are kept ordered according to LIKE, for further use

STORE: See Figure A.3.3.

YDF: Lowest factors to elastic limit for each connection subassembly.

Z: The slopes in the multi-linear idealization of connection test curve. See also X and Y in input.

A.3.2 Major variables

A: The factor that will raise connection forces and deflections to the elastic limit plus apply the first load increment beyond this limit (A = ALPMAX + PINF).

ALPMAX: The factor to the elastic limit.

ANSWER: The deflection or deflection increment for a given d.o.f. (back-substitution phase).

CE: Contributions to stiffness equations from a

given subassembly.

CRIT: A diagonal decay criterion of roundoff damage.

CYP: Resultant force in connection corresponding to the deflection imposed, as found from connection curve (see also vector CY).

DFP1(2): Uncorrected forces in the spring elements modeling the connection.

FACTOR: Convergence is assumed when the norm of the residual forces is less than or equal to FACTOR times the norm of the applied loads. Here FACTOR = 0.0001.

FPNORM: Norm of the applied loads.

F1, F2: Forces in the spring elements of a given connection before the results of the last iteration are added.

IACC: Equals 1 for one iteration after a successful acceleration. Otherwise is 0.

IALPHA: Counts the connection subassemblies up to KCOUNT or backwards.

IBA: Subscript of ELPA in back-substituion. Locates coefficient of equation.

IBAR: Right hand side of equation is located after IBAR in ELPA.

IBDIAG: Subscript of ELPA that locates diagonal coefficient of equation.

ICONV: Becomes -1 when convergence is attained in a load increment (0 otherwise) and signals the

beginning of the last iteration in that load increment.

INITL: 1 for first solution. Reverts to 0 before first back-substitution and stays 0.

IRHS: 1 when a right hand side of the equations is being processed.

IRW: Counts number of records on auxiliary storage unit 3.

ITER: Counts the number of iterations in a load increment.

JWHERE: Associated with error diagnostics. Those provided by Irons (46) have not been changed, although some have been removed.

JWHERE = 2 : Negative KUREL.

JWHERE = 3 : More than LVEND (here 40) d.o.f.s for a subassembly. (see also LVABL).

JWHERE = 5 : Size of NIX too small. (see NIXEND).

JWHERE = 6 : Zero or negative numbered d.o.f. (Repeated d.o.f. if program does not stop)

JWHERE = 7 : Provided size for wavefront, MVEND (here 80), too small. (see also MVABL).

JWHERE = 9 : NELPAZ (see Figure A.3.2) too small.

JWHERE = 10: LZ $\leq$ 0 or element segment too long for a tape record of prescribed

length MAXELT.

JWHERE = 12: Length of an equation is wrong.

JWHERE = 13: Zero pivot. (Inadequately supported structure or mechanism).

JWHERE = 14: CRIT > 10^8. Fatal ill conditioning.

JWHERE = 15: CRIT > 10^4. Suspected ill conditioning. All above errors except for JWHERE = 15, which only causes a warning message to be printed, stop the program.

KACC: Counts the number of successful accelerations in a load increment.

KCOUNT: Total number of connection subassemblies.

KDISC(K): Auxiliary storage units 4 and 8. The numbers are switched every iteration.

KKE: Counts the d.o.f.s in a connection subassembly in twos or fours.

KKUREL: Number of d.o.f.s of a finite element.

KOFAIL: Counts the number of perimeter connection subassemblies in the diaphragm, to be compared with MFAIL.

KOU: Number of spring finite elements in a connection subassembly (alias of KE for these subassemblies).

KOUNT: Counts the number of appearances of a variable (d.o.f.) in thousands plus 1000. KOUNT is also used as counter in subroutine GMESH.

KURPA: Number of active variables at a given time (current size of the wavefront).

LCUREQ: Number of stored equations when current subassembly appears.

LDES: Decoded version of LDEST.

LHS: 1 when a left hand side of the equations is being processed.

LPASS: Counts number of connection subassemblies processed in subroutine PLAST before a record is written on auxiliary storage unit 4 or 8 (max. LPASS = JPASS = 5).

LPREQ: Number of stored equations when previous subassembly was assembled.

LVEND: Maximum number of d.o.f. allowed per subassembly, thus the dimension of LVABL.

LVMAX: The maximum number of d.o.f. per subassembly actually encountered.

LZ: Length of subassembly stiffness and load record on auxiliary storage unit 1.

MAXELT: Guaranteed maximum possible LZ.

MAXNIC: Highest numbered degree of freedom encountered.

MAXPA: Maximum actual size of the wavefront, in terms of number of d.o.f.s.

MAXREC: A record on auxiliary storage unit 3 extends from MINREC to MAXREC.

MAXTAP: Limits length of buffer for length of stored equations.

MCONN: Counts connection subassemblies with different connection curves.

MFAIL: Counts number of perimeter connection subassemblies in which all connections have reached ultimate capacity.

MINREC: See MAXREC.

MSTOR: Maximum allowable number of d.o.f., however not the only factor controlling allowable d.o.f.s. See also Figures A.3.2 and A.3.3. Here MSTOR = 1500.

MVEND: Maximum allowable size of the wavefront, hence the dimension of MVABL. (see also MAXPA).

NACC: Counts the number of iterations leading to an acceleration. Acceleration is attempted when NACC = 3. Also NACC = 4 when acceleration is successful, or NACC = 5 when acceleration is not successful.

NBAXO(Z): Buffer in ELPA reserved for equations for back-substitution extends from (NBAXO + 1) to NBAXZ (see Figure A.3.2).

NBUFFA: NBAXZ - NBAXO.

NCDATA: Equals NCDAT (see input) when the connection behavior is assumed perfectly plastic after last (NCDAT) data point. Equals (NCDAT-1) if connection is assumed to break after data point before last. In the latter case, the last data point is a dummy point as explained in Appendix 1.

NCON: Preserves values of NTYPE (see input) for connection subassemblies.

NCONV: Becomes 1 at beginning of last iteration in a load increment. Changes to 0 in next load increment.

NCTART: Used to find starting locations of end connections d.o.f.s in vector NCOMP in mesh generator.

NCYP: Counts number of actual connections in a connection subassembly (Subroutine PLAST).

NDEQN: Location in ELPA of end term of an equation.

NDIAG: Location in ELPA of diagonal coefficient of the wavefront equations.

NDOF: Not the same as the vector NDOF. Used as a counter in mesh generation.

NELEM: Counts subassemblies.

NELPAZ, NELPA1, NELZ: See Figure A.3.2.

NEQ: Counts equations backwards in back-substitution.

NEW: -Pre-program: NEW = N1-NZ: range of subassembly d.o.f. numbers in NIX.

-Solution: 1 when the coefficients for a subassembly have just been assembled. 0 otherwise.

NEWRHS: -1 if convergence has not been attained in a specified number of iterations. 1 otherwise. After NEWRHS becomes -1, one more iteration is performed before program terminates.

NFAIL: Counts the number of connections that have

reached their ultimate strength, in a given perimeter connection subassembly.

NFIR, NSFIR: Artifices used in mesh generation to find the locations of and d.o.f. associated with seam connections.

NFIRST: The lowest numbered d.o.f. to be assigned to a diaphragm component for which d.o.f. will be generated in subroutine GMESH. Highest numbered d.o.f. for that component will then be NLAST.

NIC: Number of a d.o.f. (nickname).

NINT: Number of load increments actually applied to the diaphragm beyond its elastic limit. To be compared with NOPT1 (see input).

NIXEND: Effective length of NIX (see Figure A.3.2).

NIZZ: Location in NIX of last label (no. of a d.o.f.) for a subassembly.

NLAST: See NFIRST.

NOP: Counts number of pairs of spring elements in a connection subassembly. If odd numbered (n) elements, then maximum NOP = (n+1)/2.

NPAR: Location in ELPA preceding the assembled right hand sides. (see Figure A.3.2).

NPAZ: Last available location in ELPA for right hand side associated with the variables in the wavefront.

NRAT: Total number of supported d.o.f.

NRUNO: See Figure A.3.2.

NSOL: 1 for first solution. Changes to 0 just before control goes back to beginning of solution phase for the first iteration of the first load increment beyond the elastic limit.

NSPACE: Locates beginning location in NIX of labels associated with subassembly d.o.f. in mesh generation.

NSTART: Used to find starting locations of edge connections d.o.f.s in vector NCOMP in mesh generator.

NSTOR: -Allocates places for subassembly residual forces in vector STORE when recording them on auxiliary storage devices is not efficient.
-Allocates places for subassembly, accelerated deflection increments in ELPA after a successful acceleration.

NSTRES: Number of appearances of a variable.

NSUB: Counts subassemblies in mesh generation. MSUB (NSUB) is the user defined subassembly number.

NSUBP: Counts plate subassemblies in mesh generation to compare with NB (see input).

NTURN: Artifice used in routine PLAST to deal with single spring element connections (sheet to sheet seam) in pairs.

NUREL: Alias of KUREL in a loop in which KUREL is already in use.

NVABZ: Total number of d.o.f.

P:	-Norm of initially applied loads. -After elastic limit is found, it becomes a factor of the norm of the applied loads.
PBAR:	Uncorrected resultant force in a connection.
RBAR:	Resultant residual force due to a connection.
RNORM:	Norm of residual forces.
S:	Acceleration factor.
SBAR:	Resultant deformation of a connection.
S1, S2:	Deformations of first and second spring elements respectively, of a connection due to the initially applied loads.
S1I, S2I:	Same as above, except that now they are deformation increments due to residual forces, or residual forces plus new load increment.
THETA:	Shows the direction of a resultant associated with a connection.
YDFN:	Yield function in routine PLAST.

```
C                          APPENDIX 4
C
C
C                  DIAPHRAGM NON-LINEAR ANALYSIS
C
C                     PROGRAM AND FLOW CHARTS
C
C
C
C       THIS PROGRAM HAS BEEN DEVELOPED FOR THE SPECIFIC
C     PURPOSE OF ANALYZING LIGHT GAGE METAL SHEAR DIAPHRAGMS
C     IN THE LINEAR AND NON-LINEAR RANGES OF RESPONSE UP TO
C     COLLAPSE.  OPTIONS ARE AVAILABLE TO THE USER FOR SPE-
C     CIFYING THE EXTENT OF THE REQUIRED ANALYSIS.
C          THE PROGRAM HAS BEEN WRITTEN IN THE FORTRAN IV
C     LANGUAGE AND HAS BEEN TESTED AGAINST THE G-LEVEL AND
C     WATFIV COMPILERS.  AS AUXILIARY STORAGE DEVICES, IT
C     USES 2 SCRATCH DISK UNITS (UNITS 1 AND 2) FOR LINEAR
C     ANALYSIS AND 5 SCRATCH DISK UNITS (UNITS 1, 2, 3, 4,
C     AND 8) FOR NON-LINEAR ANALYSIS.  THE DIMENSION STATE-
C     MENTS IN THE PROGRAM HAVE BEEN SIZED ON A 7294 BYTE
C     RECORD LENGTH.
C          MACRO FLOW CHARTS FOR THE FOUR LONGER ROUTINES
C     MAIN, SUBK, PLAST, AND GMESH ARE GIVEN ON FIGURES
C     A.4.1 THROUGH A.4.4.  THE REST OF THE DOCUMENTATION
C     FOR THE PROGRAM  IS GIVEN IN CHAPTER 4 AND APPENDICES
C     1 THROUGH 3 OF THIS REPORT.  FULL DOCUMENTATION OF THE
C     SOLUTION ROUTINE WRITTEN BY IRONS CAN BE FOUND IN
C     REFERENCE 46.
C          THE PROGRAM MAKES NO CONVERSION  OF UNITS.  ANY
C     CONSISTENT SET OF UNITS CAN BE USED IN THE INPUT.
C          THE FOLLOWING LISTING OF THE PROGRAM IS GIVEN IN
C     A 60 COLUMN FORMAT, WITH LONGER STATEMENTS BEING CON-
C     TINUED ON THE NEXT CARD PRECEDED BY A C IN THE SIXTH
C     COLUMN OF THE LINE AND TWO BLANK COLUMNS .  THESE TWO
C     BLANK COLUMNS SHOULD BE AVOIDED WHEN A CARD DECK IS TO
C     BE MADE FROM THE LISTING.
```

```
 BLOCK DATA
 IMPLICIT REAL*8(A-H,O-Z)
 COMMON /BLK1/ RNORM,FPNORM,P,PI,IALPHA,ICONV,NCONV,KCO
C  UNT,NSTOR,
1IC,LVMAX,NIZZ,LPASS,KUREL1,KOU1,NCYP1,MSTOR,KKE,NIXEND
 COMMON /BLK2/ S1,S2,ALPMAX,PINF,CYP,NCON,NSOL,KDISK,KD
C  ISC,KOU,NOP,
1NACC,NINT,MFAIL,JPASS,NTO(50),KCONN(50),LCONN(100)
 DATA P/0. D0/,PI/3.14159 D0/,ALPMAX/1. D0/,IALPHA/0/,K
C  DISC/4/,
1KDISK/8/,MSTOR/1500/,IC/2/,NSOL/1/,NACC/-1/,ICONV/0/,N
C  CONV/0/,
2NINT/1/,KUREL1/0/,KOU1/0/,NCYP1/0/,NIXEND/10800/,NIZZ/
C  0/,LVMAX/0/,
3JPASS/5/
 END
```

```
      IMPLICIT REAL*8(A-H,O-Z)
      DIMENSION NR(10),EQVEC(10),OL(200),OLD(100),CY(100)
      DIMENSION NIX(12000),YDF(50),RES(40),NDOF(10),PP(10),N
     C  RA(10)
      COMMON /BLK1/ RNORM,FPNORM,P,PI,IALPHA,ICONV,NCONV,KCO
     C  UNT,NSTOR,
     1IC,LVMAX,NIZZ,LPASS,KUREL1,KOU1,NCYP1,MSTOR,KKE,NIXEND
      COMMON /BLK2/ S1,S2,ALPMAX,PINF,CYP,NCON,NSOL,KDISK,KD
     C  ISC,KOU,NOP,
     1NACC,NINT,MFAIL,JPASS,NTO(50),KCONN(50),LCONN(100)
      COMMON /BLK3/ STORE(2250),LOC(20),NCONVE(50)
      COMMON /BLK4/ SSK(8,8,15),X(10,5),Y(10,5),Z(9,5)
      COMMON /BLK5/ MVABL(80),LVABL(40),LDEST(40),LND(8)
      COMMON /BLK6/ ELPA(7000),EL(860),JJ(40)
      COMMON /BLK7/ INITL,NEWRHS,NELEM,KUREL,LPREQ,
     1   LZ,NELZ,NBAXO,NBZ,KL,LDES,NSTRES,KK,LIKE,KOUNT,NX,N
     C  VH
      COMMON /BLK8/ KE,KL1,NTYPE,NE
      DATA NELPAZ/5500/,LVEND/40/,MVEND/80/,KOFAIL/0/,MAXTAP
     C  /900/,
     1MAXELT/860/,NCDAT/0/,MAXNIC/0/,MAXPA/0/,NVABZ/0/,KACC/
     C  0/,
     2LCUREQ/0/,ITER/-1/,IACC/0/,NRAT/0/,NELPA1/4000/,FACTOR
     C  /1. D-4/
      EQUIVALENCE (NIX(1),ELPA(1)),(OL(1),EL(100)),(RES(1),E
     C  L(301)),
     1(OLD(1),EL(341)),(CY(1),EL(441)),(YDF(1),EL(650))
      NFUNC(I,J)=I+(J*(J-1))/2
      DO 2 I=1,8
    2 LND(I)=I
      NEWRHS=1
      INITL=1
      LOC(1) = 1
C     PROBLEM LABEL AND CONTROL DATA
      READ (5,804) (JJ(I),I=1,40)
  804 FORMAT (20A4)
      READ(5,901) NOPT1,NOPT2,NOPT3,MITER,NSU,NOOS,NOOM,PINF
  901 FORMAT(7I5,5X,F10.6)
      WRITE (6,951) (JJ(I),I=1,40)
  951 FORMAT (1X,20A4)
      WRITE (6,950) NOPT1,NOPT2,NOPT3,MITER,NSU,NOOS,NOOM,PI
     C  NF
  950 FORMAT (/,5X,'MAX. NO. OF LOAD INCREMENTS BEYOND ELAST
     C  IC LIMIT = '
     1,I5,/,5X,'ONE IF MESH GENERATOR IS REQUESTED. ELSE ZER
     C  O = ',I5,/,5
     2X,'OUTPUT CONTROL OPTION = ',I5,/,5X,'MAX. NO. OF ITER
     C  ATIONS PER L
     3OAD INCREMENT = ',I5,/,5X,'TOTAL NO. OF SUBASSEMBLIES
     C  = ',I5,/,5X,
     4'TOTAL NO. OF ORIGINAL SUBASSEMBLIES = ',I5,/,5X,'TOTA
     C  L NO. OF ORI
     5GINAL FINITE ELEMENTS = ',I5,/,5X,'RATIO OF STANDARD L
     C  OAD INCREMEN
```

```
     6T TO INITIAL LOADING = ',D14.6,/)
C      PUT ALL ELEMENT NICKNAMES IN LONG VECTOR, NIX.
       IF(NOPT2.EQ.0) GO TO 12
       CALL GMESH(NOOS,NOOM,NSU,LVEND)
       GO TO 2489
   12  DO 10 NELEM=1,NSU
       IJKL=NIXEND-8*NELEM
       I=IJKL+1
       J=IJKL+7
C      LONGER TYPE INPUT. SUBASSEMBLY INFORMATION
       READ(5,900) KUREL,(NIX(IJ),IJ=I,J)
       JWHERE=2
       IF(KUREL.LE.0) GO TO 130
       IF(KUREL.LE.LVMAX) GO TO 6
       LVMAX=KUREL
       JWHERE=3
       IF(LVMAX.GT.LVEND) GO TO 130
    6  JWHERE=5
       IF(NIZZ+KUREL+8*NELEM.GT.NIXEND) GO TO 130
C      LONGER TYPE INPUT. DEGREES OF FREEDOM FOR SUBASSEMBLY
       READ(5,900) (LVABL(I),I=1,KUREL)
       WRITE(6,9001) NELEM,(LVABL(I),I=1,KUREL)
 9001  FORMAT(5X,'SUBASSEMBLY ',I5,5X,'D.O.F.S',/,8(39X,10I5,
     C  /))
       DO 8 I=1,KUREL
       NIC=LVABL(I)
       JWHERE=6
       IF(NIC.LE.0) GO TO 130
       NIZZ=NIZZ+1
       NIX(NIZZ)=-NIC
       J=I
    7  J=J+1
       IF(J.GT.KUREL) GO TO 8
       IF(LVABL(J).EQ.NIC) WRITE(6,834) JWHERE,NIC
       GO TO 7
    8  CONTINUE
   10  NIX(8+IJKL)=NIZZ
 2489  DO 4 I=1,MVEND
    4  MVABL(I)=0
       N1=1
       MCONN=0
       WRITE(6,9002)
 9002  FORMAT(3X,'SUBASSEMBLY',3X,'KUREL',5X,'KL1',5X,'NTYPE'
     C  ,7X,'NRE',7X
     1,'KL2',7X,'LIKE',7X,'KE',8X,'NX',/)
       DO 26 NELEM=1,NSU
       LPREQ =LCUREQ
       LCUREQ=NVABZ
       IJKL=NIXEND-8*NELEM
       NZ = NIX(8+IJKL)
       NTYPE=NIX(2+IJKL)
       IF(NTYPE.EQ.-2) KOFAIL=KOFAIL+1
       IF(NTYPE.NE.3) GO TO 4441
       NX=NIX(IJKL+7)
```

```
      NVH=(NX+1)*2
 4441 LIKE=NIX(5+IJKL)
      KL2=NIX(4+IJKL)
      NRE=NIX(3+IJKL)
      KE=NIX(6+IJKL)
      KL1 = NIX(1+IJKL)
      KUREL = NZ-N1+1
      WRITE(6,9003) NELEM,KUREL,KL1,NTYPE,NRE,KL2,LIKE,KE,NX
 9003 FORMAT(9(5X,I5))
      LZ=(KUREL+1)*KUREL/2
      DO 22 NEW=N1,NZ
      NIC=NIX(NEW)
      LDES=NIC
      IF(NIC.GT.0) GO TO 20
      IF(MAXNIC+NIC.LT.0) MAXNIC=-NIC
      NCOR16=MAXPA
      IF(NCOR16.EQ.0) NCOR16=1
      DO 14 LDES=1,NCOR16
      IF(MVABL(LDES).EQ.0) GO TO 16
   14 CONTINUE
      LDES=NCOR16+1
   16 MVABL(LDES)=NIC
      IF(LDES.GT.MAXPA) MAXPA=LDES
      JWHERE=7
      IF(MAXPA.GT.MVEND) GO TO 130
      KOUNT=1000
C     RECORD FIRST, LAST AND INTERMEDIATE APPEARANCES
      DO 18 LAS=NEW,NIZZ
      IF(NIX(LAS).NE.NIC) GO TO 18
      NIX(LAS)=LDES
      KOUNT=KOUNT+1000
      LAST=LAS
   18 CONTINUE
      NIX(LAST)=LDES+1000
      LDES=LDES+KOUNT
      NIX(NEW)=LDES
   20 LDEST(NEW-N1+1)=LDES
   22 CONTINUE
      N1=NZ+1
C     RECONSTRUCT ELEMENT NICKNAMES AND COUPLE WITH DESTINAT
C       ION VECTORS
C     AND INITIAL ELEMENT STIFFNESS AND LOAD DATA
      DO 24 KL=1,KUREL
      CALL CODEST
      NIC=-MVABL(LDES)
      LVABL(KL)=NIC
      IF(NSTRES.NE.0. AND .NSTRES.NE.1) GO TO 24
      MVABL(LDES)=0
      NVABZ=NVABZ+1
   24 CONTINUE
      IF (KL1.GE.0) GO TO 305
      KL1 = -KL1
      LIKE=JJ(KL1)
      NCON=NCONVE(KL1)
```

```
      IF(NCON.EQ.0) GO TO 1113
      IALPHA=IALPHA+1
      KCONN(IALPHA)=LCONN(KL1)
 1113 DO 1002 I=1,LZ
 1002 EL(I) = STORE(LOC(KL1)-1+I)
      GO TO 320
  305 IF(NTYPE.GE.0) GO TO 1906
      LND(2)=4
      IF(LIKE.LT.0) GO TO 1907
C     CONNECTION TEST DATA INPUT
      MCONN=MCONN+1
      READ(5,1905) NCDAT,(X(I,MCONN),Y(I,MCONN),I=1,NCDAT)
 1905 FORMAT(I5,5X,7F10.6,10(/,8F10.6))
      IF(LIKE.NE.0) NIX(NIXEND+2*LIKE-1)=MCONN
      IF(LIKE.NE.0) NIX(NIXEND+2*LIKE)=NCDAT
      IF(NCDAT.EQ.1) GO TO 1907
      NCDATA=NCDAT
      IF(Y(NCDAT,MCONN).LT.0.) NCDATA=NCDAT-1
      DO 3273 M=2,NCDATA
 3273 Z(M-1,MCONN)=(Y(M,MCONN)-Y(M-1,MCONN))/(X(M,MCONN)-X(M
     C  -1,MCONN))
 1907 NCON=NTYPE
      IF(LIKE.LT.0) MCONN=NIX(NIXEND-2*LIKE-1)
      IF(LIKE.LT.0) NCDAT=NIX(NIXEND-2*LIKE)
      IALPHA=IALPHA+1
      KCONN(IALPHA)=MCONN+NCDAT*100
      NTYPE=1
      GO TO 321
 1906 NCON=0
  321 IF(KL1.EQ.0) GO TO 4258
      NCONVE(KL1)=NCON
      LCONN(KL1)=MCONN+NCDAT*100
C     ASSEMBLE SUBASSEMBLY STIFFNESS COEFFICIENTS
 4258 CALL SUBK(MCONN)
      LND(2)=2
  320 IF(NCON.NE.0) NTO(IALPHA)=(KUREL+2)/4
      IF(KL2.EQ.0) GO TO 319
C     LOADS ON SUBASSEMBLY
      READ(5,600) (NDOF(I),PP(I),I=1,KL2)
  600 FORMAT(4(I5,5X,F10.6))
      NCON=NCON+10
      NPM=LZ+1
      LZ=LZ+KUREL
      DO 1008 I=NPM,LZ
 1008 EL(I)=0.
      DO 1005 I=1,KL2
      P=P+PP(I)*PP(I)
 1005 EL(NDOF(I)+NPM-1)=PP(I)
  319 IF (NRE.EQ.0) GO TO 304
C     SUPPORTED DEGREES OF FREEDOM
      READ (5,900) (NR(I),I=1,NRE)
      DO 1007 I = 1,NRE
      NP = NR(I)+(NR(I)*(NR(I)-1))/2
      NRA(I+NRAT)=LVABL(NR(I))
```

```
 1007 EL(NP) = EL(NP) + 1.0D+20
      NRAT=NRAT+NRE
  304 WRITE(1) KUREL,LPREQ,LIKE,NCON,(LVABL(I),LDEST(I),I=1,
     C  KUREL),
     1   LZ,(EL(I),I=1,LZ)
   26 CONTINUE
      REWIND 1
      KCOUNT=IALPHA
C     PRE-PROGRAM ENDED AND SUBASSEMBLY RECORDS WRITTEN
C     ESTABLISH STOREAGE REQUIREMENTS AND AREA BOUNDARIES
   34 NELZ=NFUNC(0,LVMAX+1)*INITL+LVMAX
      IF(NELZ.GT.MAXELT) NELZ=MAXELT
      NPAR=NFUNC(0,MAXPA+1)*INITL+NELZ
      IF(INITL.EQ.0) GO TO 36
      NPAZ=MAXNIC+MAXPA
      N=NPAR+MAXPA*2
      IF(N.GT.NPAZ) NPAZ=N
      NBAXO=NPAZ+1
      IBA=NBAXO
      NBAXZ=NBAXO+MAXTAP
      IF(NBAXZ.GT.NELPAZ) NBAXZ=NELPAZ
      NBUFFA=NBAXZ-NBAXO
      JWHERE=9
      IF (NBUFFA.LT.MAXPA+4) GO TO 130
      NRUNO=NPAZ-MAXPA
   36 NCOR1=NBAXO+INITL*NBUFFA
      DO 38 I=1,NCOR1
   38 ELPA(I)=0.0
      KURPA=0
      IF(ICONV.EQ.-1) NCONV=1
      IF(NSOL.EQ.0) REWIND KDISC
      IF(NCONV.EQ.1) WRITE(6,5555) NINT
 5555 FORMAT(//,5X,'RESULTS FOR END OF LOAD INCREMENT',I5,'
     C   BEYOND ELAS
     1TIC LIMIT',//)
C     SEEK AND ASSEMBLE NEW SUBASSEMBLY
      DO 90 NELEM=1,NSU
      IF (INITL.EQ.0) GO TO 39
      READ(1) KUREL,LPREQ,LIKE,NCON,(LVABL(I),LDEST(I),I=1,K
     C  UREL)
     1,LZ,(ELPA(I),I=1,LZ)
      IF(NCON.GT.0) GO TO 4443
      NPM=LZ+1
      LZ=LZ+KUREL
      DO 4442 I=NPM,LZ
 4442 ELPA(I)=0.
      GO TO 41
 4443 NCON=NCON-10
      GO TO 41
   39 BACKSPACE 1
      IF(IACC.EQ.1.OR.NACC.EQ.5.OR.(ITER.EQ.0.AND.NINT.EQ.1)
     C  ) GO TO 45
      READ(1) KUREL,LPREQ,LIKE,NCCN,(LVABL(I),LDEST(I),ELPA(
     C  I),I=1,
```

```
     1KUREL)
      GO TO 47
   45 READ(1) KUREL,LPREQ,LIKE,NCON,(LVABL(I),LDEST(I),I=1,K
     C  UREL)
      IF(NCON.EQ.0) GO TO 53
      NSTOR=NSTOR-KUREL
      DO 51 I=1,KUREL
   51 ELPA(I)=STORE(NSTOR+I)
      GO TO 47
   53 DO 55 I=1,KUREL
   55 ELPA(I)=0.
   47 BACKSPACE 1
   41 WRITE(2) KUREL,LPREQ,LIKE,NCON,(LVABL(I),LDEST(I),I=1,
     C  KUREL),
     1 IBA,(ELPA(I),I=NBAXO,IBA)
      IF(NSOL.EQ.0) GO TO 43
      JWHERE=10
      IF(LZ.GT.NELZ. OR .LZ.LE.0) GO TO 130
   43 IBA=NBAXO
      NEW=1
      L=0
      DO 40 KL=1,KUREL
      CALL CODEST
      MVABL(LDES)=LVABL(KL)
      LVABL(KL)=LDES
   40 IF(LDES.GT.KURPA) KURPA=LDES
      NCOR2=2-INITL
      DO 66 LHSRHS=NCOR2,2
      LHS=2-LHSRHS
      IRHS=1-LHS
      NCOR3=LHS*KUREL+IRHS
      DO 66 KL=1,NCOR3
      GO TO (42,44),LHSRHS
   42 KG=LVABL(KL)
      MGO=NFUNC(0,KG)+NELZ
      GO TO 46
   44 MGO=(KL-1)*MAXPA+NPAR
   46 NCOR4=LHS*KL+IRHS*KUREL
      DO 66 IL=1,NCOR4
      IG=LVABL(IL)
      L=L+1
   48 CE=ELPA(L)
      GO TO (50,56),LHSRHS
   50 IF(KG-IG) 52,54,56
   52 MG=NFUNC(KG,IG)+NELZ
      GO TO 66
   54 IF(KL.NE.IL) CE=CE+CE
   56 MG=MGO+IG
   66 ELPA(MG)=ELPA(MG)+CE
      IF(NSOL.EQ.0) GO TO 57
      JWHERE=12
      IF(L.NE.LZ) GO TO 130
C     ELIMINATE VARIABLE IN POSITION LDES, AND WRITE EQUATIO
C       N FOR TAPE
```

```
   57 DO 90 KL=1,KUREL
      CALL CODEST
      IF(NSTRES.NE.0. AND .NSTRES.NE.1) GO TO 90
   68 NDEQN=IBA+KURPA+4
      IF(NDEQN.LE.NBAXZ. AND .NEW.EQ.0) GO TO 70
      IF(NEW.EQ.0) WRITE(2) IBA,(ELPA(I),I=NBAXO,IBA)
      IBA=NBAXO
      NEW=0
      IF(INITL.NE.0) GO TO 68
      BACKSPACE 1
      READ(1) NBZ,(ELPA(I),I=NBAXO,NBZ)
      BACKSPACE 1
      GO TO 68
   70 IBDIAG=IBA+LDES
      NDIAG=IBDIAG
      IF(INITL.NE.0) NDIAG=NFUNC(0,LDES+1)+NELZ
      PIVOT=ELPA(NDIAG)
      ELPA(NDIAG)=0.0
      JWHERE=13
      IF(PIVOT.EQ.0) GO TO 130
      MGZ=NELZ
      JGZ=KURPA
      IBO=IBA
      IF(INITL.EQ.0) IBA=IBA+KURPA
      NCOR5=2-INITL
      DO 84 LHSRHS=NCOR5,2
      IF(LHSRHS.EQ.2) JGZ=1
      DO 84 JG=1,JGZ
      IBA=IBA+1
      GO TO (72,76),LHSRHS
   72 MGO=MGZ
      MGZ=MGO+JG
      IF(LDES.GT.JG) GO TO 74
      MG=MGO+LDES
      GO TO 78
   74 MG=NFUNC(JG,LDES)+NELZ
      GO TO 78
   76 MGO=(JG-1)*MAXPA+NPAR
      MG=MGO+LDES
      MGZ=MGO+KURPA
   78 NDELT=IBO-MGO
      CONST=ELPA(MG)
      ELPA(IBA)=CONST
      IF(CONST.EQ.0) GO TO 84
      CONST=CONST/PIVOT
      ELPA(MG)=0.0
      IF(INITL.NE.LHSRHS) GO TO 80
C     SIMULTANEOUSLY, CREATE A SIMPLE ROUNDOFF CRITERION
      MG=NPAR+MAXPA+JG
      ELPA(MG)=ELPA(MG)+ELPA(MGZ)**2
   80 NCOR6=MGO+1
      DO 82 I=NCOR6,MGZ
   82 ELPA(I)=ELPA(I)-CONST*ELPA(I+NDELT)
   84 CONTINUE
```

```
      ELPA(IBDIAG)=PIVOT
      IBA=NDEQN
      ELPA(IBA)=KURPA
      ELPA(IBA-1)=LDES
      NIC=MVABL(LDES)
      ELPA(IBA-2)=NIC
      IF(INITL.EQ.0) GO TO 88
      MG=NPAR+MAXPA+LDES
      CRIT = DSQRT(ELPA(MG))/DABS(PIVOT)
      ELPA(MG)=0.0
      JWHERE=14
      IF(CRIT.GT.1.0E8) GO TO 130
      JWHERE = 15
      IF(CRIT.GT.1.0E4. OR .PIVOT.LT.0.)
     1 WRITE(6,834) JWHERE,NIC,CRIT,PIVOT,LZ,NELZ,NELEM
   88 MVABL(LDES)=0
      IF(MVABL(KURPA).NE.0) GO TO 90
      KURPA=KURPA-1
      IF(KURPA.NE.0) GO TO 88
   90 CONTINUE
      DO 94 I=1,NELZ
   94 ELPA(I)=0.0
C     BACK-SUBSTITUTE INTO EQUATIONS, TAKEN IN REVERSE ORDER
      IF(NSOL.EQ.0) REWIND KDISK
      IF(INITL.NE.0) REWIND 1
      INITL=0
      MDISK=KDISK
      KDISK=KDISC
      KDISC=MDISK
      NBZ=IBA
      NEQ=NVABZ
      LPREQ=LCUREQ
      NELEM=NSU
      IALPHA=KCOUNT
      RNORM=0.
      LPASS=0
      NSTOR=MSTOR
      IF(NACC.EQ.5) NACC=0
      NACC=NACC+1
      IF(NACC.EQ.3.AND.(NCONV.EQ.1.OR.NEWRHS.EQ.-1)) NACC=1
  100 IF(IBA.NE.NBAXO) GO TO 102
      BACKSPACE 2
      READ(2) NBZ,(ELPA(I),I=NBAXO,NBZ)
      BACKSPACE 2
      IBA=NBZ
  102 KURPA=ELPA(IBA)
      LDES=ELPA(IBA-1)
      NIC=ELPA(IBA-2)
      IBAR=IBA-4
      IBA=IBAR-KURPA
      IBDIAG=IBA+LDES
      PIVOT=ELPA(IBDIAG)
      ELPA(IBDIAG)=0.0
      MGO=NRUNO
```

```
      MGZ=MGO+KURPA
      CONST=ELPA(IBAR+1)
      NDELT=IBA-MGO
      NCOR8=MGO+1
      DO 104 I=NCOR8,MGZ
  104 CONST=CONST-ELPA(I)*ELPA(I+NDELT)
C     PLACE ANSWERS AND PREPARE FOR NEW ITERATIVE LOOP
      ANSWER=CONST/PIVOT
      ELPA(MGO+LDES)=ANSWER
      ELPA(NIC)=ANSWER
      IF(NACC.EQ.2) ELPA(NELPAZ+NIC)=ANSWER
  106 ELPA(IBDIAG)=PIVOT
      IF(IBA.EQ.NBAXO. AND .NEWRHS.EQ.1)
     1   WRITE(1) NBZ,(ELPA(I),I=NBAXO,NBZ)
      NEQ=NEQ-1
  108 IF(NEQ.NE.LPREQ) GO TO 100
      BACKSPACE 2
      READ(2) KUREL,LPREQ,LIKE,NCON,(LVABL(I),LDEST(I),I=1,K
     C  UREL),
     1   NBZ,(ELPA(I),I=NBAXO,NBZ)
      BACKSPACE 2
      IBA=NBZ
      IF((NSOL.EQ.1.OR.NACC.EQ.3).AND.NEWRHS.EQ.1) WRITE(1)
     C  KUREL,LPREQ,
     1LIKE,NCON,(LVABL(I),LDEST(I),I=1,KUREL)
      IF(NCON.EQ.0) GO TO 1810
C     PLACE ANSWERS FOR CONNECTION SUBASSEMBLIES ALSO
      DO 112 KL=1,KUREL
      CALL CCDEST
      IF(NACC.EQ.3) GO TO 109
      EL(KL)=ELPA(NRUNO+LDES)
      IF(IACC.EQ.1) EL(KL)=EL(KL)-ELPA(NELPA1+NSTOR+KL)
      GO TO 112
  109 STORE(NSTOR+KL)=ELPA(NRUNO+LDES)
  112 CONTINUE
      NSTOR=NSTOR+KUREL
  117 IF(NACC.EQ.3) GO TO 99
  113 NOP=0
      KKE=0
  907 KKE=KKE+2
  957 PPM=KKE/2
      IF (DCOS(PPM*PI)) 95,3,3
   95 S1=EL(KKE)-EL(KKE-1)
      IF(KKE.LT.KUREL) GO TO 907
      S2=0.
      KKE=KKE+2
      GO TO 2793
    3 S2= EL(KKE)-EL(KKE-1)
 2793 NOP=NOP+1
      NKKE=KKE/2
      EL(NKKE-1)=S1*SSK(1,1,LIKE)
      EL(NKKE)=S2*SSK(1,1,LIKE)
      IF (NSOL.EQ.0) GO TO 908
C     FIND FACTOR TO ELASTIC LIMIT
```

```
      IF(NCON.NE.-1) GO TO 2788
      EQVEC(NOP)=EL(NKKE-1)*EL(NKKE-1)
      SQE=EL(NKKE)*EL(NKKE)
      IF(EQVEC(NOP).LT.SQE) EQVEC(NOP)=SQE
      GO TO 2790
 2788 EQVEC(NOP)=EL(NKKE-1)*EL(NKKE-1)+EL(NKKE)*EL(NKKE)
 2790 IF (NOP.NE.NTO(IALPHA)) GO TO 907
      NCONVE(IC/2)=NCON
      LCONN(IC-1)=LIKE
      LCONN(IC)=KUREL
      NTO(IALPHA)=NELEM
      IC=IC+2
      NSTOR=NSTOR-KUREL
      KOU=KUREL/2
      DO 222 IJ=1,KOU
  222 STORE(NSTOR+IJ)=EL(IJ)
      NSTOR=NSTOR+KUREL
      YDFMAX=EQVEC(1)
      DO 11 IJ=2,NOP
   11 IF(EQVEC(IJ).GT.YDFMAX) YDFMAX=EQVEC(IJ)
      MCONN=KCONN(IALPHA)
      DO 5000 I=1,10000
      IF(MCONN.LT.100) GO TO 5001
 5000 MCONN=MCONN-100
 5001 YDF(IALPHA)=Y(1,MCONN)/DSQRT(YDFMAX)
      IALPHA=IALPHA-1
      IF(IALPHA.NE.0) GO TO 99
      ALPMAX=YDF(1)
      DO 15 KJ=2,KCOUNT
   15 IF(YDF(KJ).LT.ALPMAX) ALPMAX=YDF(KJ)
C     ALPMAX IS THE FACTOR TO ELASTIC LIMIT
      WRITE(6,1901) ALPMAX
 1901 FORMAT(///,6X,'STRUCTURAL FACTOR TO ELASTIC LIMIT =',D
     C  20.8,//)
      P=P*FACTOR
      FPNORM=P*((ALPMAX+PINF)**2)
      CALL PLAST(NOPT1,NOPT3)
      GO TO 99
  908 IF(KKE.LT.KUREL) GO TO 907
      IF((NCONV.EQ.1.OR.NOPT3.NE.0.OR.NEWRHS.EQ.-1).AND.IALP
     C  HA.EQ.KCOUNT
     1) WRITE(6,5007)
 5007 FORMAT(/,10X,' CONNECTION SPRING ELEMENTS INTERNAL FOR
     C  CES',/)
      CALL PLAST(NOPT1,NOPT3)
      IF(NACC.LT.4) GO TO 909
      DO 747 I=1,KUREL
  747 STORE(NSTOR+I)=RES(I)
      NSTOR=NSTOR+KUREL
      IC=IC+2
      IF(IC.LE.2*KCOUNT) GO TO 738
      IF(NACC-4) 130,740,732
 1810 IF(NSOL.EQ.1.OR.NACC.EQ.3) GO TO 99
      DO 1817 I=1,KUREL
```

```
 1817 RES(I)=0.
  909 IF(NEWRHS.EQ.1) WRITE(1) KUREL,LPREQ,LIKE,NCON,(LVABL(
     C  I),
     1LDEST(I),RES(I),I=1,KUREL)
   99 DO 116 KL=1,KUREL
      CALL CODEST
      IF(NSTRES.LE.0) GO TO 116
      NIC=LVABL(KL)
  116 CONTINUE
      NELEM=NELEM-1
      IF(NELEM.NE.0) GO TO 108
      IF (NSOL.EQ.0) GO TO 97
      DO 101 I=1,MAXNIC
  101 STORE(I)=ALPMAX*ELPA(I)
      IF(NOPT1.EQ.0) GO TO 732
C     FIRST ORDER DEFLECTIONS CORRESPONDING TO STANDARD LOAD
C        INCREMENT
C     TO BE WRITTEN ON UNIT 3
      DO 762 I=1,MAXNIC
  762 ELPA(I)=PINF*ELPA(I)
      MINREC=1
      IRW=1
      IF(MAXNIC.LE.MAXTAP) GO TO 5016
      IRW=MAXNIC/MAXTAP
      DO 5010 I=1,IRW
      MAXREC=I*MAXTAP
      WRITE(3) MINREC,MAXREC,(ELPA(J),J=MINREC,MAXREC)
 5010 MINREC=MINREC+MAXTAP
      IF(MAXREC.EQ.MAXNIC) GO TO 732
      IRW=IRW+1
 5016 MAXREC=MAXNIC
      WRITE(3) MINREC,MAXREC,(ELPA(J),J=MINREC,MAXREC)
      GO TO 732
   97 DO 731 I=1,MAXNIC
  731 STORE(I)=ELPA(I)+STORE(I)
      IACC=0
      IF (NACC.EQ.3) GO TO 6658
  732 IF(NEWRHS.EQ.-1) GO TO 5050
      IF(NOPT3.EQ.0.AND.NSOL.EQ.0.AND.NCONV.NE.1) GO TO 5005
C     PRINT DEFLECTIONS AND SUPPORT REACTIONS
 5050 WRITE(6,5006)
 5006 FORMAT(/,10X,' DEFLECTIONS',/)
      DO 400 I=1,NRAT
  400 EL(I) =STORE(NRA(I))*(-1.0D+20)
  729 WRITE (6,840) (I,STORE(I),I=1,MAXNIC)
  840 FORMAT(5(4H DOF,I4,2X,D14.6))
      WRITE (6,843)
  843 FORMAT (1H0)
      WRITE (6,841) (NRA(I),EL(I),I=1,NRAT)
  841 FORMAT (6X,32HREACTION ASSOCIATED WITH DOF NO.,I5,3H I
     C  S,D20.8)
      IF(NOPT1.EQ.0) STOP
 5005 GO TO (6659,6660,6652,742),NACC
 6659 IF(NSOL.EQ.1) GO TO 733
```

```
 6660 IF(MFAIL.EQ.KOFAIL.AND.NCONV.EQ.0) GO TO 4548
      IF(NCONV.EQ.0) MFAIL=0
      IF(NCONV.EQ.0) GO TO 734
      DO 5020 I=1,IRW
 5020 READ(3) MINREC,MAXREC,(ELPA(J),J=MINREC,MAXREC)
  733 DO 730 I=1,MAXNIC
  730 STORE(I)=STORE(I)+ELPA(I)
  734 IF(NACC.NE.3.OR.NEWRHS.EQ.-1) GO TO 736
C     MODIFIED AITKEN ACCELERATOR.  S IS THE ACCELERATION FA
C       CTOR
 6658 DENOM=0.
      ZNUM=0.
      DO 735 I=1,MAXNIC
      SQE=ELPA(I)
      IF(DABS(SQE).LT.1.E-12) SQE=0.
      EL6=ELPA(I+NELPAZ)
      IF(DABS(EL6).LT.1.E-12) EL6=0.
      DENOM=DENOM+(SQE-EL6)**2
  735 ZNUM=ZNUM-(SQE-EL6)*SQE
      S=ZNUM/DENOM
      IF(S.LE.0.) GO TO 7001
      KACC=KACC+1
      IF(NOPT3.EQ.1) GO TO 732
      NACC=4
      GO TO 6655
 7001 IF(NOPT3.EQ.1) WRITE(6,6653) S
 6653 FORMAT(//,'ACCELERATION FACTOR IS ',D20.8,' .NO ACCELE
     C  RATION DONE.
     1 ITERATION CONTINUES')
      NACC=5
      GO TO 6655
 6652 DO 737 I=1,MAXNIC
      ELPA(I)=S*ELPA(I)
  737 STORE(I)=STORE(I)+ELPA(I)
      WRITE(6,2000)
 2000 FORMAT(10X,'ACCELERATED VALUES ARE')
      NACC=4
      GO TO 732
  742 DO 751 I=1,MAXNIC
  751 STORE(I)=STORE(I)-ELPA(I)
 6655 IC=2
      NSTOR=MSTOR
  738 NCON=NCONVE(IC/2)
      LIKE=LCONN(IC-1)
      KUREL=LCONN(IC)
      IF(NACC.EQ.4) GO TO 6656
      DO 6657 I=1,KUREL
 6657 EL(I)=STORE(NSTOR+I)
      GO TO 113
 6656 DO 739 I=1,KUREL
      EL(I)=STORE(NSTOR+I)*(S+1.)
  739 ELPA(NELPA1+NSTOR+I)=EL(I)-STORE(NSTOR+I)
      GO TO 113
  740 NACC=0
```

```
      IACC=1
  736 ITER=ITER+1
      IF(NEWRHS.EQ.1) GO TO 1052
      WRITE(6,1903) MITER,ITER
 1903 FORMAT(10X,' NO CONVERGENCE IN  ',I4,'  ITERATIONS.RES
     C  ULTS GIVEN A
     1RE FOR ',I4,'  ITERATIONS')
      STOP
 1052 NSOL=0
      REWIND 3
      IF(ICONV.EQ.0.AND.ITER.EQ.MITER) NEWRHS=-1
C     GO BACK FOR NEW ITERATION IN SAME LOAD INCREMENT
      IF(NCONV.EQ.0) GO TO 34
      WRITE(6,1902) ITER,KACC
 1902 FORMAT(10X,' CONVERGED IN ',I4,' ITERATIONS AND ',I4,'
     C   ACCELERATIO
     1NS')
      IF(MFAIL.LT.KOFAIL) GO TO 4457
 4548 WRITE(6,4447)
 4447 FORMAT(//,5X,'FAILURE IN ALL PERIMETER CONNECTIONS')
      STOP
 4457 NACC=0
      IF(NINT.GE.NOPT1) STOP
C     GET READY FOR FIRST ITERATION OF NEW LOAD INCREMENT
      NINT=NINT+1
      KACC=0
      MFAIL=0
      ITER=0
      NCONV=0
      ICONV=0
      GO TO 34
C     ERROR DIAGNOSTICS AND FINISH
  130 WRITE(6,832)
  832 FORMAT(/6H ERROR)
      WRITE(6,834) JWHERE,NIC,CRIT,PIVOT,LZ,NELZ,NELEM,NRHS,
     1   NBUFFA,LVMAX,NIZZ,NELPAZ,LVEND,MVEND,NIXEND
      A=0.0
      A=1.0/A
  140 STOP
  834 FORMAT(/9H JWHERE =,I3,5X,5HNIC =,I4,5X,6HCRIT =,E9.2,
     C  3X,
     1   7HPIVOT =,E12.4,3X,4HLZ =,I5,11X,6HNELZ =,I5/
     2   8H NELEM =,I4,5X,6HNRHS =,I3,5X,8HNBUFFA =,I6,4X,
     3   7HLVMAX =,I5,10X,6HNIZZ =,I5,9X,8HNELPAZ =,I5/
     4   8H LVEND =,I4,5X,7HMVEND =,I4,3X,8HNIXEND =,I6)
  900 FORMAT(16I5)
      END
```

```
      SUBROUTINE CODEST
C     (INTERPRETS CODED ELEMENT DESTINATIONS FROM LDEST.)
      IMPLICIT REAL*8(A-H,O-Z)
      COMMON /BLK5/ MVABL(80),LVABL(40),LDEST(40),LND(8)
      COMMON /BLK7/ INITL,NEWRHS,NELEM,KUREL,LPREQ,
     1   LZ,NELZ,NBAXO,NBZ,KL,LDES,NSTRES,KK,LIKE,KOUNT,NX,N
     C  VH
      LDES=LDEST(KL)
      DO 2 NSTRES=1,1000000
      IF(LDES.LT.1000) GO TO 4
    2 LDES=LDES-1000
    4 NSTRES=NSTRES-2
      RETURN
      END
```

```
      SUBROUTINE PLATE(UXY,UYX,YL,XL,EX,EY,T,G)
C     ORTHOTROPIC PLANE STRESS ELEMENT STIFFNESS MATRIX GENER
C        ATOR
      IMPLICIT REAL*8(A-H,O-Z)
      DIMENSION S(8,8)
      COMMON /BLK6/ ELPA(7000),EL(860),JJ(40)
      EQUIVALENCE (S(1,1),ELPA(6101))
      A=EX/(1.-UXY*UYX)
      B=EY/(1.-UXY*UYX)
      C=EX*UYX/(1.-UXY*UYX)
      D=YL/XL
      DO 100 I = 1,7,2
      S(I,I) = T*((A*D/3.)+(G/(3.*D)))
  100 S(I+1,I+1) = T*((B/(3.*D))+(G*D/3.))
      S(2,1) = T*(C+G)/4.
      S(4,3) = -S(2,1)
      S(6,5) = S(2,1)
      S(8,7) = -S(2,1)
      S(3,2) = T*(-C+G)/4.
      S(5,4)= S(3,2)
      S(7,6) = S(3,2)
      S(4,1) = -S(3,2)
      S(6,3) = S(4,1)
      S(8,5) = S(4,1)
      S(5,2) = -S(2,1)
      S(7,4) = S(2,1)
      S(6,1) = -S(2,1)
      S(8,3) = S(2,1)
      S(7,2) = -S(3,2)
      S(8,1) = -S(7,2)
      S(3,1) = T*((-A*D/3.)+G/(6.*D))
      S(4,2) =-T*((-B/(6.*D))+(G*D/3.))
      S(5,3) = T*((A*D/6.)-(G/(3.*D)))
      S(6,4) = T*((-B/(3.*D))+(G*D/6.))
      S(7,5) = S(3,1)
      S(8,6) = S(4,2)
      S(5,1) = -S(1,1)/2.
      S(6,2) = -S(2,2)/2.
      S(7,3) = S(5,1)
      S(8,4) = S(6,2)
      S(7,1) = S(5,3)
      S(8,2) = S(6,4)
      DO 101 I = 2,8
      DO 102 J = 1,7
      IF (I.LE.J) GO TO 101
  102 S(J,I) = S(I,J)
  101 CONTINUE
      RETURN
      END
```

```
      SUBROUTINE BEAM(ALEN,ZI,AX,YM)
C     BEAM ELEMENT STIFFNESS MATRIX GENERATOR
      IMPLICIT REAL*8(A-H,O-Z)
      DIMENSION BMK(8,8)
      COMMON /BLK6/ ELPA(7000),EL(860),JJ(40)
      EQUIVALENCE (BMK(1,1),ELPA(6101))
      DO 100 I = 1,6
      DO 100 J = 1,6
  100 BMK(I,J) = 0.0
  108 BMK(1,1) = AX*YM/ALEN
      BMK(1,4) = -BMK(1,1)
      ST = ZI*YM
      BMK(2,2) = 12.*ST/ALEN**3
      BMK(2,3) = -6.*ST/ALEN**2
      BMK(2,5) = -BMK(2,2)
      BMK(2,6) = BMK(2,3)
      BMK(3,3) = (4.*ST/ALEN)
      BMK(3,5) = -BMK(2,3)
      BMK(3,6) = (2.*ST/ALEN)
      BMK(4,4) = BMK(1,1)
      BMK(5,5) = BMK(2,2)
      BMK(5,6) = BMK(3,5)
      BMK(6,6) = BMK(3,3)
      DO 109 I = 2,6
      DO 109 J = 1,5
      IF (I.LE.J) GO TO 109
      BMK(I,J) = BMK(J,I)
  109 CONTINUE
      RETURN
      END
```

```
      SUBROUTINE COLUM(ALEN,ZI,AX,YM)
C     COLUMN ELEMENT STIFFNESS MATRIX GENERATOR
      IMPLICIT REAL*8(A-H,O-Z)
      DIMENSION CLK(8,8)
      COMMON /BLK6/ ELPA(7000),EL(860),JJ(40)
      EQUIVALENCE (CLK(1,1),ELPA(6101))
      DO 100 I = 1,6
      DO 100 J = 1,6
  100 CLK(I,J) = 0.0
  104 SZ = YM*ZI
      CLK(1,1) = 12.*SZ/ALEN**3
      CLK(1,3) = 6.*SZ/ALEN**2
      CLK(1,4) = -CLK(1,1)
      CLK(1,6)=CLK(1,3)
      CLK(2,2) = AX*YM/ALEN
      CLK(2,5) = -CLK(2,2)
      CLK(3,3) = (4.*SZ/ALEN)
      CLK(3,4) = -6.*SZ/ALEN**2
      CLK(3,6) = (2.*SZ/ALEN)
      DO 103 I = 1,3
  103 CLK(I+3,I+3) = CLK(I,I)
      CLK(4,6) = CLK(3,4)
      DO 105 I = 2,6
      DO 105 J = 1,5
      IF (I.LE.J) GO TO 105
      CLK(I,J) = CLK(J,I)
  105 CONTINUE
      RETURN
      END
```

```
      SUBROUTINE SUBK(MCONN)
C     GENERATES ELEMENT D.O.F. IN SUBASSEMBLY NUMBERING
C     SYSTEM AND ASSEMBLES SUBASSEMBLY STIFFNESS
C     COEFFICIENTS
      IMPLICIT REAL*8(A-H,O-Z)
      DIMENSION NVABL(8),SK(8,8)
      COMMON /BLK2/ S1,S2,ALPMAX,PINF,CYP,NCON,NSOL,KDISK,KD
     C  ISC,KOU,NOP,
     1NACC,NINT,MFAIL,JPASS,NTO(50),KCONN(50),LCONN(100)
      COMMON /BLK3/ STORE(2250),LOC(20),NCONVE(50)
      COMMON /BLK4/ SSK(8,8,15),X(10,5),Y(10,5),Z(9,5)
      COMMON /BLK5/ MVABL(80),LVABL(40),LDEST(40),LND(8)
      COMMON /BLK6/ ELPA(7000),EL(860),JJ(40)
      COMMON /BLK7/ INITL,NEWRHS,NELEM,KUREL,LPREQ,
     1   LZ,NELZ,NBAXO,NBZ,KL,LDES,NSTRES,KK,LIKE,KOUNT,NX,N
     C  VH
      COMMON /BLK8/ KE,KL1,NTYPE,NE
      EQUIVALENCE (SK(1,1),ELPA(6101)),(NVABL(1),ELPA(6201))
      DO 100 I=1,LZ
  100 EL(I)=0.0
  900 FORMAT (16I5)
      NPL=0
      NENO=0
      MEG=KE
      IF(KE.LT.0) KE=-KE
      IF(LIKE.GT.0) GO TO 118
      NENO=NENO+1
      LIKE=-LIKE
  118 DO 120 NE = 1,KE
      IF(MEG.LT.0) GO TO 988
C     GENERATE ELEMENT D. O. F. IN SUBASSEMBLY NUMBERING SYS
C       TEM
      IF(NCON.EQ.0) GO TO 981
      KKUREL=2
      NVABL(1)=2*NE-1
      NVABL(2)=2*NE
      GO TO 982
  981 IF(NTYPE.EQ.3) GO TO 983
      KKUREL=6
      DO 984 I=1,6
  984 NVABL(I)=3*NE-3+I
      GO TO 982
  983 KKUREL=8
      KCNE=NE-NX
      DO 985 I=1,1000
      IF(KONE.LE.1) GO TO 986
  985 KONE=KONE-NX
  986 IF(KONE.EQ.1) NPL=NPL+1
      J=1
      DO 987 I=1,4
      IF(I.EQ.3) J=-1
      NVABL(I)=2*NE-2+I+NPL*2
  987 NVABL(I+4)=NVH+NVABL(I)+J*2
      GO TO 982
```

```
  988 READ(5,900) KKUREL,(NVABL(I),I=1,KKUREL)
  982 NENO=NENO+1
      IF(NENO.GT.1) GO TO 743
C     INTRODUCE (ANOTHER) ORIGINAL FINITE ELEMENT
      GO TO (301,302,303), NTYPE
  301 IF(NCON.EQ.0) GO TO 304
      AX=Y(1,MCONN)/X(1,MCONN)
      ALEN=1.
      YM=1.
      ZI=0.
      GO TO 641
  304 READ(5,601) ALEN,ZI,AX,YM
  601 FORMAT(8F10.6)
  641 CALL BEAM(ALEN,ZI,AX,YM)
      GO TO 647
  302 READ(5,601) ALEN,ZI,AX,YM
      CALL COLUM(ALEN,ZI,AX,YM)
      GO TO 647
  303 READ(5,601) UXY,UYX,YL,XL,EX,EY,T,G
      CALL PLATE(UXY,UYX,YL,XL,EX,EY,T,G)
  647 IF(LIKE.EQ.0) GO TO 980
      DO 734 I = 1,KKUREL
      DO 734 J = 1,KKUREL
  734 SSK(I,J,LIKE)=SK(LND(I),LND(J))
      GO TO 980
  743 DO 755 I = 1,KKUREL
      DO 755 J = 1,KKUREL
  755 SK(LND(I),LND(J))=SSK(I,J,LIKE)
C     PLACE ELEMENT COEFFICIENTS IN SUBASSEMBLY MATRIX (EL)
  980 DO 103 I=1,KKUREL
      DO 103 J = 1,I
      IF (NVABL(J).LE .NVABL(I)) GO TO 141
      NP=NVABL(I)+(NVABL(J)*(NVABL(J)-1))/2
      GO TO 150
  141 NP = NVABL(J) + (NVABL(I)*(NVABL(I)-1))/2
  150 EL(NP)=SK(LND(J),LND(I))+EL(NP)
  103 CONTINUE
  120 CONTINUE
      IF (KL1.EQ.0) RETURN
      JJ(KL1)=LIKE
C     KEEP SUBASSEMBLY STIFFNESS COEFFICIENTS FOR FURTHER US
C       E
      DO 130 I = 1,LZ
  130 STORE(LOC(KL1)-1+I) = EL(I)
      LOC(KL1+1) = LOC(KL1) + LZ
      RETURN
      END
```

```
      SUBROUTINE PLAST(NOPT1,NOPT3)
C     ANALYZES CONNECTIONS IN THE NON-LINEAR RANGE
      IMPLICIT REAL*8(A-H,O-Z)
      DIMENSION OL(200),RES(40),OLD(100),CY(100),OU(20)
      COMMON /BLK1/ RNORM,FPNORM,P,PI,IALPHA,ICONV,NCONV,KCO
     C  UNT,NSTOR,
     1IC,LVMAX,NIZZ,LPASS,KUREL1,KOU1,NCYP1,MSTOR,KKE,NIXEND
      COMMON /BLK2/ S1,S2,ALPMAX,PINF,CYP,NCON,NSOL,KDISK,KD
     C  ISC,KOU,NOP,
     1NACC,NINT,MFAIL,JPASS,NTO(50),KCONN(50),LCONN(100)
      COMMON /BLK3/ STORE(2250),LOC(20),NCONVE(50)
      COMMON /BLK4/ SSK(8,8,15),X(10,5),Y(10,5),Z(9,5)
      COMMON /BLK5/ MVABL(80),LVABL(40),LDEST(40),LND(8)
      COMMON /BLK6/ ELPA(7000),EL(860),JJ(40)
      COMMON /BLK7/ INITL,NEWRHS,NELEM,KUREL,LPREQ,
     1   LZ,NELZ,NBAXO,NBZ,KL,LDES,NSTRES,KK,LIKE,KOUNT,NX,N
     C  VH
      EQUIVALENCE (OL(1),EL(100)),(RES(1),EL(301)),(OLD(1),E
     C  L(341))
      EQUIVALENCE (CY(1),EL(441)),(OU(1),EL(650))
      IF(NSOL.EQ.0) GO TO 3
C     RETRIEVE BASIC SUBASSEMBLY INFORMATION AND INITIALIZE
C       VARIABLES
      MFAIL=0
      WRITE(6,201)
  201 FORMAT(//,6X,'CONNECTION SPRING ELEMENTS INTERNAL FORC
     C  ES AT ELASTI
     1C LIMIT',//)
      IC=2
      NSTOR=MSTOR
      IALPHA=KOUNT
      A=ALPMAX+PINF
   32 NCON=NCONVE(IC/2)
      LIKE=LCONN(IC-1)
      KUREL=LCONN(IC)
      IC=IC+2
  410 SPS=SSK(1,1,LIKE)
      MCONN=KCONN(IALPHA)
      DO 420 I=1,10000
      IF(MCONN.LT.100) GO TO 421
  420 MCONN=MCONN-100
  421 NCDAT=I-1
      NCDATA=NCDAT
      IF(Y(NCDAT,MCONN).LT.0.) NCDATA=NCDAT-1
      KOU=KUREL/2
      NCYP=KOU
      IF(NCON.NE.-1) NCYP=KOU/2
      L=0
      AN=DCOS(KOU*PI)
      IF(AN.LT.0.) L=1
      KKE=0
      NKKE=0
      KOUNT=0
      IF(NSOL.EQ.0) GO TO 422
```

```
      DO 77 I=1,KOU
      EL(I)=STORE(NSTOR+I)
   77 OU(I)=ALPMAX*EL(I)
C     PRINT SPRING FORCES AT ELASTIC LIMIT
      WRITE(6,202) NTO(IALPHA),(I,OU(I),I=1,KOU)
      IF(NOPT1.NE.0) GO TO 15
      IALPHA=IALPHA-1
      GO TO 424
C     ACTUAL ANALYSIS AFTER FIRST SOLUTION STARTS HERE
   15 NKKE=NKKE+2
      KKE=KKE+4
      CYP=Y(1,MCONN)
      F1=EL(NKKE-1)
      KOUNT=KOUNT+1
C     DFP1, DFP2 REFLECT NEW LOAD INCREMENT  (SEE A)
      DFP1=A*F1
      OL(KUREL1+KOU+NKKE-1)=PINF*F1
      OLD(KOU1+NKKE-1)=ALPMAX*F1/SPS
      S1I=OL(KUREL1+KOU+NKKE-1)/SPS
      IF(KOUNT.EQ.KOU) GO TO 11
      IF(NCON.EQ.-1) CYP1=Y(1,MCONN)
      DFP2=A*EL(NKKE)
      KOUNT=KOUNT+1
      OL(KUREL1+KOU+NKKE)=PINF*EL(NKKE)
      OLD(KOU1+NKKE)=ALPMAX*EL(NKKE)/SPS
      S2I=OL(KUREL1+KOU+NKKE)/SPS
      IF(NCON.NE.-1) GO TO 10
C     SHEET TO SHEET SEAM CONNECTIONS ANALYSIS
   11 NTURN=1
      OLD(KOU1+NKKE-1)=OLD(KOU1+NKKE-1)+S1I
      PBAR=DABS(DFP1)
   17 YDFN=PBAR-CYP
      IF(YDFN.GT.0.) GO TO 18
      IF(NTURN.EQ.0) GO TO 56
      CY(NCYP1+NKKE-1)=CYP
      RES(KKE-2)=0.
      OL(KUREL1+NKKE-1)=DFP1
      IF(KOUNT.EQ.KOU) GO TO 31
  206 OLD(KOU1+NKKE)=OLD(KOU1+NKKE)+S2I
      CYP=CYP1
      PBAR=DABS(DFP2)
      NTURN=0
      GO TO 17
   18 SBAR=DABS(OLD(KOU1+NKKE-1))
      IF(NTURN.EQ.1) GO TO 106
      SBAR=DABS(OLD(KOU1+NKKE))
      GO TO 106
C     NON-LINEAR ANALYSIS IN RE-SOLUTION
    3 IF(LPASS.NE.0) GO TO 410
C     READY TO READ RECORD
      READ(KDISK) KUREL1,KOU1,NCYP1,(OL(I),I=1,KUREL1),(OLD(
     C  I),I=1,KOU1)
     1,(CY(I),I=1,NCYP1)
      KUREL1=0
```

```
      KOU1=0
      NCYP1=0
      GO TO 410
  422 NFAIL=0
      IF(NCONV.NE.1) GO TO 16
      DO 402 I=1,KOU
  402 OU(I)=OL(KUREL1+I)
C     PRINT SPRING FORCES IN RE-SOLUTION
      WRITE(6,202) NTO(IALPHA),(I,OU(I),I=1,KOU)
   16 KKE=KKE+4
      NKKE=NKKE+2
      CYP=CY(NCYP1+NKKE/2)
      IF(NCON.EQ.-1) CYP=CY(NCYP1+NKKE-1)
      F1=OL(KUREL1+NKKE-1)
      KOUNT=KOUNT+1
      IF(KOUNT.EQ.KOU) GO TO 33
      IF(NCON.EQ.-1) CYP1=CY(NCYP1+NKKE)
      F2=OL(KUREL1+NKKE)
      KOUNT=KOUNT+1
   33 IF(NCONV.EQ.1) GO TO 2
      DFP1=EL(NKKE-1)+F1
      S1I=EL(NKKE-1)/SPS
      IF(KOUNT.EQ.KOU.AND.L.EQ.1) GO TO 11
      DFP2=EL(NKKE)+F2
      S2I=EL(NKKE)/SPS
      IF(NCON+2) 10,10,11
    2 S1I=OL(KUREL1+KOU+NKKE-1)+EL(NKKE-1)
      DFP1=F1+S1I
      S1I=S1I/SPS
      IF(KOUNT.EQ.KOU.AND.L.EQ.1) GO TO 11
      S2I=OL(KUREL1+KOU+NKKE)+EL(NKKE)
      DFP2=F2+S2I
      S2I=S2I/SPS
      IF(NCON.EQ.-1) GO TO 11
   10 PBAR=DSQRT(DFP1*DFP1+DFP2*DFP2)
      OLD(KOU1+NKKE-1)=OLD(KOU1+NKKE-1)+S1I
      OLD(KOU1+NKKE)=OLD(KOU1+NKKE)+S2I
      YDFN=PBAR-CYP
      IF(YDFN.LT.0.) GO TO 5
      SBAR=DSQRT(OLD(KOU1+NKKE-1)**2+OLD(KOU1+NKKE)**2)
C     COMPARE RESULTANT DEFORMATION WITH CONNECTION CURVE AN
C       D FIND
C     CORRECT RESULTANT FORCE
  106 IF(SBAR.GT.X(1,MCONN).AND.SBAR.LT.X(NCDATA,MCONN)) GO
     C  TO 104
      IF(SBAR.GE.X(NCDATA,MCONN)) GO TO 303
      CYP=Y(1,MCONN)
      GO TO 105
  303 IF(NSOL.EQ.1) GO TO 304
      IF(NCON.EQ.-2) NFAIL=NFAIL+1
  304 CYP=Y(NCDATA,MCONN)
      IF(NCDATA.LT.NCDAT) CYP=0.
      GO TO 105
  104 DO 302 M=2,NCDATA
```

```
      IF(SBAR-X(M,MCONN)) 301,301,302
  301 CYP=Y(M-1,MCONN)+(SBAR-X(M-1,MCONN))*Z(M-1,MCONN)
      GO TO 105
  302 CONTINUE
C     FIND RESULTANT AND NODAL RESIDUAL FORCES
  105 RBAR=PBAR-CYP
      IF(NCON.EQ.-1) GO TO 14
      THETA=DABS(DATAN(DFP2/DFP1))
      RES(KKE-2)=RBAR*DCOS(THETA)*DABS(DFP1)/DFP1
      RES(KKE)=RBAR*DSIN(THETA)*DABS(DFP2)/DFP2
      CY(NCYP1+NKKE/2)=CYP
      OL(KUREL1+NKKE-1)=DFP1-RES(KKE-2)
      OL(KUREL1+NKKE)=DFP2-RES(KKE)
      GO TO 30
   14 IF(NTURN.EQ.1) GO TO 58
      RES(KKE)=RBAR*PBAR/DFP2
      OL(KUREL1+NKKE)=DFP2-RES(KKE)
      CY(NCYP1+NKKE)=CYP
      GO TO 30
   58 RES(KKE-2)=RBAR*PBAR/DFP1
      OL(KUREL1+NKKE-1)=DFP1-RES(KKE-2)
      CY(NCYP1+NKKE-1)=CYP
      IF(KOUNT.EQ.KOU.AND.L.EQ.1) GO TO 31
      GO TO 206
    5 RES(KKE-2)=0.
      OL(KUREL1+NKKE-1)=DFP1
      CY(NCYP1+NKKE/2)=CYP
   56 RES(KKE)=0.
      OL(KUREL1+NKKE)=DFP2
      IF(NCON.EQ.-1) CY(NCYP1+NKKE)=CYP
   30 RES(KKE-1)=-RES(KKE)
   31 RES(KKE-3)=-RES(KKE-2)
      IF(KKE.GT.KUREL) RES(KKE)=0.
      CALL CONV (RES(KKE-2),RES(KKE))
      IF(NSOL.EQ.0.) GO TO 13
   99 IF(KOU.NE.KOUNT) GO TO 15
  404 LPASS=LPASS+1
      KUREL1=KUREL1+KUREL
      KOU1=KOU1+KOU
      NCYP1=NCYP1+NCYP
      IF(LPASS.LT.JPASS.AND.IALPHA.NE.0) GO TO 406
      IF(NSOL-1) 405,403,403
  406 IF(NSOL-1) 408,12,12
C     WRITE RECORD ( AT THIS POINT AFTER ONLY INITIAL SOLUTI
C       ON)
  403 WRITE(8) KUREL1,KOU1,NCYP1,(OL(I),I=1,KUREL1),(OLD(I),
     C  I=1,KOU1),(C
     1Y(I),I=1,NCYP1)
      IF(IALPHA.EQ.0) GO TO 12
  407 LPASS=0
      IF(NSOL.EQ.0) RETURN
C     UP TO NEXT 'RETURN' FIRST SOLUTION ONLY
      KUREL1=0
      KOU1=0
```

```
      NCYP1=0
   12 DO 78 I=1,KUREL
   78 STORE(NSTOR+I)=RES(I)
  424 NSTOR=NSTOR+KUREL
   35 IF(IALPHA.NE.0) GO TO 32
      IF(NOPT1.NE.0) REWIND 8
      RETURN
C     RE-SOLUTION ONLY
   13 IF(KOU.NE.KOUNT) GO TO 16
      IF(NFAIL.EQ.NCYP) MFAIL=MFAIL+1
      IF((NCONV.EQ.1.OR.NOPT3.EQ.0).AND.NEWRHS.EQ.1) GO TO 4
     C  04
      KKOB=KUREL1+1
      KKOE=KUREL1+KOU
      KALPHA=IALPHA+1
C     PRINT SPRING FORCES IN RE-SOLUTIONS
      WRITE(6,202) NTO(KALPHA),(I,OL(I),I=KKOB,KKOE)
      GO TO 404
C     WRITE RECORDS IN RE-SOLUTION
  405 IF(NEWRHS.EQ.1) WRITE(KDISC) KUREL1,KOU1,NCYP1,(OL(I),
     C  I=1,KUREL1),
     1(OLD(I),I=1,KOU1),(CY(I),I=1,NCYP1)
      IF(IALPHA.GT.0) GO TO 407
  202 FORMAT(/,10X,'SUBASSEMBLY ',I3,/,4(2X,'ELEMENT',I3,2X,
     C  D16.8))
  408 RETURN
      END
```

```
      SUBROUTINE CONV (DFDP1,DFDP2)
C     CHECKS CONVERGENCE
      IMPLICIT REAL*8(A-H,O-Z)
      COMMON /BLK1/ RNORM,FPNORM,P,PI,IALPHA,ICONV,NCONV,KCO
     C  UNT,NSTCR,
     1IC,LVMAX,NIZZ,LPASS,KUREL1,KOU1,NCYP1,MSTOR,KKE,NIXEND
      COMMON /BLK2/ S1,S2,ALPMAX,PINF,CYP,NCON,NSOL,KDISK,KD
     C  ISC,KOU,NOP,
     1NACC,NINT,MFAIL,JPASS,NTO(50),KCONN(50),LCONN(100)
      COMMON /BLK7/ INITL,NEWRHS,NELEM,KUREL,LPREQ,
     1    LZ,NELZ,NBAXO,NBZ,KL,LDES,NSTRES,KK,LIKE,KOUNT,NX,N
     C  VH
      RNORM=RNORM+2.*(DFDP1*DFDP1+DFDP2*DFDP2)
      IF(KOU.NE.KOUNT) RETURN
      IALPHA=IALPHA-1
      IF(IALPHA.NE.0) RETURN
      WRITE(6,100) RNORM
  100 FORMAT(5X,' RES. FORCE NORM = ',D20.8)
      IF(NCONV.EQ.1.OR.NACC.EQ.4) RETURN
      IF(RNORM.LE.FPNORM) ICONV=-1
      IF(ICONV.NE.-1) RETURN
      FPNORM=P*((ALPMAX+(NINT+1)*PINF)**2)
      RETURN
      END
```

```
      SUBROUTINE GMESH(NOOS,NOOM,NSU,LVEND)
C     GENERATES DIAPHRAGM FINITE ELEMENT MESH D.O.F.
      IMPLICIT REAL*8(A-H,O-Z)
      DIMENSION NIX(12000),NCOMP(200),MSUB(100),NCEND(200),N
     C  CEDGE(100),
     1NSHARE(20),NXV(20),NYV(20),NCY(20),MPURC(20),MPURL(20)
     C  ,NPURC(500)
     2,NDV(20)
      COMMON /BLK1/ RNORM,FPNORM,P,PI,IALPHA,ICONV,NCONV,KCO
     C  UNT,NSTOR,
     1IC,LVMAX,NIZZ,LPASS,KUREL1,KOU1,NCYP1,MSTOR,KKE,NIXEND
      COMMON /BLK5/ NS(80),LVABL(40),NEV(40),LND(8)
      COMMON /BLK6/ ELPA(7000),EL(860),NSEAM(40)
      COMMON /BLK7/ INITL,NEWRHS,NELEM,KUREL,LPREQ,
     1   LZ,NELZ,NBAXO,NBZ,KL,LDES,NSTRES,KK,LIKE,KOUNT,NX,N
     C  VH
      EQUIVALENCE (NIX(1),ELPA(1)),(NCOMP(1),ELPA(6501)),(MS
     C  UB(1),ELPA(6
     1601)),(NCEND(1),ELPA(6656)),(NCEDGE(1),ELPA(6756)),(NS
     C  HARE(1),ELPA
     2(6806)),(NXV(1),ELPA(6816)),(NYV(1),ELPA(6826)),(NCY(1
     C  ),ELPA(6836)
     3),(MPURC(1),ELPA(6851)),(MPURL(1),ELPA(6871)),(NPURC(1
     C  ),EL(1))
C     READ BASIC MESH DATA
      READ(5,200) NA,NB,NC,ND,NE,NF1,NFB,NFB1,NFBB,NFBB1,NG,
     C  NGB,NGBB,NGB
     11,NGB2,NH,NHB,NBX,NBY,NPUR,(NS(I),I=1,NF1),(NEV(I),I=1
     C  ,NG),(NXV(I)
     2,I=1,NBX),(NYV(I),I=1,NBY),(NCY(I),I=1,NBY)
C     ARE THERE INTERMEDIATE PURLINS?
      IF(NPUR.EQ.0) GO TO 110
      READ(5,200) NPUR1,NPUR2,NPUR3,NPUR4,NPURB1,NPURB2,NSE,
     C  (MPURC(I),I=
     11,NA),(MPURL(I),I=1,NA)
      NSUM=0
      NPURN=0
      NPURL=0
      DO 111 I=1,NA
      NPURN=NPURN+MPURC(I)
  111 NPURL=NPURL+MPURL(I)
      NPUR5=0
      NPUR6=NPUR4
C     MATCH SUBASSEMBLY NUMBERS AND INITIALIZE VARIABLES
  110 READ(5,200) NCORR,(MSUB(I),I=1,NSU)
      IF(NCORR.EQ.1) READ(5,200) (NDV(I),I=1,NB)
      NDT=0
      DO 168 I=1,NB
      IF(NCORR.EQ.0) NDV(I)=ND
  168 NDT=NDT+NDV(I)
      NF=NSE*NPUR
      NG2=0
      NBX1=0
      NBY1=0
```

```
      DO 2 I=1,NF1
    2 NF=NF+NS(I)
      DO 4 I=1,NBX
    4 NBX1=NBX1+NXV(I)
      DO 6 I=1,NBY
    6 NBY1=NBY1+NYV(I)
      DO 80 I=1,NG
   80 NG2=NG2+NEV(I)*4
      NBD=2*(NDT+1)
      NFIRST=1
      NLAST=NBD*(NE*NC+1)
      LAST=NLAST
      NSUB=1
      NSPACE=(MSUB(1)-1)*LVEND+1
      NTOTAL=NA*NH*4
C     GENERATE D. O. F. NUMBERS FOR PLATE AND SEAM CONNECTIO
C       N
C     SUBASSEMBLIES.  OTHER CONNECTION D.O.F.S PARTIALLY GEN
C       ERATED IN
C     THIS LOOP
      DO 44 NP=1,NA
      NFIR=2*NFB+1
      NSFIR=2*NFB1+1
      K=1
      KK=1
      DO 12 I=NFIRST,NLAST
      IF(NP.EQ.1.OR.K.GT.NF) GO TO 10
      IF(NFIR-I+NFIRST-K) 10,8,10
    8 NCOMP(I-NFIRST+K)=I
      NCOMP(I-NFIRST+K+1)=NSHARE(K)
      IF(NSFIR-I+NFIRST-K) 150,148,150
  148 NSEAM(2*KK-1)=NSHARE(K)-1
      NSEAM(2*KK)=I
      KK=KK+1
      NSFIR=NSFIR+2*NFBB1
  150 NFIR=NFIR+2*NFBB
      K=K+1
      GO TO 12
   10 NCOMP(I-NFIRST+K)=I
   12 CONTINUE
      IF(NPUR.EQ.0) GO TO 108
      NUM=MPURC(NP)*4
      DO 112 MP=1,NPUR
      J=0
      NCONST=NPUR1*2+(MP-1)*NPUR2*2+NBD*(NPUR4+NPUR5)
      DO 112 I=4,NUM,4
      NPURC(I-3+(MP-1)*NPURN*4+NSUM)=NCOMP(1+NBD*NPUR3*J+NCO
     C  NST)
      NPURC(I-1+(MP-1)*NPURN*4+NSUM)=NCOMP(2+NBD*NPUR3*J+NCO
     C  NST)
  112 J=J+1
      NSUM=NSUM+NUM
      NPUR4=0
      IF(NSE.EQ.0) NPUR5=NPUR6
```

```
108 IF(NA.NE.1.AND.NP.EQ.NA) GO TO 38
    NSTART=NBD*NC*NE+(NFB+1)*2
    IF(NP.NE.1) GO TO 38
    NCTART=2*NGB+1
    DO 14 I=1,NG2,4
    NCEDGE(I)=NCOMP(NCTART)
    NCEDGE(I+2)=NCOMP(NCTART+1)
 14 NCTART=NCTART+2*NGBB
    GO TO 16
 38 LIMIT=0
    DO 42 J=1,NF1
    NUREL=NS(J)*2
    DO 40 I=1,NUREL
 40 NIX(NSPACE+I-1)=NSEAM(LIMIT+I)
    CALL NPLACE(NUREL,-1,NS(J),NSPACE,NSUB,LVEND,NIXEND)
 42 LIMIT=LIMIT+NUREL
    IF(NP.EQ.NA) GO TO 20
 16 IF(NF.EQ.0) GO TO 20
    DO 18 I=1,NF
    NSHARE(I)=NCOMP(NSTART)
 18 NSTART=NSTART+2*NFBB
 20 NCTART=1
    NH1=(NP-1)*NH*4
    NH2=NH*4
    DO 22 I=1,NH2,4
    NCEND(NH1+I)=NCOMP(NCTART)
    NCEND(NH1+I+2)=NCOMP(NCTART+1)
    NCEND(NH1+NTOTAL+I)=NCOMP(NCTART+NBD-2)
    NCEND(NH1+NTOTAL+I+2)=NCOMP(NCTART+NBD-1)
 22 NCTART=NCTART+NBD*NHB
    IF(NP.NE.NA) GO TO 26
    NCTART=NC*NE*NBD+2*NGB+1
    DO 24 I=1,NG2,4
    NCEDGE(NG2+I)=NCOMP(NCTART)
    NCEDGE(NG2+I+2)=NCOMP(NCTART+1)
 24 NCTART=NCTART+2*NGBB
 26 N=NE+1
    L=0
    NB1=NB
 28 NSUBP=1
    ND2=0
 30 NROW=0
    ND=NDV(NSUBP)
    LIMIT=(ND+1)*2
    KUREL=(ND+1)*(NE+1)*2
    DO 34 J=1,N
    DO 32 I=1,LIMIT
 32 LVABL(I+NROW)=NCOMP(NBD*(L*NE+J-1)+I+ND2)
 34 NROW=NROW+LIMIT
    DO 36 I=1,KUREL
 36 NIX(NSPACE+I-1)=LVABL(I)
    NIX(NIXEND+7-8*MSUB(NSUB))=ND
    CALL NPLACE(KUREL,3,ND*NE,NSPACE,NSUB,LVEND,NIXEND)
    ND2=ND2+ND*2
```

```
      NSUBP=NSUBP+1
      IF(NSUBP.LE.NB) GO TO 30
      IF(NB1.EQ.NB*NC) GO TO 76
      NB1=NB1+NB
      L=L+1
      GO TO 28
   76 IF(NP.EQ.NA) GO TO 46
      NFIRST=NLAST+1
   44 NLAST=NLAST+LAST-NF
   46 NGB3=NGB1*3+1
      NGB2=NGB2*3
C     GENERATE D.O.F. NUMBERS FOR THE SUBASSEMBLIES OF THE T
C       WO X - DIR.
C     BEAMS AND THE REST OF THE EDGE CONNECTION SUBASSEMBLY
C       D.O.F.S
      DO 60 J=1,2
      LIMIT=0
      NFIRST=NLAST+1
      NLAST=NLAST+(NBX1+1)*3
      DO 48 I=NFIRST,NLAST
   48 NCOMP(I-NFIRST+1)=I
C     THESE TWO SMALL LOOPS TREAT SHARED D.O.F.S AT INTERNAL
C        HINGES
      DO 50 I=1,2
      NSHARE((J-1)*4+I)=NCOMP(I)
   50 NSHARE((J-1)*4+I+2)=NCOMP(NLAST-NFIRST+I-2)
      IF(NPUR.EQ.0) GO TO 130
      DO 128 I=1,NPUR
      NSHARE(7+2*((J-1)*NPUR+I))=NCOMP(NPURB1*3+1+(I-1)*NPUR
     C  B2*3)
  128 NSHARE(8+2*((J-1)*NPUR+I))=NCOMP(NPURB1*3+2+(I-1)*NPUR
     C  B2*3)
  130 DO 54 JJ=1,NBX
      KUREL=(NXV(JJ)+1)*3
      DO 52 I=1,KUREL
   52 NIX(NSPACE+I-1)=NCOMP(LIMIT+I)
      CALL NPLACE(KUREL,1,NXV(JJ),NSPACE,NSUB,LVEND,NIXEND)
   54 LIMIT=LIMIT+KUREL-3
      KOUNT=NGB3-NGB1+5
      K=NGB3
      NBX4=NGB3+3*(NG2/4-1)
      DO 56 I=NGB3,NBX4,3
      NCEDGE((J-1)*NG2+2+I+I-KOUNT)=NCOMP(K)
      NCEDGE((J-1)*NG2+2+I+I-KOUNT+2)=NCOMP(K+1)
      K=K+NGB2
   56 KOUNT=KOUNT+2
      LIMIT=(J-1)*NG2
      DO 60 I=1,NG
      KUREL=NEV(I)*4
      DO 58 JJ=1,KUREL
   58 NIX(NSPACE+JJ-1)=NCEDGE(LIMIT+JJ)
      CALL NPLACE(KUREL,-2,KUREL/2,NSPACE,NSUB,LVEND,NIXEND)
   60 LIMIT=LIMIT+KUREL
C     GENERATE D.O.F. NUMBERS FOR SUBASSEMBLIES OF THE TWO Y
```

```
C       -DIR. BEAMS
C     AND COMPLETE GENERATION OF END CONNECTIONS D.O.F.S
      DO 74 J=1,2
      MTOTAL=(J-1)*NTOTAL
      NFIRST=NLAST+J
      NLAST=NLAST+(NBY1+1)*3-6+J
      DO 62 I=1,2
      NCOMP(I)=NSHARE((J-1)*2+I)
   62 NCOMP(NBY1*3+I)=NSHARE((J-1)*2+I+4)
      NCOMP((NBY1+1)*3)=NLAST+1
      DO 64 I=NFIRST,NLAST
   64 NCOMP(I-NFIRST+3)=I
      LIMIT=0
      DO 68 JJ=1,NBY
      KUREL=(NYV(JJ)+1)*3
      DO 66 I=1,KUREL
   66 NIX(NSPACE+I-1)=NCOMP(LIMIT+I)
      CALL NPLACE(KUREL,2,NYV(JJ),NSPACE,NSUB,LVEND,NIXEND)
   68 LIMIT=LIMIT+KUREL-3
      NZ=1
      JJ=0
      DO 70 I=4,NTOTAL,4
      JJ=JJ+3
      IF(I.NE.NZ*NH*4+4) GO TO 78
      JJ=JJ-3
      NZ=NZ+1
   78 NCEND(MTOTAL+I-2)=NCOMP(JJ-2)
   70 NCEND(MTOTAL+I)=NCOMP(JJ-1)
      LIMIT=0
      DO 74 I=1,NBY
      KUREL=4*NCY(I)
      DO 72 JJ=1,KUREL
   72 NIX(NSPACE+JJ-1)=NCEND(LIMIT+JJ+NTOTAL*(J-1))
      CALL NPLACE(KUREL,-2,KUREL/2,NSPACE,NSUB,LVEND,NIXEND)
   74 LIMIT=LIMIT+KUREL
      IF(NPUR.EQ.0) GO TO 120
C     GENERATE D.O.F. NUMBERS FOR INTERMEDIATE PURLINS AND S
C       HEET TO
C     PURLIN CONNECTIONS
      DO 138 J=1,NPUR
      NFIRST=NLAST+2
      NLAST=NLAST+(NPURL+1)*3-4
      DO 114 K=1,2
      NCOMP(K+(J-1)*(NPURL+1)*3)=NSHARE(8+K+2*(J-1))
  114 NCOMP(K+NPURL*3+(J-1)*(NPURL+1)*3)=NSHARE(8+K+2*(J-1)+
     C  NPUR*2)
      NCOMP((NPURL+1)*3+(J-1)*(NPURL+1)*3)=NLAST+1
      DO 140 K=NFIRST,NLAST
  140 NCOMP(K-NFIRST+3+(J-1)*(NPURL+1)*3)=K
  138 CONTINUE
      LIMIT=0
      DO 115 I=1,NPUR
      KUREL=NPURN*4
      NSUM=MPURC(1)*4
```

```
      NODEC=(I-1)*NPURN*4
      NODEP=(I-1)*(NPURL+1)*3
      JJ=0
      J=1
      DO 116 K=4,KUREL,4
      JJ=JJ+3
      IF(K.NE.NSUM+4) GO TO 117
      JJ=JJ-3*NSE+(1-NSE)*3*NPUR6
      J=J+1
      IF(J.LE.NA) NSUM=NSUM+MPURC(J)*4
  117 NPURC(K-2+LIMIT)=NCOMP(JJ+1+NODEP)
  116 NPURC(K+LIMIT)=NCOMP(JJ+2+NODEP)
      LIMIT=LIMIT+KUREL
      NDOF=0
      NDOFP=0
      DO 118 NP=1,NA
      KUREL=MPURC(NP)*4
      DO 119 K=1,KUREL
  119 NIX(NSPACE+K-1)=NPURC(K+NDOF+NODEC)
      CALL NPLACE(KUREL,-3,KUREL/2,NSPACE,NSUB,LVEND,NIXEND)
      NDOF=NDOF+KUREL
      KUREL=(MPURL(NP)+1)*3
      DO 121 K=1,KUREL
  121 NIX(NSPACE+K-1)=NCOMP(K+NDOFP+NODEP)
      CALL NPLACE(KUREL,2,MPURL(NP),NSPACE,NSUB,LVEND,NIXEND
     C  )
  118 NDOFP=NDOFP+KUREL-3
  115 CONTINUE
C     GENERATE KL1 AND LIKE
  120 DO 84 I=1,2
      DO 172 J=1,NOOS
      READ(5,200) NOS,(MSUB(K),K=1,NOS)
      IF(NOS.GT.1.OR.I.EQ.2) GO TO 170
      NIX(NIXEND+1-8*MSUB(1))=0
      GO TO 172
  170 NIX(NIXEND-3-8*MSUB(1)+4*I)=J
      IJKL=NIXEND-3+4*I
      DO 82 K=2,NOS
   82 NIX(IJKL-8*MSUB(K))=-J
  172 CONTINUE
   84 NOOS=NOOM
C     SUPPORTS AND LOADED D.O.F.S. ALSO REARRANGE D.O.F.S IN
C        NIX
      READ(5,200) NRE1,NRE11,NRE2,NRE22,KLS,KL2
      DO 86 I=1,NSU
      IJKL=NIXEND-8*I
      KUREL=NIX(IJKL+8)
      IF(KUREL.GT.LVMAX) LVMAX=KUREL
      IF(I.EQ.NRE1) GO TO 102
      NIX(IJKL+3)=0
      GO TO 100
  102 NIX(IJKL+3)=NRE11
      NRE1=NRE2
      NRE11=NRE22
```

```
100 IF(KLS.EQ.I) GO TO 104
    NIX(IJKL+4)=0
    GO TO 98
104 NIX(IJKL+4)=KL2
 98 DO 88 J=1,KUREL
    NIZZ=NIZZ+1
 88 NIX(NIZZ)=-NIX((I-1)*40+J)
 86 NIX(IJKL+8)=NIZZ
200 FORMAT(16I5)
    RETURN
    END
```

```
      SUBROUTINE NPLACE(KUREL,NTYPE,KE,NSPACE,NSUB,LVEND,NIX
     C  END)
C     PRINTS D.O.F. GENERATED IN GMESH AND PLACES
C     SUBASSEMBLY DATA IN ARRAY NIX
      IMPLICIT REAL*8(A-H,O-Z)
      DIMENSION NIX(12000),MSUB(100)
      COMMON /BLK6/ ELPA(7000),EL(860),JJ(40)
      EQUIVALENCE (NIX(1),ELPA(1)),(MSUB(1),ELPA(6601))
      NSPAND=NSPACE+KUREL-1
      WRITE(6,201) NSUB,MSUB(NSUB)
  201 FORMAT(/,5X,'MESH GENERATOR SUBASSEMBLY NO.',I5,/,5X,'
     C  USER SUBASSE
     1MBLY NO.',I5,/)
      IF(NTYPE.LT.0) GO TO 1
      JUMP=2
      IF(NTYPE.EQ.1.OR.NTYPE.EQ.2) JUMP=3
      NSPAC1=NSPACE+1
      WRITE(6,202) (NIX(I),I=NSPACE,NSPAND,JUMP)
  202 FORMAT(8X,'D.O.F. IN X-DIR. ',8(/,5X,10I8),/)
      WRITE(6,203) (NIX(I),I=NSPAC1,NSPAND,JUMP)
  203 FORMAT(8X,'D.O.F. IN Y-DIR. ',8(/,5X,10I8),/)
      NSPAC1=NSPACE+2
      IF(JUMP.EQ.3) WRITE(6,204) (NIX(I),I=NSPAC1,NSPAND,JUM
     C  P)
  204 FORMAT(8X,'ROTATIONAL D.O.F.',2(/,5X,10I8),/)
      GO TO 2
    1 IF(NTYPE.EQ.-1) WRITE(6,205) (NIX(I),I=NSPACE,NSPAND)
  205 FORMAT(8X,'D.O.F. IN X-DIR. AND CONNECTIVITY ',8(/,5X,
     C  5(I8,' --'I5
     1)),/)
      IF(NTYPE.NE.-1) WRITE(6,206) (NIX(I),I=NSPACE,NSPAND)
  206 FORMAT(8X,'D.O.F. AND CONNECTIVITY. DIRECTIONS INDICAT
     C  ED BY X OR Y
     1 ',8(/,5X,3('X:',I6,' --',I5,'   Y:',I5,' --',I5,2X)),
     C  /)
    2 IJKL=NIXEND-8*MSUB(NSUB)
      NIX(IJKL+6)=KE
      NIX(IJKL+2)=NTYPE
      NIX(IJKL+8)=KUREL
      NSUB=NSUB+1
      IF(NSUB.LE.NSU) NSPACE=(MSUB(NSUB)-1)*LVEND+1
      RETURN
      END
```

$$
\begin{bmatrix}
B1 & & & & & & & \\
B2 & B6 & & & & & & \\
B3 & -B4 & B1 & & & \text{Symm.} & & \\
B4 & B7 & -B2 & B6 & & & & \\
-\frac{B1}{2} & -B2 & B5 & -B4 & B1 & & & \\
-B2 & -\frac{B6}{2} & B4 & B8 & B2 & B6 & & \\
B5 & B4 & -\frac{B1}{2} & B2 & B3 & -B4 & B1 & \\
-B4 & B8 & B2 & -\frac{B6}{2} & B4 & B7 & -B2 & B6
\end{bmatrix}
$$

where,

$$B1 = \frac{t}{3}\left(\frac{E_x}{\lambda}\frac{b}{a} + G_{xy}\frac{a}{b}\right)$$

$$B2 = \frac{t}{4}\left(\mu_{yx}\frac{E_x}{\lambda} + G_{xy}\right)$$

$$B3 = \frac{t}{6}\left(\frac{-2E_x}{\lambda}\frac{b}{a} + G_{xy}\frac{a}{b}\right)$$

$$B4 = \frac{t}{4}\left(\mu_{yx}\frac{E_x}{\lambda} - G_{xy}\right)$$

$$B5 = \frac{t}{6}\left(\frac{E_x}{\lambda}\frac{b}{a} - 2G_{xy}\frac{a}{b}\right)$$

$$B6 = \frac{t}{3}\left(\frac{E_y}{\lambda}\frac{a}{b} + G_{xy}\frac{b}{a}\right)$$

$$B7 = \frac{t}{6}\left(\frac{E_y}{\lambda}\frac{a}{b} - 2G_{xy}\frac{b}{a}\right)$$

$$B8 = \frac{t}{6}\left(\frac{-2E_y}{\lambda}\frac{a}{b} + G_{xy}\frac{b}{a}\right)$$

and,

$$\lambda = 1 - \mu_{xy}\mu_{yx}$$

Table 3.1 Orthotropic Plane Stress Plate Element Stiffness Matrix (Reference 26)

	Seam Slip (10^{-3} in.)					
	Gage G		Gage H		Gage I	
Load (kip)	Test*	F.E.	Test*	F.E.	Test*	F.E.
13.477	4.6	3.84	4.0	3.89	4.6	3.93
(Elastic limit)						
18.477	8.0	8.16	7.3	8.38	8.0	8.45
23.477	13.3	13.39	11.4	13.80	13.3	13.83
28.477	20.4	23.02	18.0	23.78	21.3	23.76
33.477	30.0	34.05	26.5	35.10	31.3	35.11
38.477**	52.0	58.73	42.0	59.74	53.0	59.96

* Test results noted above have been picked from curves in Reference (53). The curves were drawn from test data at loads different than those above.

** Test results extrapolated from available curves for this load level.

Table 5.1 Comparison of test seam slip with finite element analysis results

Total number of subassemblies: 57

Total degrees of freedom: 827

Analysis with IBM 370/168 computer:

	Solution Time (sec.)	
	CPU	I/O
Linear analysis up to elastic limit	10.36	17.01
Full non-linear analysis*	383.07	1545.27
Linear analysis up to elastic limit**	10.40	17.29

* Other statistics for the full non-linear analysis are as follows:

Load increment beyond elastic limit	No. of Iterations	No. of Accelerations
1	5	1
2	6	1
3	6	1
4	8	2
5	14	4
6	21	6

** With more recent version of the program including the mesh generator

Table 5.2 Analysis and Iteration Statistics for the 10' x 12' Welded Diaphragm

	Elastic Limit		
Case*	Load (kip)	Deflection (in.)	Elastic Slope (k/in.)
Test	Cannot be properly identified from curve		55.0
1	0.5429	0.01132	47.978
2	0.5408	0.01039	52.060
3	0.5406	0.01028	52.594
4	0.5444	0.01344	40.492
5	0.5419	0.01137	47.673

* See Section 5.4.3.1 for a list of the above cases 1 - 5.

Table 5.3 Results of Linear Analyses on Different Models of the 10' x 12' Standard Corrugated Diaphragm

	Seam slip (in.) at the following seam lines (1 to 4 in positive y-dir. on Figure 5.19)			
Load (kip)	1	2	3	4
Elastic Limit (0.5406 k.)	0.00115	0.00121	0.00124	0.00126
1.5406	0.00444	0.00464	0.00476	0.00485
2.5406	0.01335	0.01379	0.01403	0.01418
3.5406	0.03043	0.03121	0.03150	0.03155
4.5406	0.06714	0.06969	0.06984	0.06810

Table 5.4 Seam Slip Computed in Finite Element Analysis of Case 3 (see Section 5.4.3.1) for the 10' x 12' Standard Corrugated Diaphragm

	Model A	Model B	Model C
Total number of subassemblies	68	88	88
Total degrees of freedom	606	766	766

Analysis with IBM 370/168 computer:

Linear Analyses up to Elastic Limit			Non-Linear Analyses		
	Solution Time (sec.)			Solution Time (sec.)	
Model	CPU	I/O	Model	CPU	I/O
A	8.70	17.73	A*	53.52	217.03
B	10.30	21.64	A***	367.00	1580.71
C	10.07	21.64	C**	62.27	264.21
A*	9.18	18.70			

* Later analysis after some additions to program

** Only one load increment beyond elastic limit, with a total of 8 iterations and 2 accelerations

*** Full analysis (conducted later than linear analysis A*), the number of iterations and accelerations at each load increment being as follows:

Load increment beyond elastic limit	No. of Iterations	No. of Accelerations
1	5	1
2	8	2
3	11	3
4	15	4
5	26	7

Table 5.5 Analysis and Iteration Statistics for the 10' x 12' Standard Corrugated Diaphragm

	Seam Slip (in.) at the following seam lines (1 to 5 in positive y-dir. on Figure 5.29)				
Load (kip)	1	2	3	4	5
Elastic Limit (0.3434 k.)	0.0012	0.0012	0.0012	0.0012	0.0012
0.8434	0.0065	0.0066	0.0067	0.0066	0.0066
1.3434	0.0162	0.0163	0.0166	0.0163	0.0162
1.8434	0.038	0.0381	0.0387	0.0381	0.0374
2.3434	0.0937	0.094	0.0953	0.094	0.0941
2.8434*	0.375	0.363	0.365	0.363	0.375

* Results after 76 iterations at this load. Given values of seam slip only lower bound.

Table 5.6 Seam Slip Computed in the Non-Linear Analysis of Model AT, 10' x 12' Trapezoidally Corrugated Diaphragm of Section 5.5

		Model AT	Model BT
Total number of subassemblies		47	83
Total degrees of freedom		463	583
Analysis with IBM 370/168 computer:			
		Solution Time (sec.)	
		CPU	I/O
Linear analysis up	Model AT	5.07	12.35
to Elastic Limit	Model BT	6.92	19.35
Full non-linear Analysis*	Model AT	515.27	2413.96

* Iterations are as follows:

Load increment beyond elastic limit	No. of Iterations	No. of Accelerations
1	5	1
2	11	3
3	12	3
4	32	9
5	76	23

Table 5.7 Analysis and Iteration Statistics for the 10' x 12' Trapezoidally Corrugated Diaphragm

```
24 IN. X 28 IN. DIAPH. NON-LINEAR ANALYSIS. MAX. NO. OF LOAD INC. 5, 0.1 K EACH
MAX. NO. OF ITER. PER LOAD INC. 40,    INITIAL LOAD 1 KIP
    5     0     0    40    11     0     0       .1
   12     1     2     0     0     1     3     0
  101   102   119   120   121   122   123   124   125   110   111   126
   16     2    -2     0     0     2     8     0
    1   101     2   102    31   120    32   121    61   123    62   124    91   110    92   111
    9     3     1     3     0     3     2     0
  101   102   103   104   105   106   107   108   109
    4     4    -2     0     0    -2     2     0
    5   104     6   105
   40     5     3     0     0     4    12     4
    1     2     3     4     5     6     7     8     9    10    11    12    13    14    15    16
   17    18    19    20    21    22    23    24    25    26    27    28    29    30    31    32
   33    34    35    36    37    38    39    40
   40    -5     3     0     0     0     0     0
   31    32    33    34    35    36    37    38    39    40    41    42    43    44    45    46
   47    48    49    50    51    52    53    54    55    56    57    58    59    60    61    62
   63    64    65    66    67    68    69    70
   40    -5     3     0     0     0     0     0
   61    62    63    64    65    66    67    68    69    70    71    72    73    74    75    76
   77    78    79    80    81    82    83    84    85    86    87    88    89    90    91    92
   93    94    95    96    97    98    99   100
    4    -4    -2     0     0     0     0     0
   95   113    96   114
    9    -3     1     0     1     0     0     0
  110   111   112   113   114   115   116   117   118
   16    -2    -2     0     0     0     0     0
    9   107    10   108    39   128    40   129    69   131    70   132    99   116   100   117
   12    -1     2     0     0     0     0     0
  107   108   127   128   129   130   131   132   133   116   117   134
   8.        0.14        0.69        29500.
    9       .002375       .25         .0075        .375         .015         .465        .02625
 .545       .0425         .61          .0625       .66          .09875       .715        .126875
 .74        .15           .75
  14.       .14           .69         29500.
   2    7    8
  .3       .0003         2.67          7.         33000.       33.           .018       500.
   7       -1.
```

Table A.1.1 24" x 28" diaphragm, manual input

```
DIAPH. OF FIG. A.1.5. NON-LINEAR ANALYSIS. MAX. NO. OF LOAD INCR. 5.  1.5 K EACH
INIT. LOAD 1 K.,MAX. ITER. PER INCR. 40,MATERIAL PROPS. AS CASE 3,SECT. 5.4.3.1
    5    1    0   40   39   12    7       1.5
    3    3    1    4    2    1    1    1    2    4    1    3    2    3    1    3
    1    3    2    2    3    5    3    4    1    3    3    5    4
    3    4    1    1    3    2    1    2    3    2    2    2    2
    0    7   10   13   16   17   20   23   24   27   30   33    1    2    3    4
   37   38   39   36    5   25    6   26   15   35   14   34    8    9   18   19
   28   29   11   12   21   22   31   32
    2    1   37
    2    2   38
    2    3   39
    2    4   36
    4    5   15   25   35
    2    6   14
    9    7   10   13   17   20   23   27   30   33
    4    8   11   28   31
    6    9   12   19   22   29   32
    2   16   24
    2   18   21
    2   26   34
    4    1    3   37   39
    2    2   38
   12    4    6    8   11   14   18   21   26   28   31   34   36
    4    5   15   25   35
    9    7   10   13   17   20   23   27   30   33
    6    9   12   19   22   29   32
    2   16   24
    5    1   25    2   35    1
  10.      .117      .655     29500.
  20.      .117      .655     29500.
    9     .002375    .25      .0075     .375      .015      .465     .02625
 .545     .0425      .61       .0625    .66      .09875     .715     .126875
 .74       .15       .75
  12.      .117      .655     29500.
   1
 .3       .000065   12.       10.      32100.    6.955     .01875    10450.
  12.       .0951     .526    29500.
    9     .00125     .07      .0075     .1375     .0175     .19      .0275
 .22      .03875     .24       .06125   .265      .08125    .2775    .09
 .28       .125      .2825
  10   11
  11    -1.
```

Table A.1.2 Diaphragm model of Figure A.1.5, input using the mesh generator

```
10' * 12' WELDED CELLULAR DIAPHRAGM   INITIAL LOAD 10 K., INCR. LOAD 5 K.
MAX. NO. OF ITER PER LOAD INCR. 35, MAX. NO. OF 6 LOAD INCREMENTS
  6     1     1    35    57     7     6          .5
  6     4     1     5     2     1     1     1     3     3     1     4     4     1     1     3
  1     1     6     0     7     4     5     2     2     2     2     2     2     3     3     3
  3     3     3
  0     5     6     7     8    11    14    15    16    17    20    23    24    25    26    29
 32    33    34    35    38    41    42    43    44    47    50    51    52    53     1     2
 57    56     3    12    21    30    39    48     4    13    22    31    40    49    10    19
 28    37    46    55     9    18    27    36    45    54
  2     1    57
  2     2    56
  6     3    12    21    30    39    48
 12     4     9    13    18    22    27    31    36    40    45    49    54
 24     5     6     7     8    14    15    16    17    23    24    25    26    32    33    34
 35    41    42    43    44    50    51    52    53
  6    10    19    28    37    46    55
  5    11    20    29    38    47
  2     1    57
 14     2     4     9    13    18    22    27    31    36    40    45    49    54    56
  6     3    12    21    30    39    48
 24     5     6     7     8    14    15    16    17    23    24    25    26    32    33    34
 35    41    42    43    44    50    51    52    53
  6    10    19    28    37    46    55
  5    11    20    29    38    47
  3     1    48     2    55     1
24.          16.6          7.97          29500.
  5          .00434        4.5           .02           5.37          .04555        6.            .11258
6.75         .26291        7.272
 12.         9.7           6.19          29500.
  1
.3           .3            12.           6.            29500.        29500.        .06           11346.15
12.          36.5          9.71          29500.
  5          .003936       1.703         .011942       2.496         .029926       3.079         .08
3.62         .163038       3.808
  7    8
  8          -10.
```

Table A.1.3 10' x 12' welded cellular metal deck, input using the mesh generator

```
10' * 12' STANDARD CORRUGATED DIAPHRAGM   INITIAL LOAD 1 K.,INCR. LOAD 1 K.
MAX. NO. OF ITER PER LOAD INCR. 40, MAX. NO. OF 8 LOAD INCREMENTS
  8    1    0   40   68    8    6        1.
  5    2    1    4    3    1    1    1    1    2    1    1    1    1    1    4
  1    1    5    3    4    7    8    3    3    3    3    3    4    4    4    4
  4
  2    2    1    1    2    2    1    3    4    4    4    3    3    3    3    3
  3
  0    5   10   15   18   23   28   31   36   41   44   49   54   57   62    1
  2   68   67    3   16   29   42   55    4   17   30   43   56   14   27   40
 53   66   13   26   39   52   65    6    7   19   20   32   33   45   46   58
 59    8    9   21   22   34   35   47   48   60   61   11   12   24   25   37
 38   50   51   63   64
  2    1   68
  2    2   67
 10    3   14   16   27   29   40   42   53   55   66
 19    4   13   17   19   21   24   26   30   32   34   37   39   43   45   47
 50   52   56   65
 10    5   10   18   23   31   36   44   49   57   62
  6    6    8   11   58   60   63
 15    7    9   12   20   22   25   33   35   38   46   48   51   59   61   64
  4   15   28   41   54
  2    1   68
 27    2    4    6    8   11   13   17   19   21   24   26   30   32   34   37
 39   43   45   47   50   52   56   58   60   63   65   67
 10    3   14   16   27   29   40   42   53   55   66
 10    5   10   18   23   31   36   44   49   57   62
 15    7    9   12   20   22   25   33   35   38   46   48   51   59   61   64
  4   15   28   41   54
  1    3    0    0   68    1
 18.     .117      .655     29500.
  1    2   26
  9     .002375    .25       .0075     .375      .015      .465     .02625
.545    .0425      .61       .0625     .66       .09875    .715     .126875
.74     .15        .75
 8.     .117       .655     29500.
 .3     .000065    8.        18.      32100.     6.955     .01875   10450.
  8.     .0951     .526     29500.
  9     .00125     .07       .0075     .1375     .0175     .19      .0275
.22     .03875     .24       .06125    .265      .08125    .2775    .09
.28     .125       .2825
  1     1.
```

Table A.1.4 10' x 12' standard corrugated diaphragm Model A, input using the mesh generator

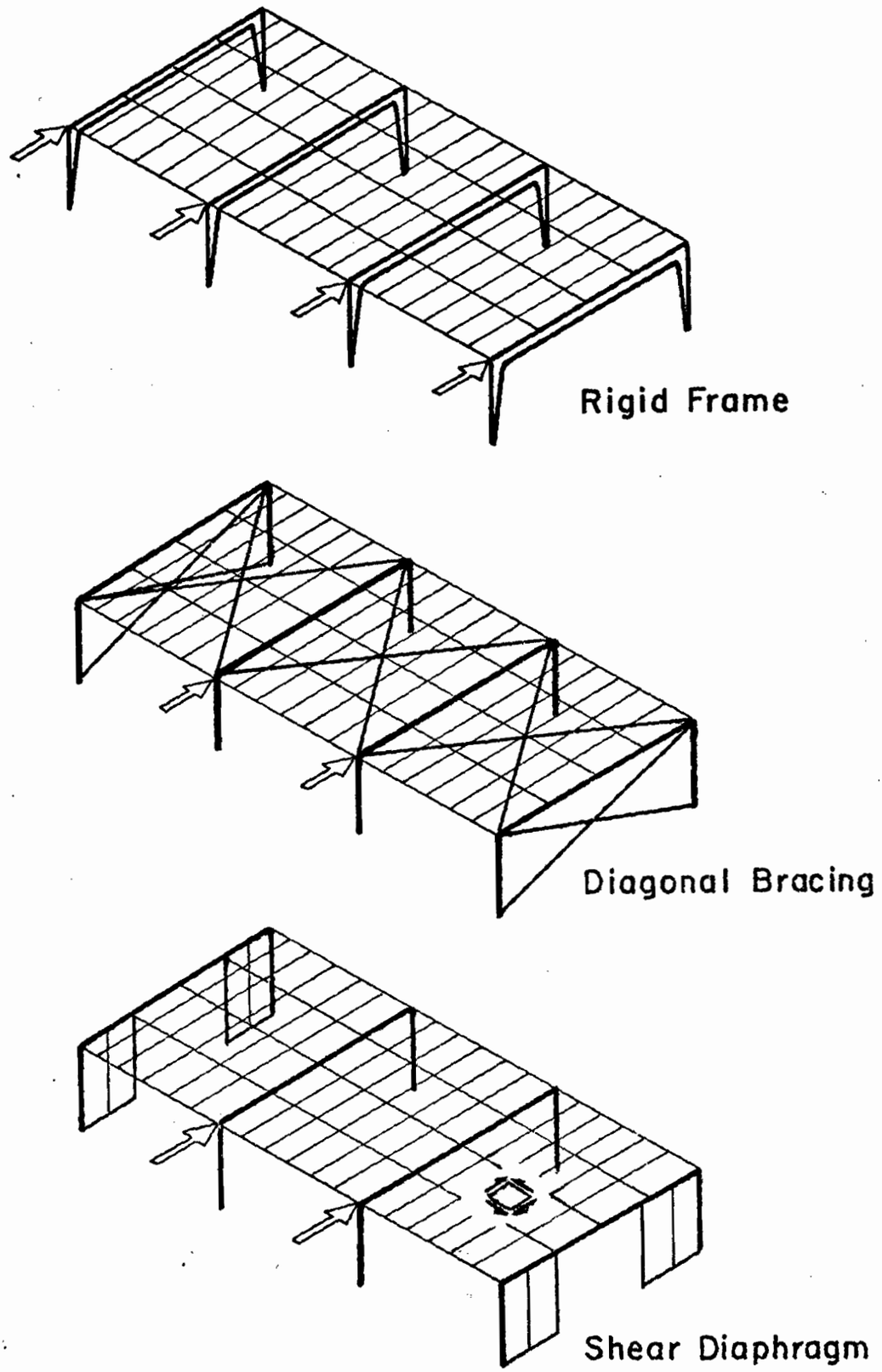

Figure 1.1 Alternative methods for resisting lateral forces

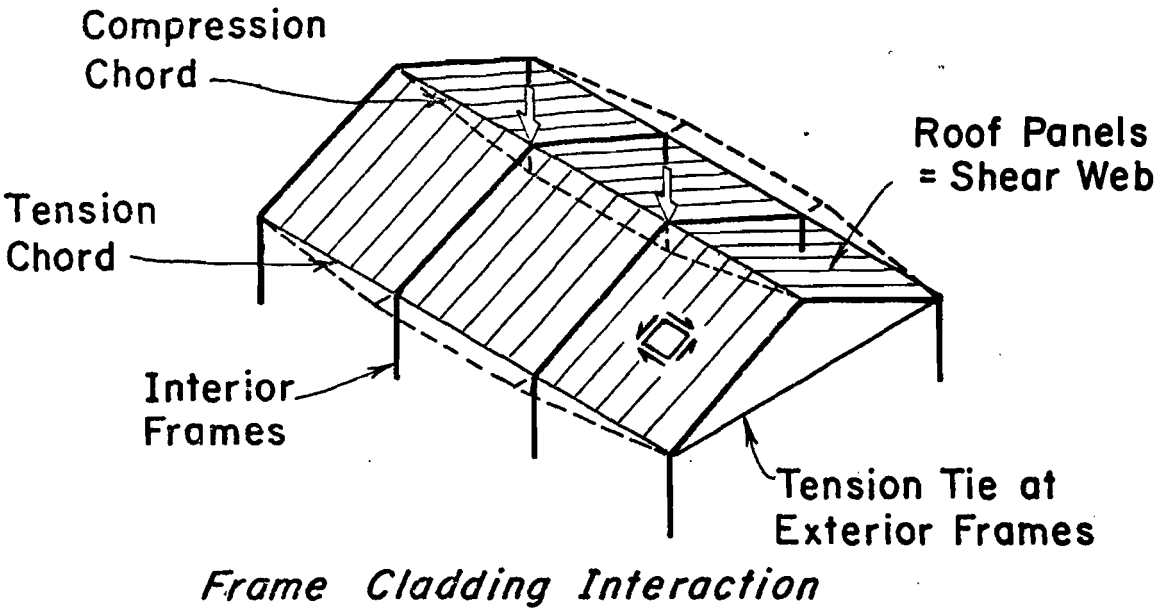

Frame Cladding Interaction

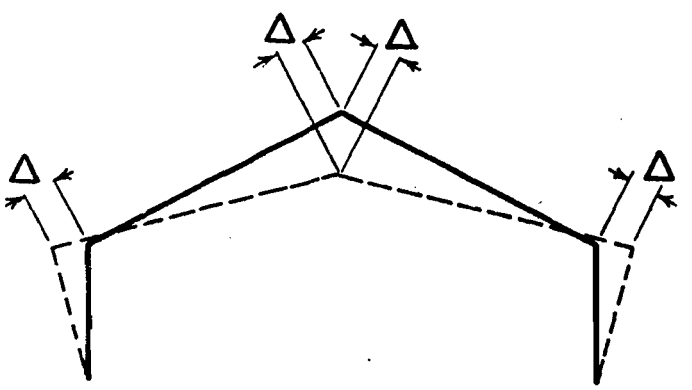

Cross Section at Interior Frames

Figure 1.2 Interaction of sheathing and moment resisting frames to carry vertical loads

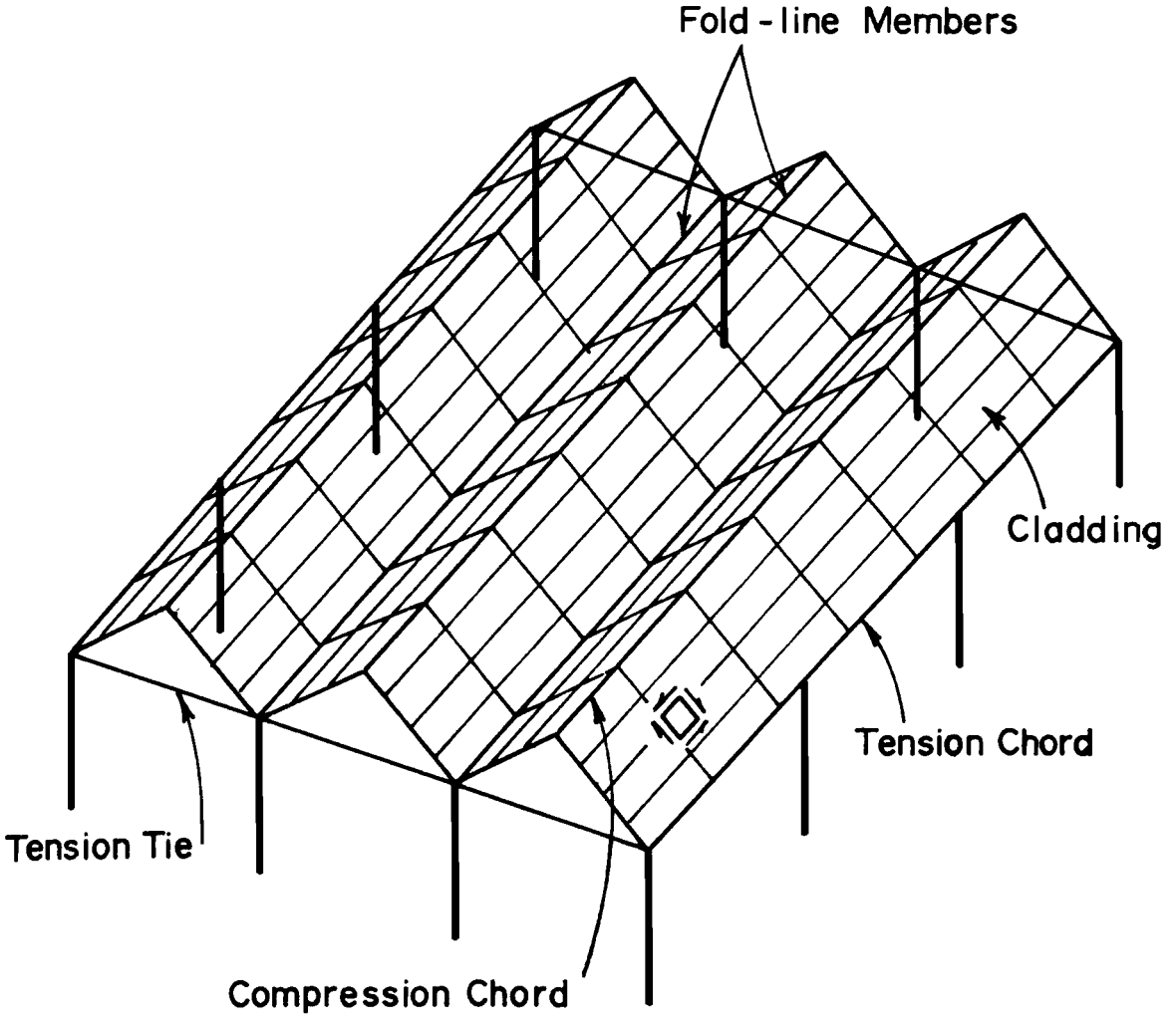

Figure 1.3 Folded plate structure

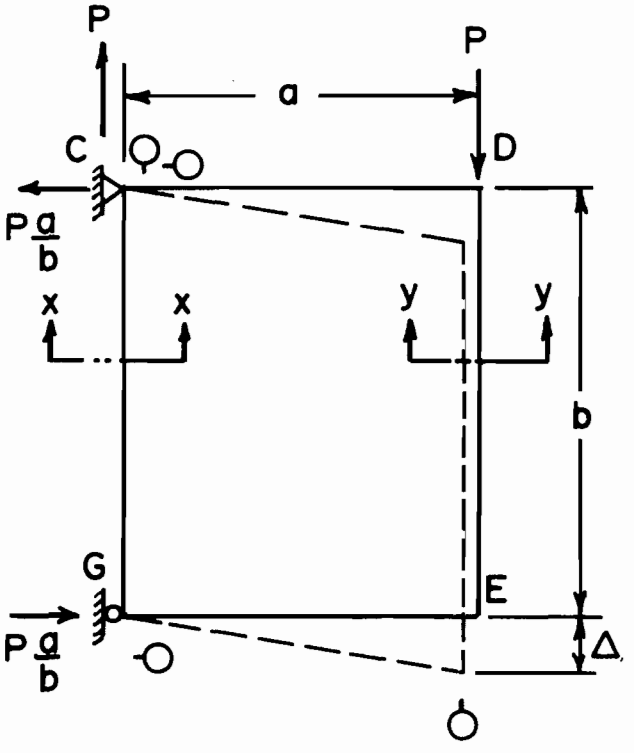

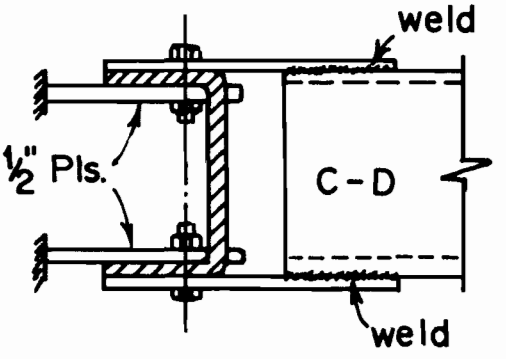

Section x-x
Pinned connection details at C

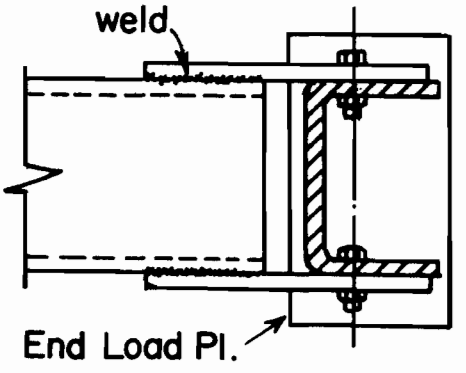

Section y-y
Details at corner D

Notes:

1. Symbol ○ represents dial gage
2. Pinned connection or double-link connection should be provided at corner (G) for reversed loading
3. See Figure 2.1b for cantilever test

Figure 2.1a Plan of cantilever test frame (Ref. 4)

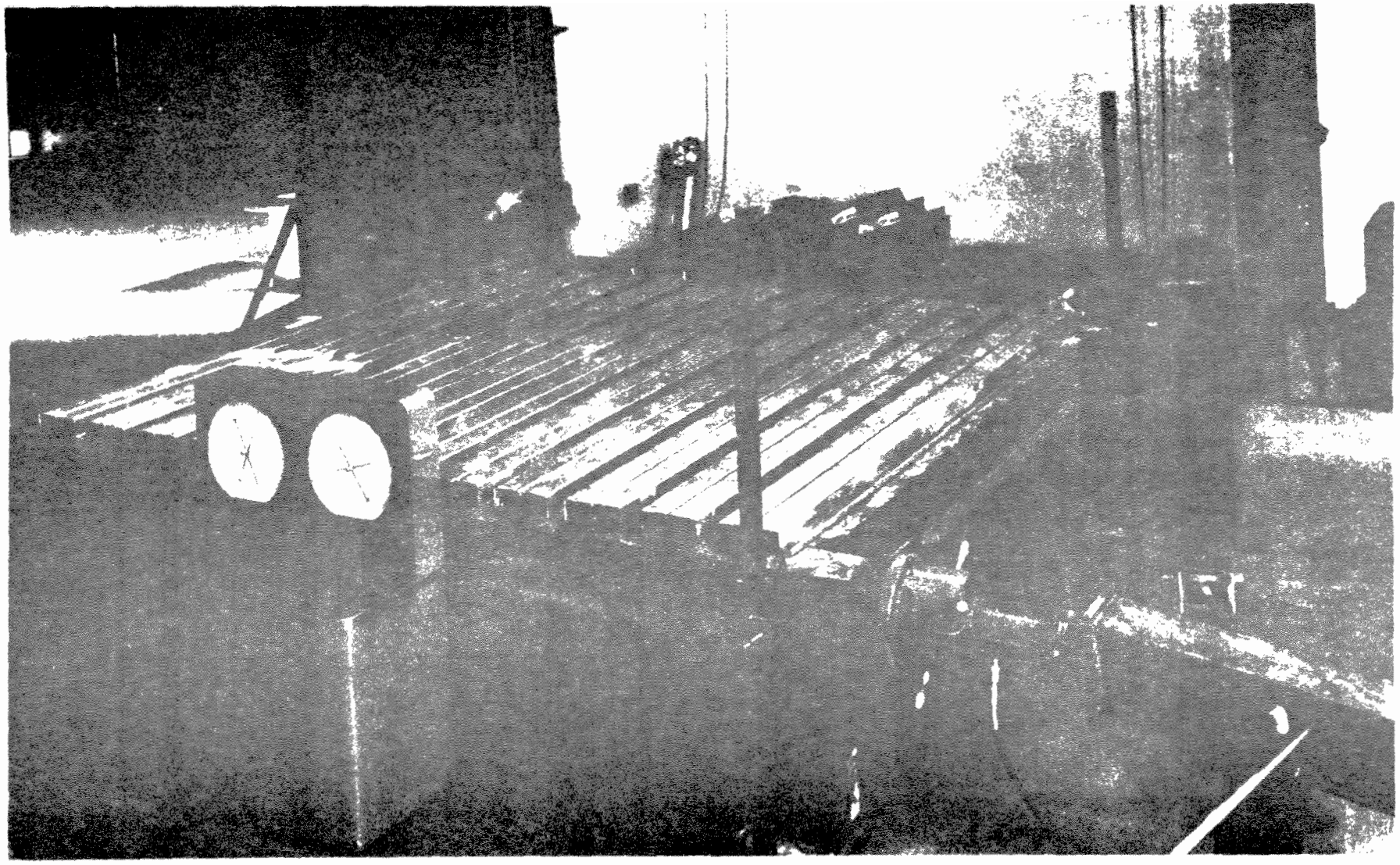

Figure 2.1b Cantilever test

a. Rectangular corrugations with attachments at every valley

single-sided attachment

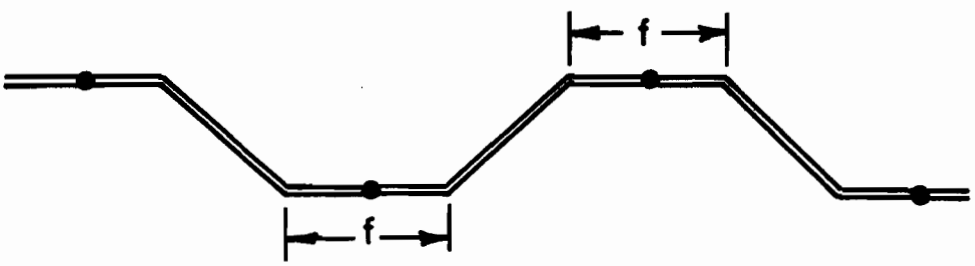

double-sided attachment

b. Corrugations and attachment analyzed by Rothwell (20)

Figure 2.2 Some geometries on which earlier analyses have been conducted

1. Trapezoidal Corrugation

a. small attachments at the valleys

b. small attachments at the valleys and crests

c. wide attachments to a rigid flange

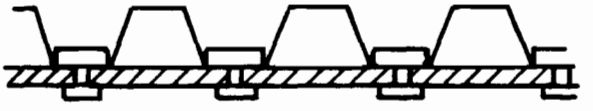

d. small attachment to a rigid flange

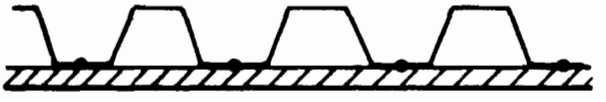

Special Cases

Type of Attachment	(I) Zero-Width Crests	(II) Zero-Width Valleys	(III) Zero-Width Valleys and Crests
a			
b			
c	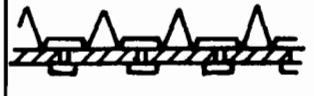		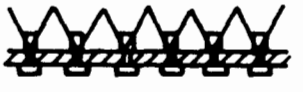
d	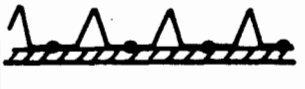		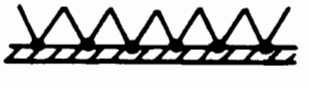

Figure 2.3 Corrugation geometries and manners of attachment analyzed by Libove and co-workers (cont.)

2. Circular arc corrugations

3. Sinusoidal corrugations

Cases of attachment considered for 2 and 3 above:
(drawn only for case 2)

a. small attachments at the valleys

b. small attachments at crests and valleys

c. small attachments at mid-height

d. combination of b and c

Figure 2.3 (cont.) Corrugation geometries and manners of attachment analyzed by Libove and co-workers

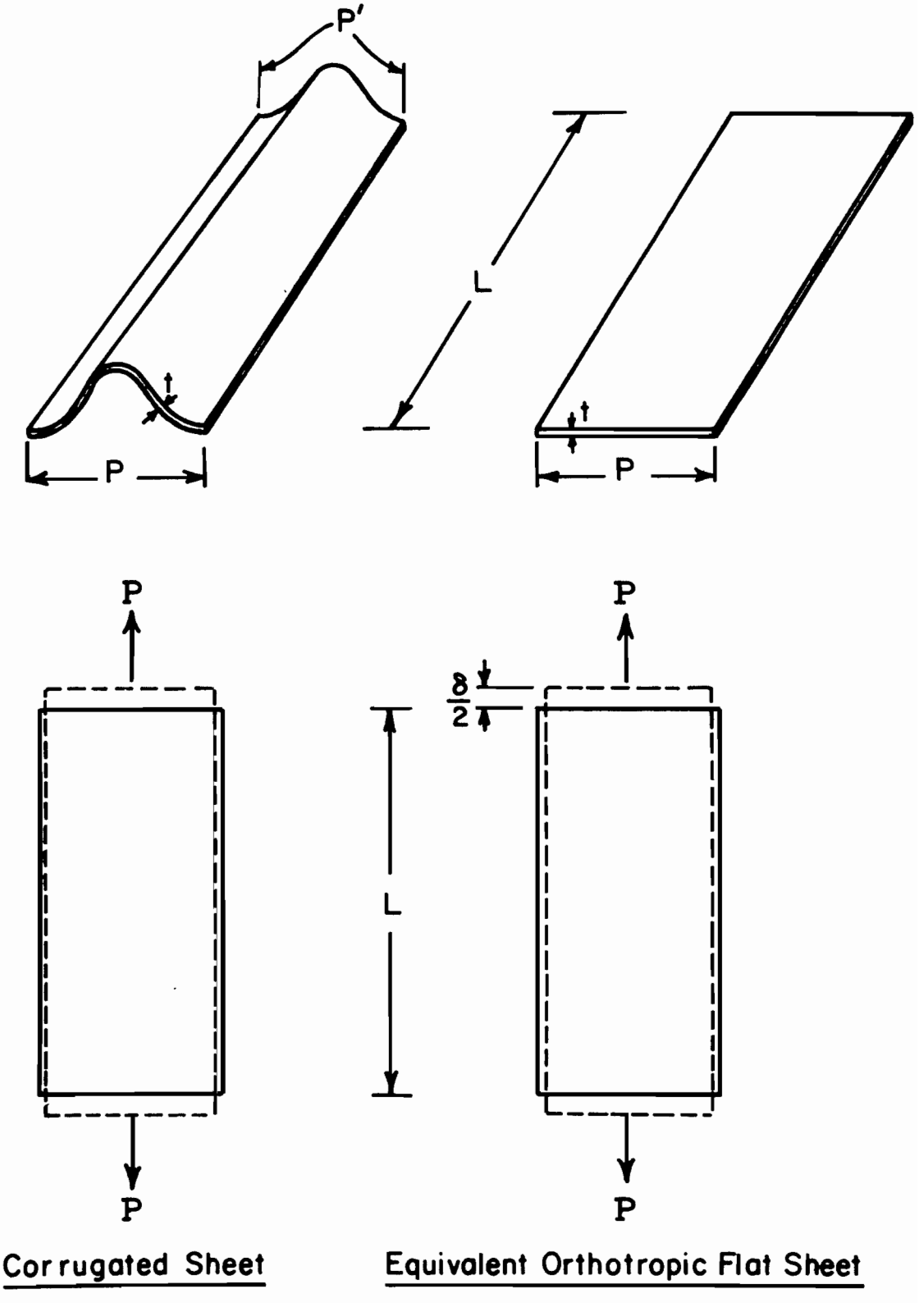

Figure 3.1 Idealization of corrugated sheeting

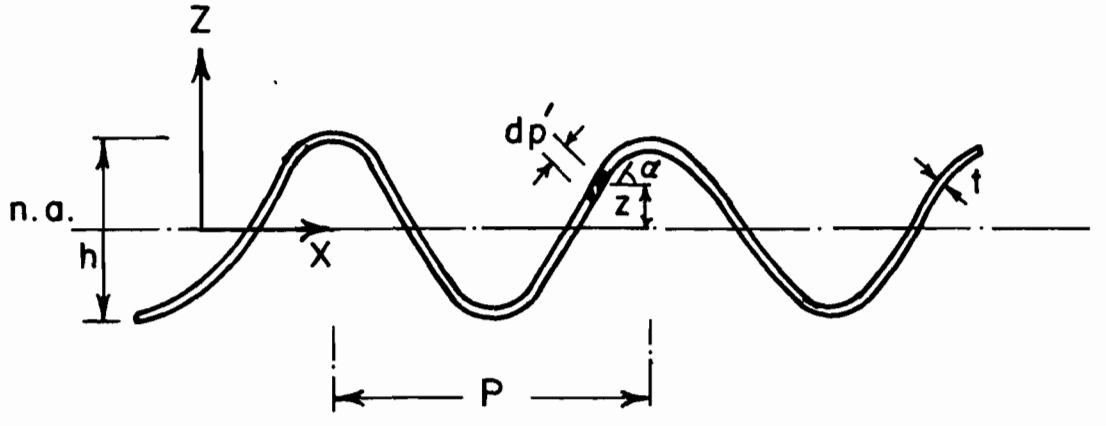

Corrugation shape assumed in Ref. 26: $Z = \frac{h}{2} \sin\left(\frac{2\pi X}{P}\right)$

Figure 3.2 Definition of variables in Equations 3.6 and 3.7

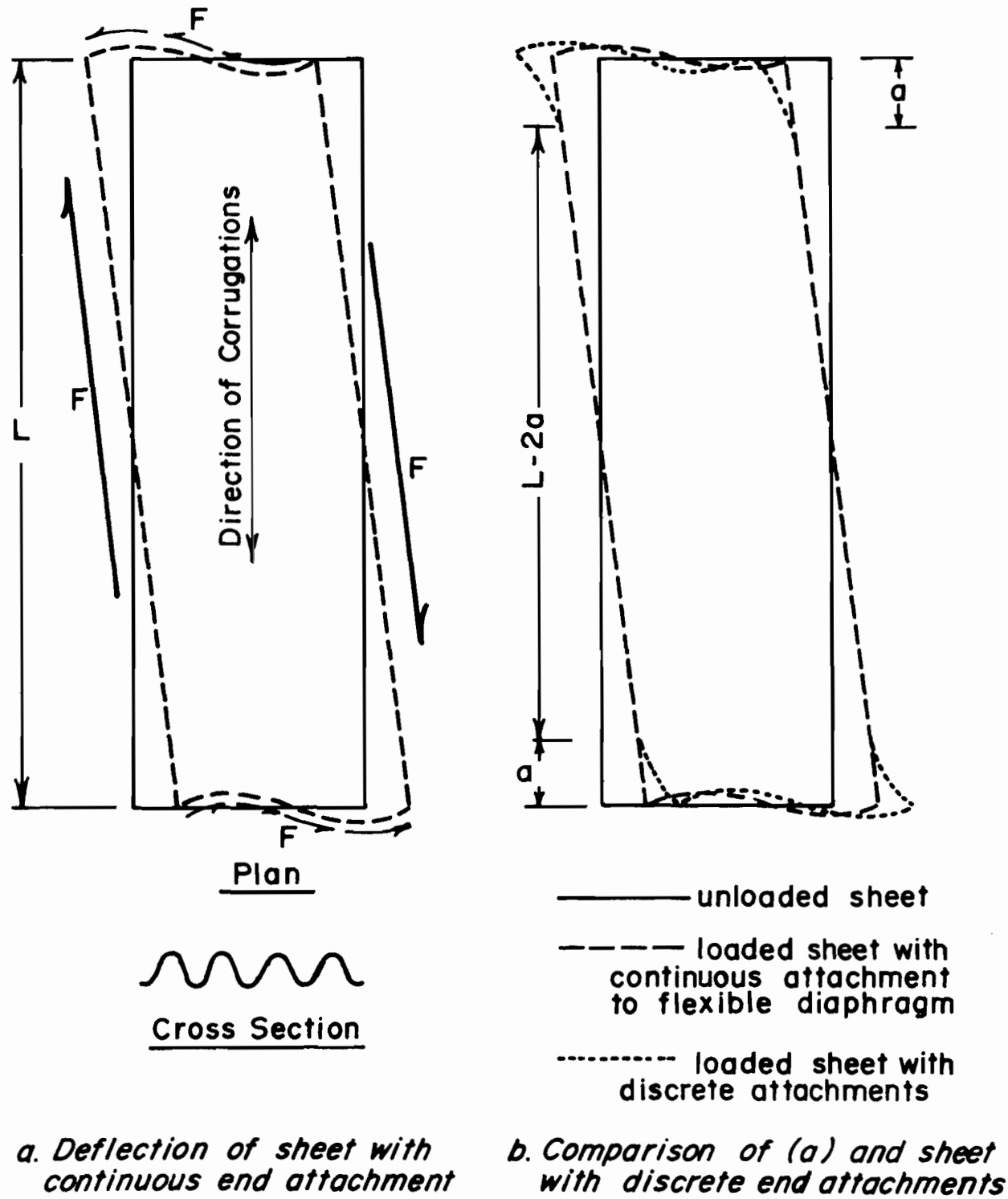

Figure 3.3 Shear deflection of corrugated sheeting (cont.)

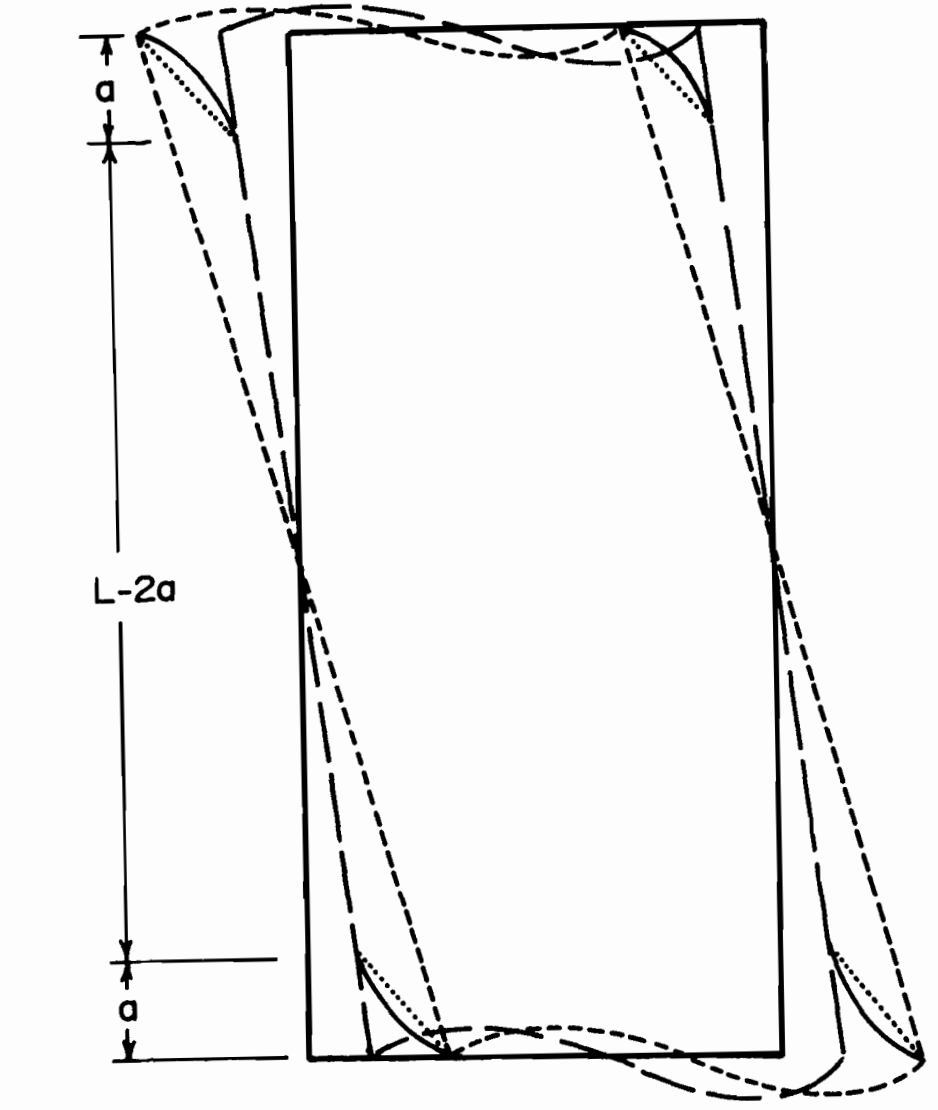

unloaded sheet

case of Figure 3.3a

approximation of deflection of sheet with discrete end attachments by using an average G_{eff}

approximation of same by using G_{ae} and G_{L-2a}

actual shape of end sweep

c. Comparison of three cases of using shear moduli

Figure 3.3 (cont.) Shear deflection of corrugated sheeting

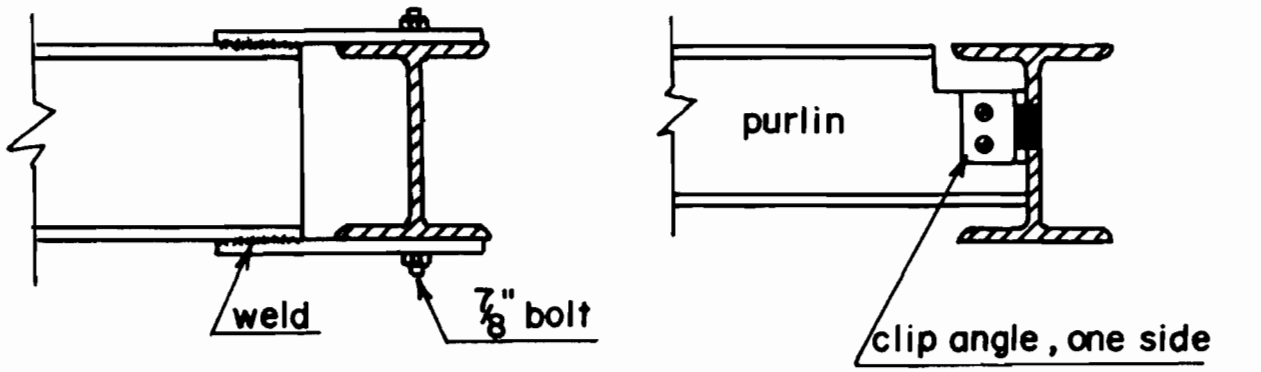

Perimeter member connection

Perimeter beam to intermediate purlin connection

Heavy Frame Connections

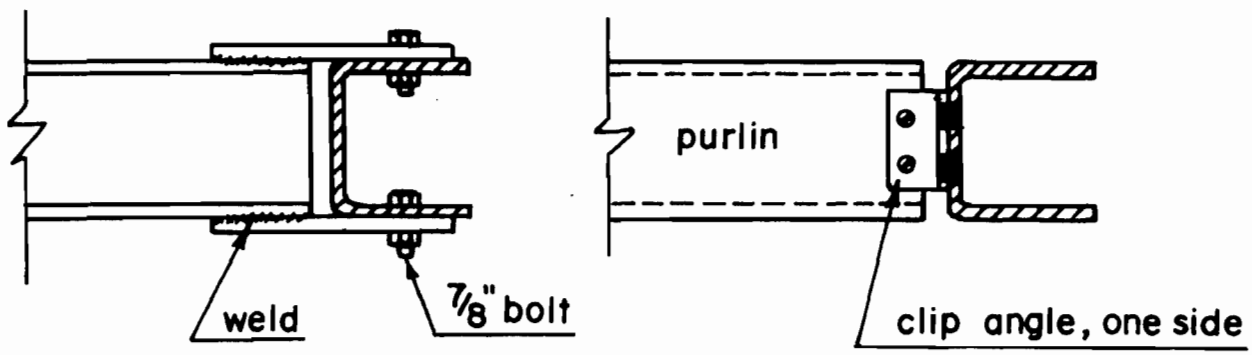

Perimeter member connection

Perimeter beam to intermediate purlin connection

Light Frame Connections

Figure 3.4 Diaphragm test frame connections

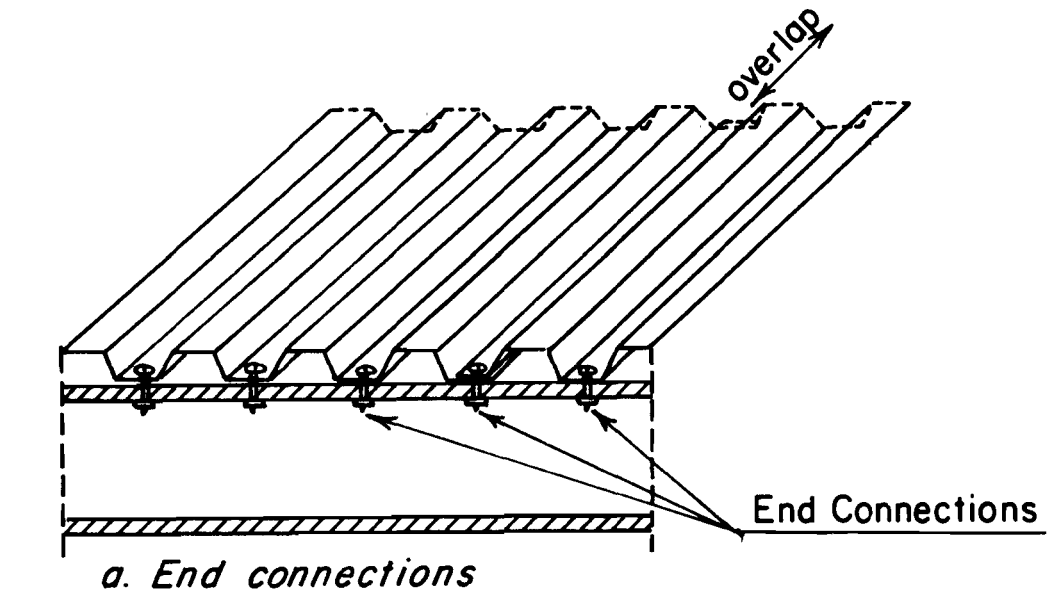

a. End connections

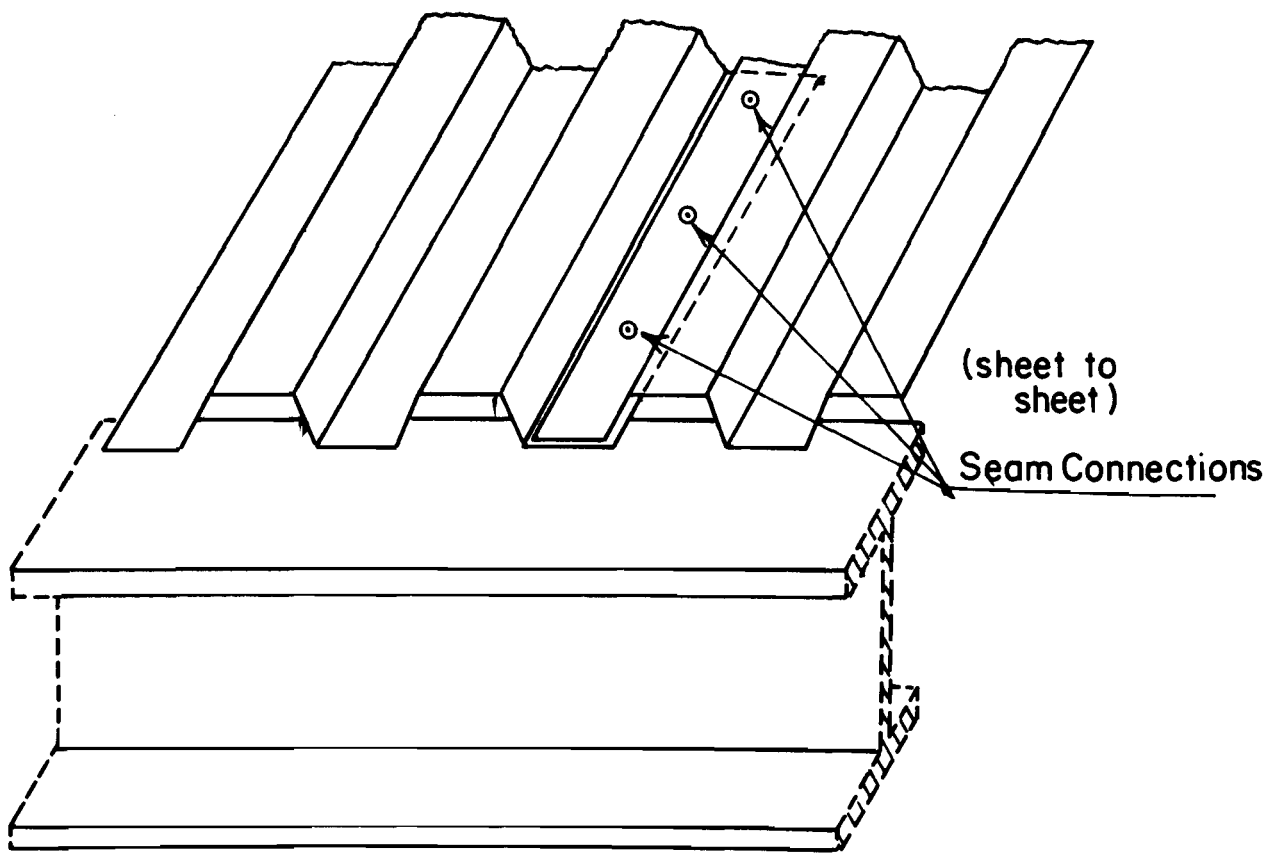

b. Sheet to sheet seam connections

Figure 3.5 Sheet connections (cont.)

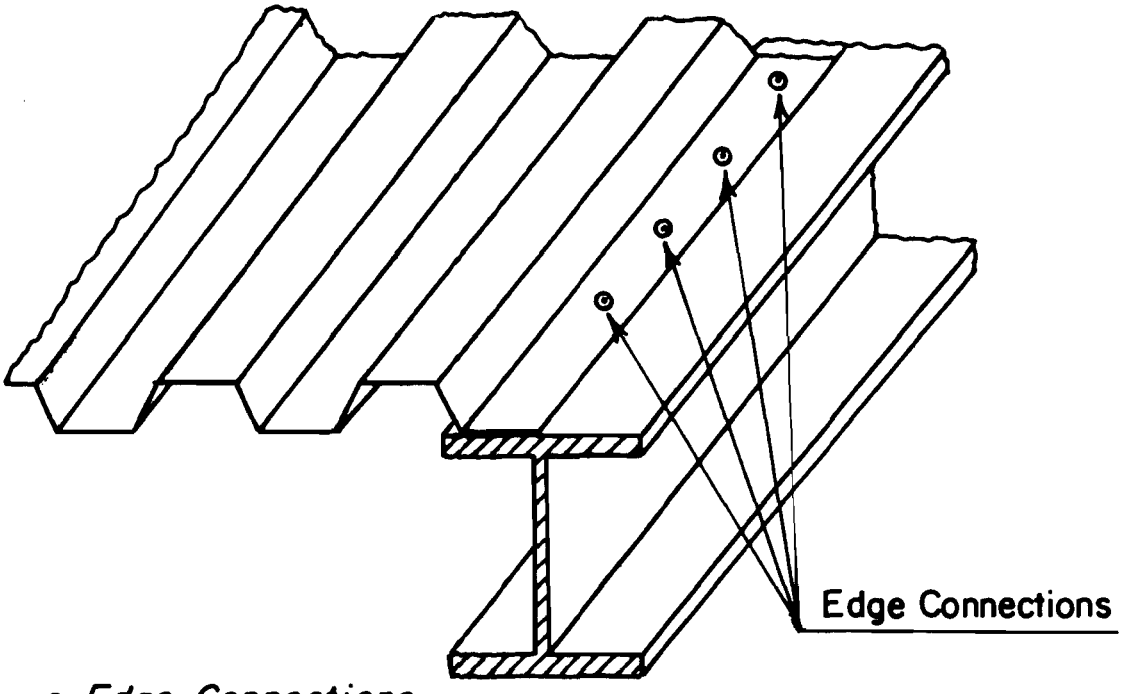

c. Edge Connections

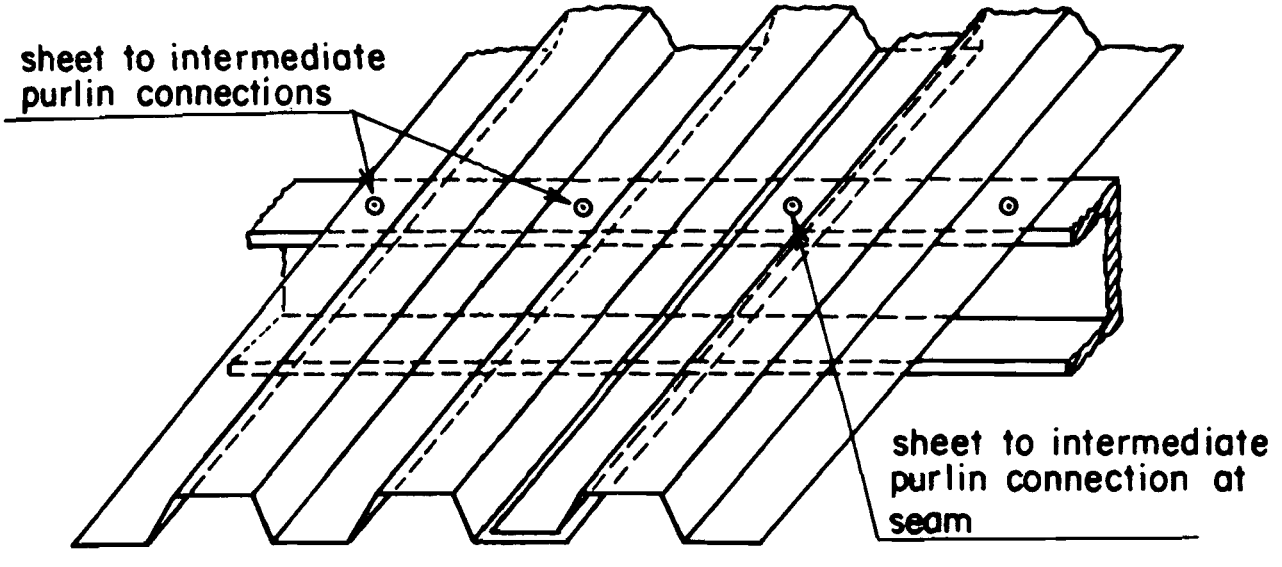

d. Sheet to intermediate purlin connections

Figure 3.5 (cont.) Sheet connections (cont.)

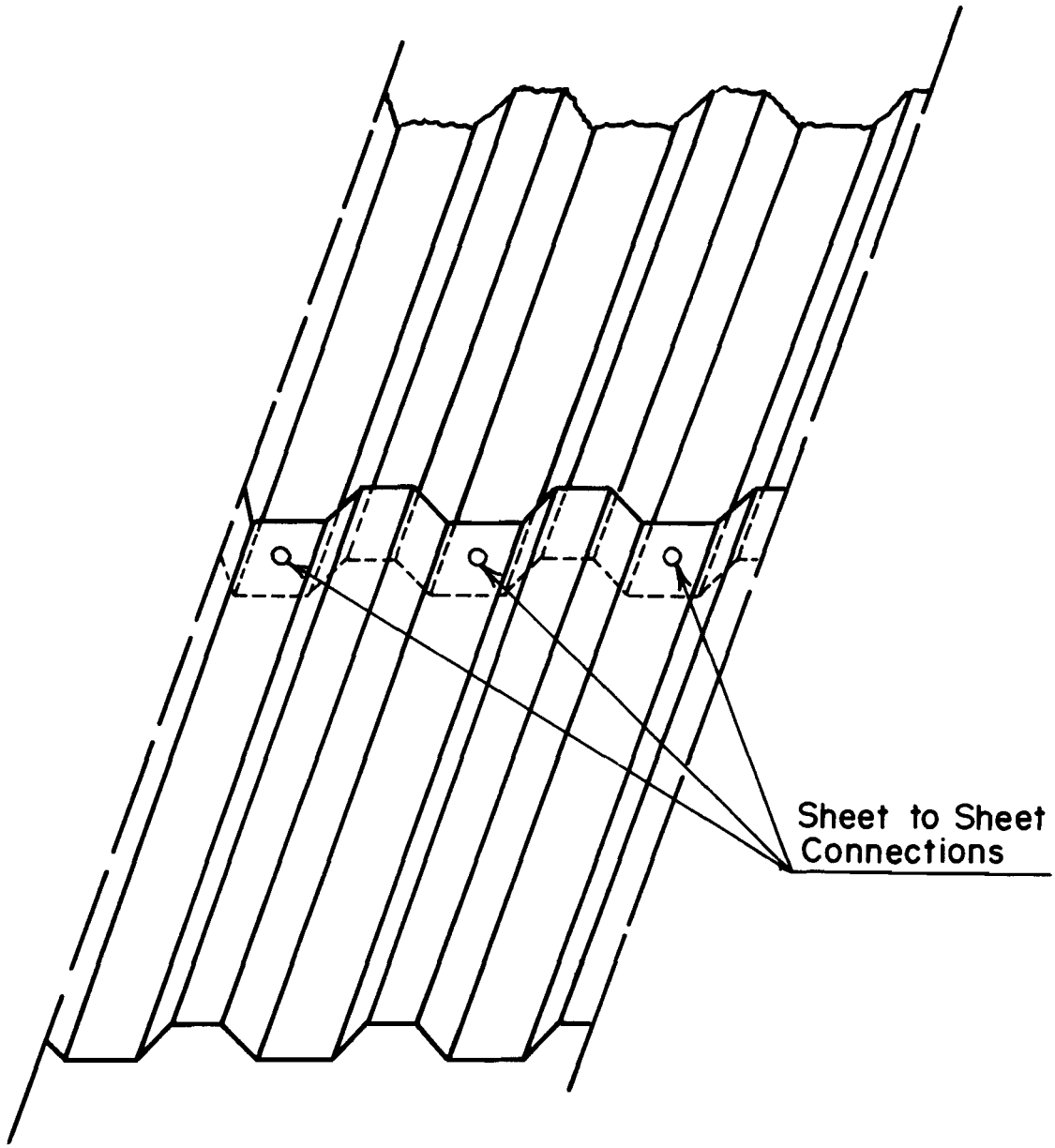

e. Lengthwise connection of two sheets

Figure 3.5 (cont.) Sheet connections

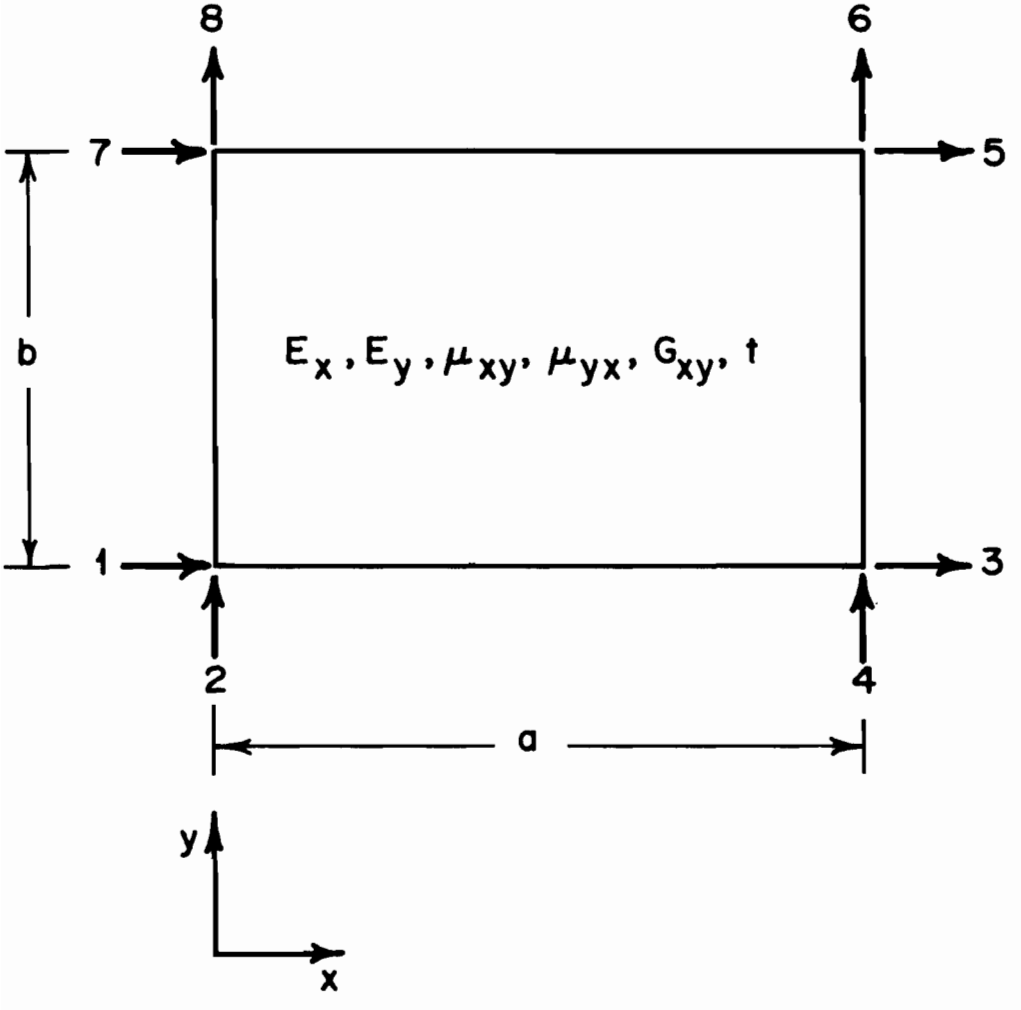

Figure 3.6 Orthotropic plane stress plate element

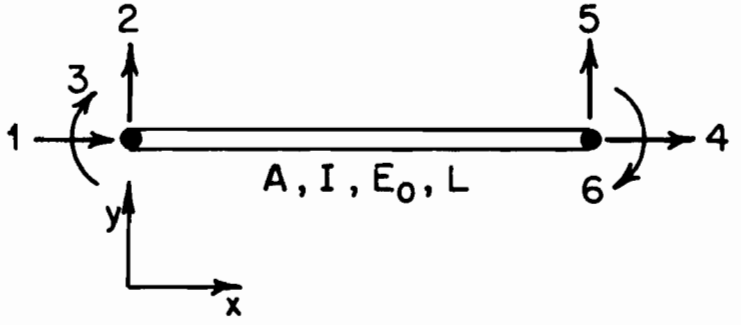

a. Beam finite element

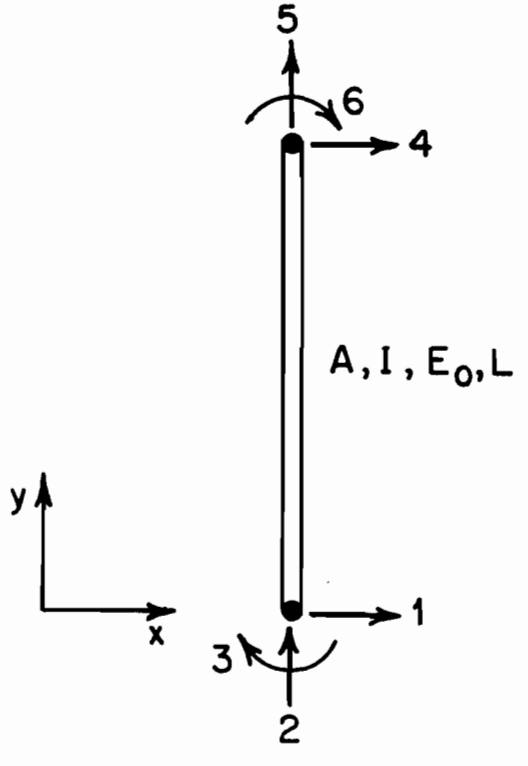

b. Column finite element

Figure 3.7 Flexural member representation

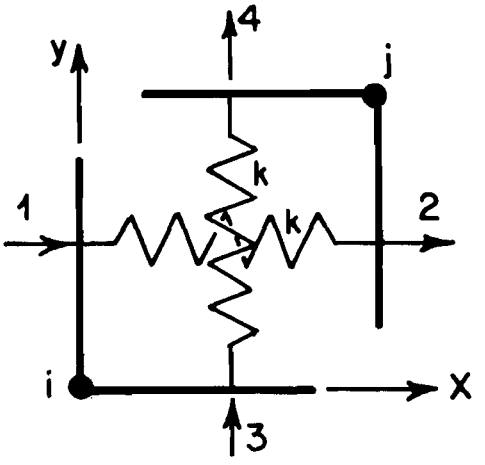

a. Connection model with springs in two directions

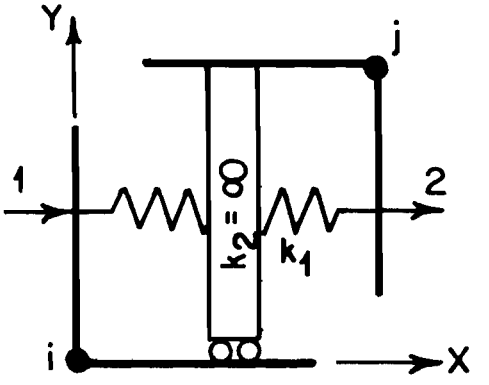

b. Connection model with spring only in one direction (used for sheet to sheet seam connections)*

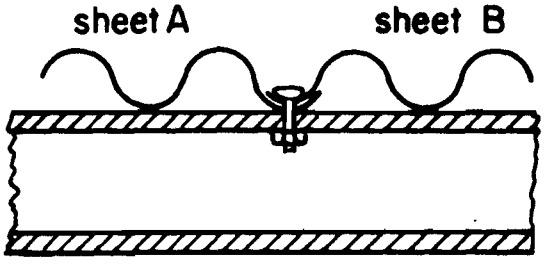

c. Mechanical end connector at sheet sidelap

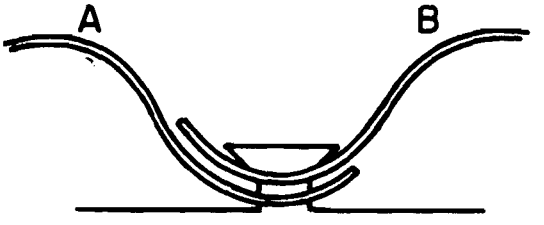

d. Sheets A and B connected to flange independently

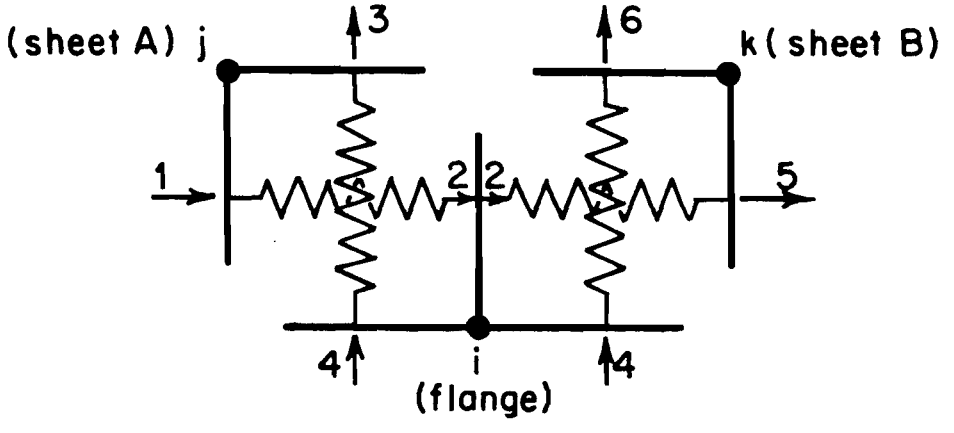

e. Model of the independent connections of Figures (c) and (d)

* the X and Y directions are interchangeable

Figure 3.8 Connection models (cont.)

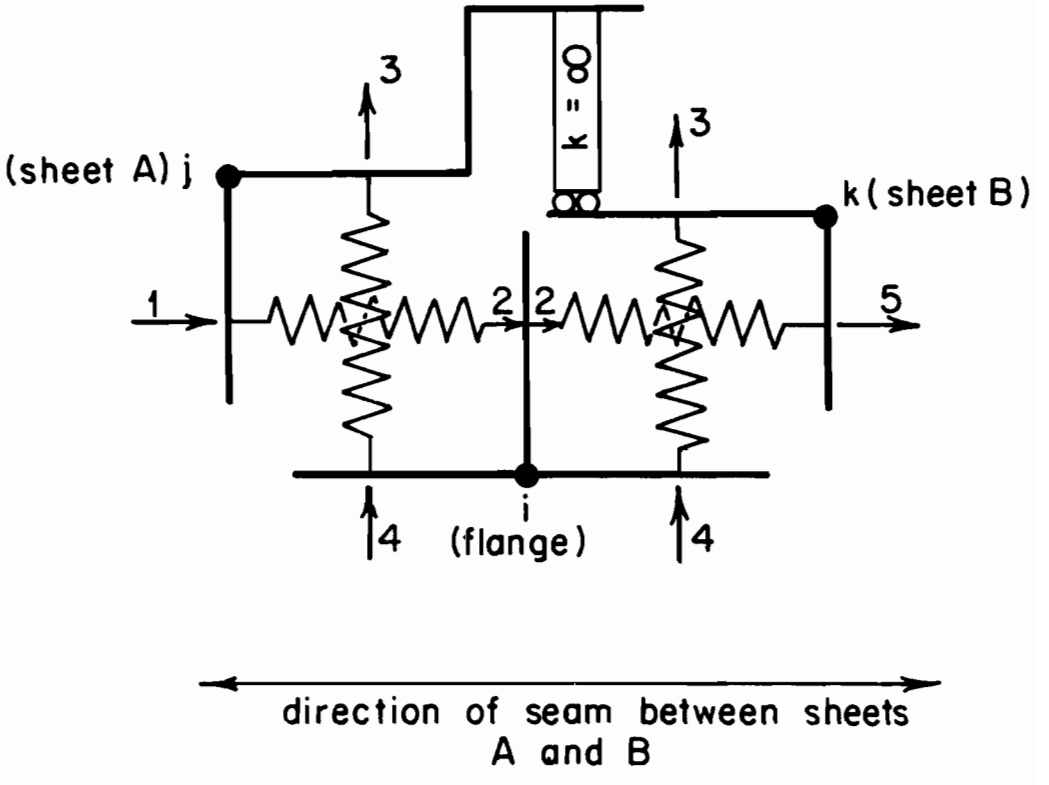

f. Model of sheet to intermediate purlin connection at sheet sidelap

Figure 3.8 (cont.) Connection models

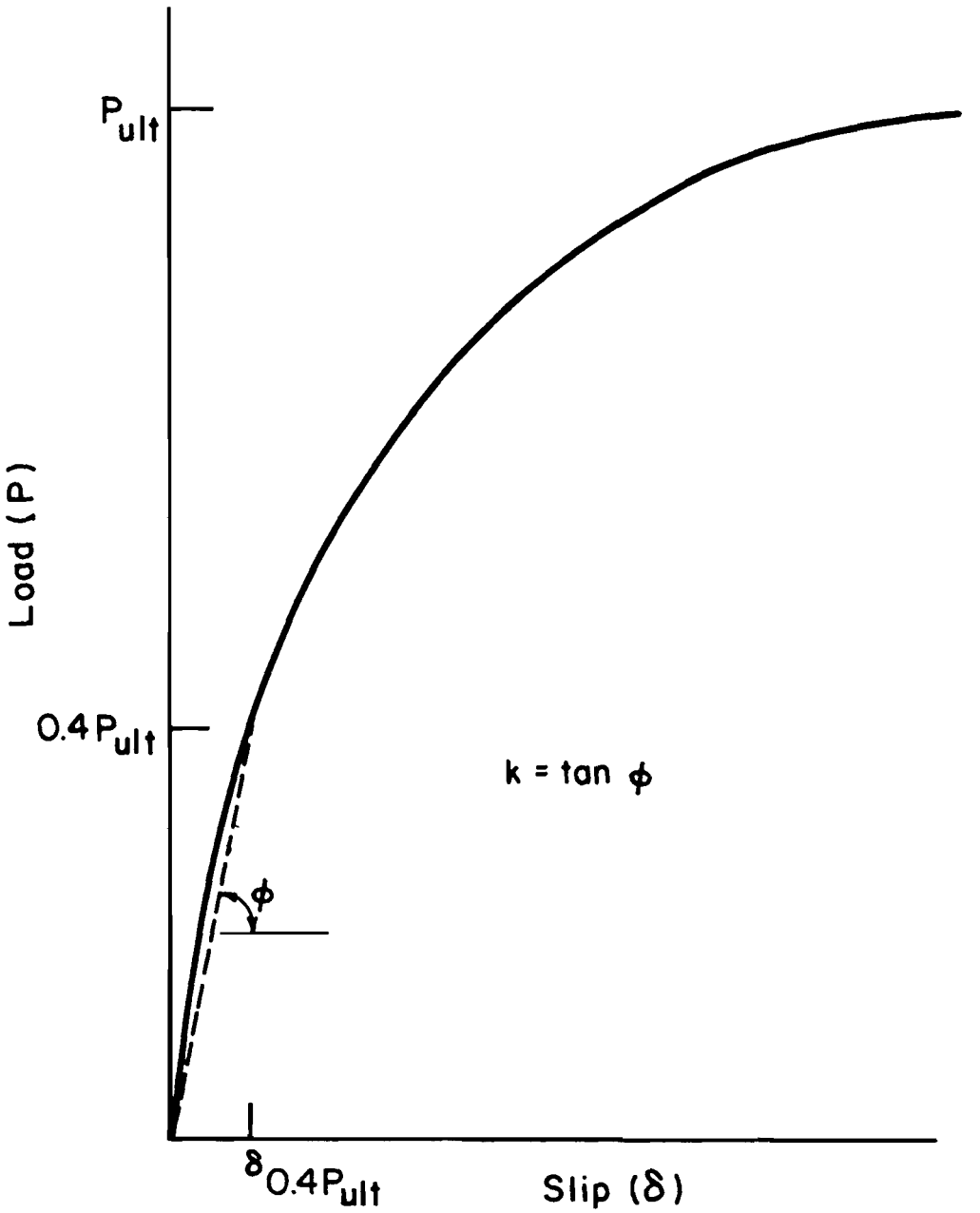

Figure 3.9 Approximation of connection behavior for first order analysis

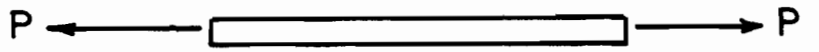

a. Axial element in structure

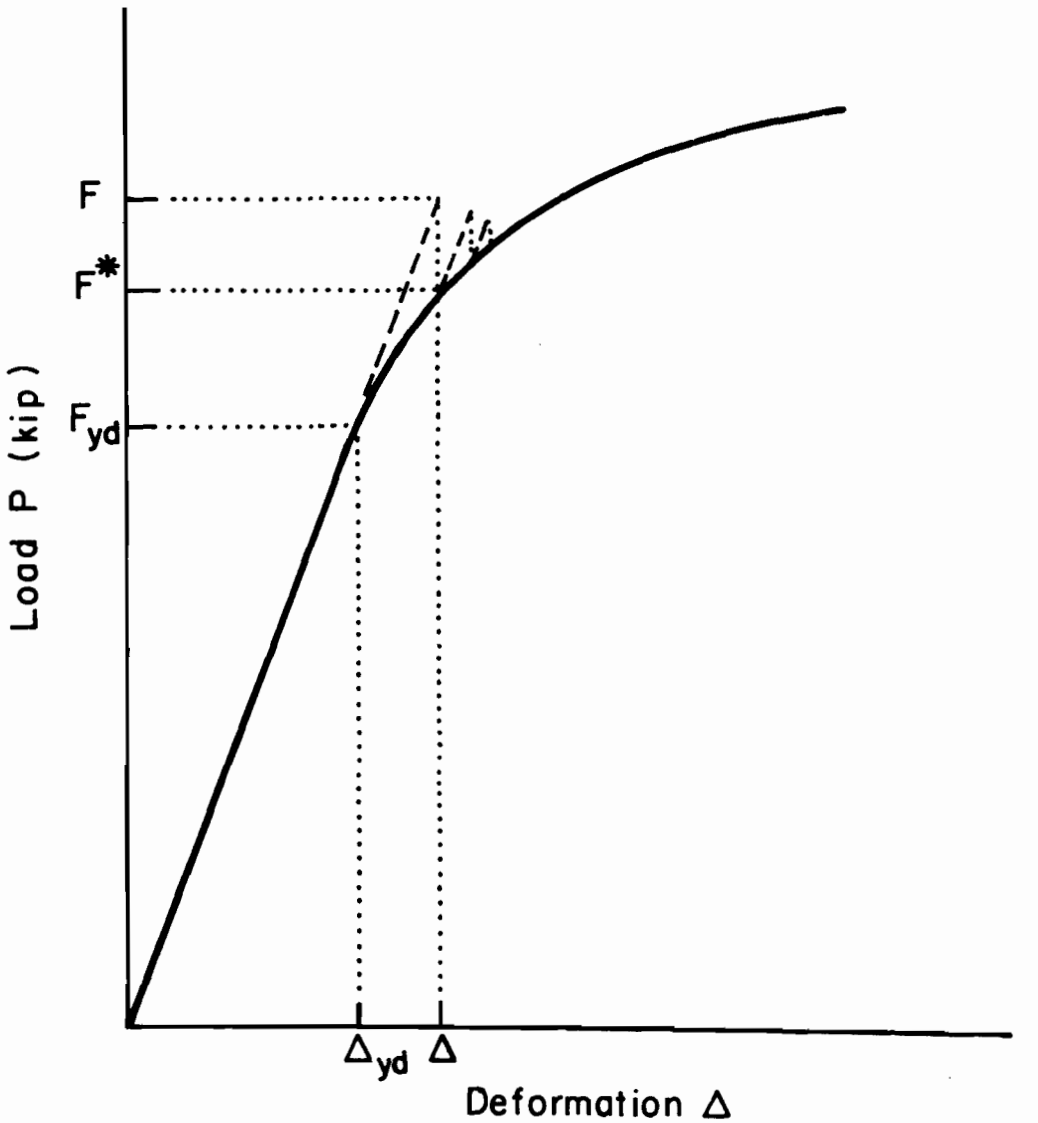

b. Tension test behavior of element of Figure 4.1 a

Figure 4.1 Residual force approach for axial element

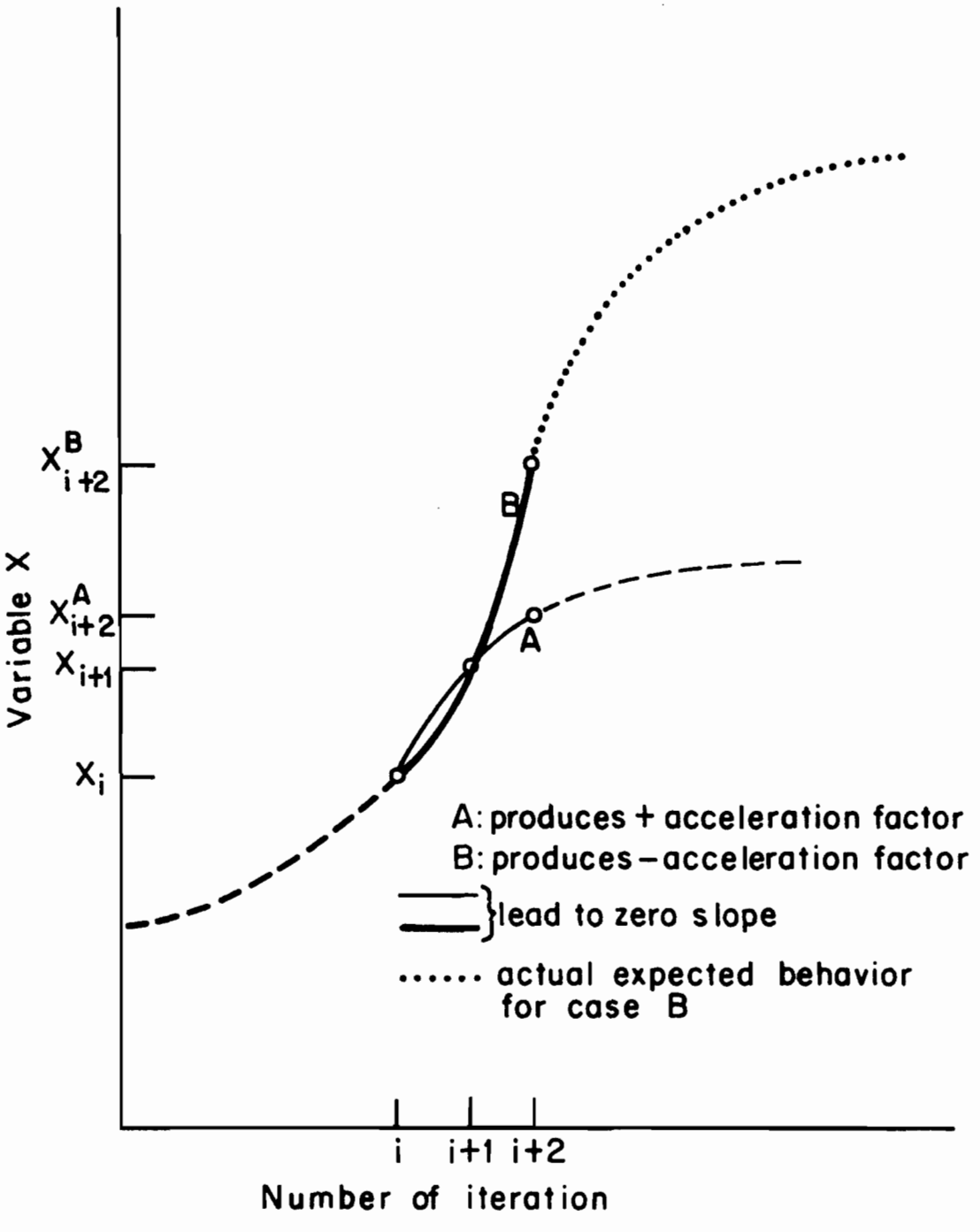

Figure 4.2 Effect of the third iteration of a triplet, on the acceleration factor S

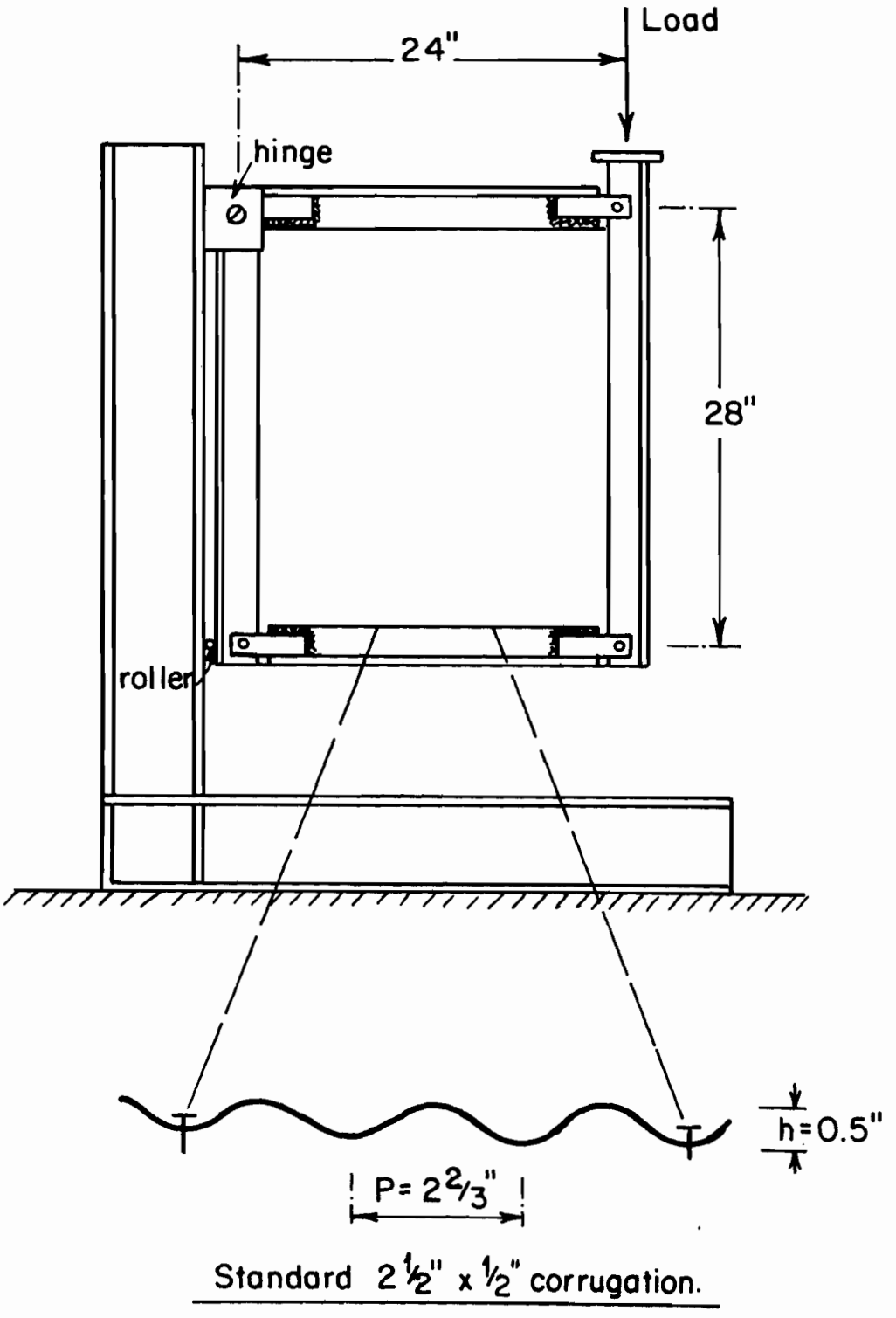

Figure 5.1 Test arrangement of the 24" x 28" diaphragm

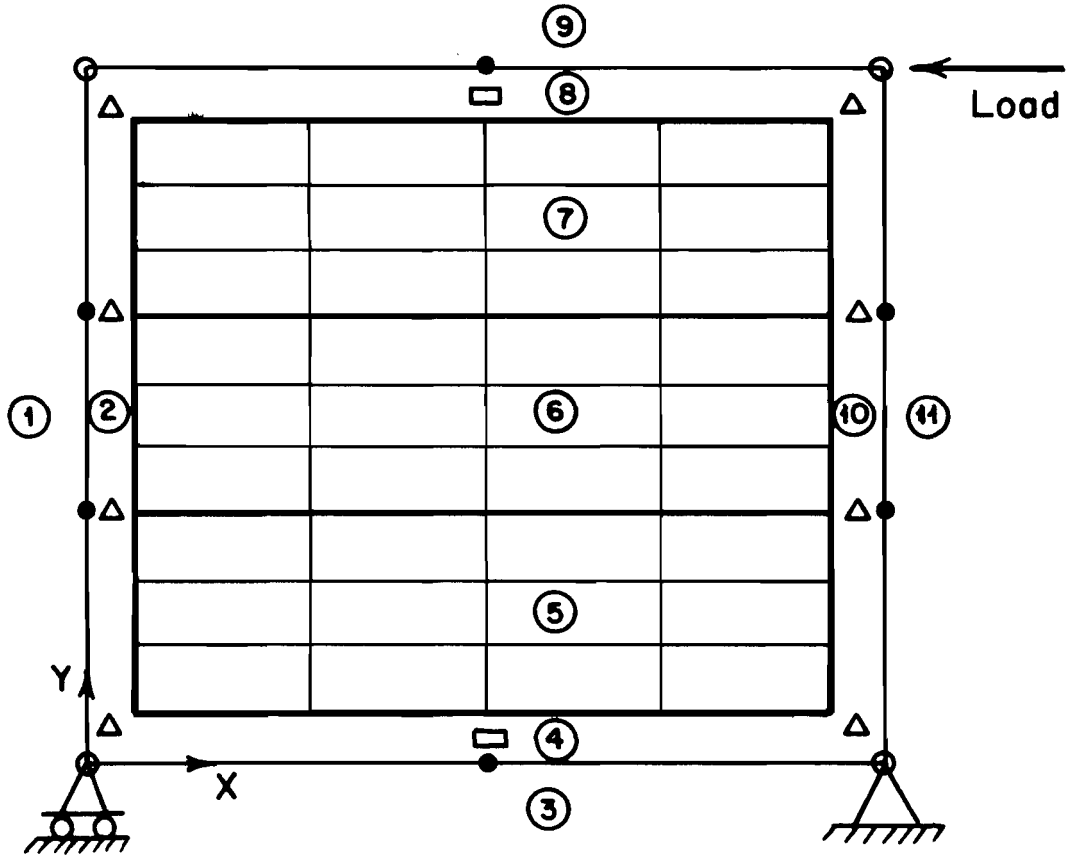

(i) : subassembly number

△ : end connector

▭ : edge connector

——— plate element borders

——— plate subassembly borders

—●— beam nodal point

—○— end of beam subassembly

Figure 5.2 Finite element mesh and the sequence of sub-assemblies for the 24" x 28" diaphragm

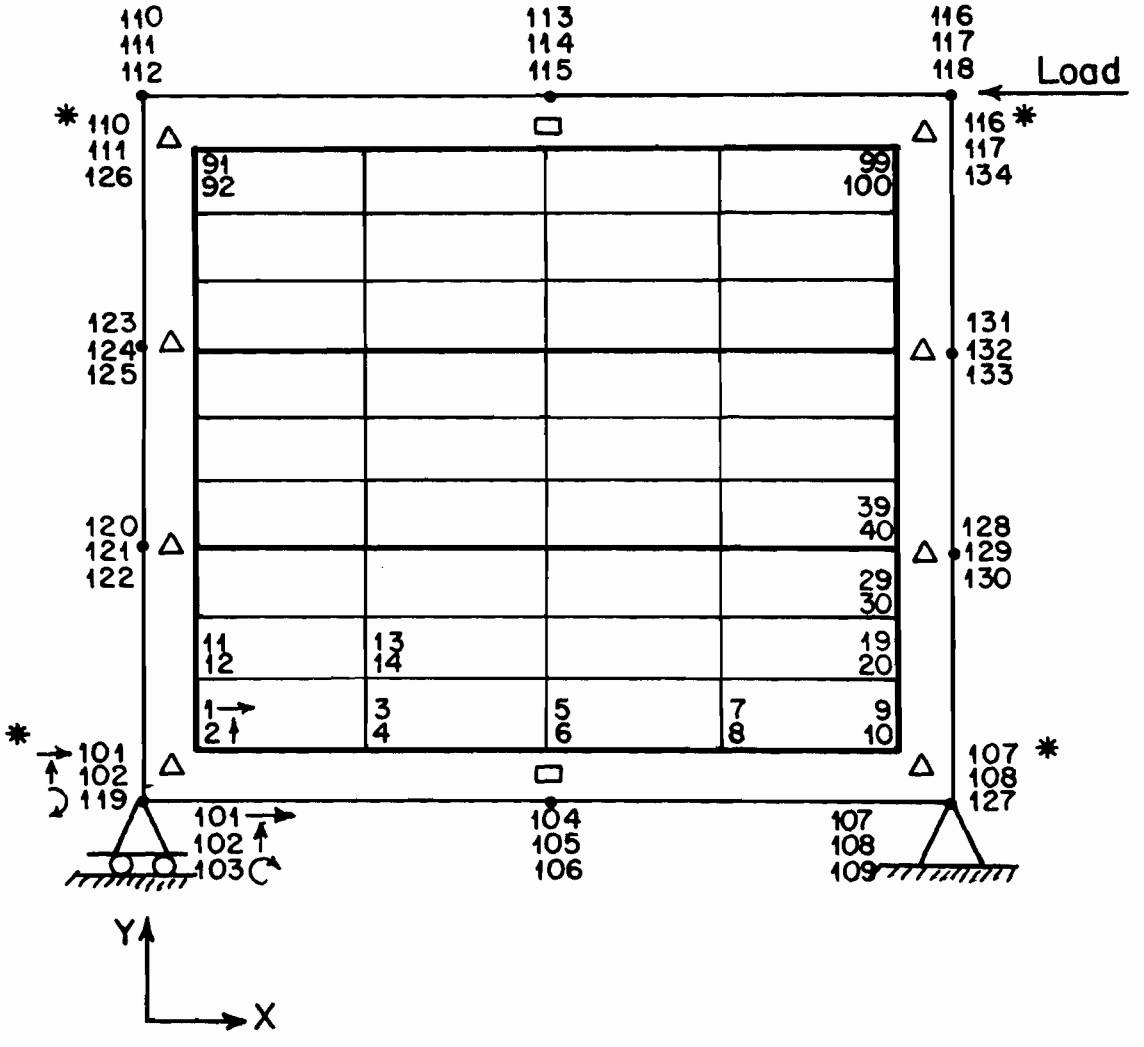

* beamsin y direction share same translational d.o.f.s. with beams in x direction, but not the rotational d.o.f (internal hinges).

Figure 5.3 Numbering of structural d.o.f. for the 24" x 28" diaphragm

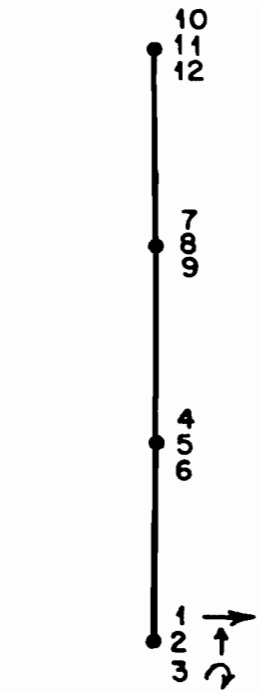

End Beam
(Y-dir.)
Subassembly

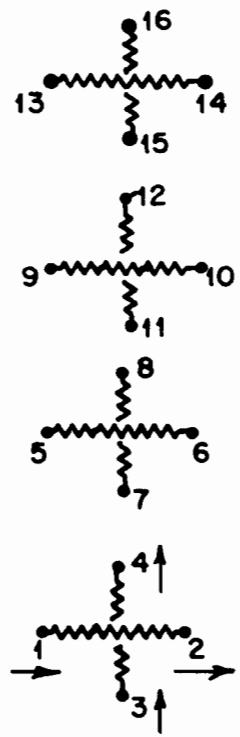

End Connection
Subassembly

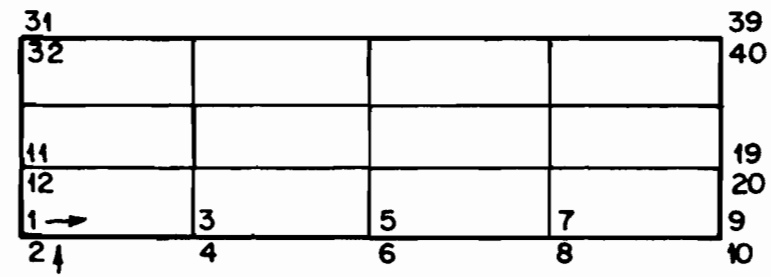

Plate Subassembly

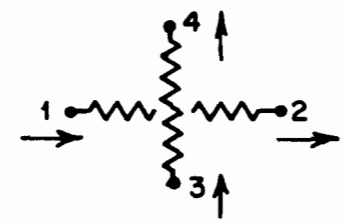

Edge Connection Subassembly

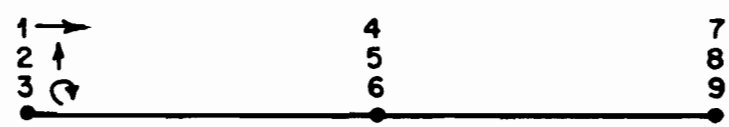

Edge Beam (X-dir) Subassembly

Figure 5.4 Basic subassemblies of the 24" x 28" diaphragm and subassembly d.o.f. numbering

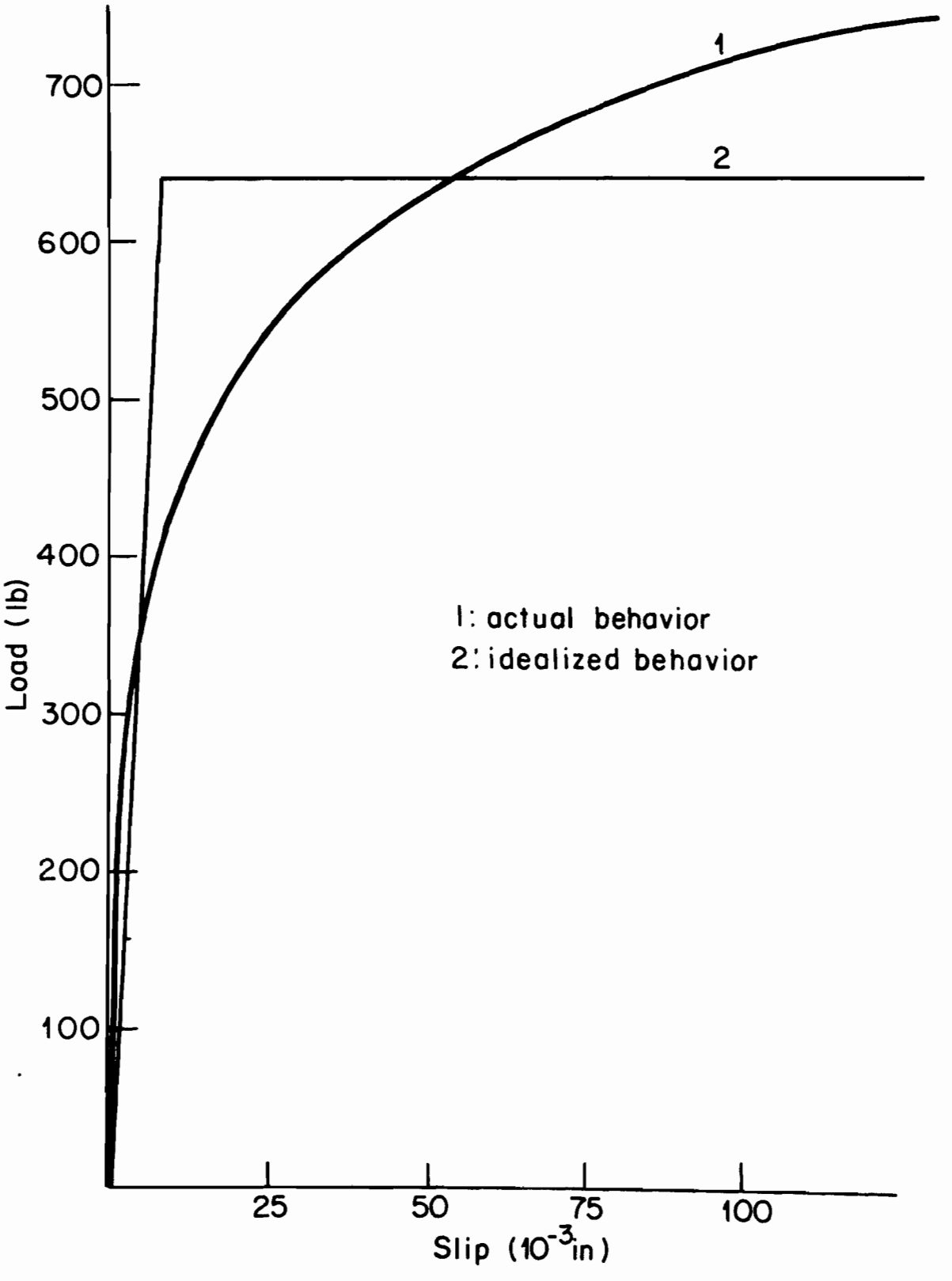

Figure 5.5 No. 14 screw in 26 gage steel

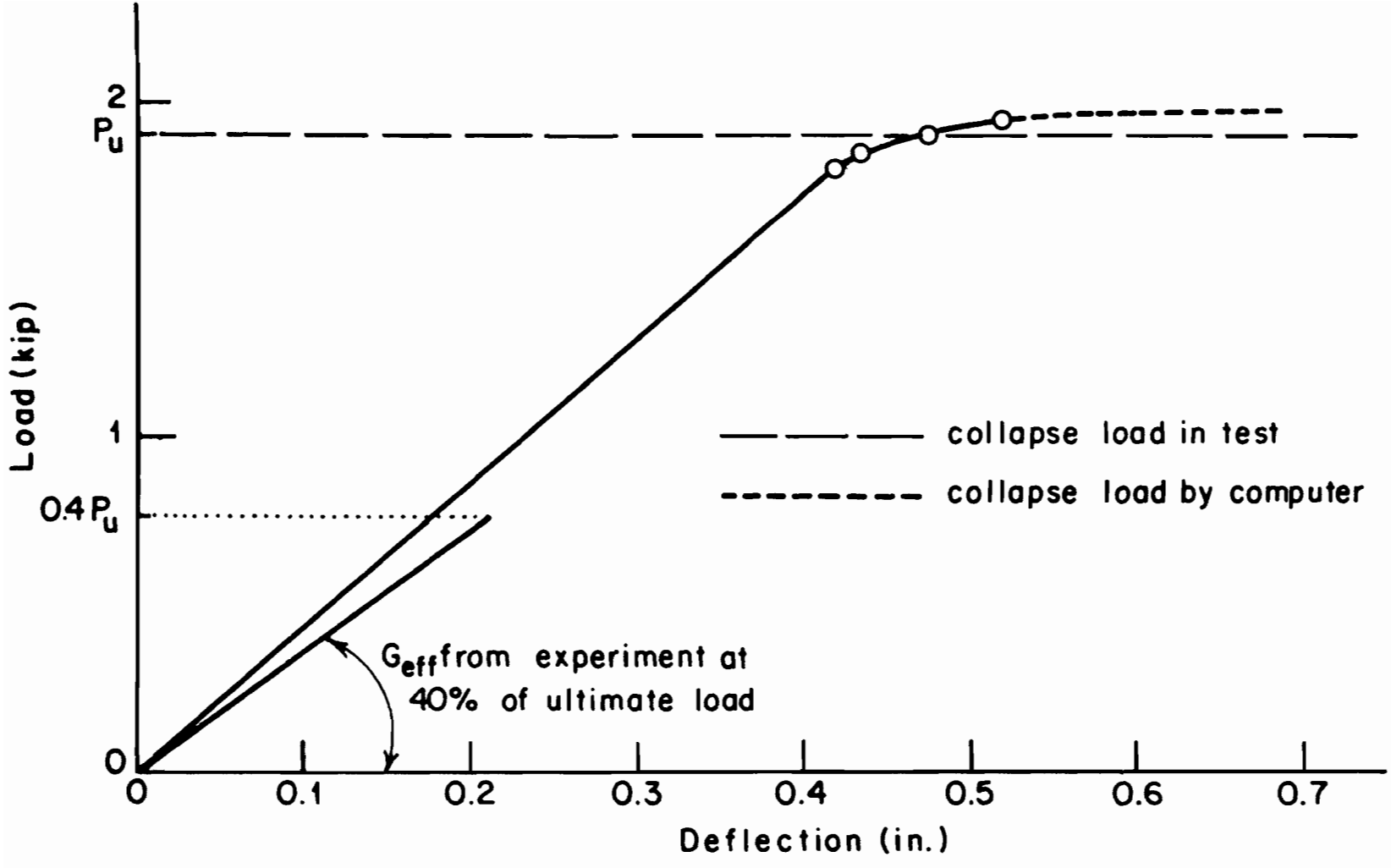

Figure 5.6 24" x 28" shear diaphragm. Deflection of representative d.o.f.

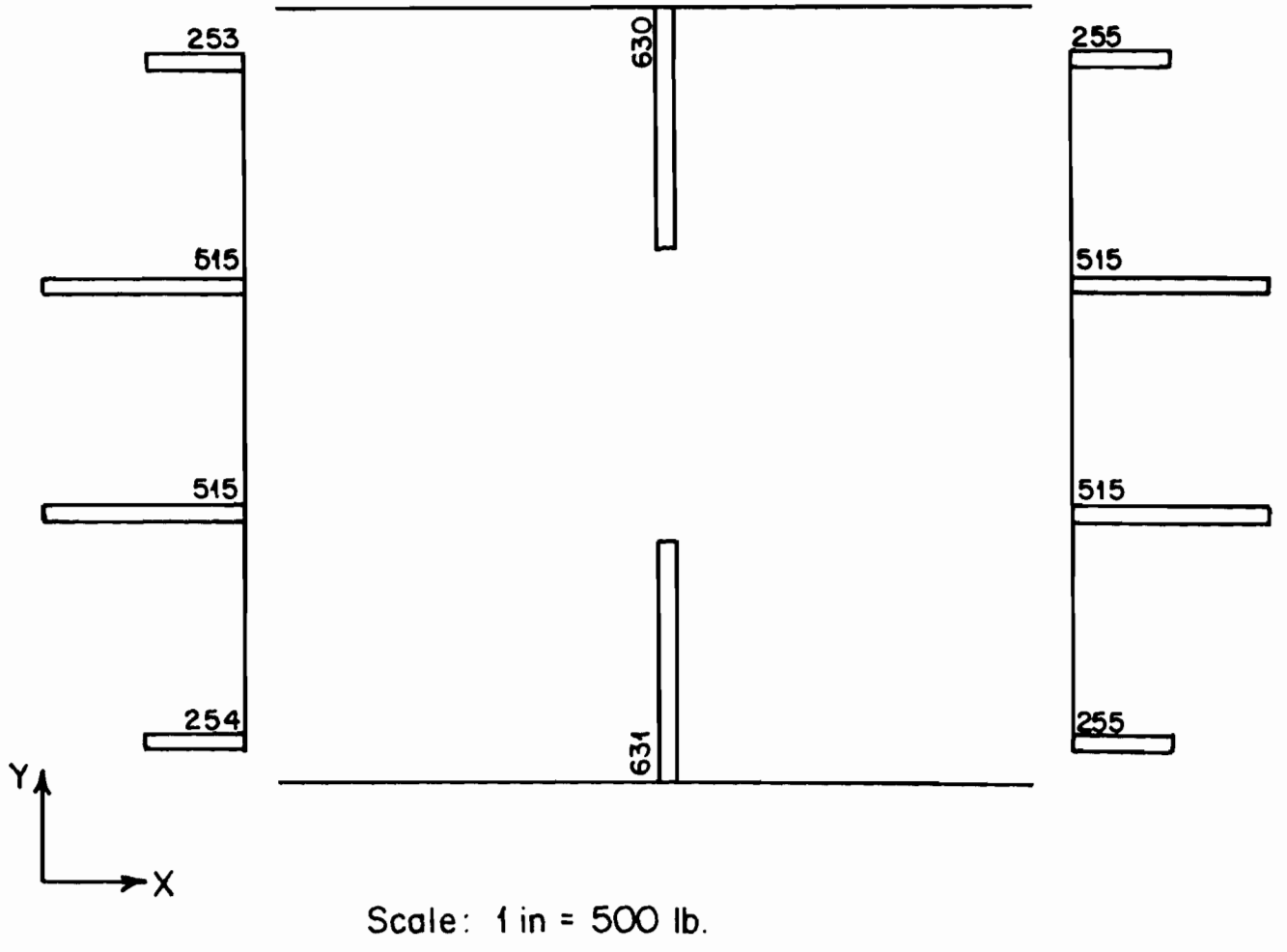

Figure 5.7 Longitudinal forces on the perimeter beams of the 24" x 28" diaphragm, at the elastic limit

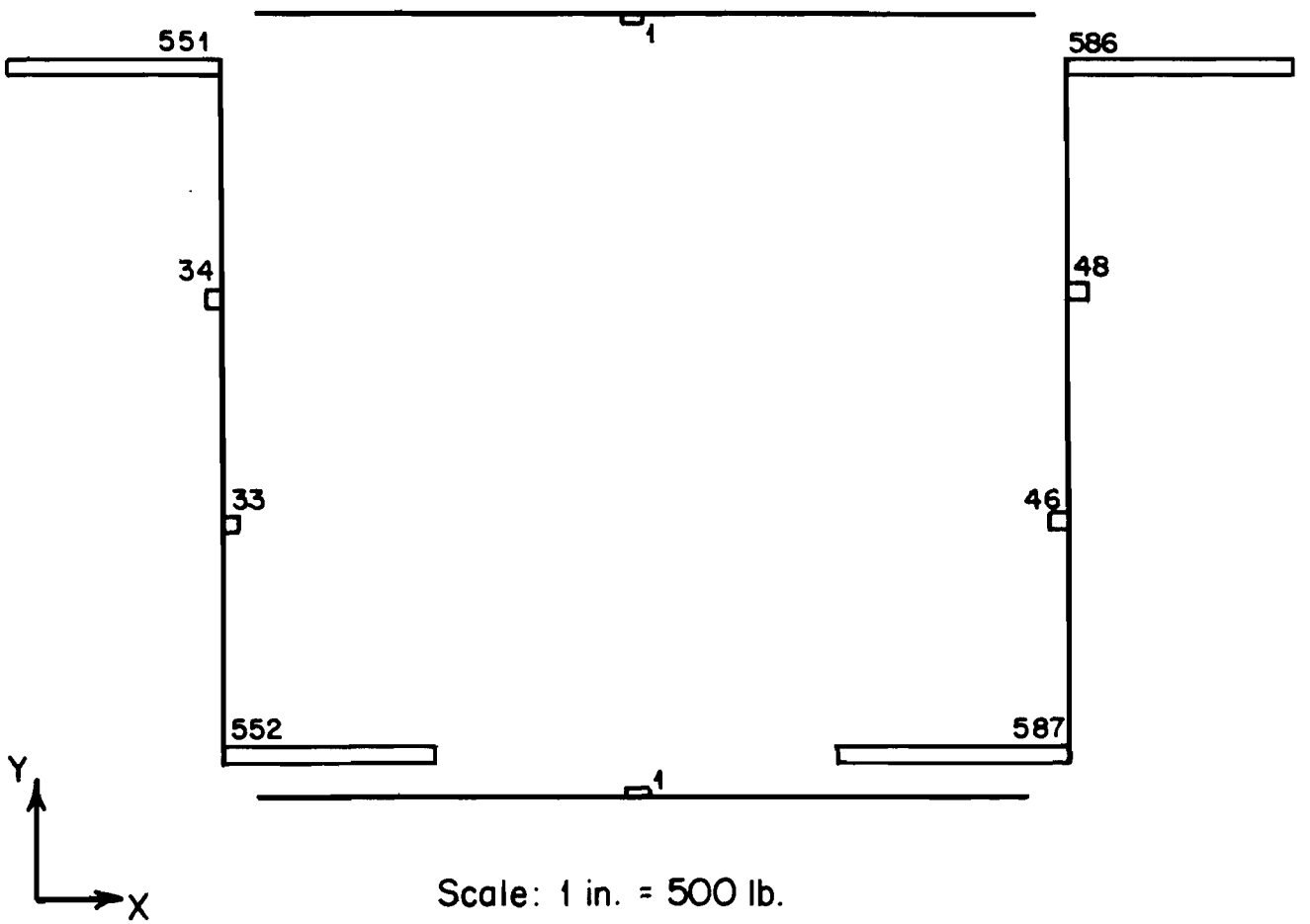

Figure 5.8 Lateral forces on the perimeter beams of the 24" x 28" diaphragm, at the elastic limit

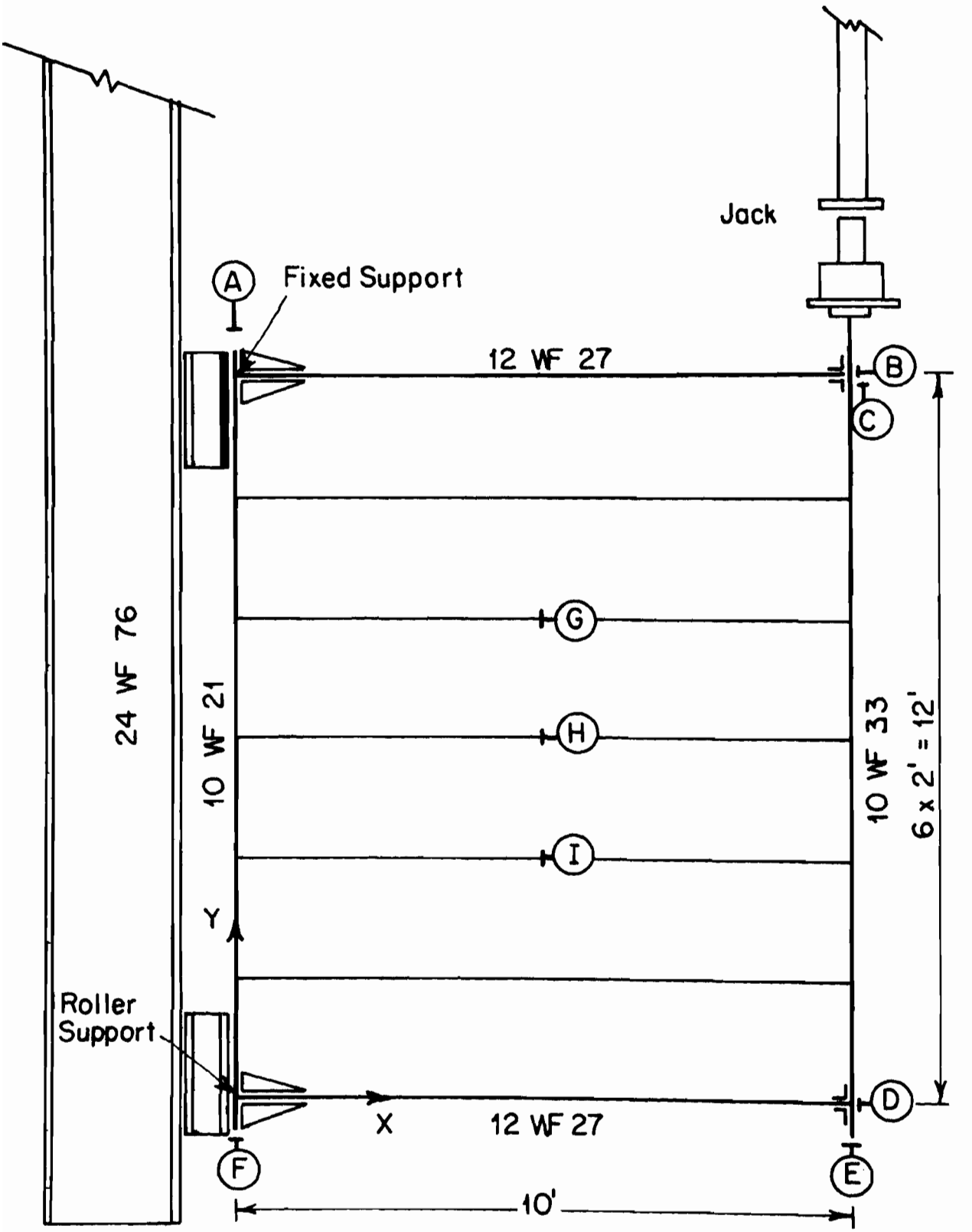

Figure 5.9 Test arrangement of the 10' x 12' welded diaphragm

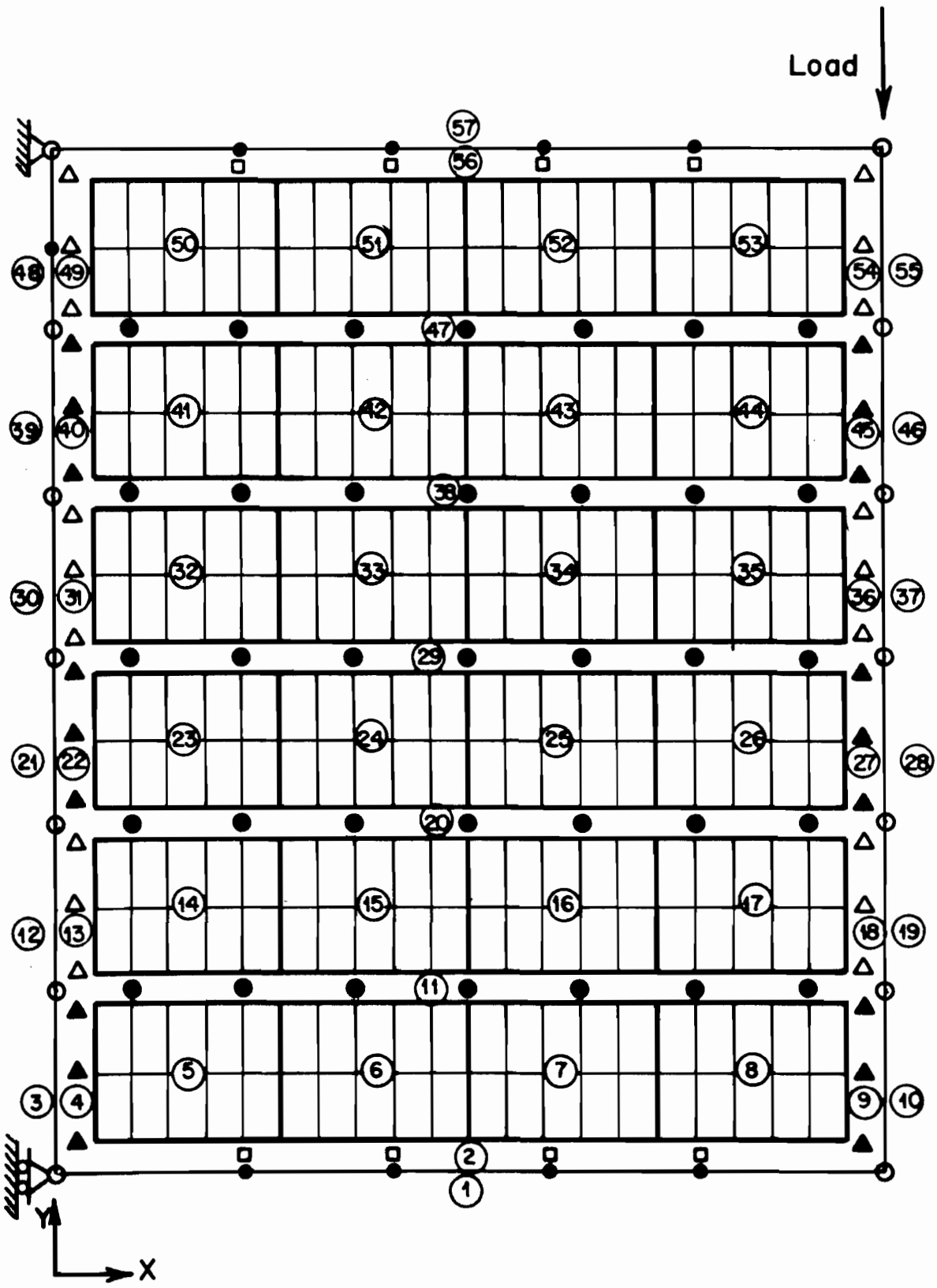

Figure 5.10 Finite element mesh and the sequence of sub-assemblies for the 10' x 12' welded diaphragm

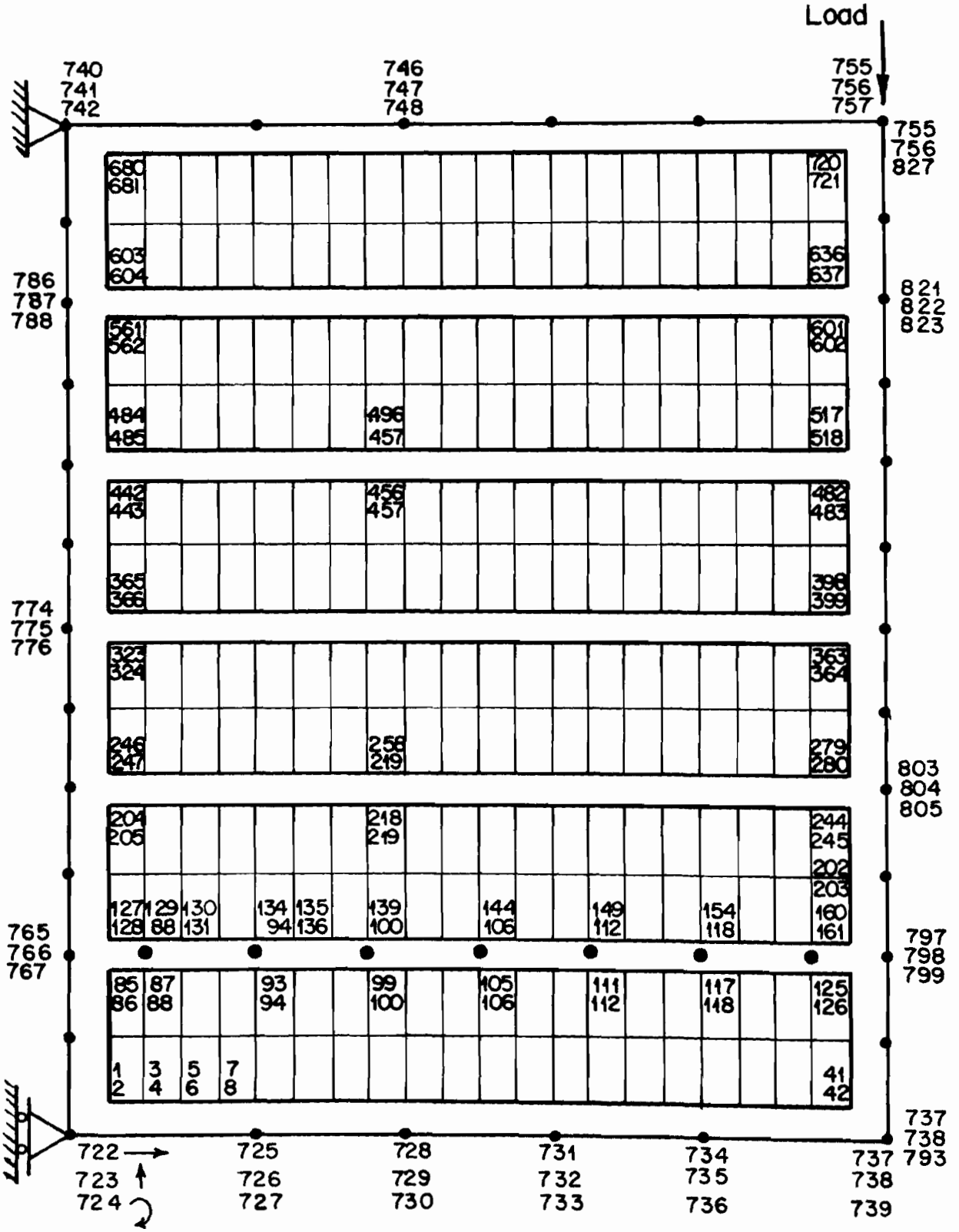

Figure 5.11 Numbering of structural d.o.f. for the 10' x 12' welded diaphragm

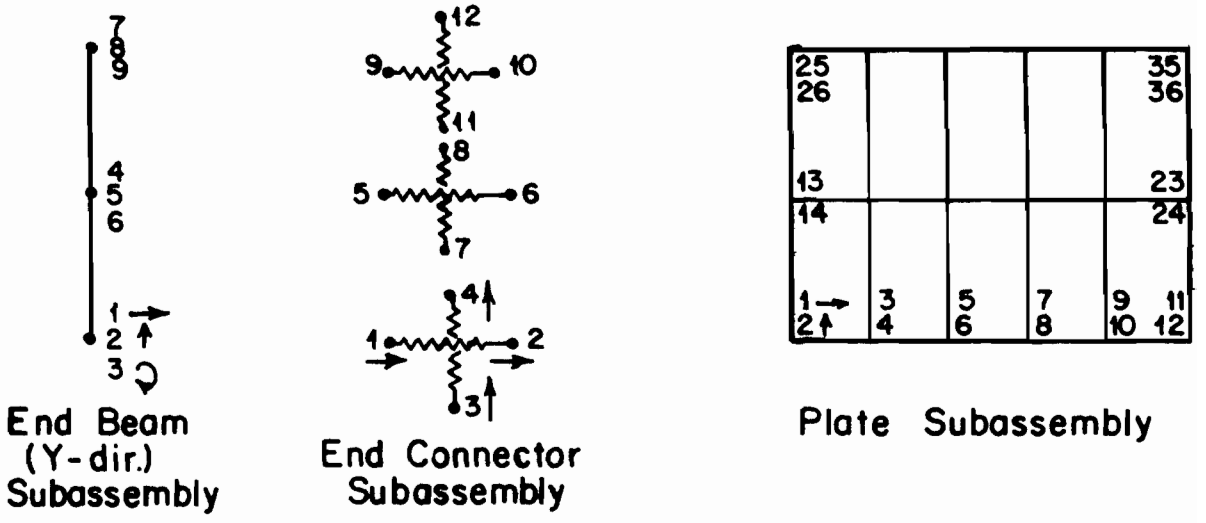

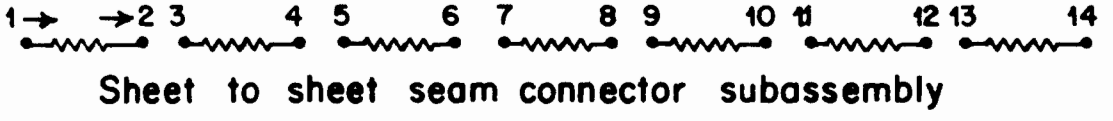

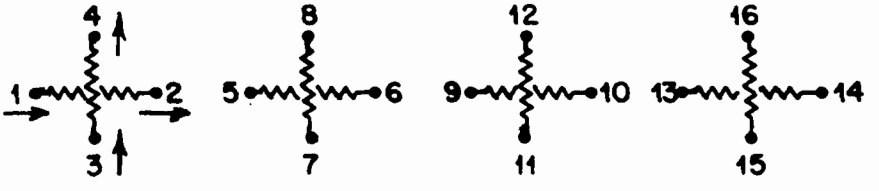

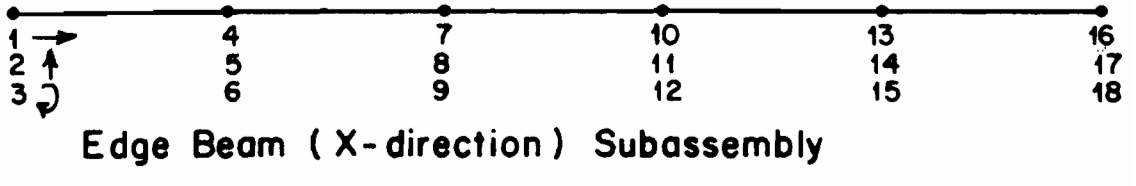

Figure 5.12 Basic subassemblies of the 10' x 12' welded diaphragm

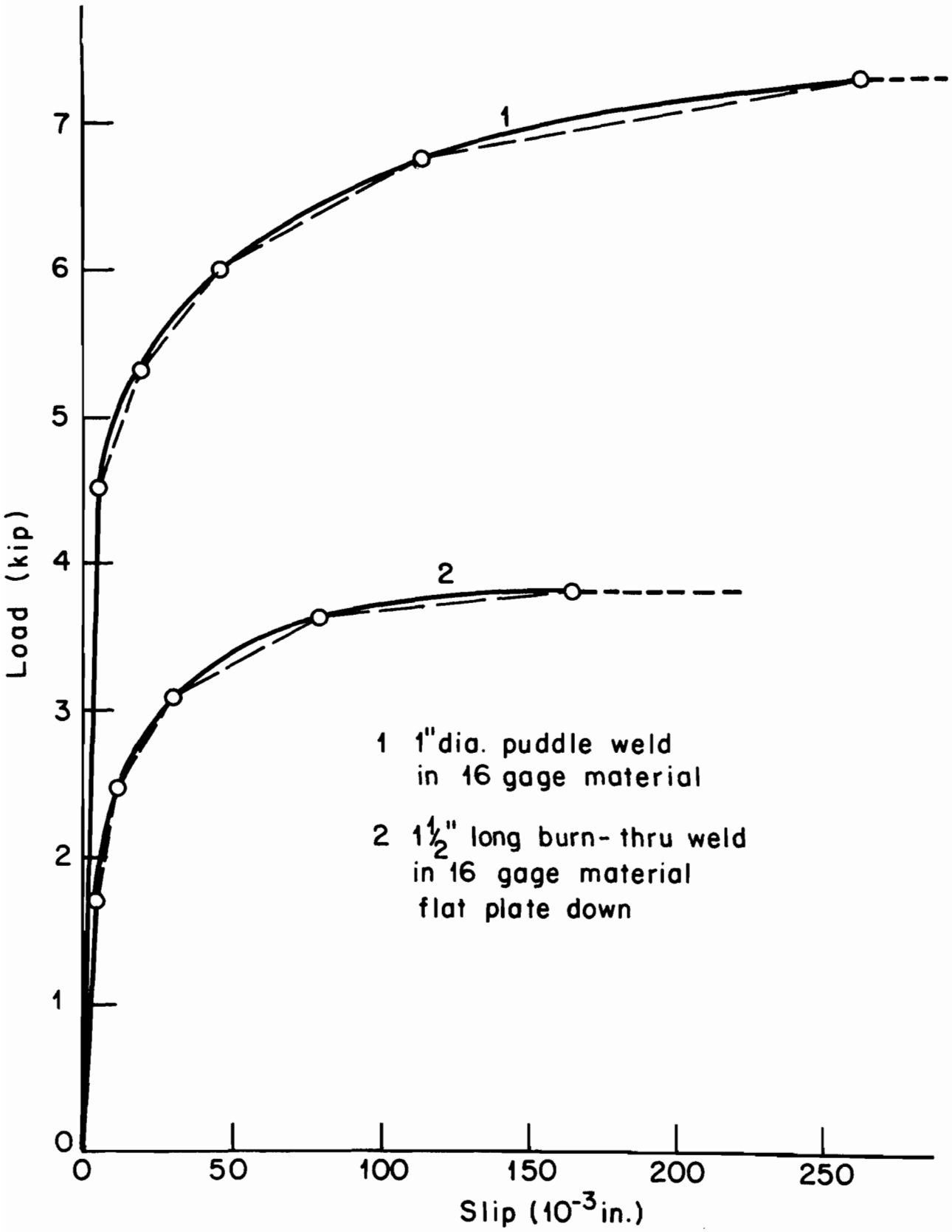

Figure 5.13 Interpolated curves. Connections of welded diaphragm

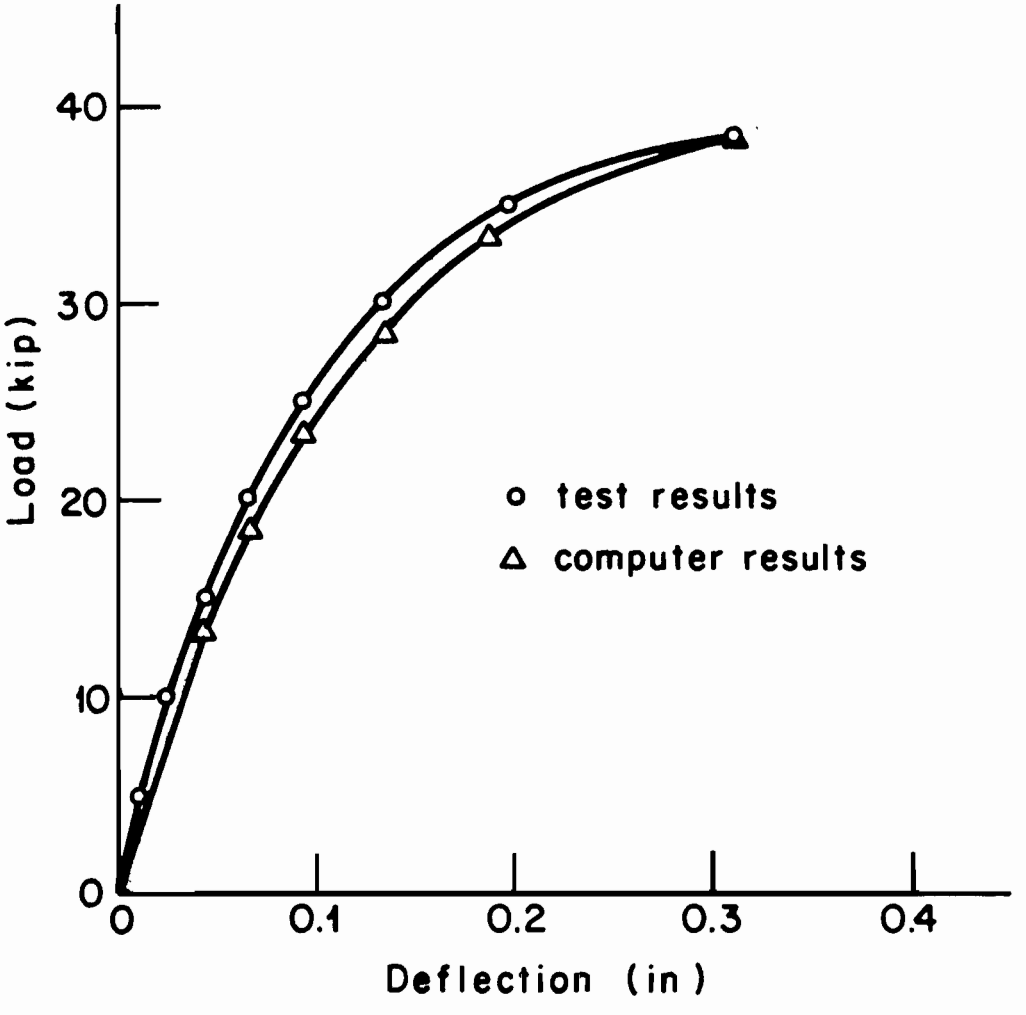

Figure 5.14 10' x 12' welded diaphragm. Deflection of representative d.o.f.

Forces at the elastic limit (13477 lbs.)

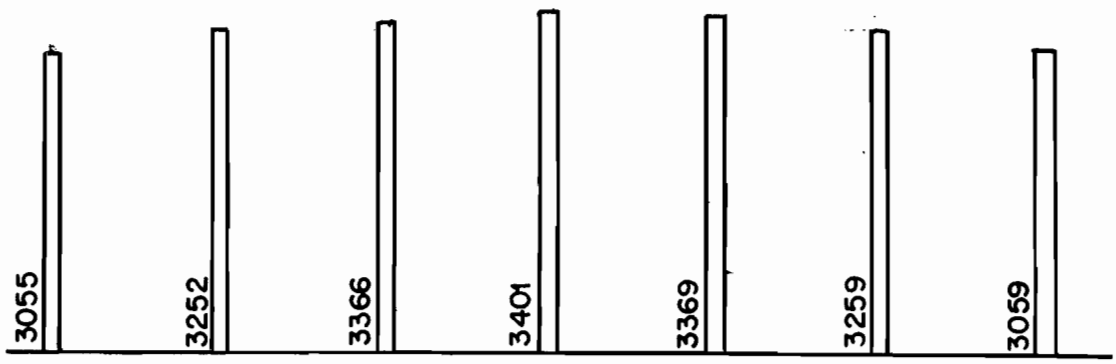

Forces at the 5th increment of load (38477 lbs.)

Scale: 1 in = 2000 lbs.

Figure 5.15 Forces in the connectors of the middle seam line of 10' x 12' welded diaphragm

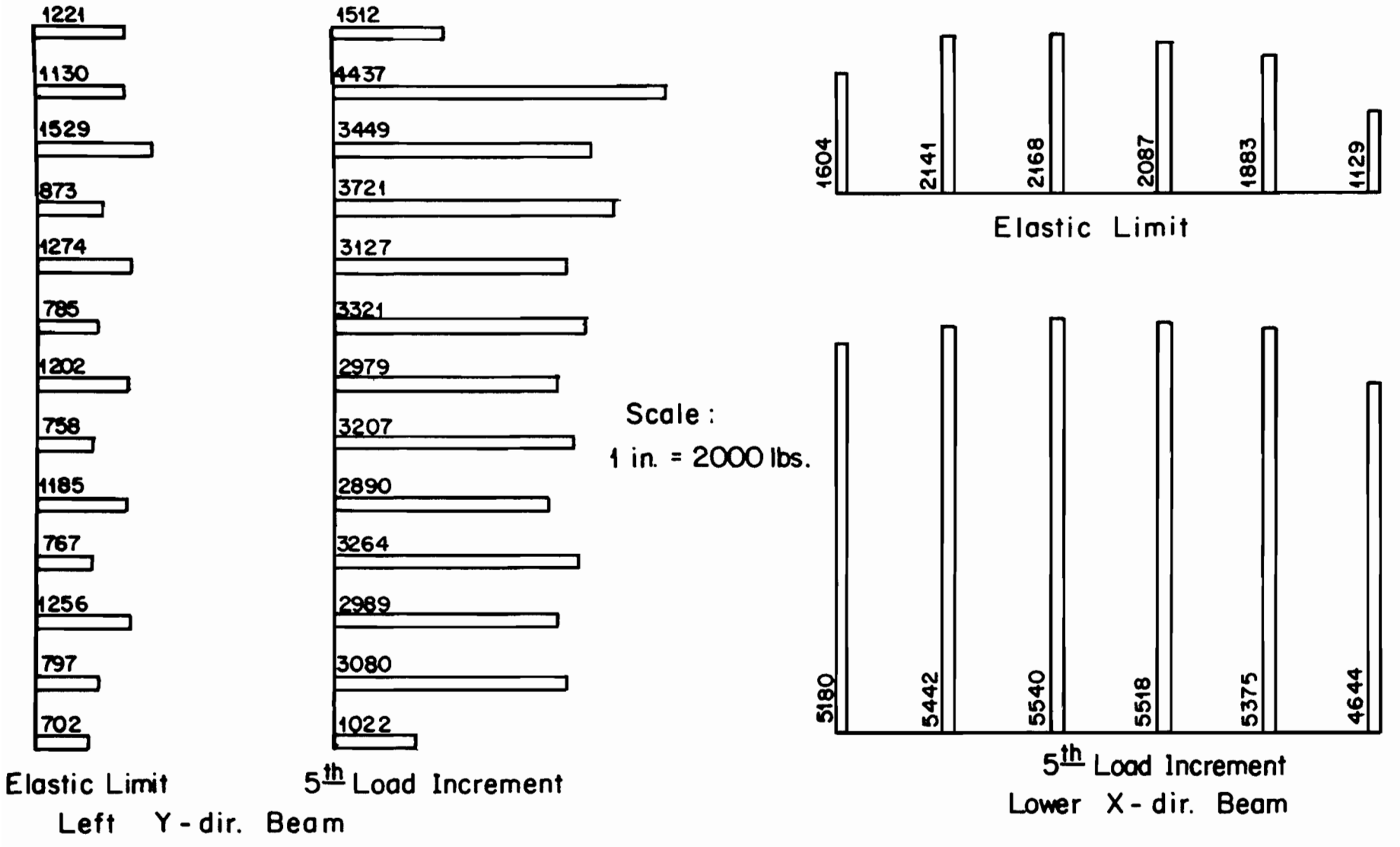

Figure 5.16 Longitudinal forces on the perimeter of beams of 10' x 12' welded diaphragm (cont.)

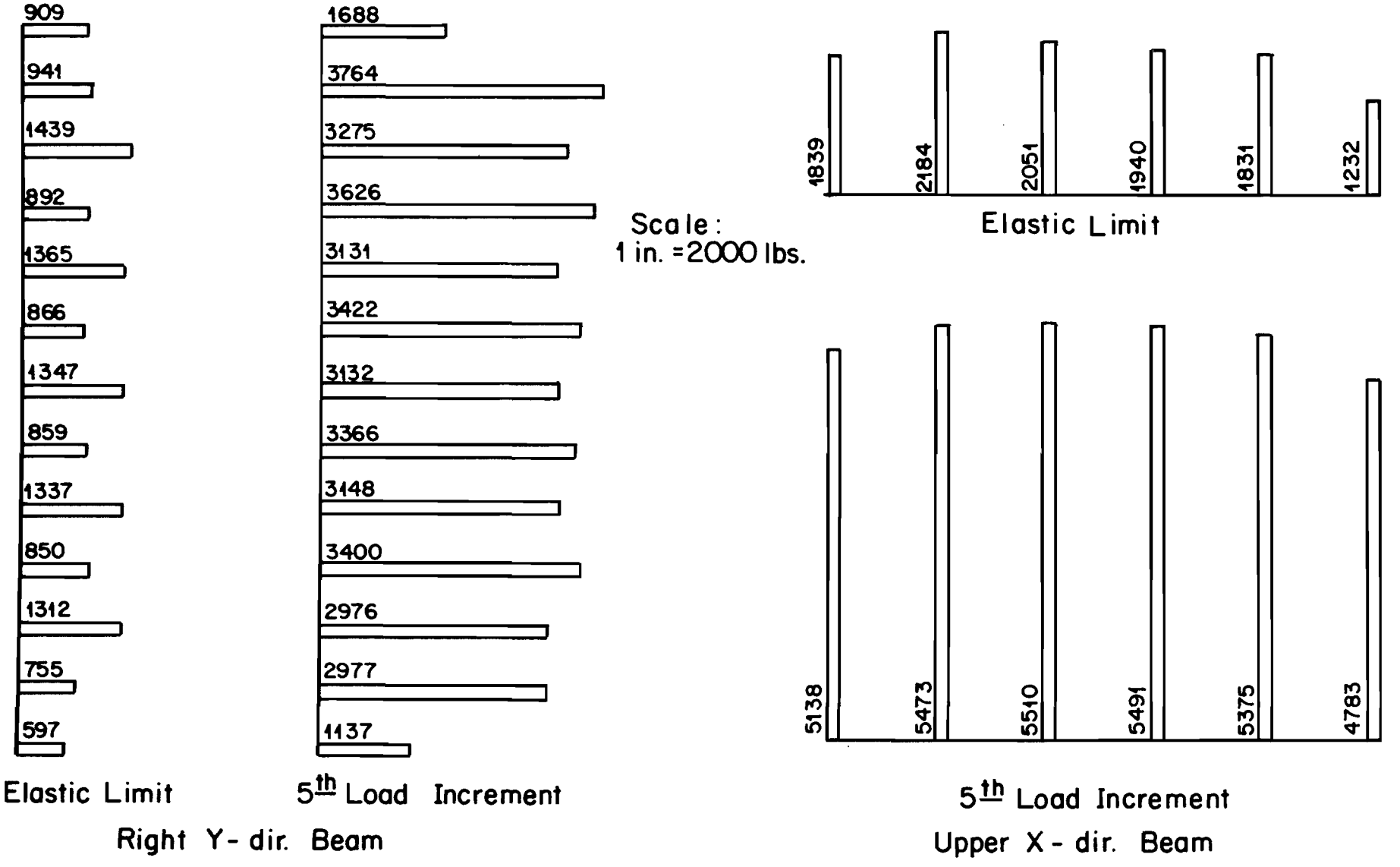

Figure 5.16 (cont.) Longitudinal forces on the perimeter beams of 10' x 12' welded diaphragm

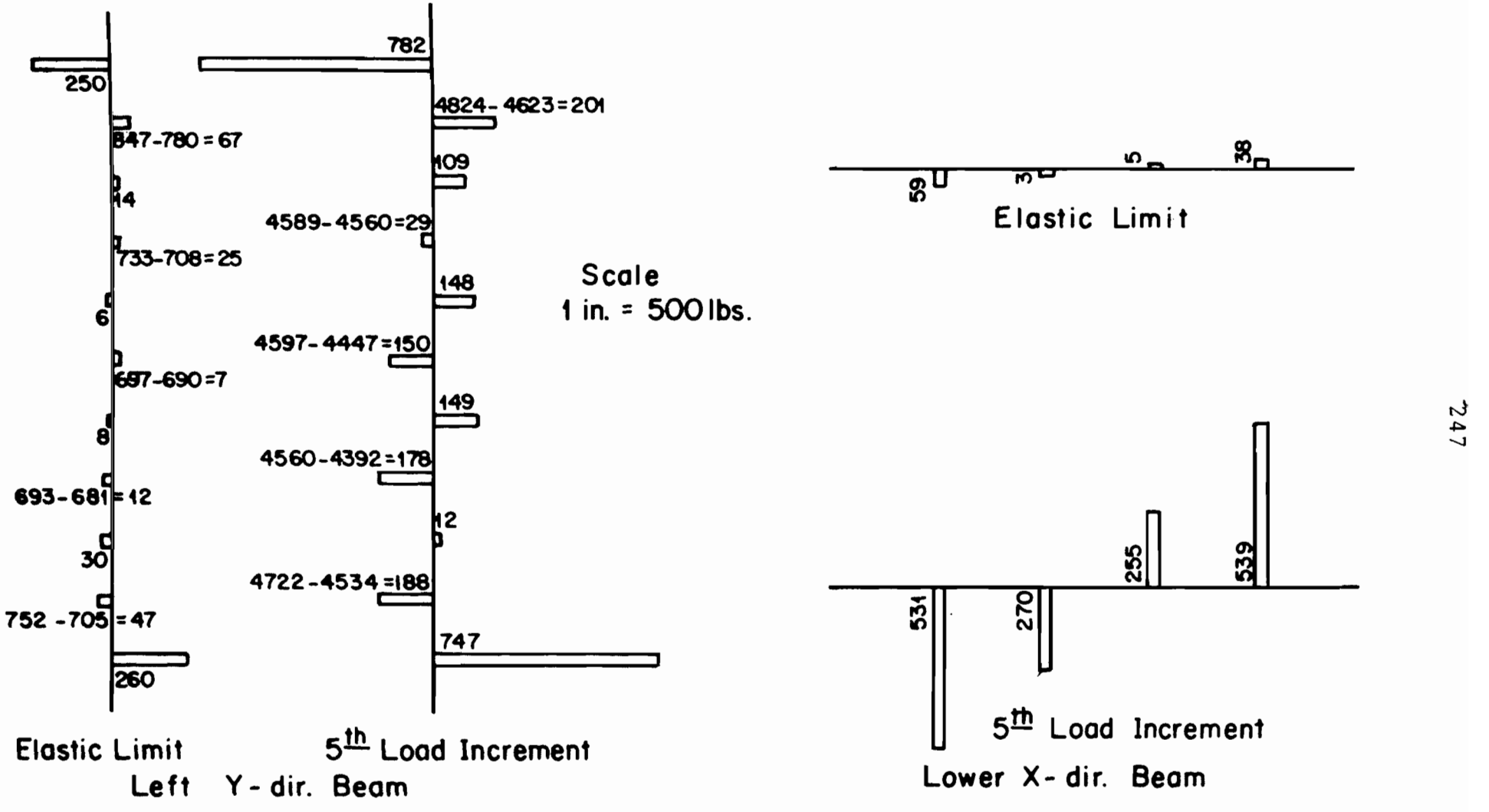

Figure 5.17 Lateral forces on the perimeter beams of 10' x 12' welded diaphragm (cont.)

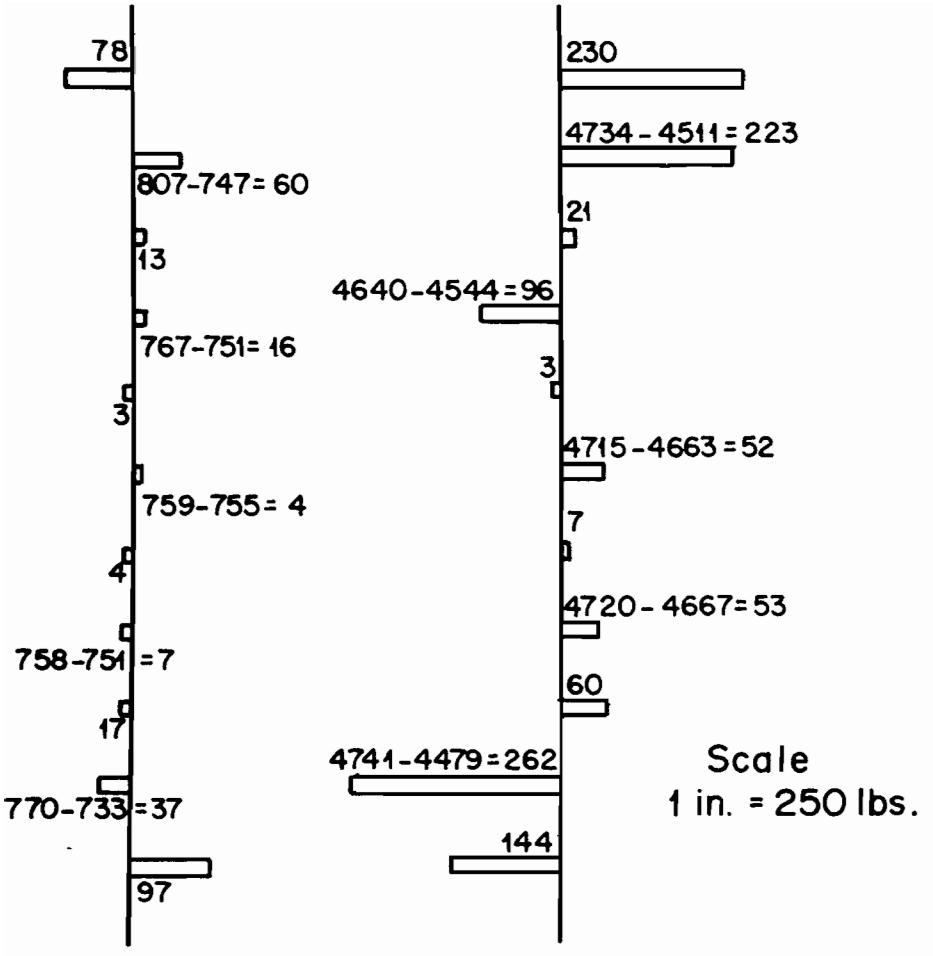

Scale
1 in. = 250 lbs.

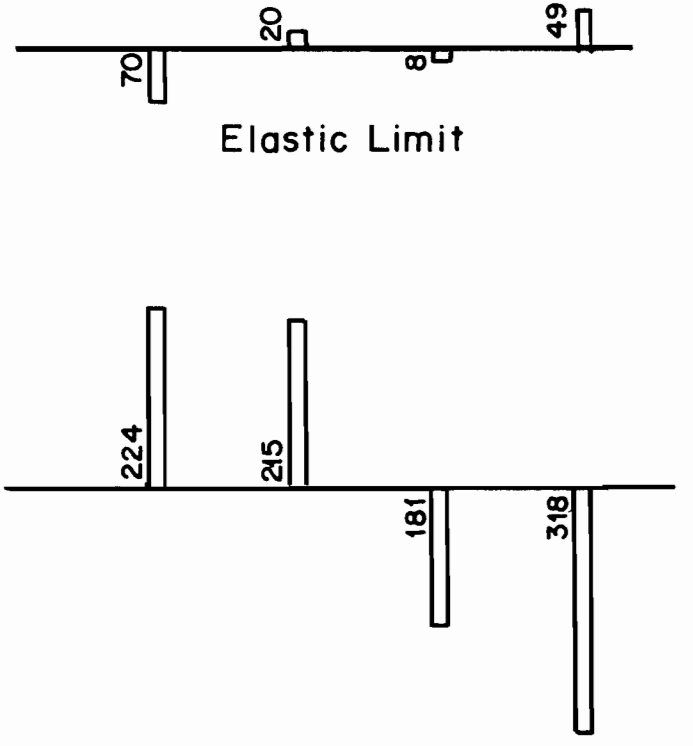

Figure 5.17 (cont.) Lateral forces on the perimeter beams of 10' x 12' welded diaphragm

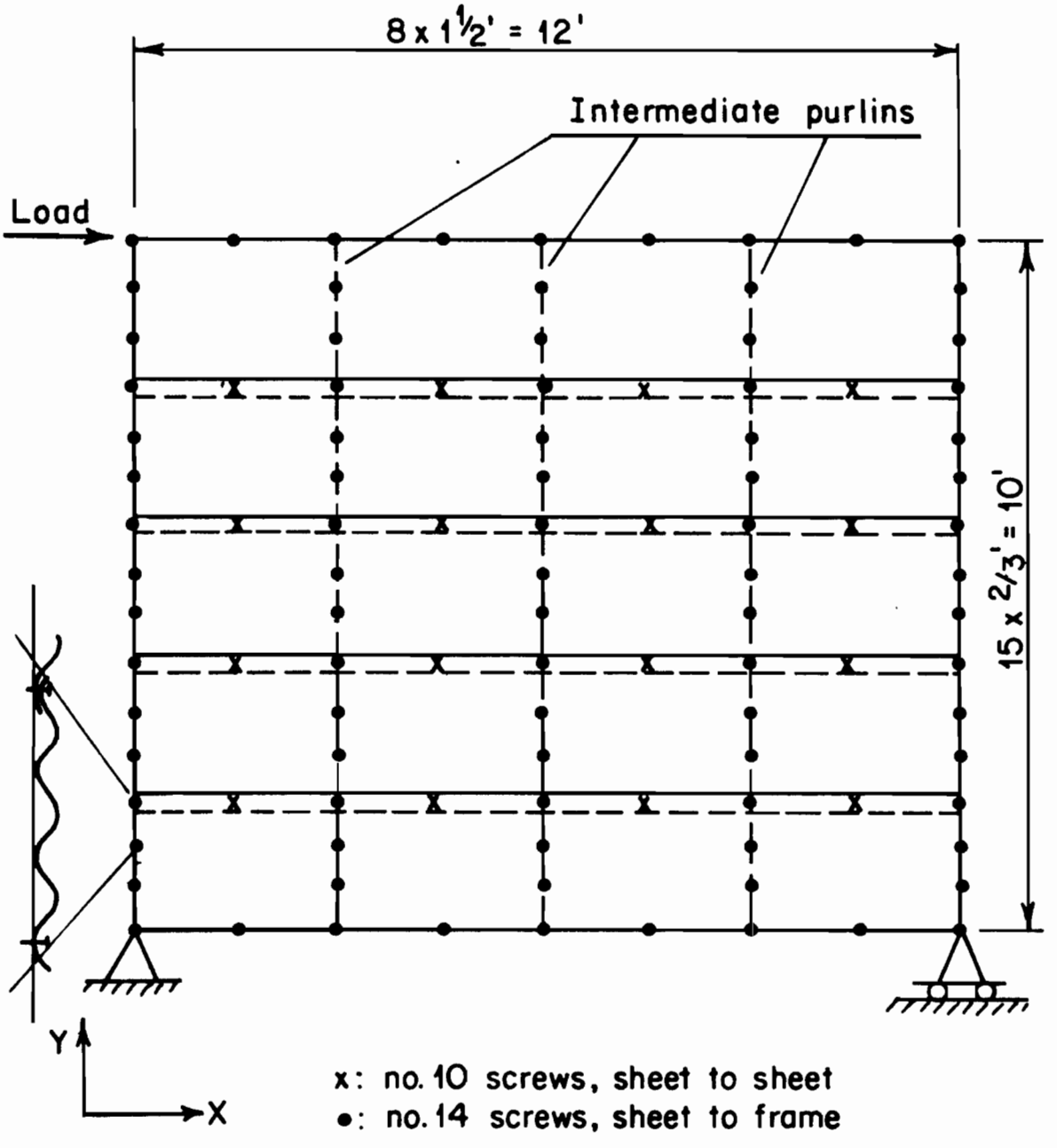

All sheets 2½"x ½" standard corrugation (see Figure 5.1)
Perimeter beams: 14 gage ⊏ 6" x 1½"
Intermediate purlins: 16 gage ⊏ 6" x 1½"

Figure 5.18 Test arrangement of the 10' x 12' standard corrugated diaphragm

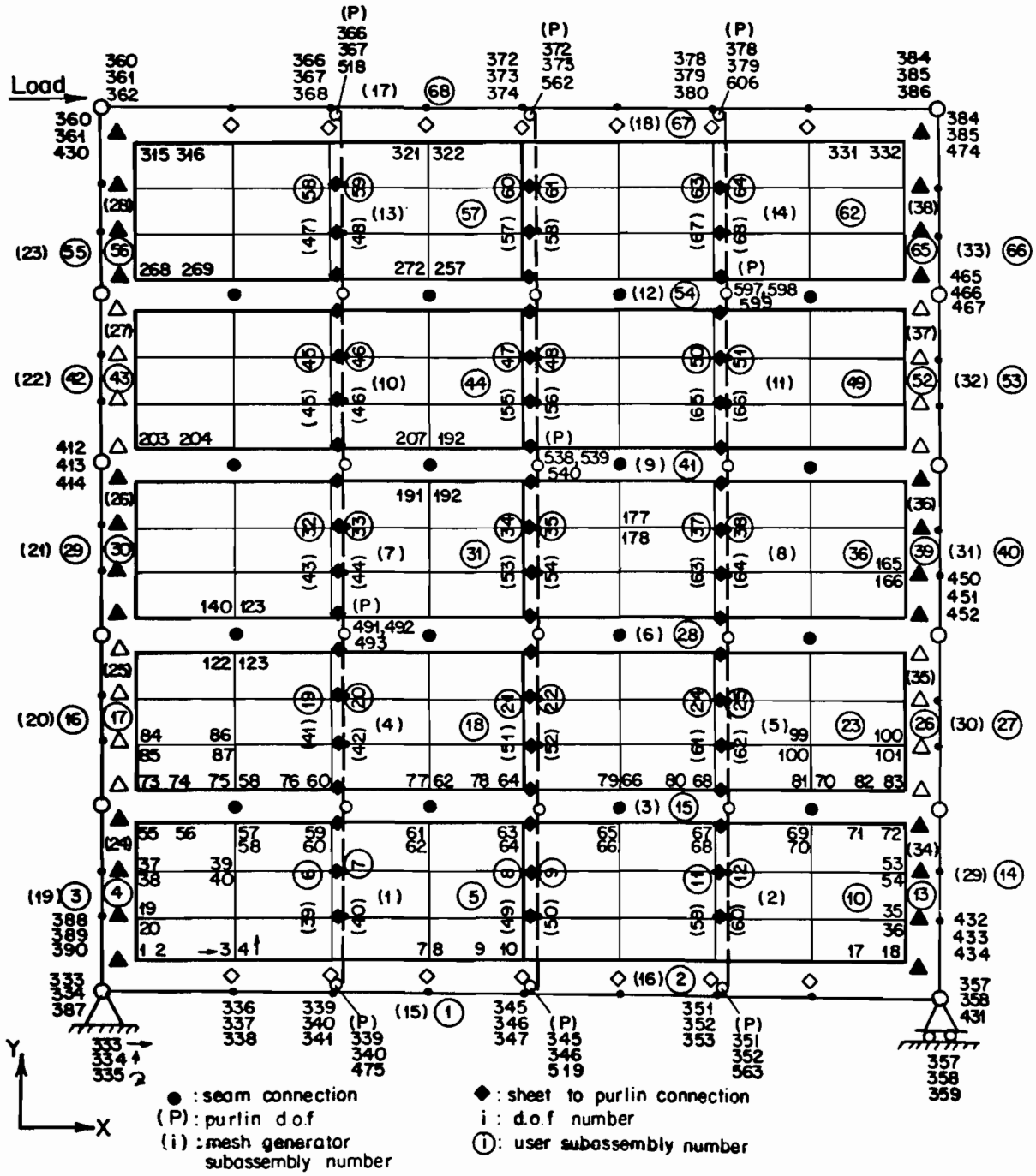

Figure 5.19 10' x 12' standard corrugated diaphragm Model A

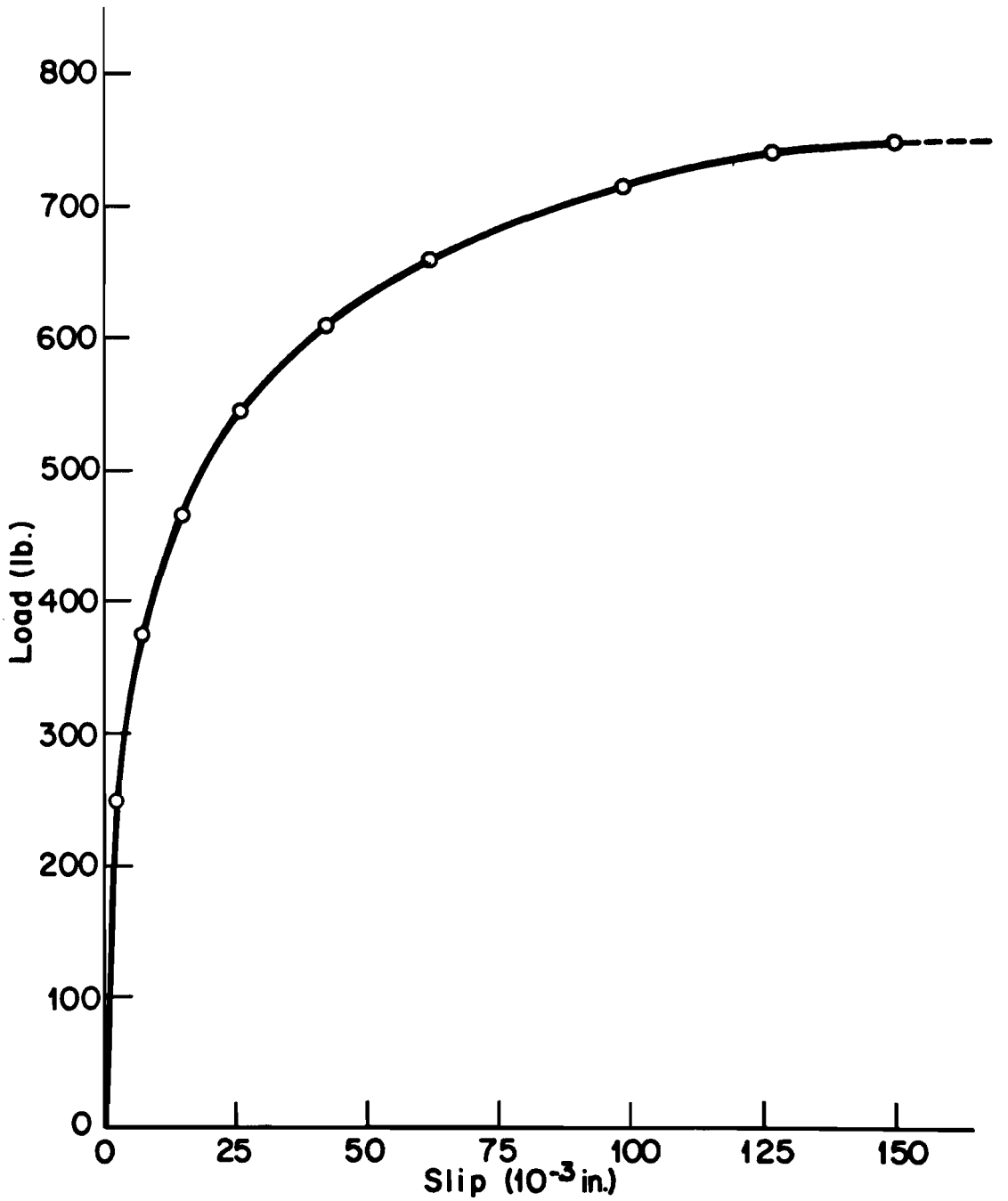

Figure 5.20 Edge connection with no. 14 self tapping screw to 26 gage steel

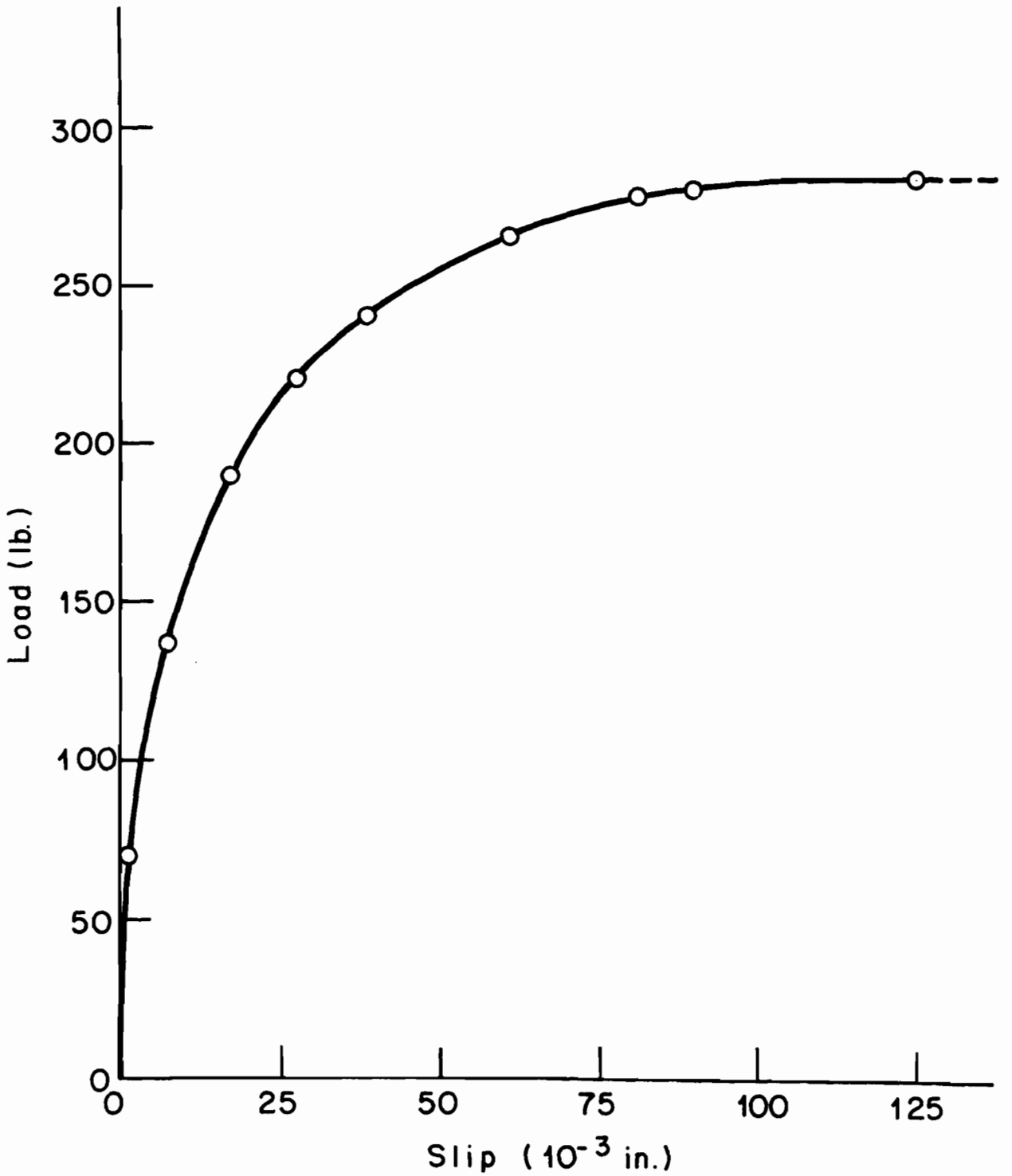

Figure 5.21 #10 screw fastened sidelap connection in 26 gage steel

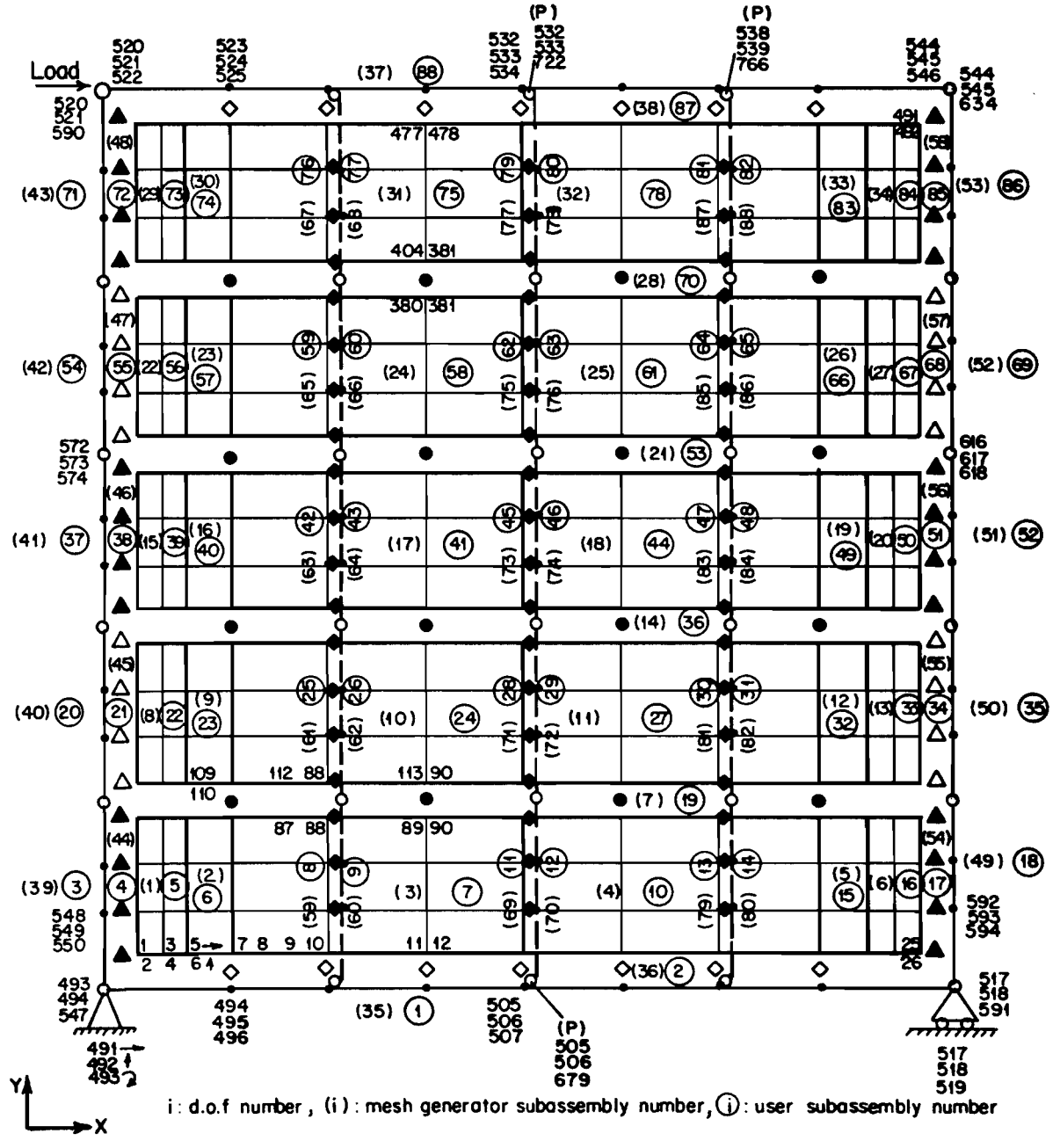

Figure 5.22 10' x 12' standard corrugated diaphragm Model B

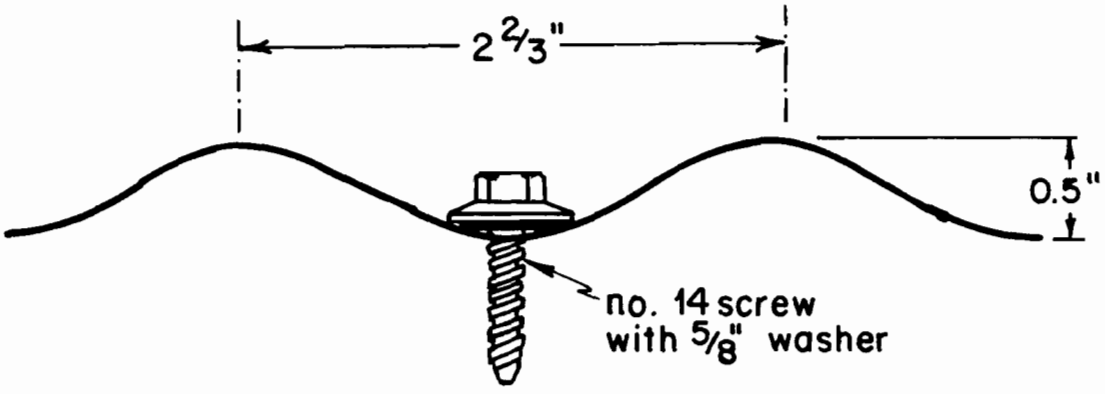

Scale: actual size

a. Relative sizes of screws and corrugation.

b. Quasi-sinusoidal corrugation with point attachments at mid-heights of corrugations.

Figure 5.23 End attachment of standard corrugation and possible idealization to find the effective shear modulus

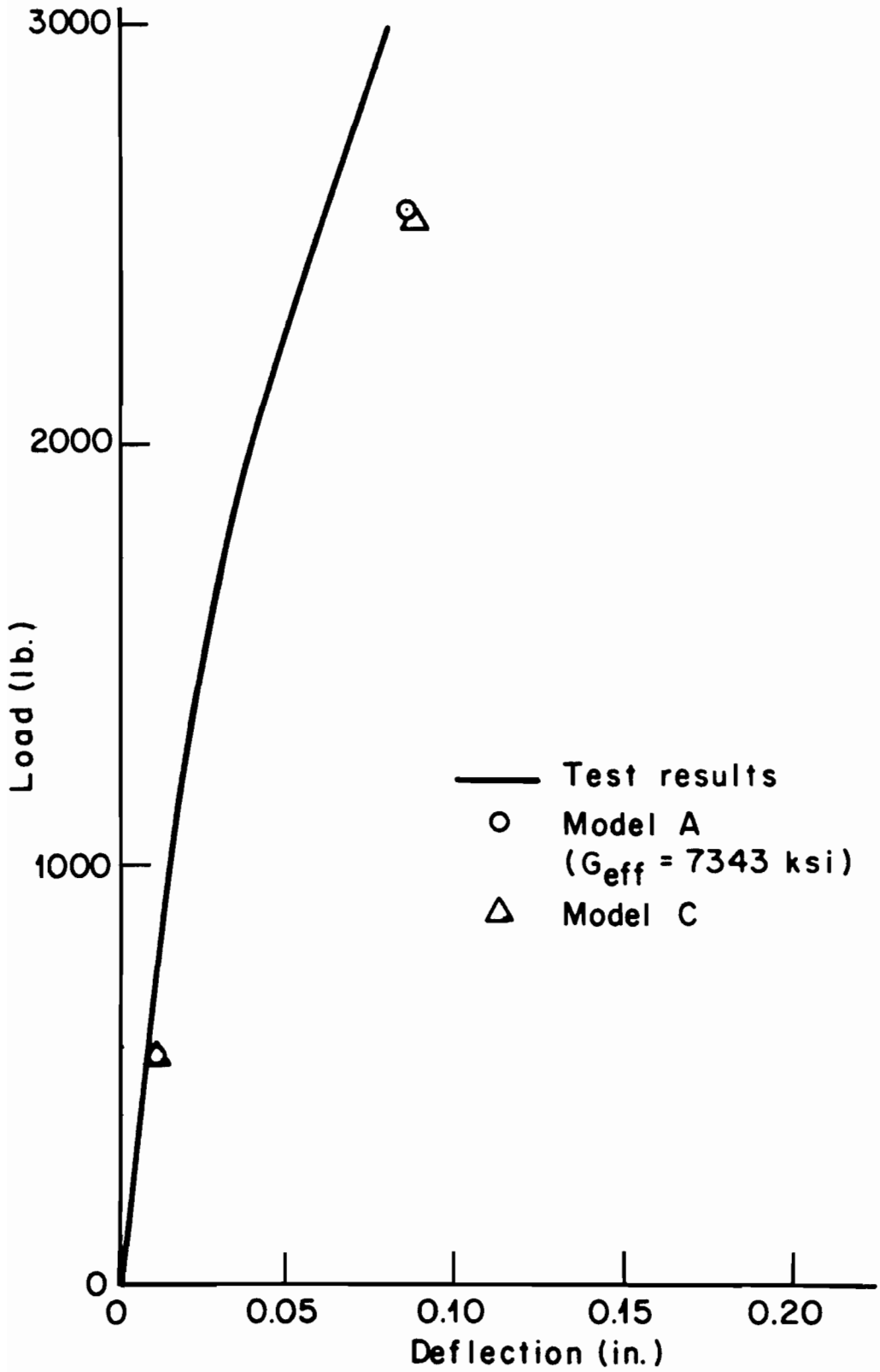

Figure 5.24 Models A and C compared against the initial portion of the test results

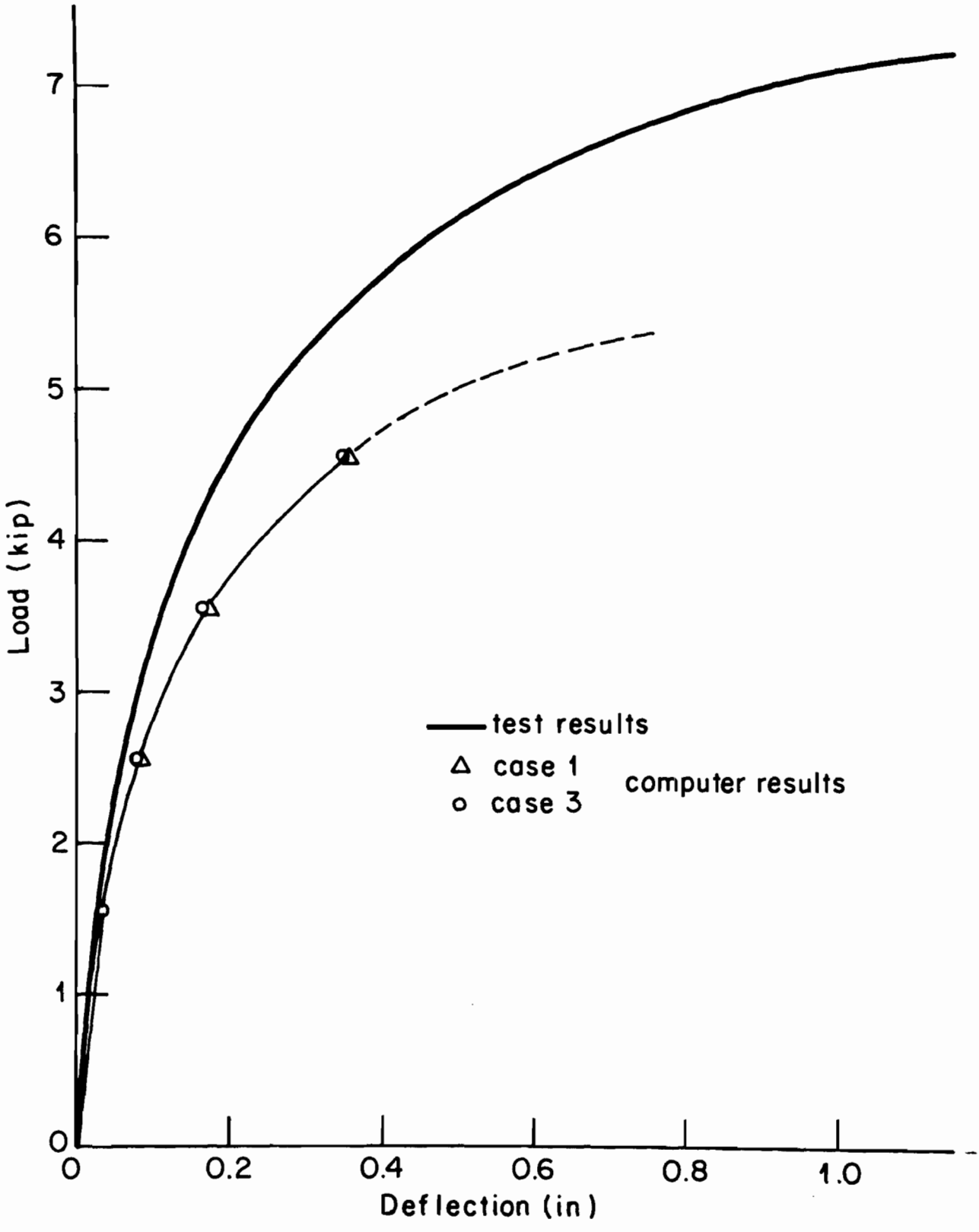

Figure 5.25 10' x 12' standard corrugated diaphragm behavior under static load

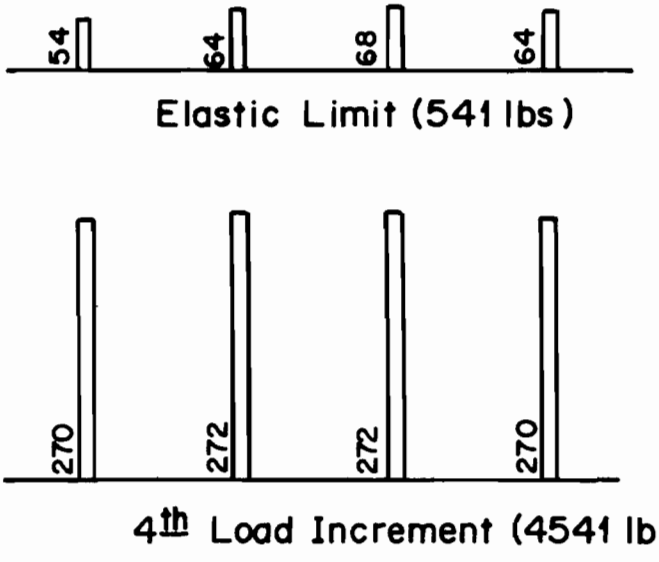

Second seam line (counted in positive Y-dir.)

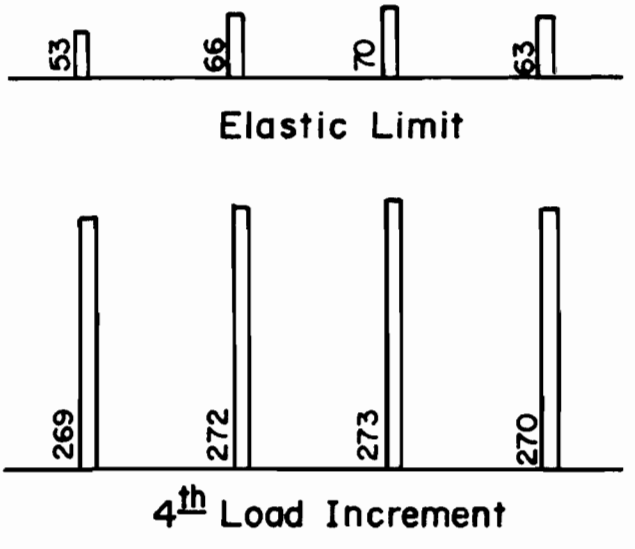

Third seam line

Figure 5.26 Forces in sheet to sheet connectors of 10' x 12' standard corrugated diaphragm

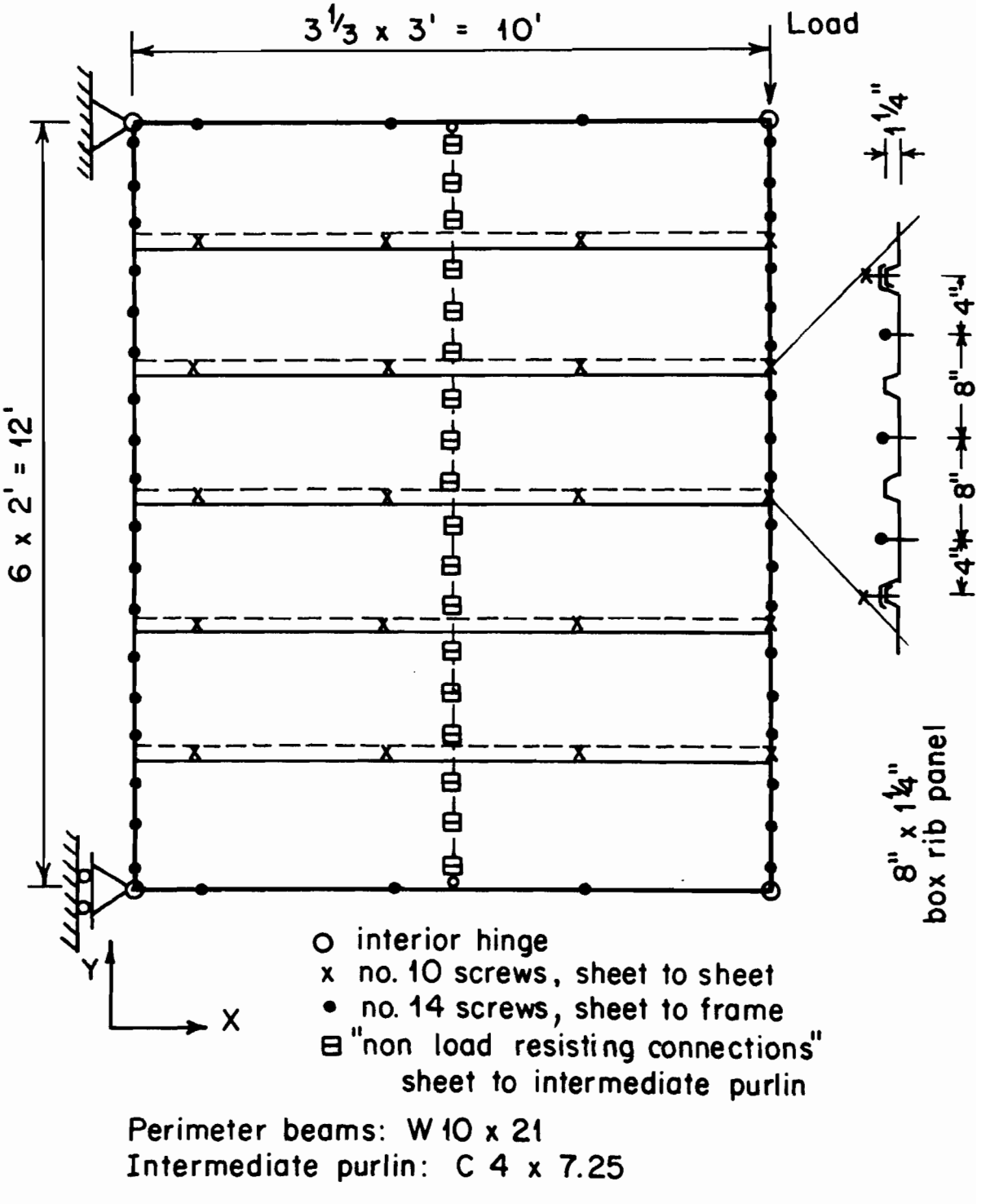

Figure 5.27 Test arrangement of the 10' x 12' trapezoidally corrugated diaphragm

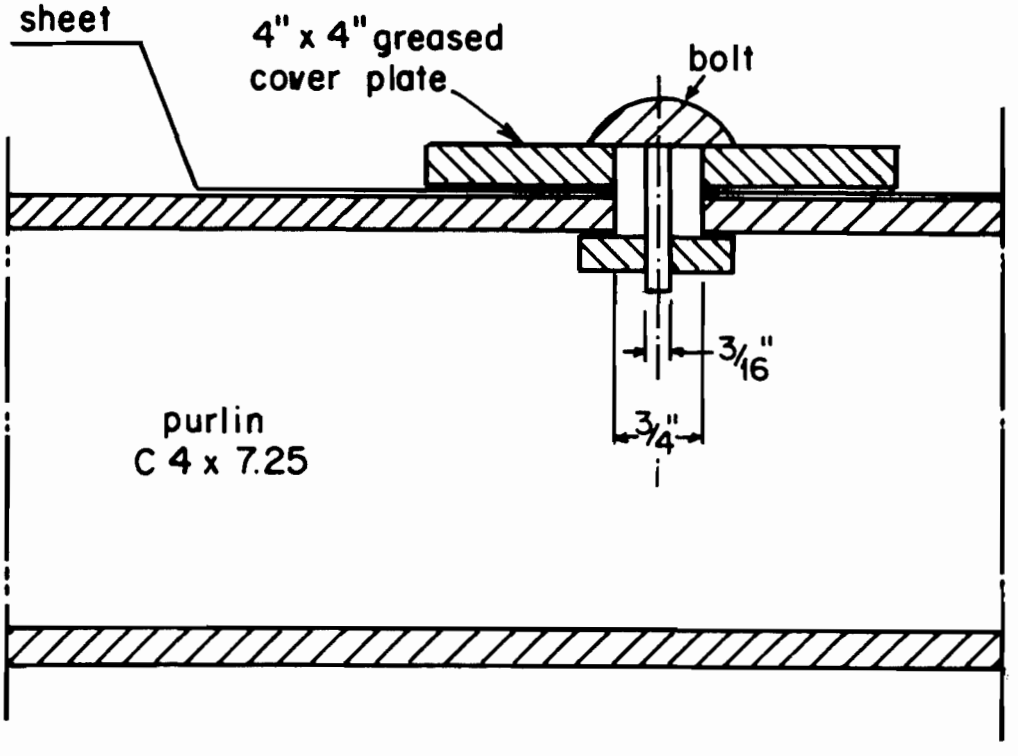

Figure 5.28 Cross-section detail of "non-load resisting connection" between sheet and intermediate purlin

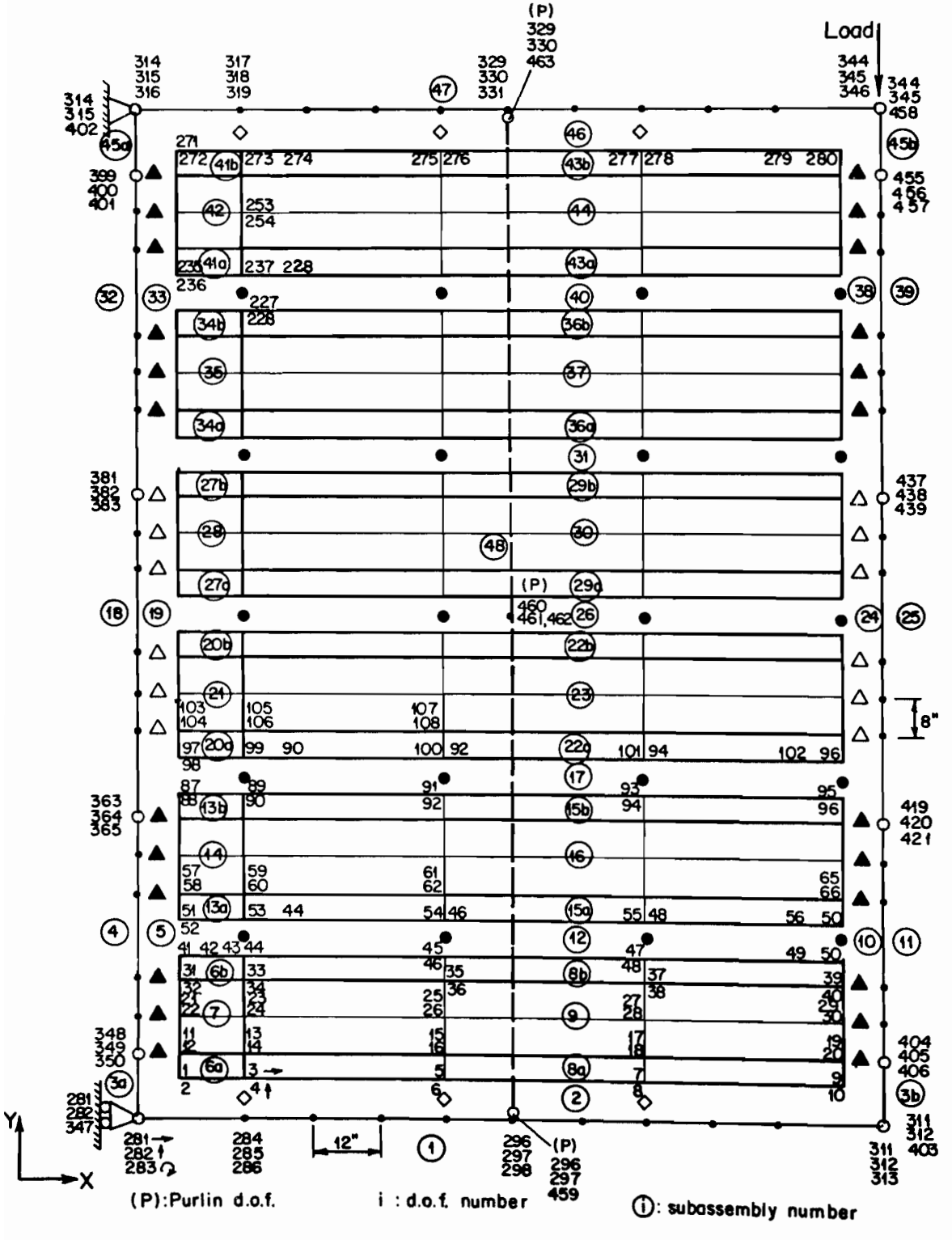

Figure 5.29 10' x 12' trapezoidally corrugated diaphragm Model AT

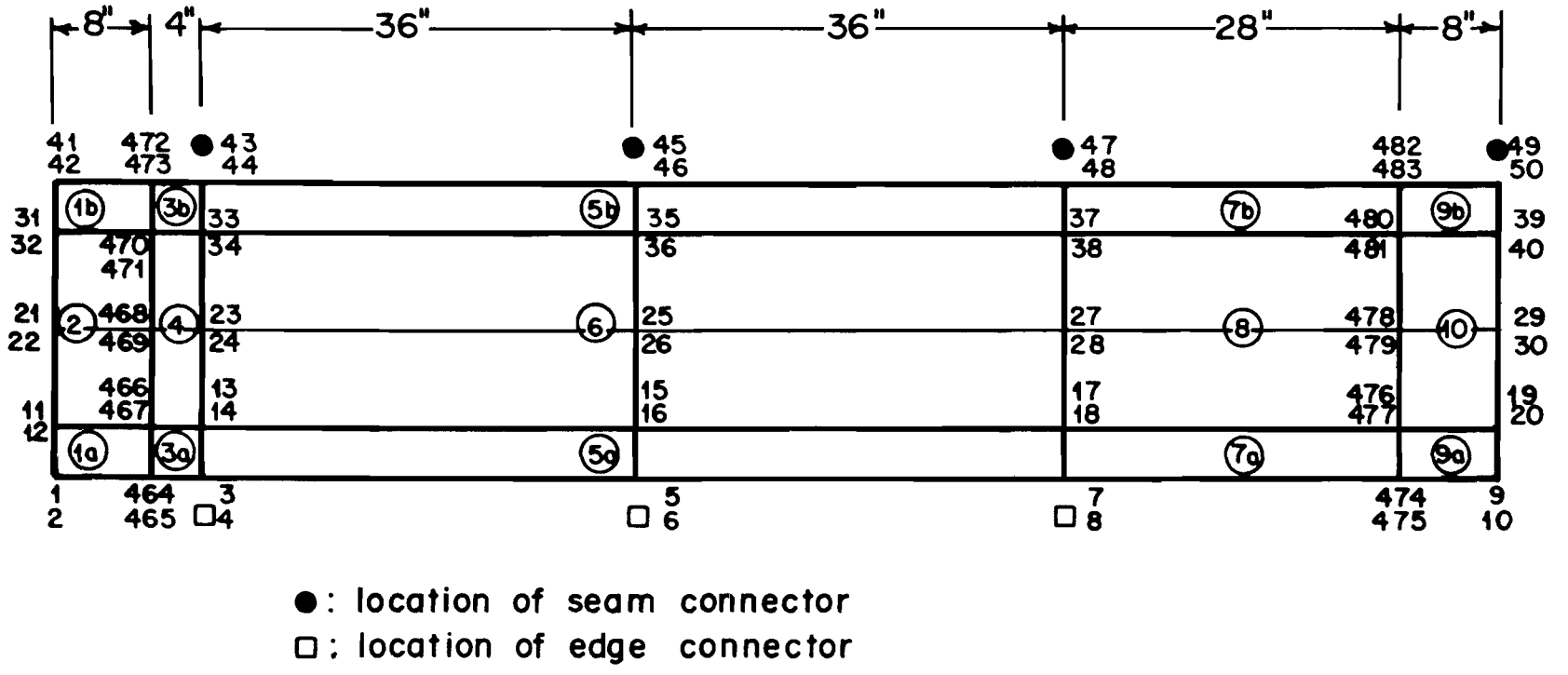

Figure 5.30 Finite element mesh of a sheet of the 10' x 12' trapezoidally corrugated diaphragm for the case of Model BT

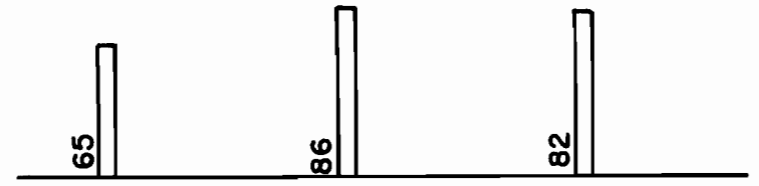

Model AT

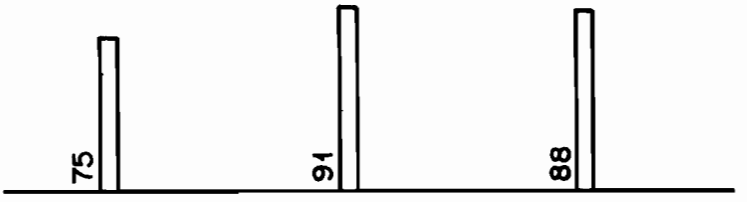

Model BT

Longitudinal forces (lb.) on the X-dir. perimeter beams

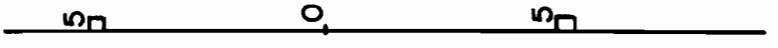

Model AT

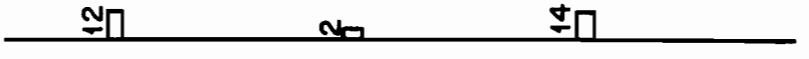

Model BT

Lateral forces (lb.) on the X-dir. perimeter beams

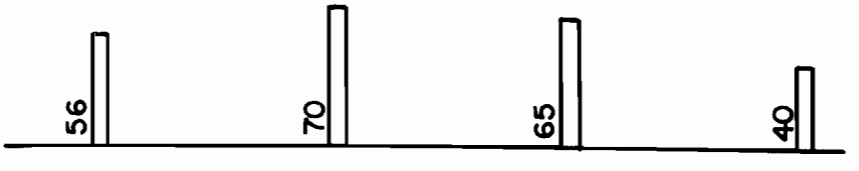

Scale
1 in. = 100 lbs.

Model AT

Model BT

Forces (lb.) in connectors of middle seam line

Figure 5.31 Comparison of force distribution in Models AT and BT (cont.)

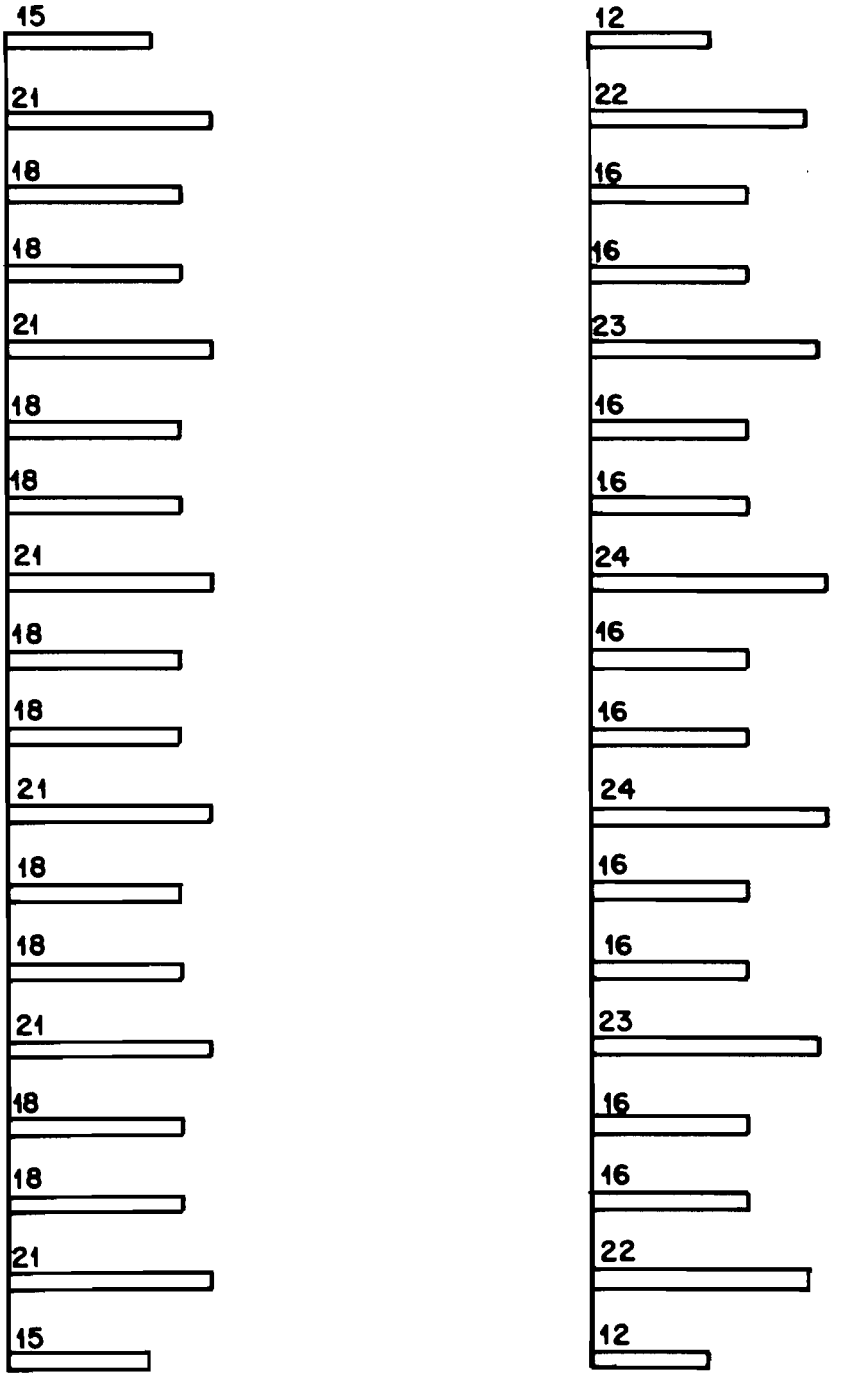

Longitudinal forces (lb) on left Y-dir. perimeter beam
Scale: 1 in = 20 lbs.

Figure 5.31 (cont.) Comparison of force distribution in Models AT and BT

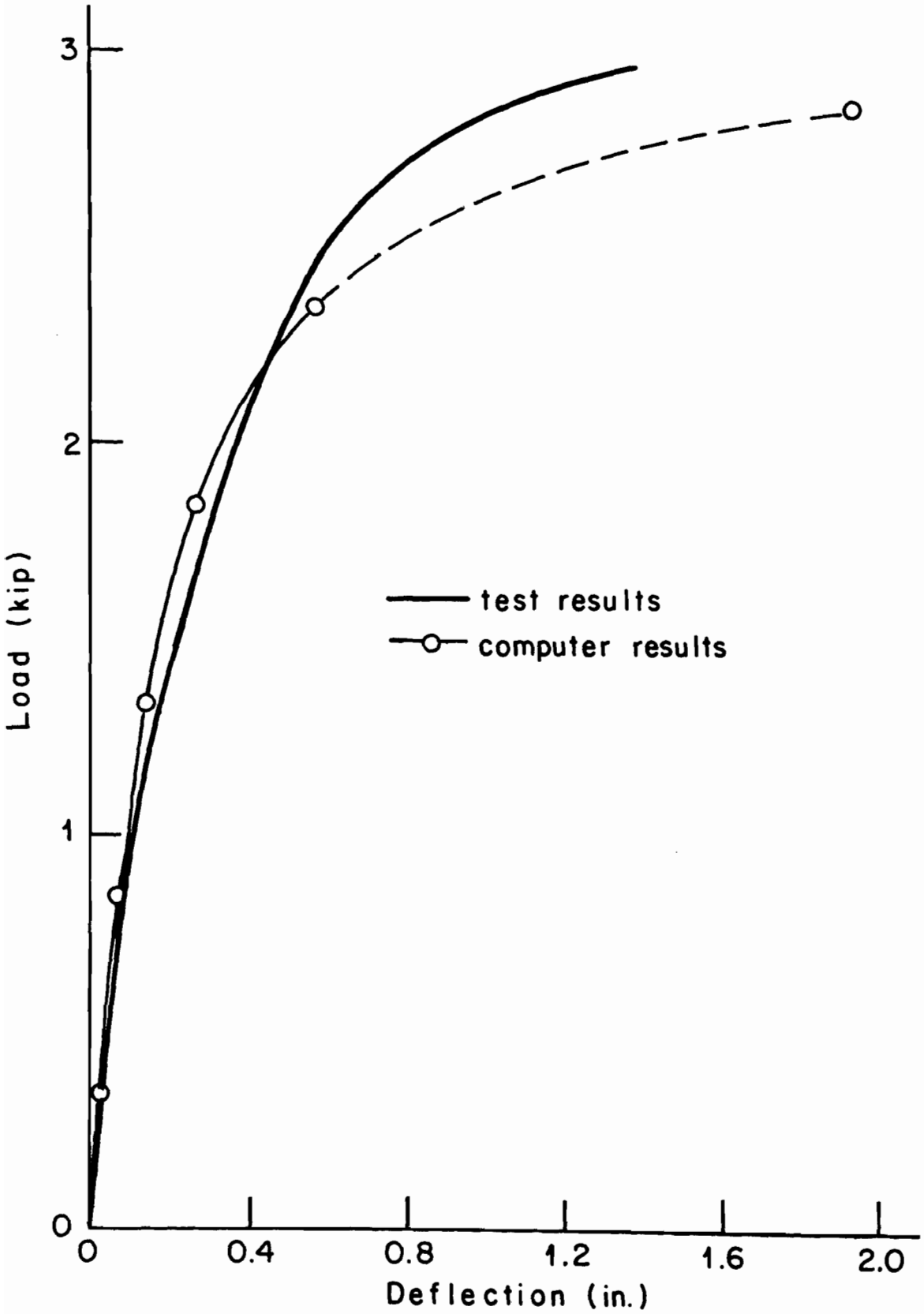

Figure 5.32 Trapezoidally corrugated diaphragm. Deflection of representative d.o.f.

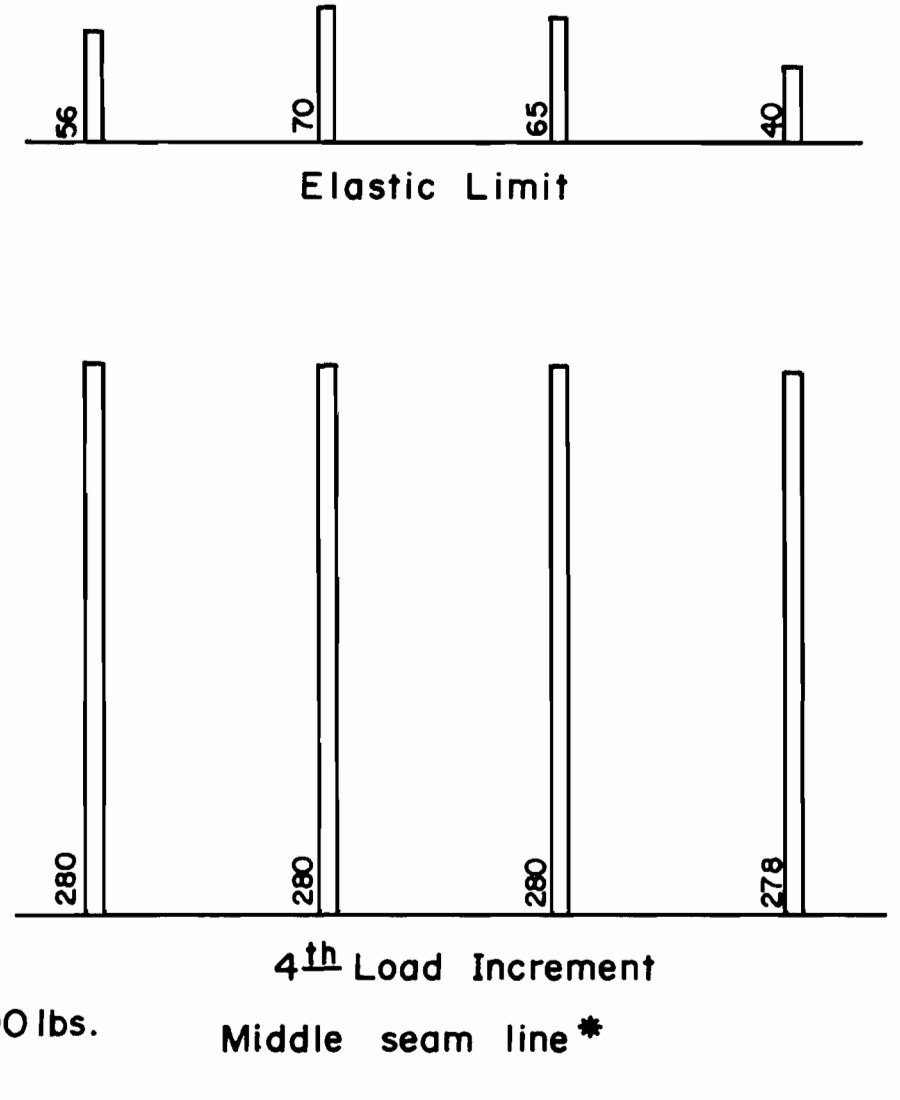

* Forces at other seams practically the same as these shown here.

Figure 5.33 Forces in the seam connectors of the 10' x 12' trapezoidally corrugated diaphragm

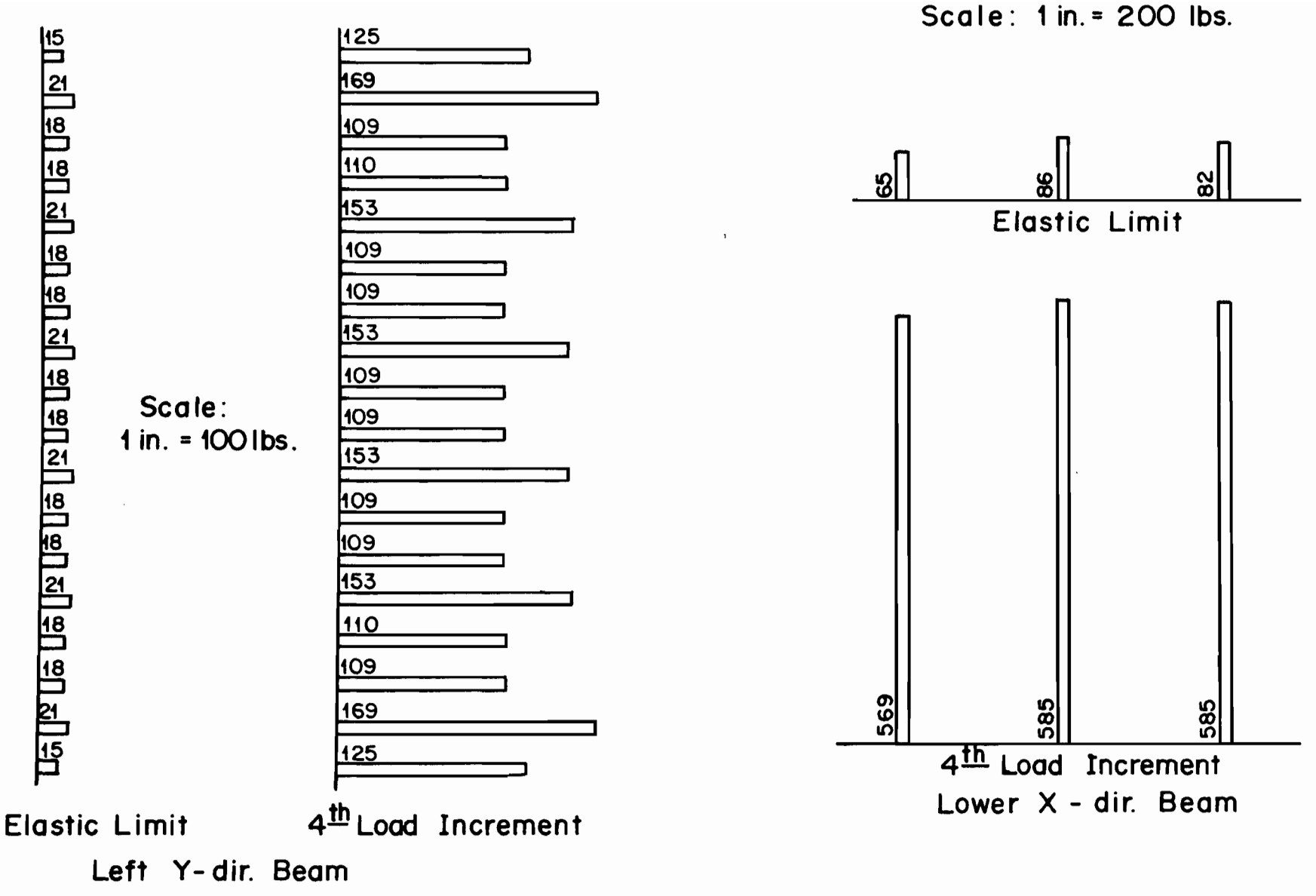

Figure 5.34 Longitudinal forces on the perimeter beams of the 10' x 12' trapezoidally corrugated diaphragm (cont.)

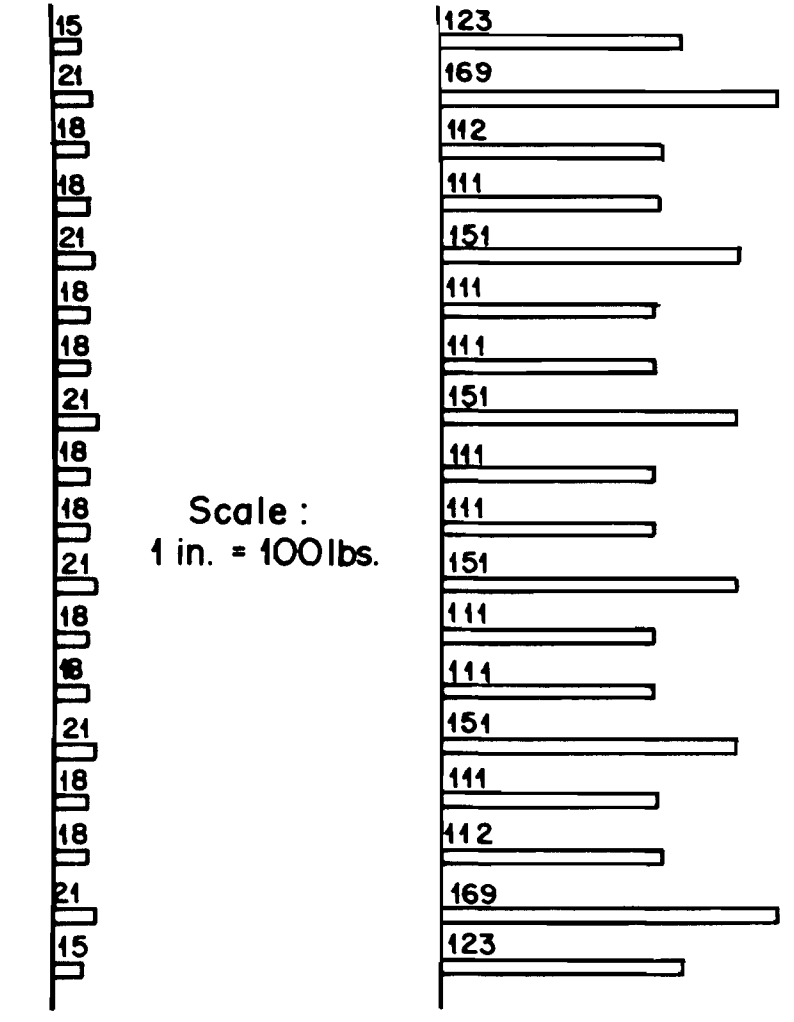

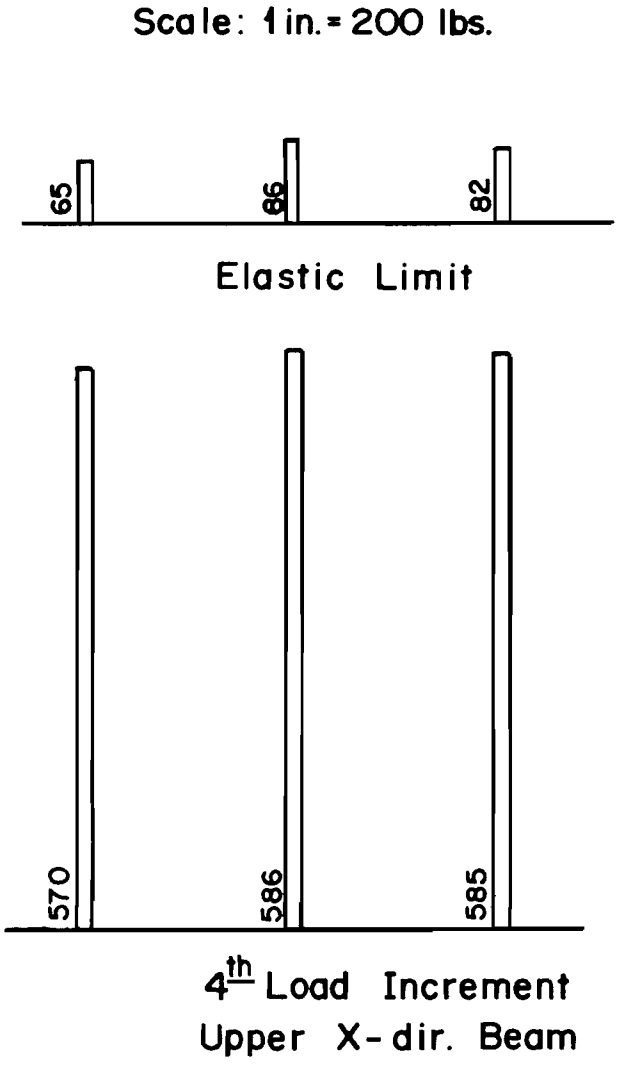

Figure 5.34 (cont.) Longitudinal forces on the perimeter beams of the 10' x 12' trapezoidally corrugated diaphragm

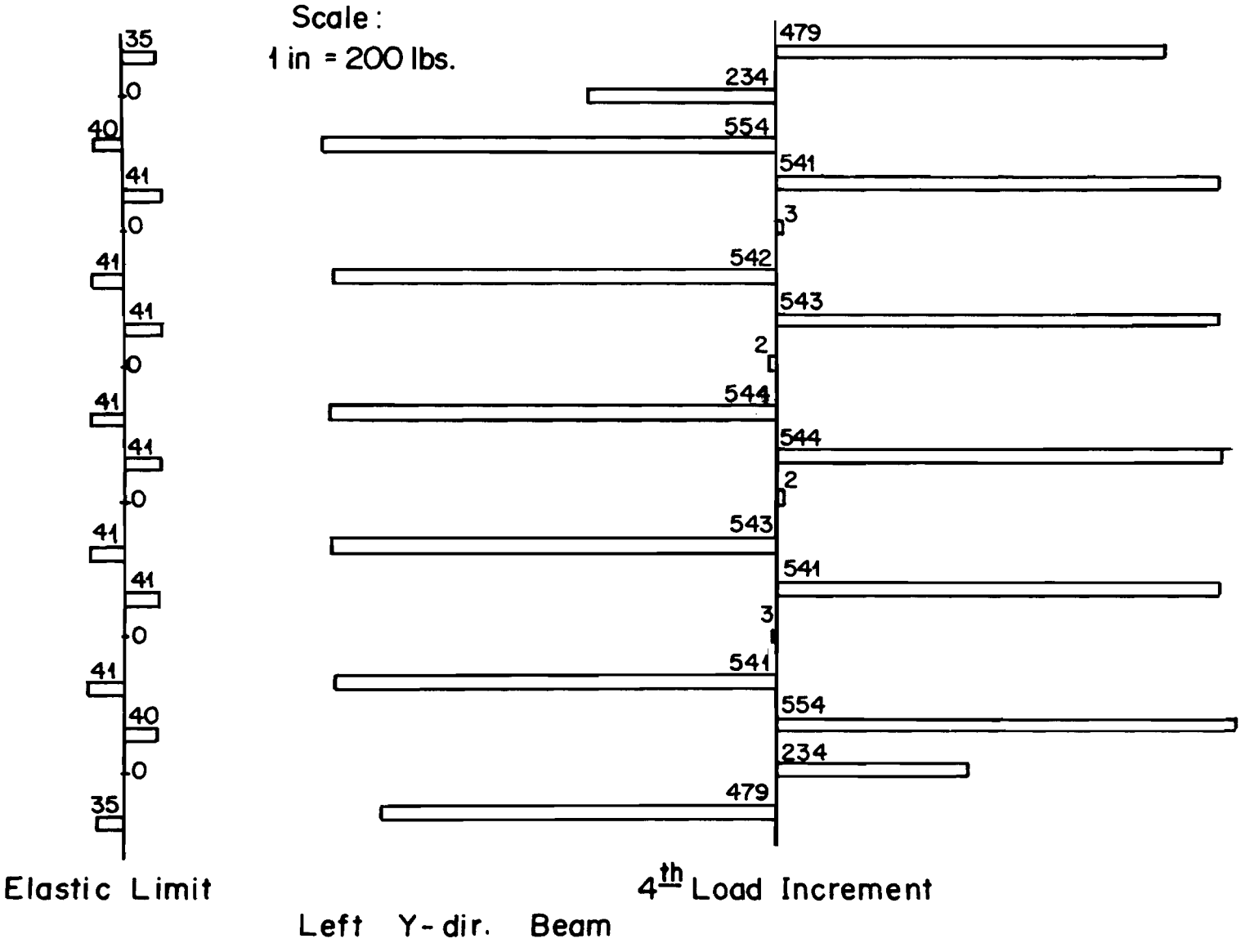

Figure 5.35 Lateral forces on the perimeter beams of the 10' x 12' trapezoidally corrugated diaphragm (cont.)

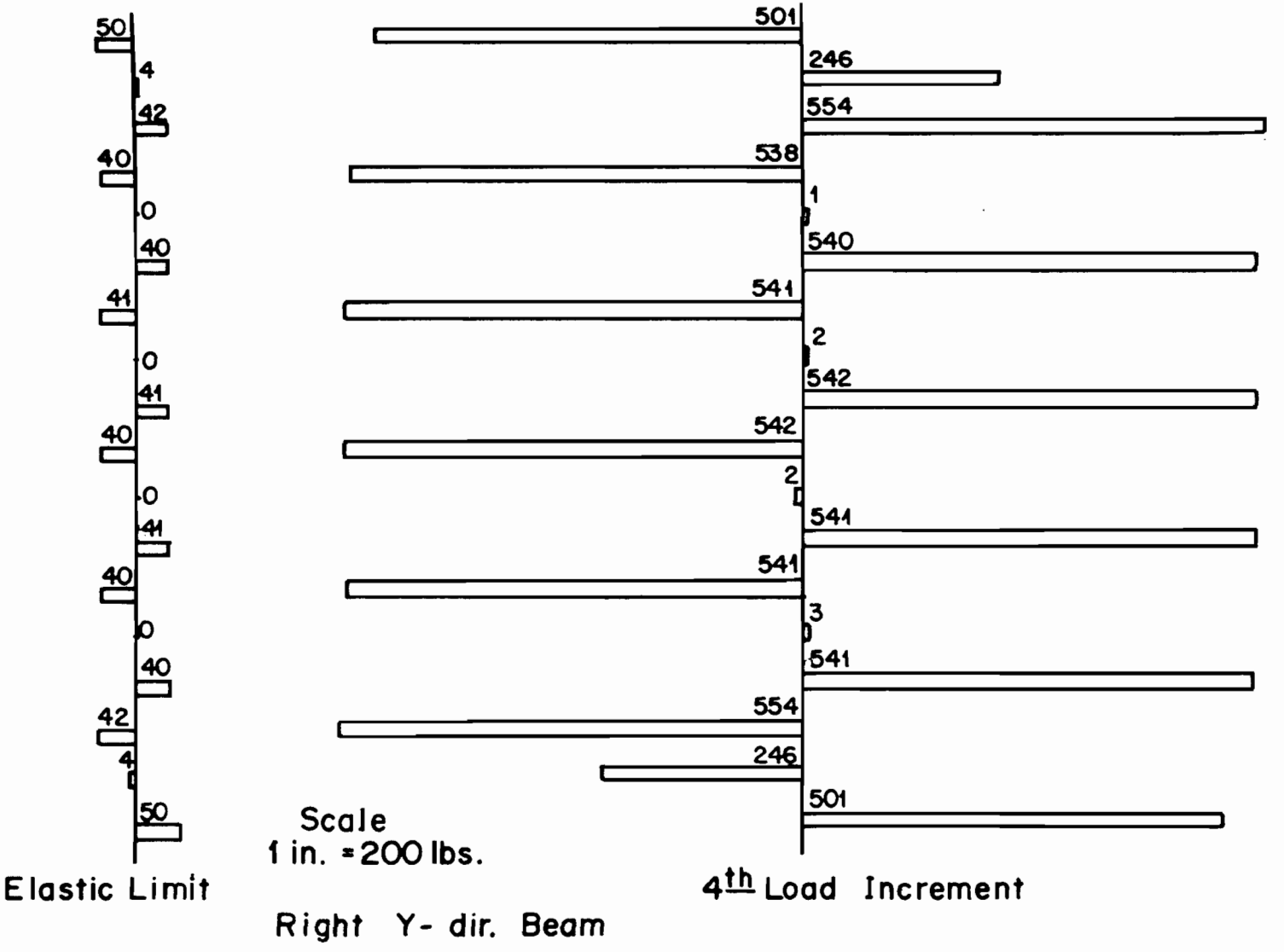

Figure 5.35 (cont.) Lateral forces on the perimeter beams of the 10' x 12' trapezoidally corrugated diaphragm (cont.)

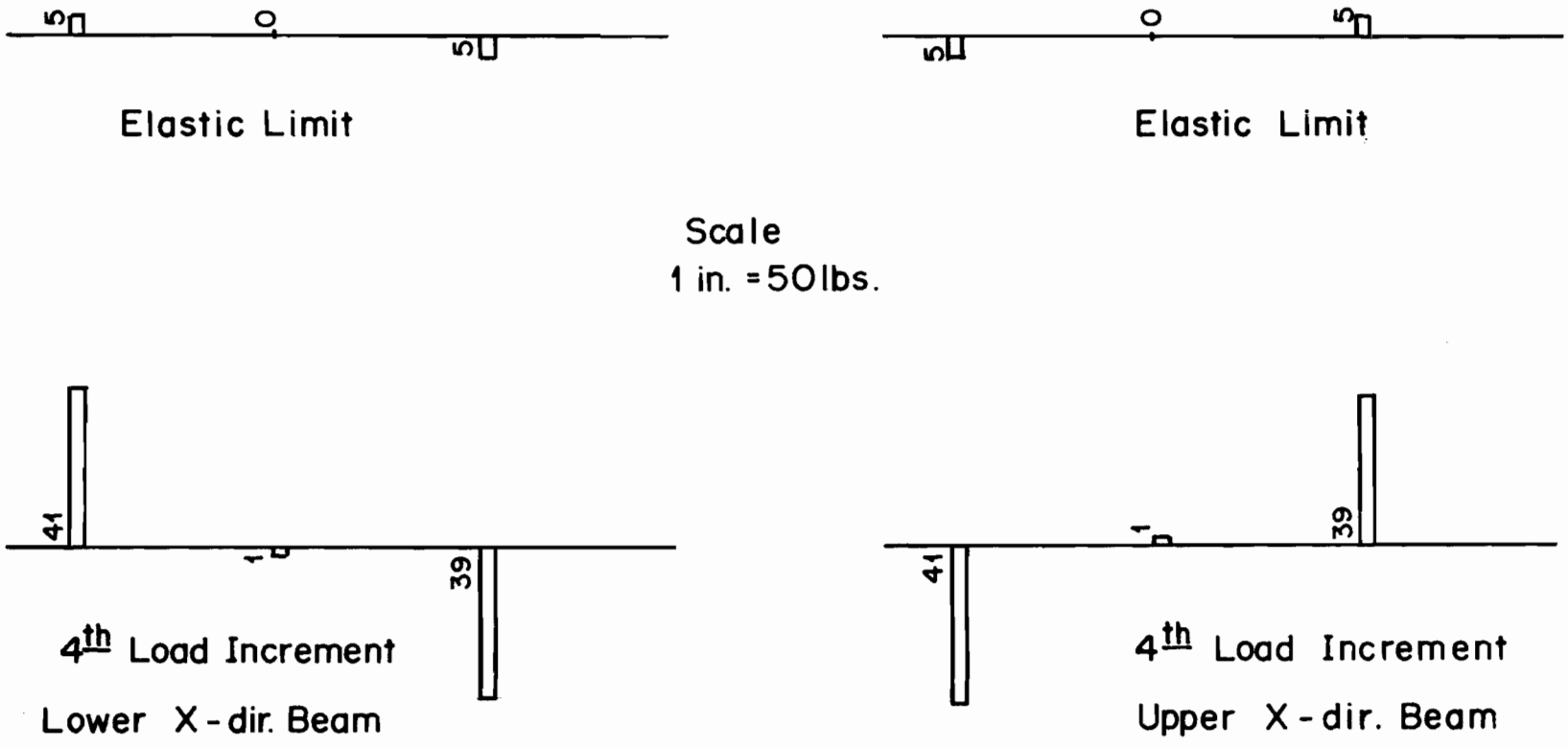

Figure 5.35 (cont.) Lateral forces on the perimeter beams of the 10' x 12' trapezoidally corrugated diaphragm

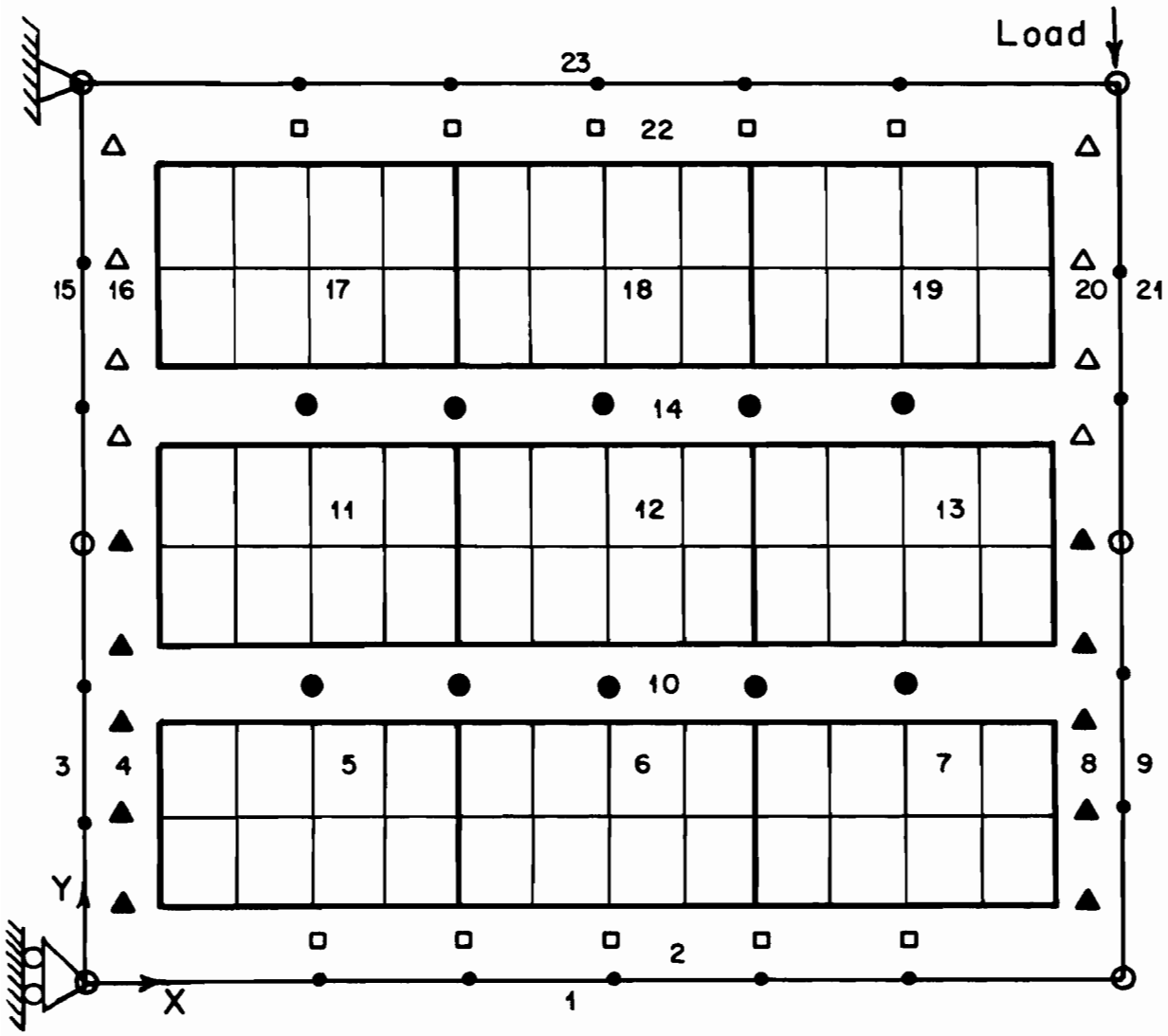

Figure A.1.1 Finite element mesh and subassembly sequence for a hypothetical diaphragm

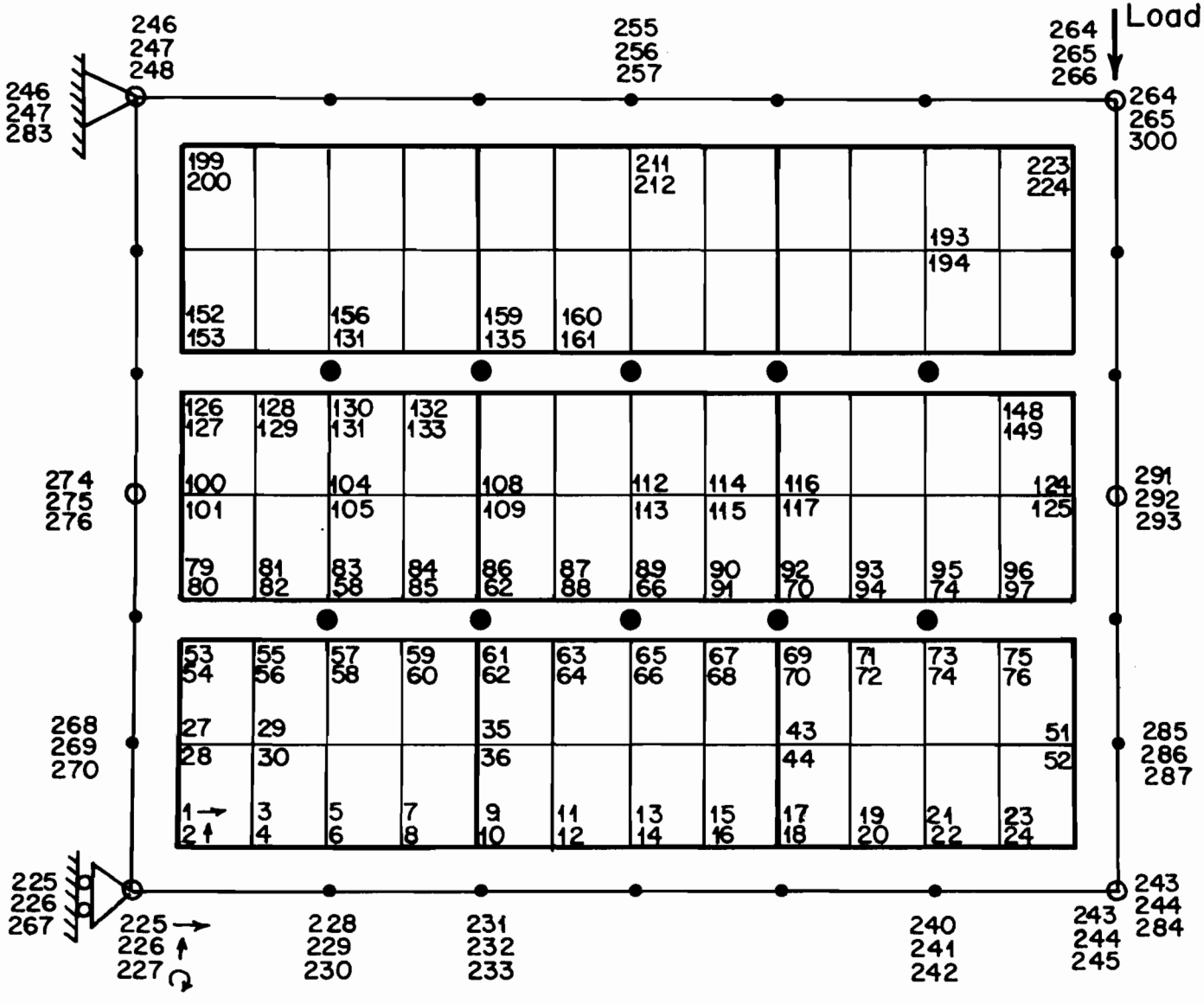

Figure A.1.2 Structural d.o.f.s for diaphragm of Figure A.1.1

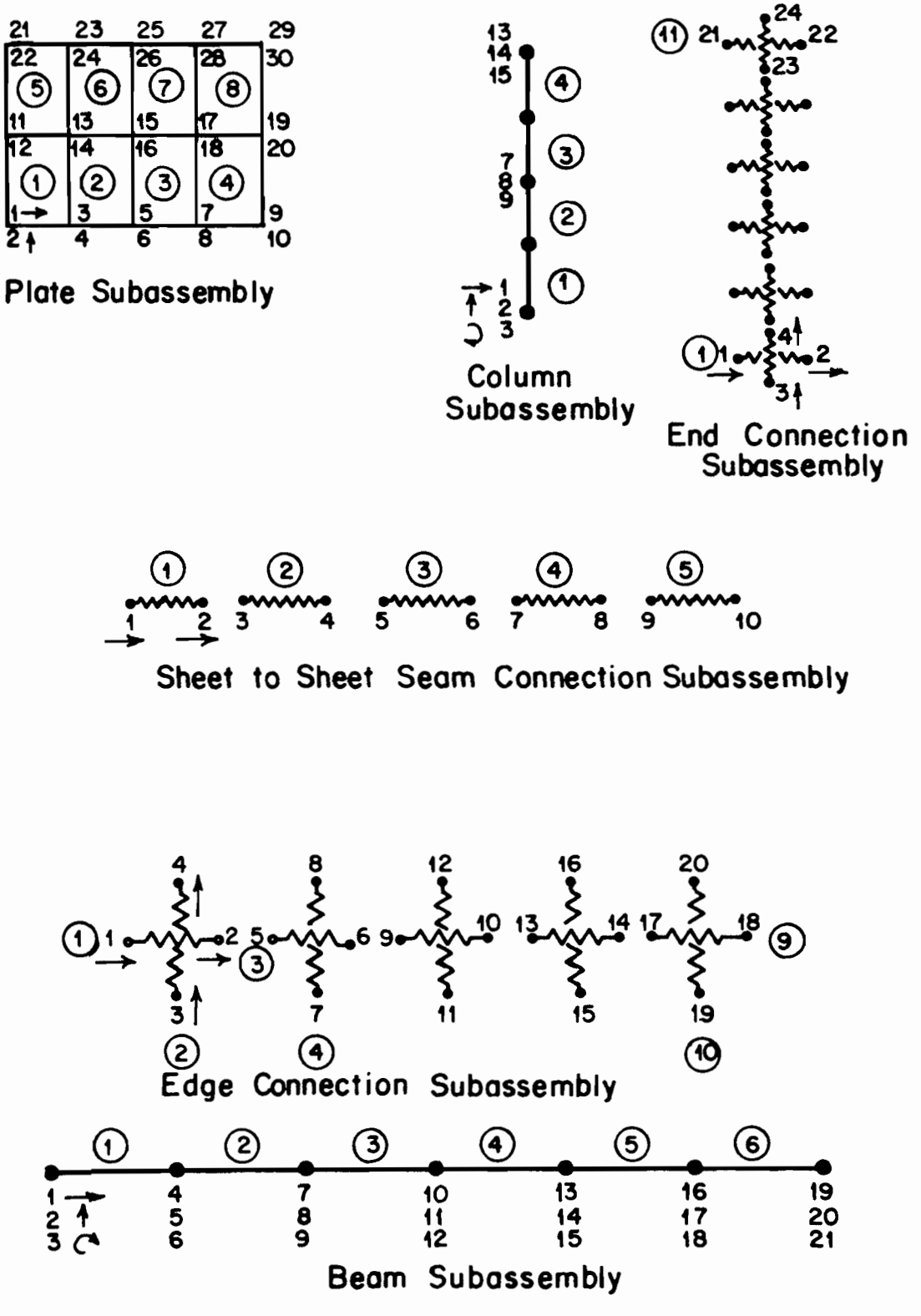

Figure A.1.3 Degrees of freedom in subassembly numbering system

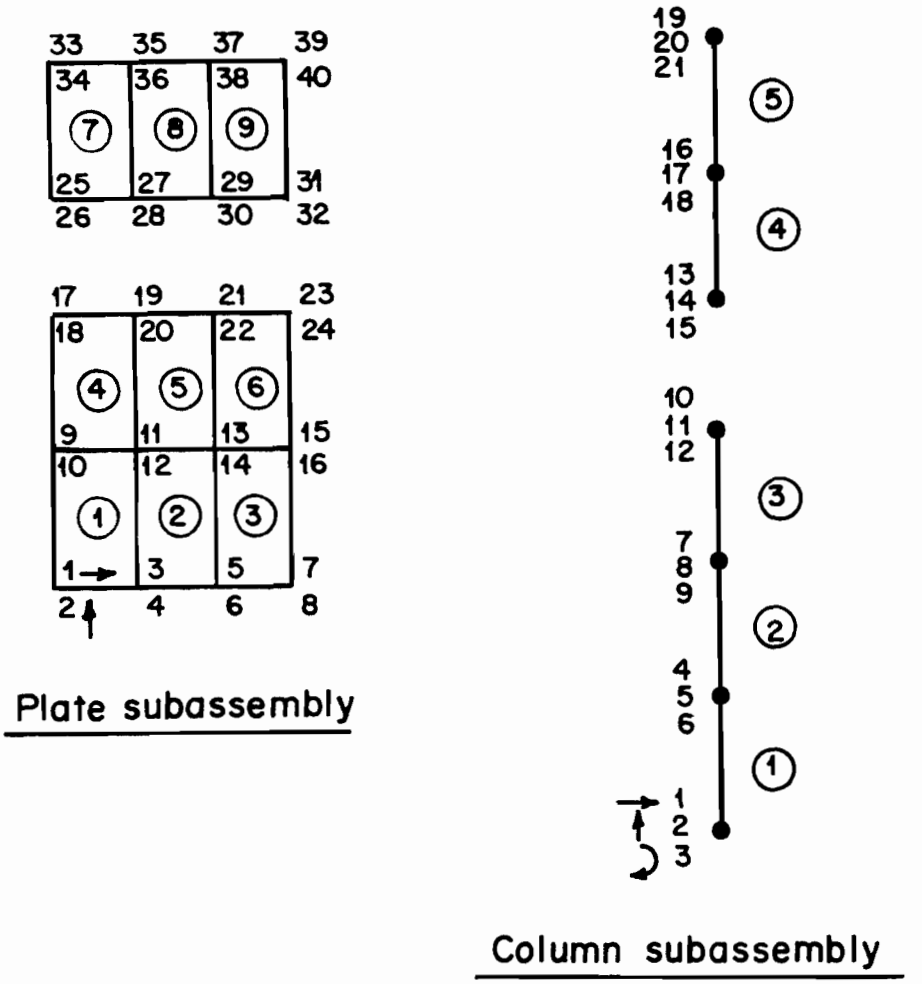

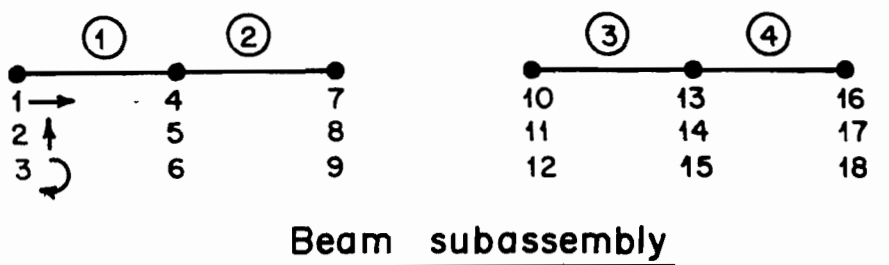

Figure A.1.4 Examples of split subassemblies

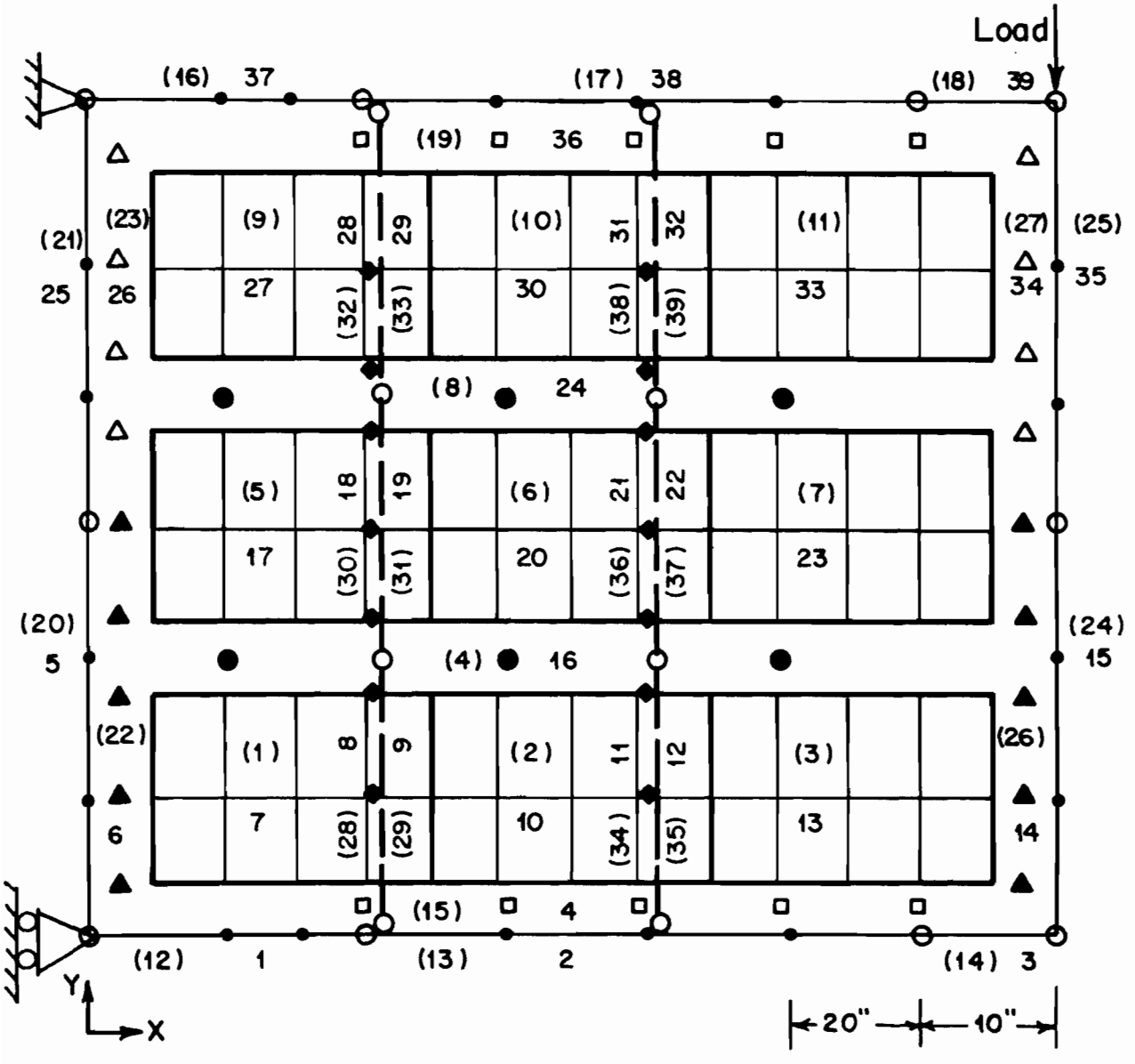

▲,△: end connections
□ edge connections
◆ sheet to purlin connections
● sheet to sheet connections
(28),(30),(32);(34),(36),(38): sheet to purlin connection subassemblies
(29),(31),(33),(35),(37),(39): purlin subassemblies
(i): mesh generator sequence of subassembly numbering
j : possible user defined sequence

Figure A.1.5 Subassembly numbering and matching for a hypothetical diaphragm model

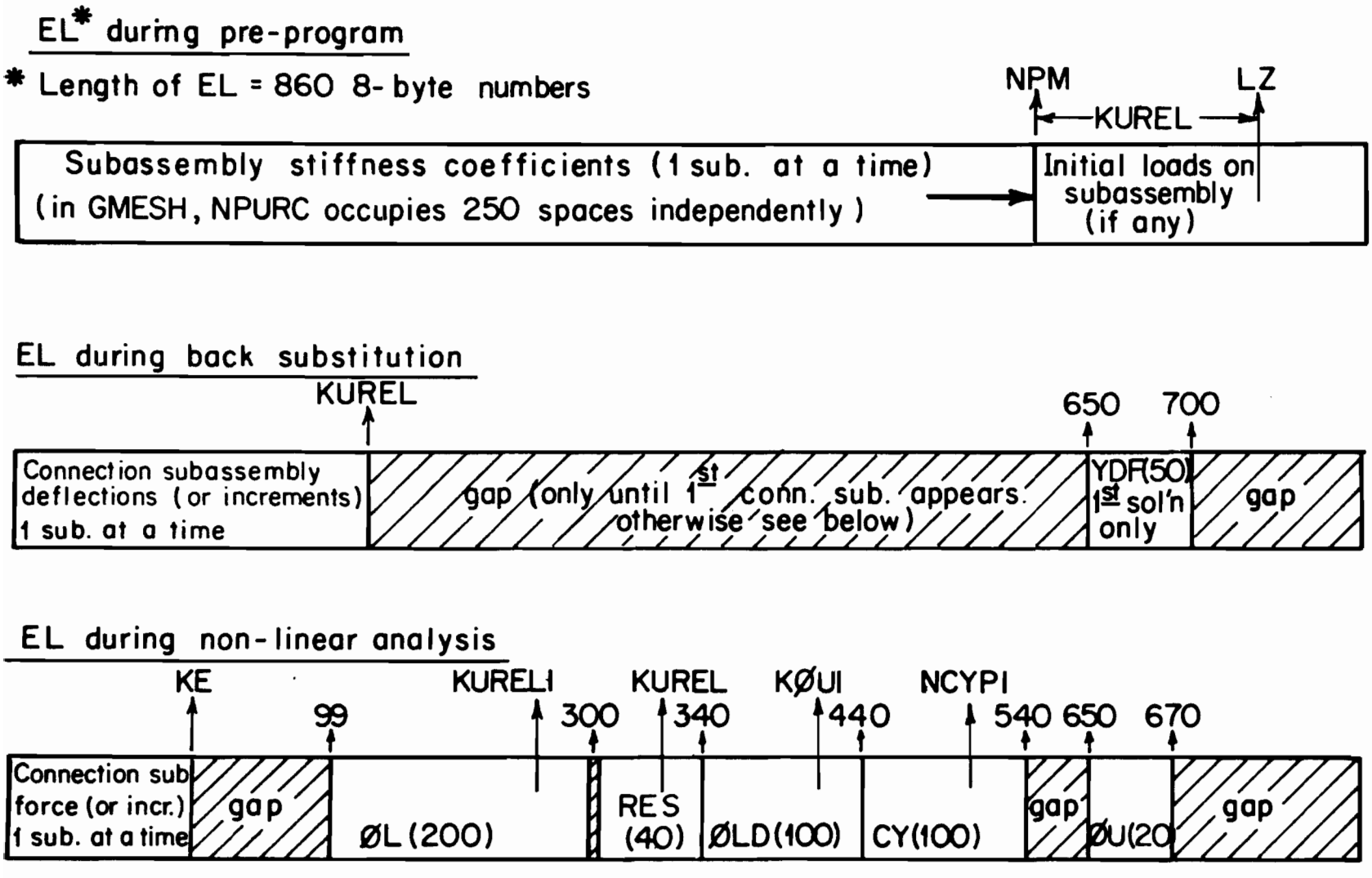

Figure A.3.1 Map of array EL at different stages

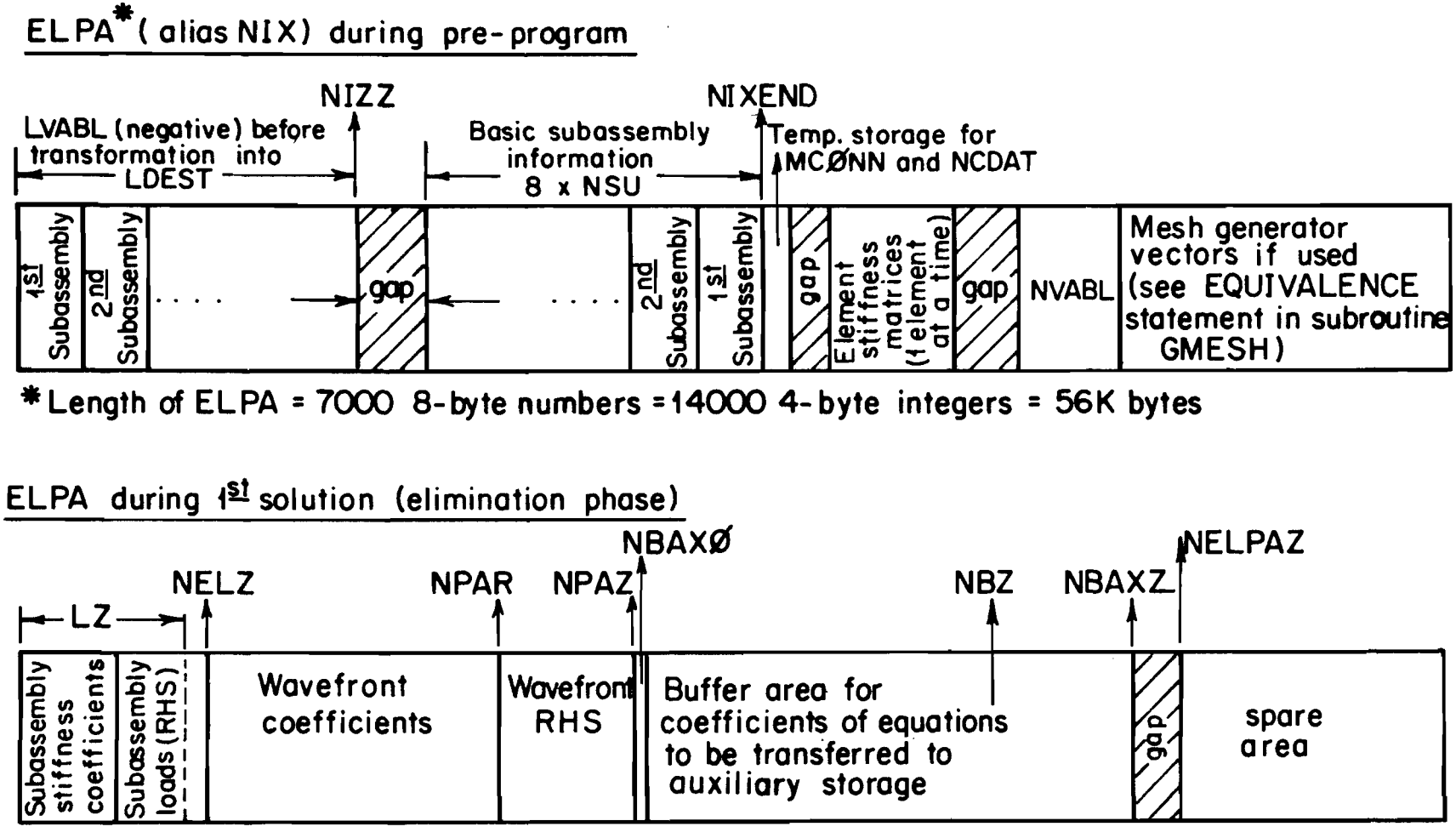

Figure A.3.2 Map of array ELPA at different stages (cont.)

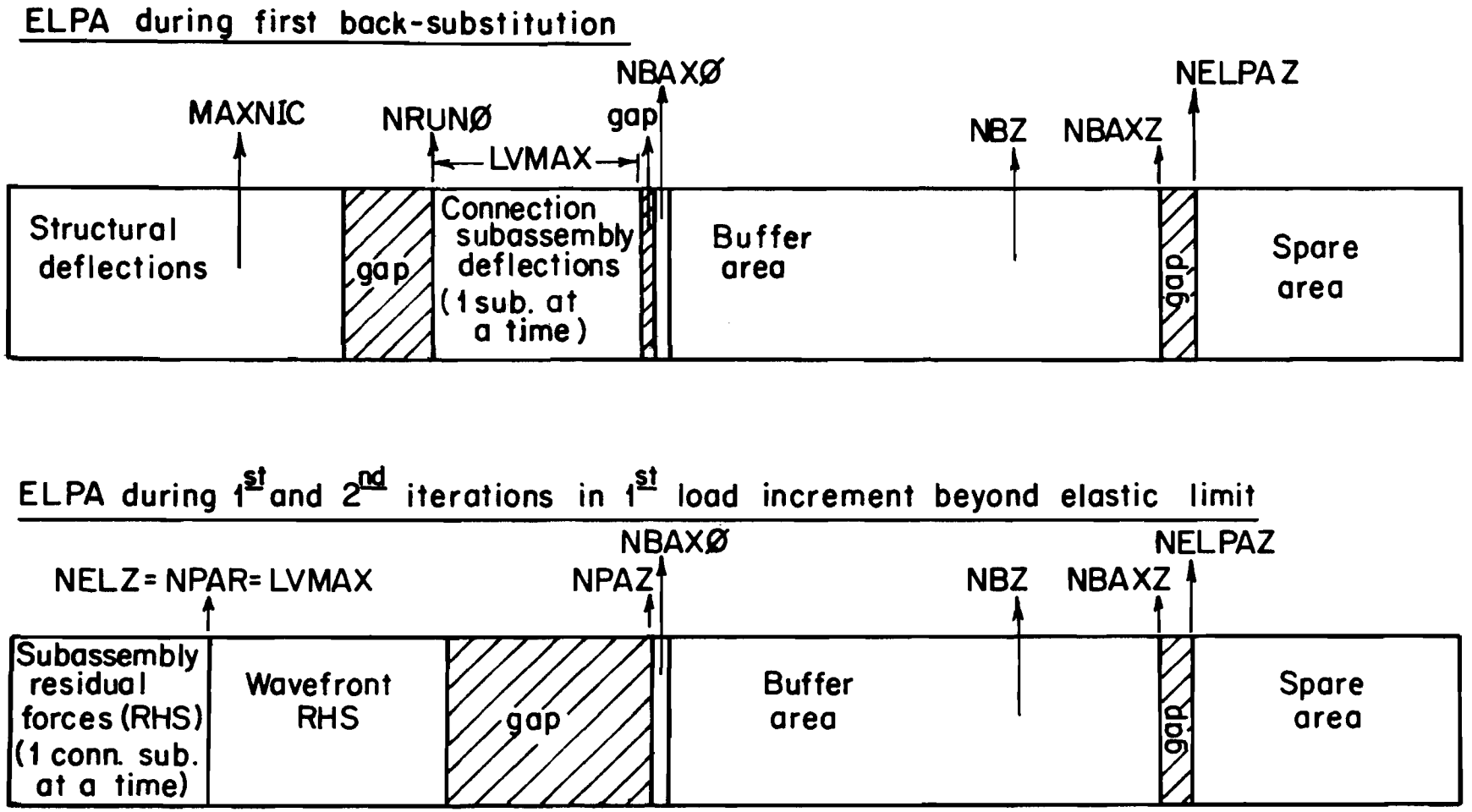

Figure A.3.2 (cont.) Map of array ELPA at different stages (cont.)

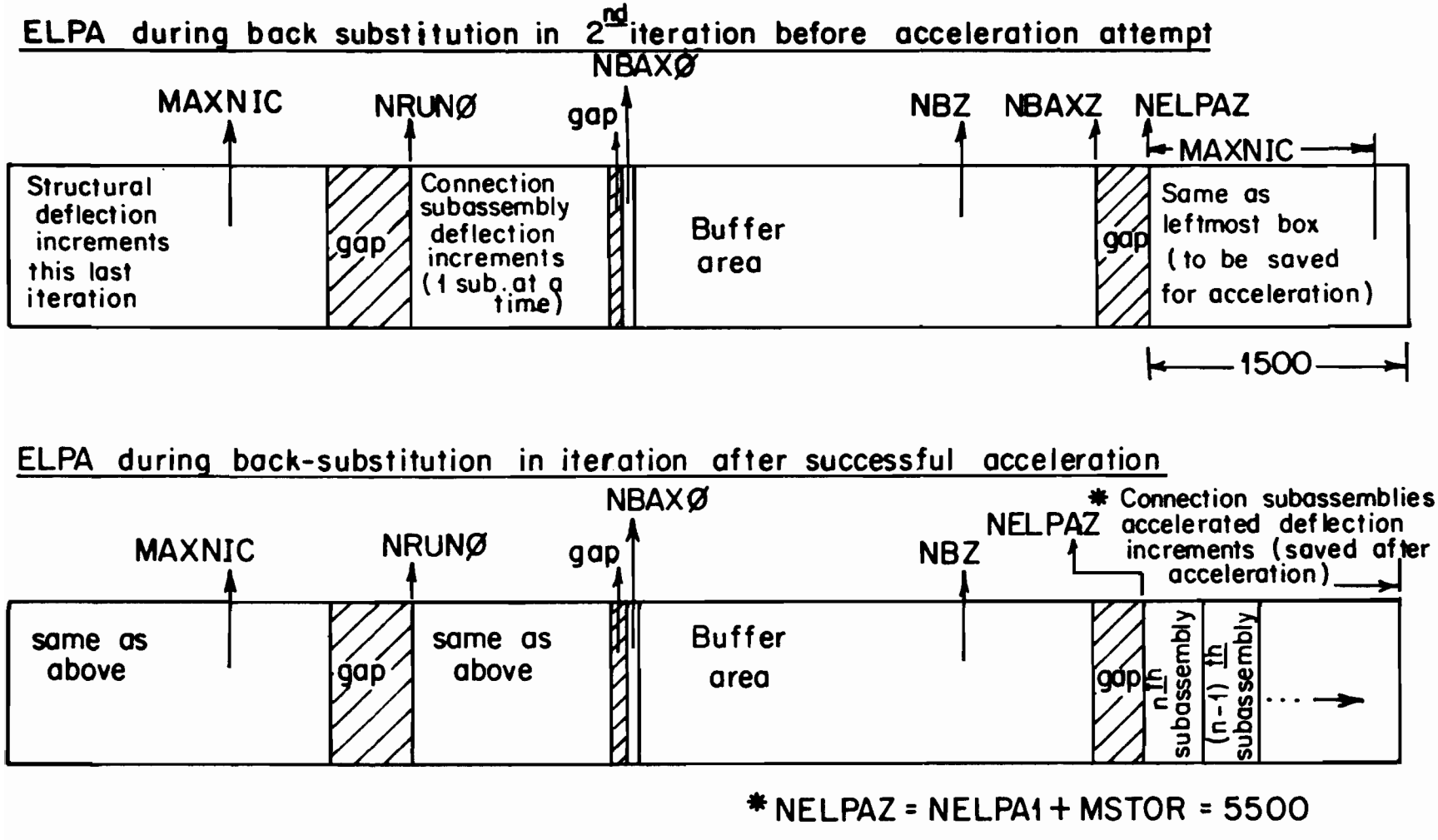

Figure A.3.2 (cont.) Map of array ELPA at different stages

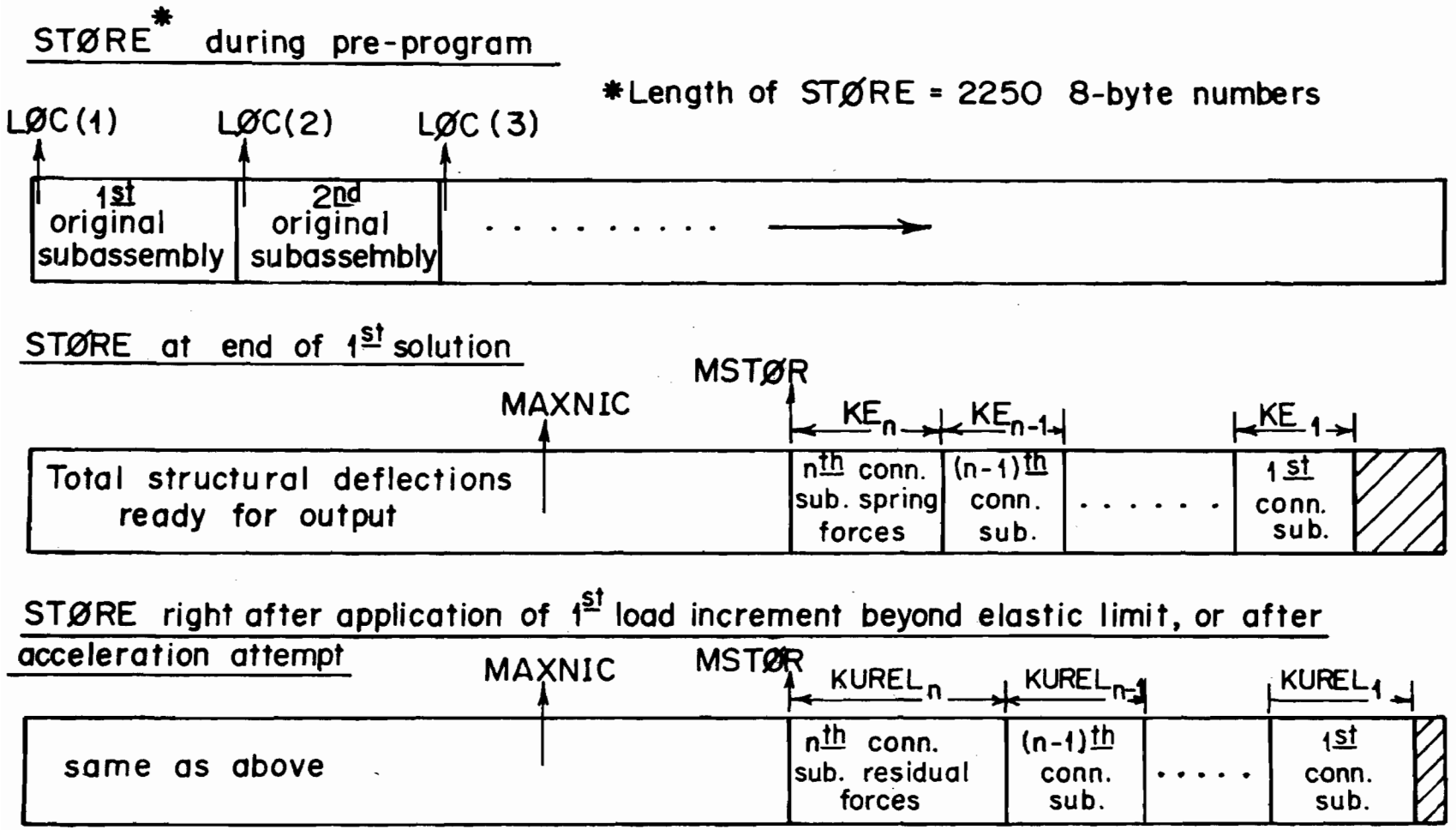

Figure A.3.3 Map of array STORE at different stages

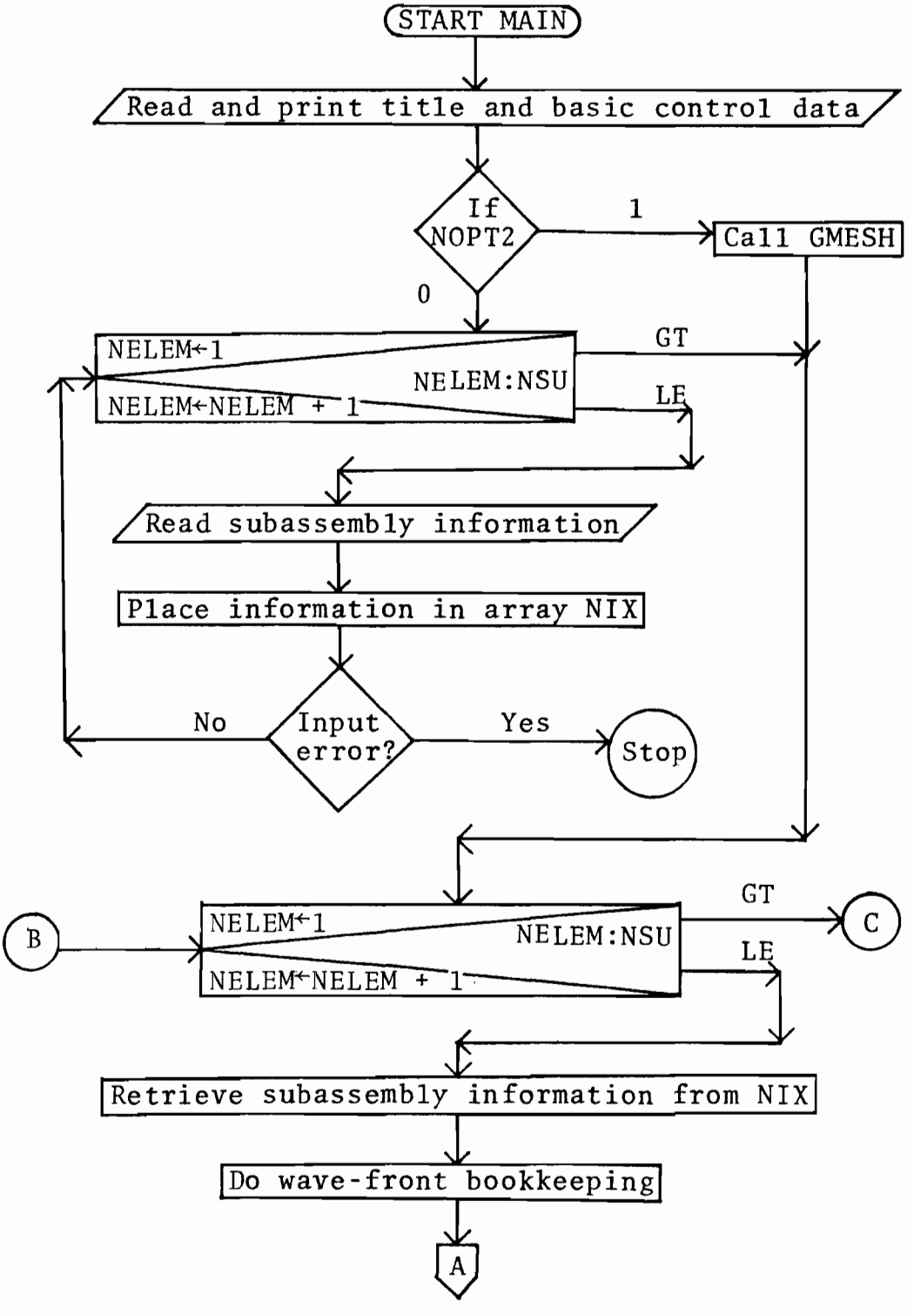

Figure A.4.1 Flow chart for main routine (cont.)

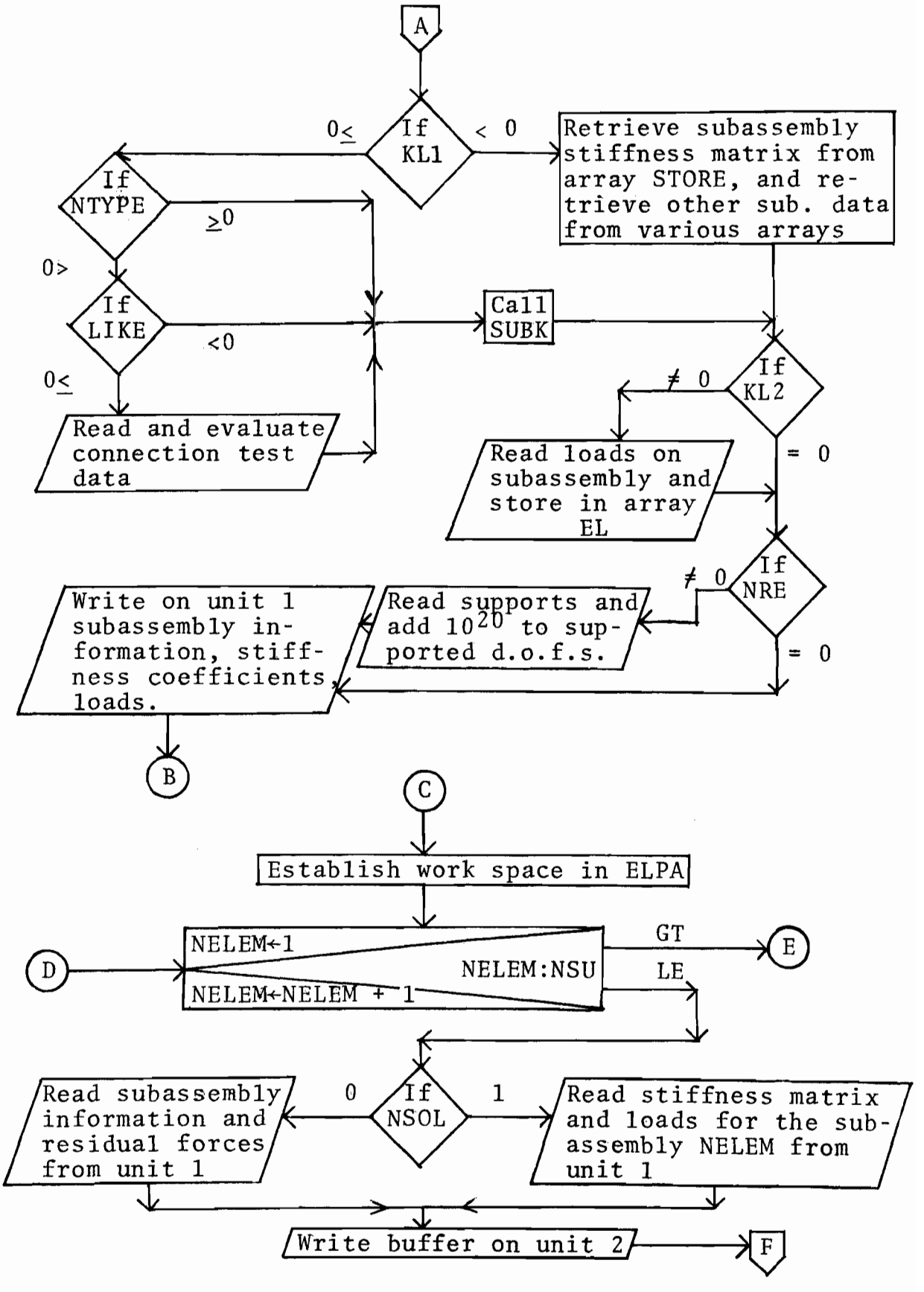

Figure A.4.1 (cont.) Flow chart for main routine

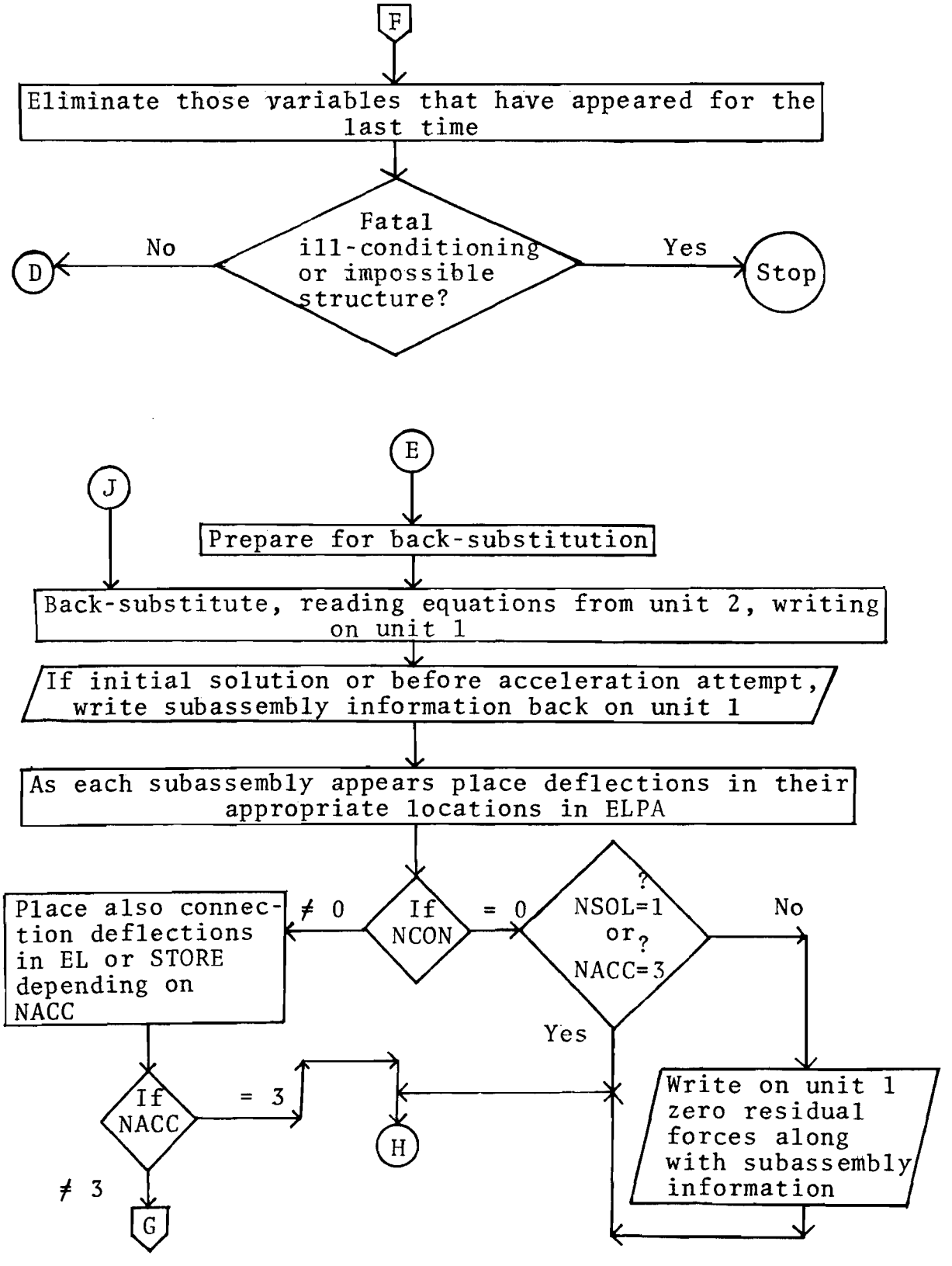

Figure A.4.1 (cont.) Flow chart for main routine

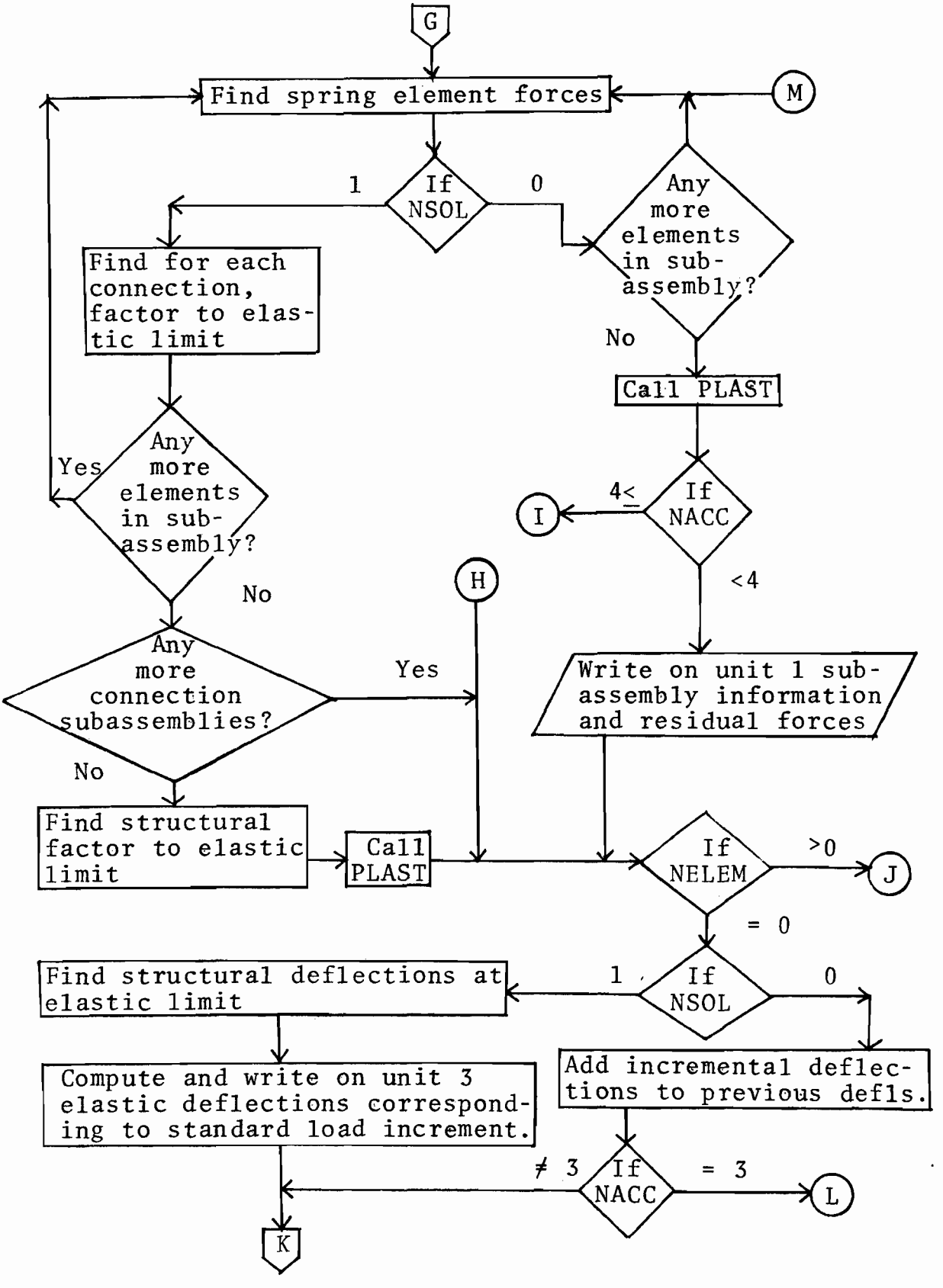

Figure A.4.1 (cont.) Flow chart for main routine

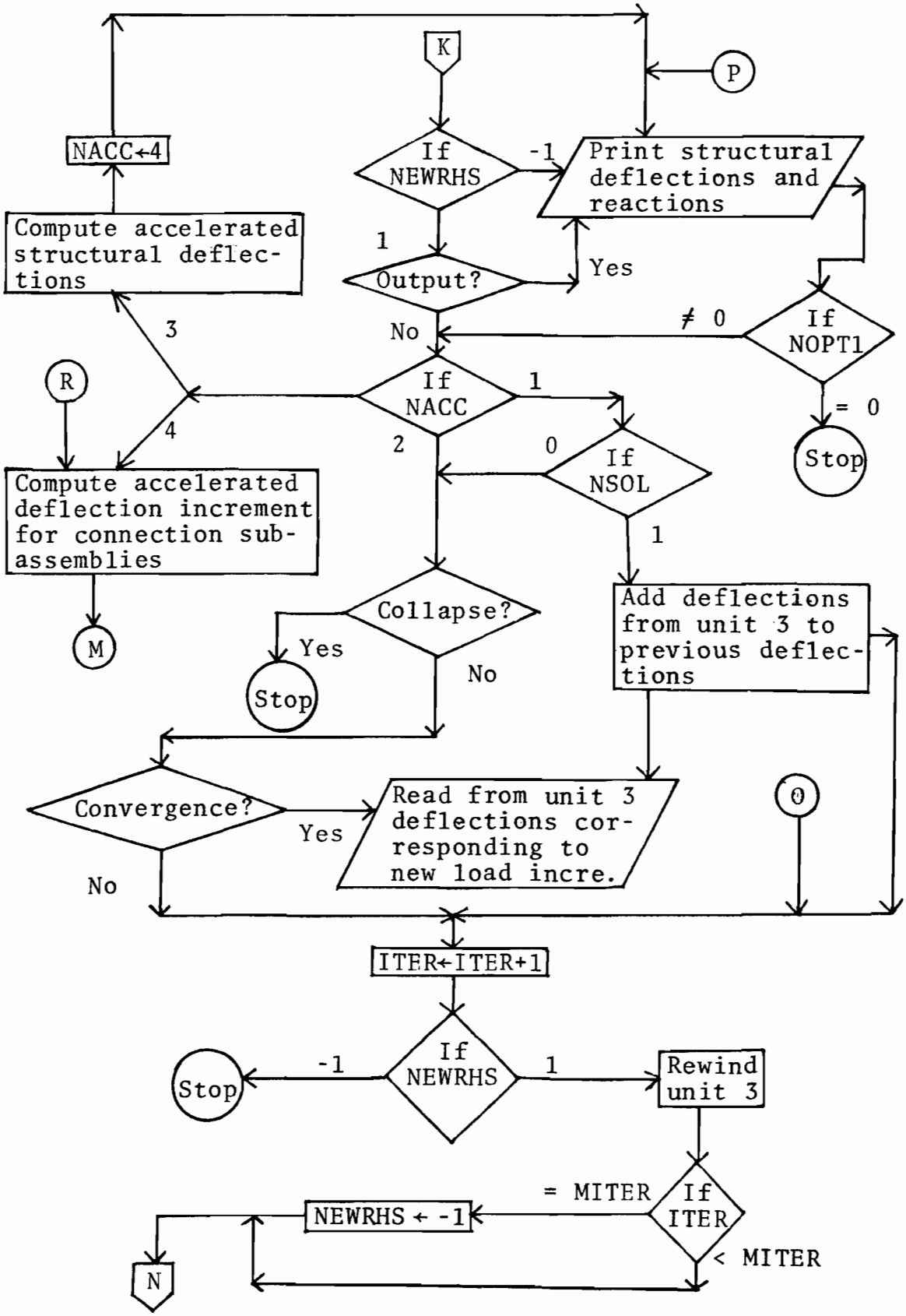

Figure A.4.1 (cont.) Flow chart for main routine

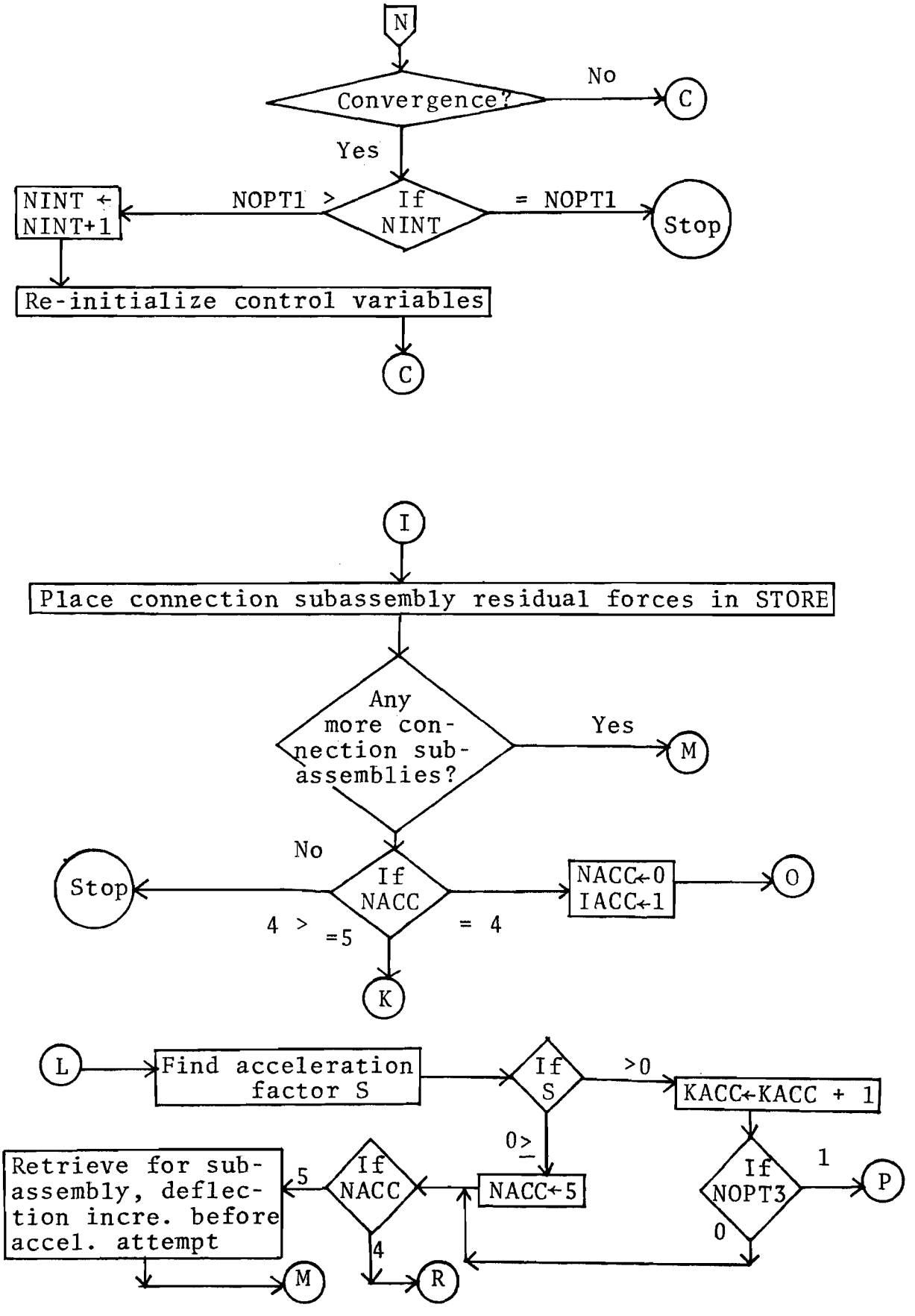

Figure A.4.1 (cont.) Flow chart for main routine

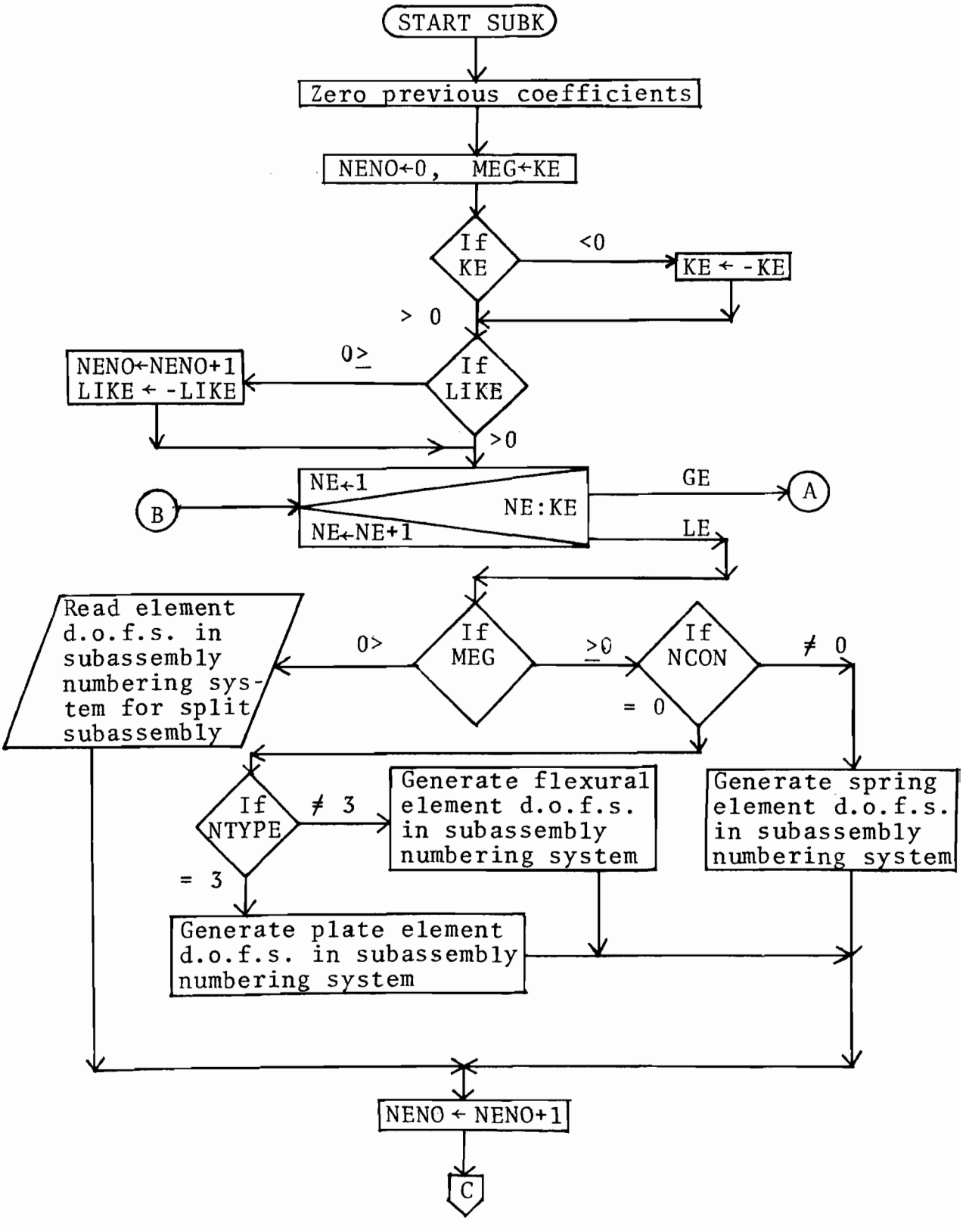

Figure A.4.2 Flow chart for subroutine SUBK (cont.)

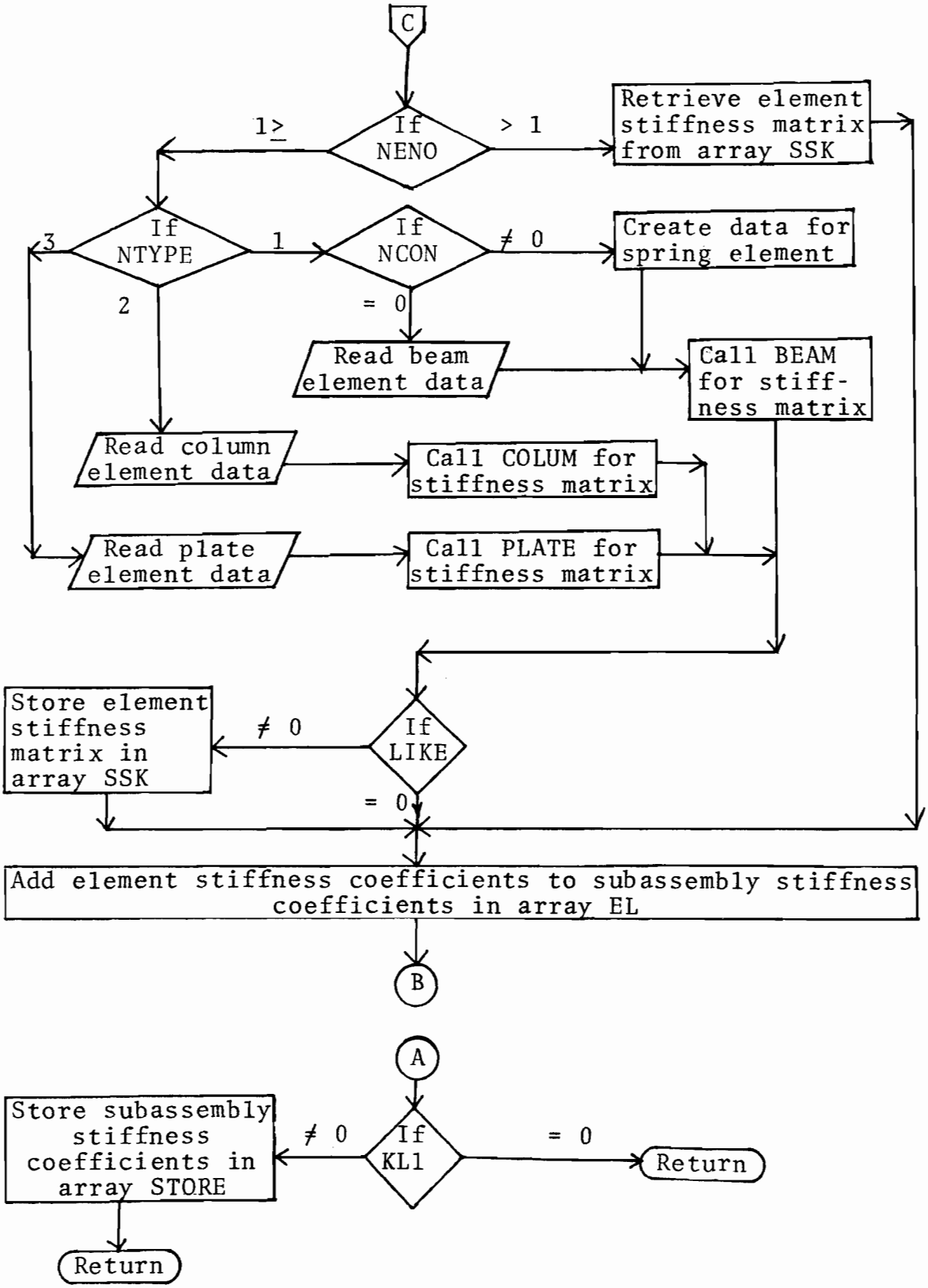

Figure A.4.2 (cont.) Flow chart for subroutine SUBK

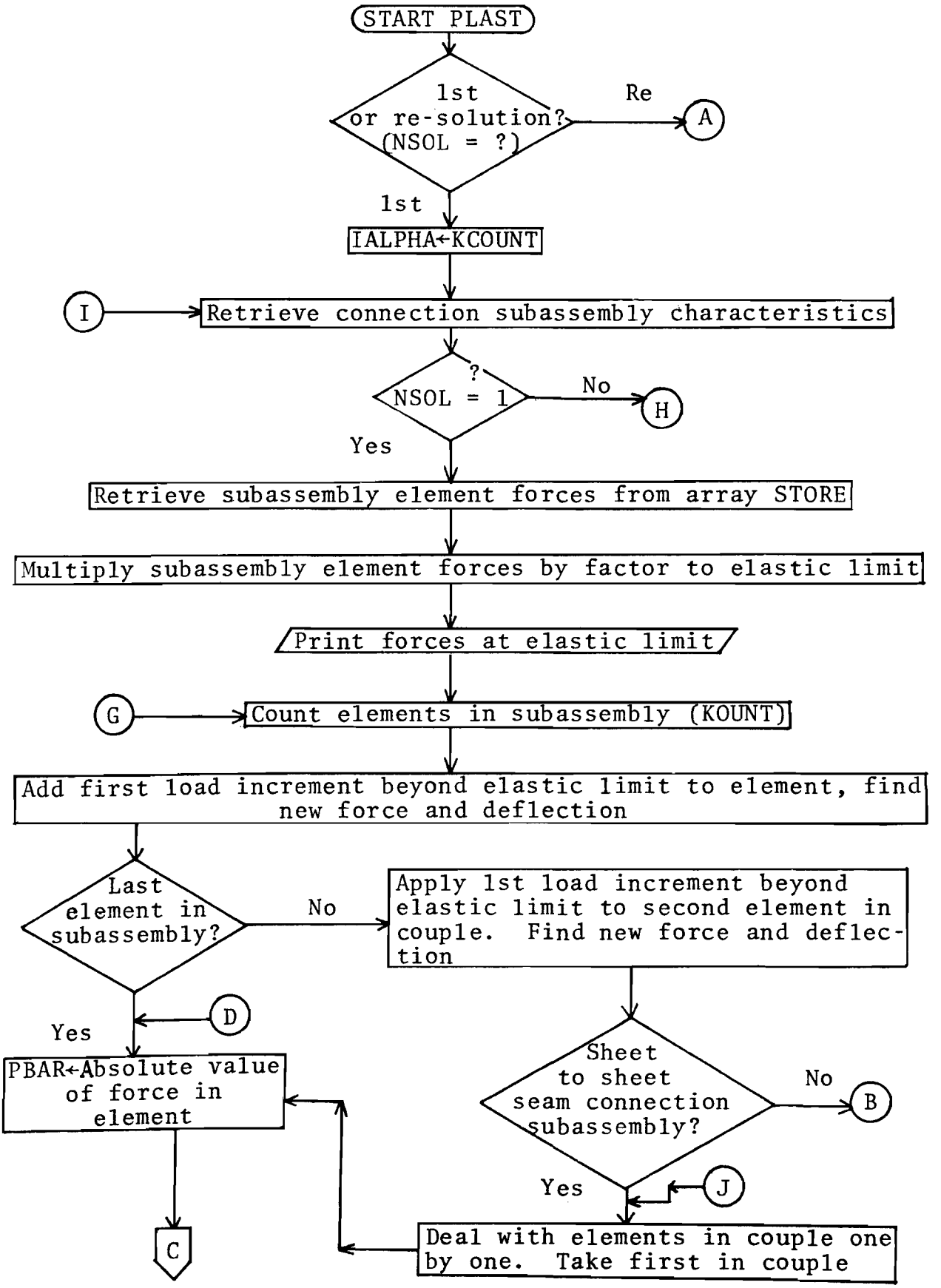

Figure A.4.3 Flow chart for subroutine PLAST (cont.)

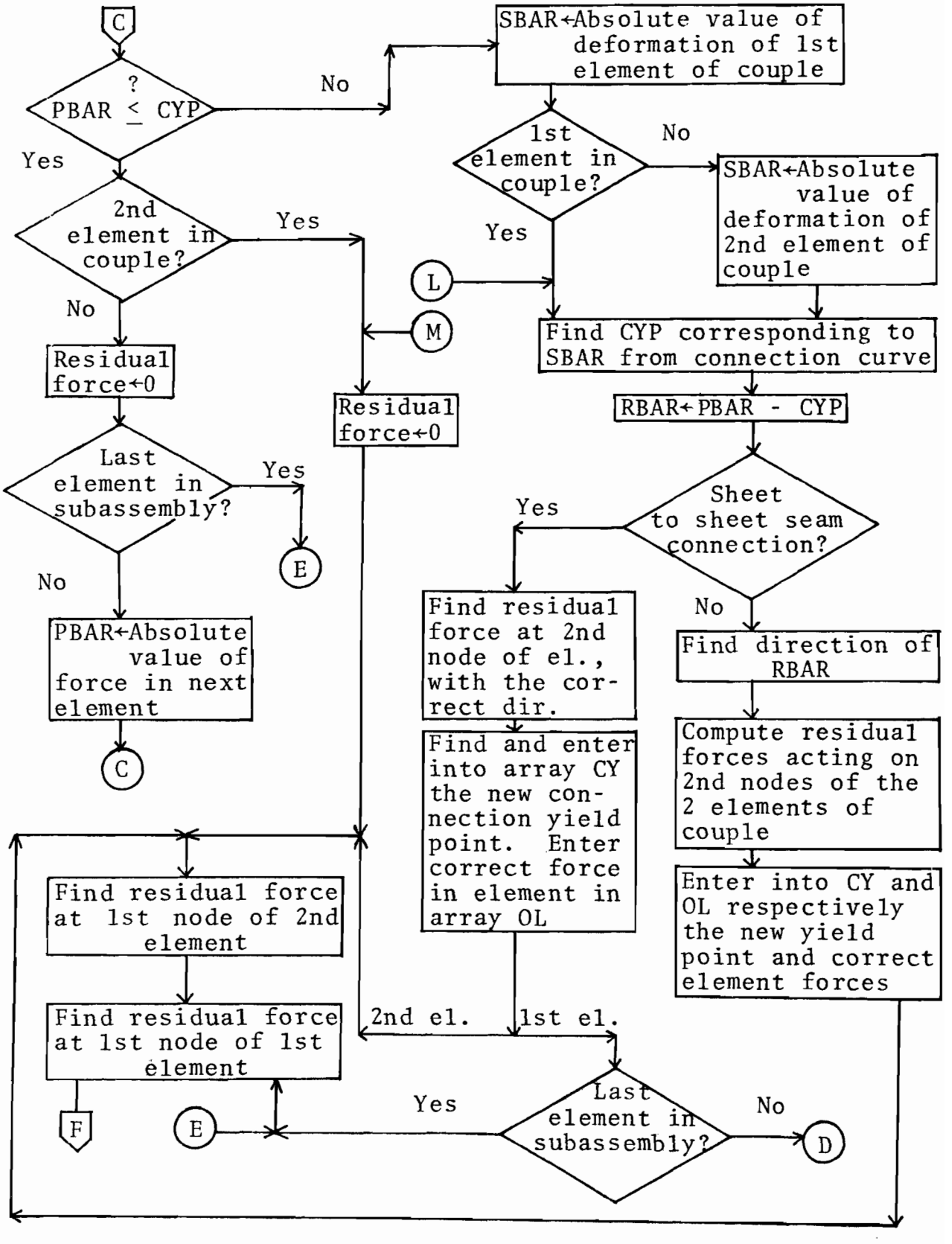

Figure A.4.3 (cont.) Flow chart for subroutine PLAST

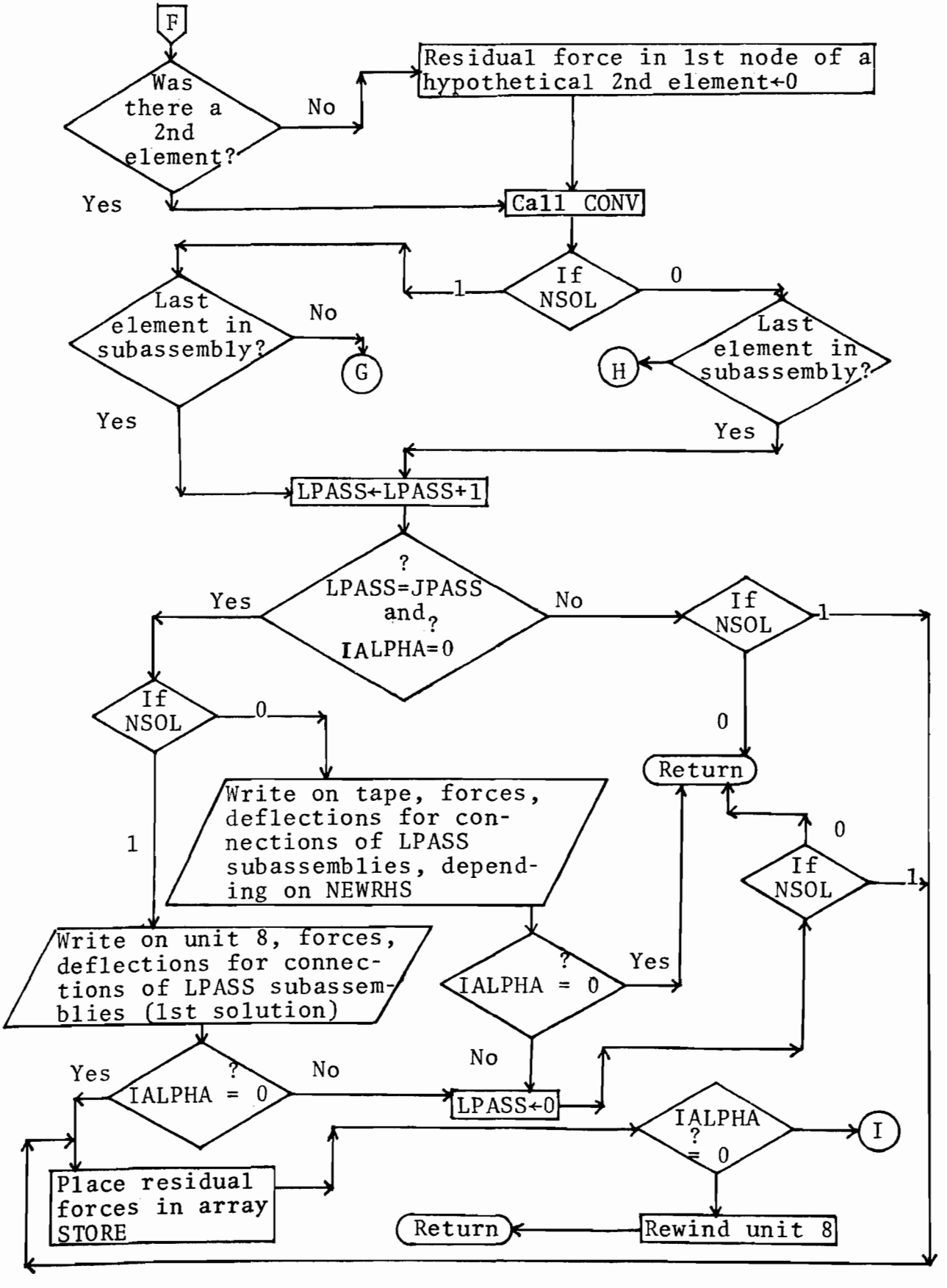

Figure A.4.3 (cont.) Flow chart for subroutine PLAST

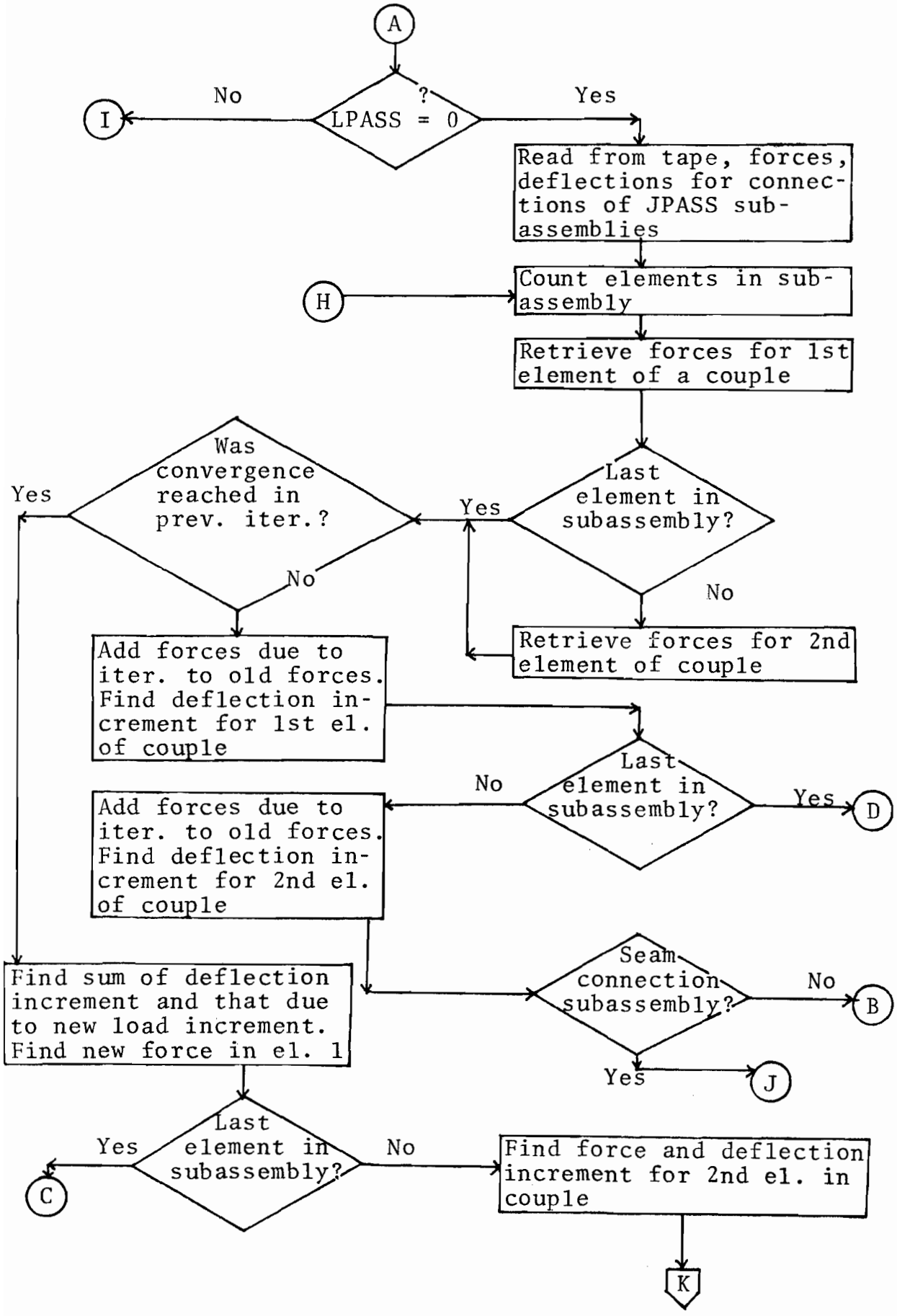

Figure A.4.3 (cont.) Flow chart for subroutine PLAST

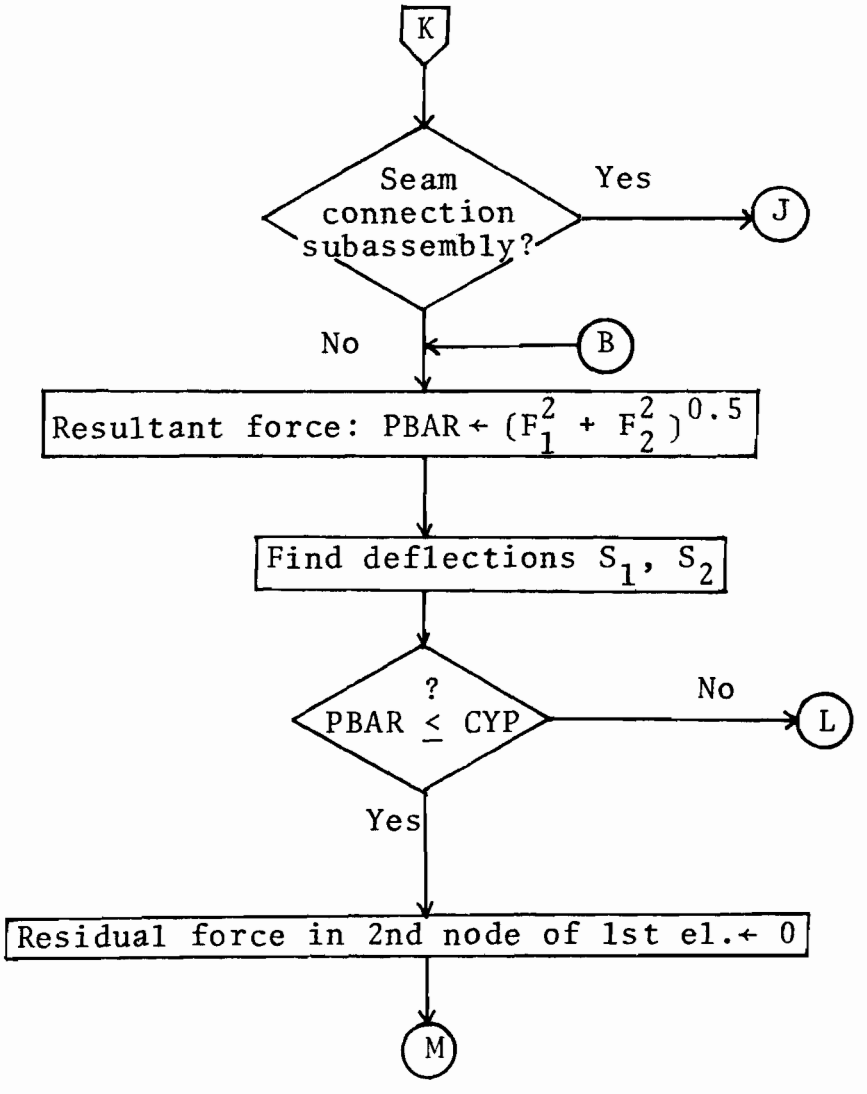

Figure A.4.3 (cont.) Flow chart for subroutine PLAST

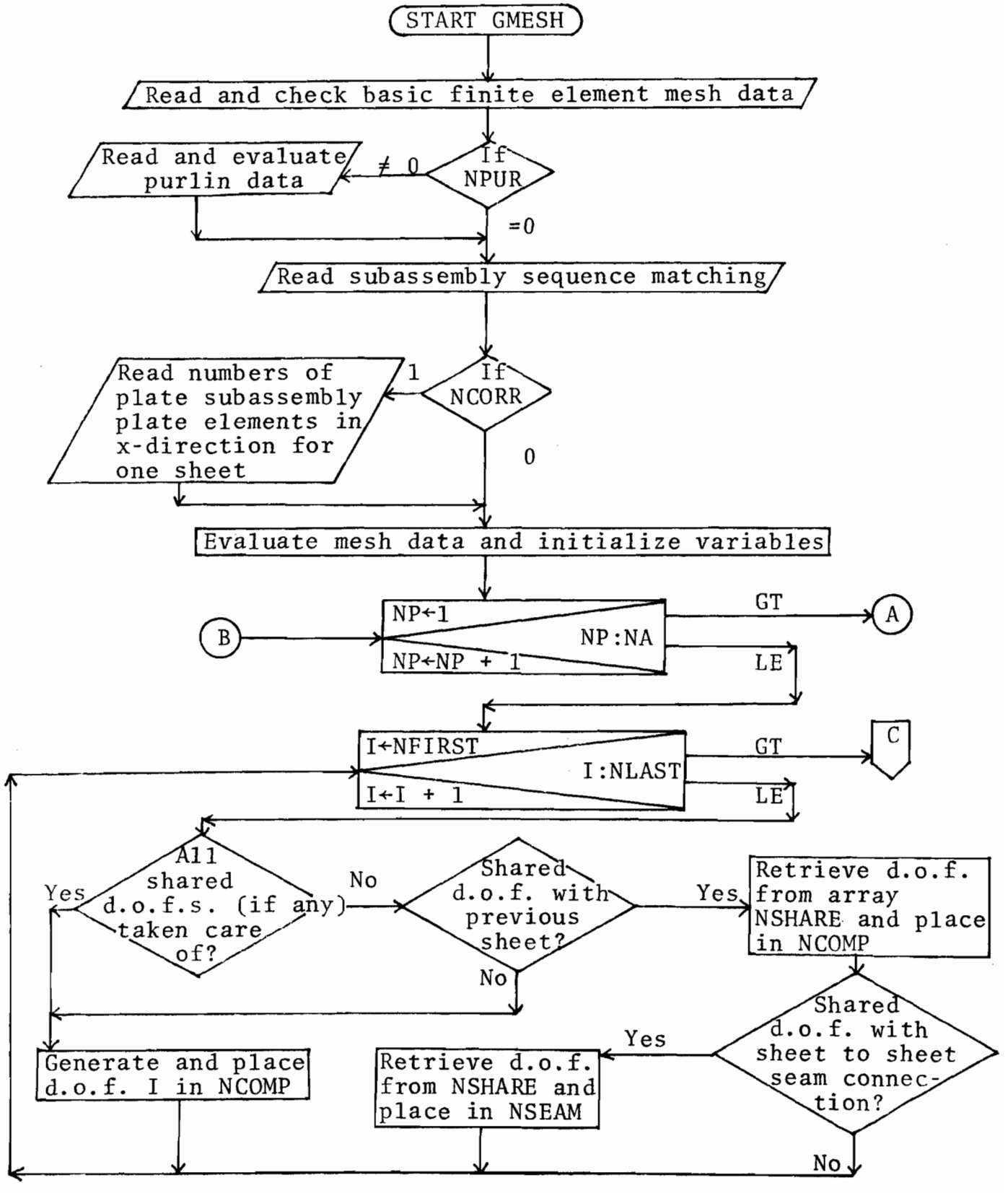

Figure A.4.4 Flow chart for subroutine GMESH (cont.)

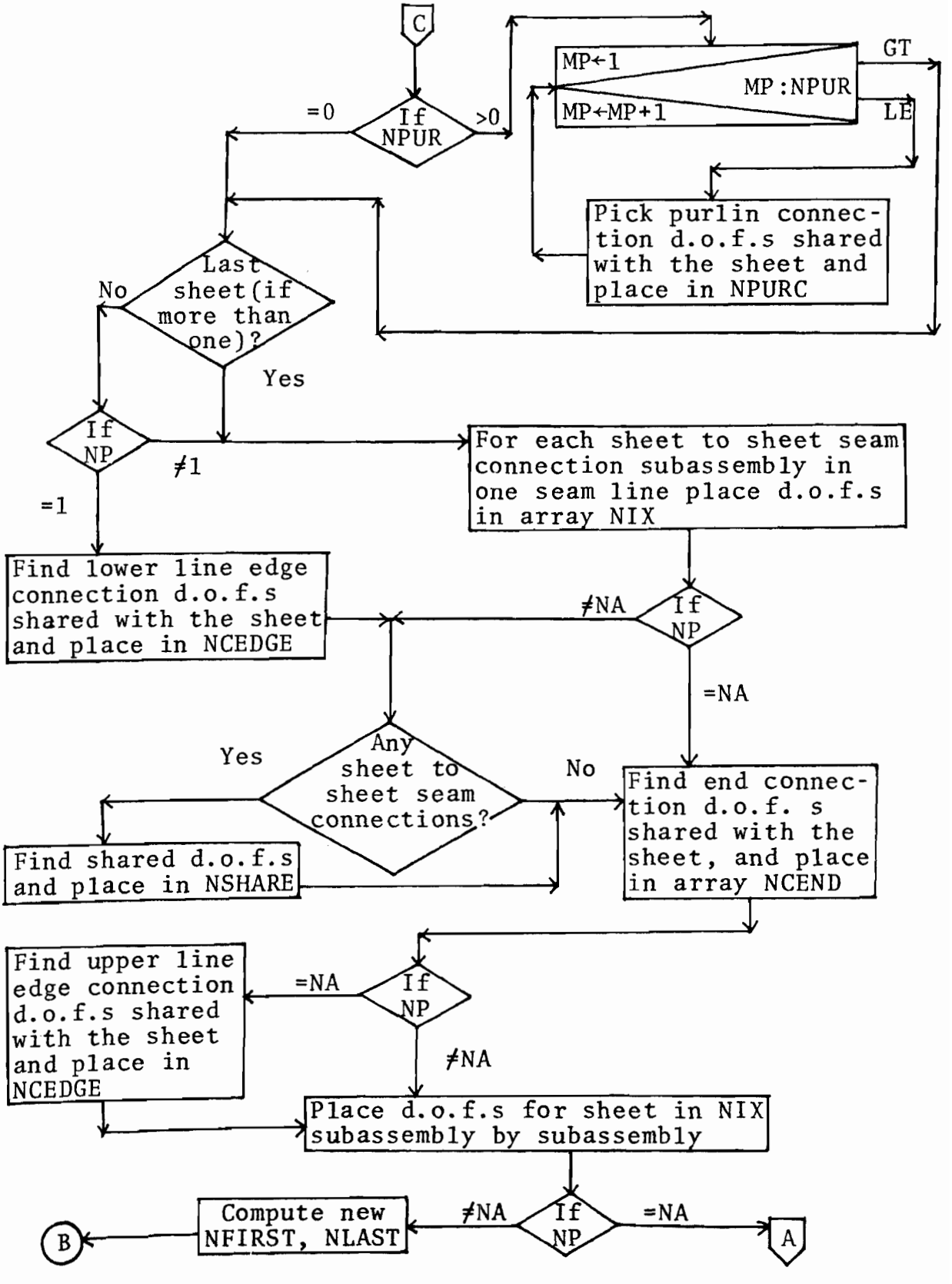

Figure A.4.4 (cont.) Flow chart for subroutine GMESH

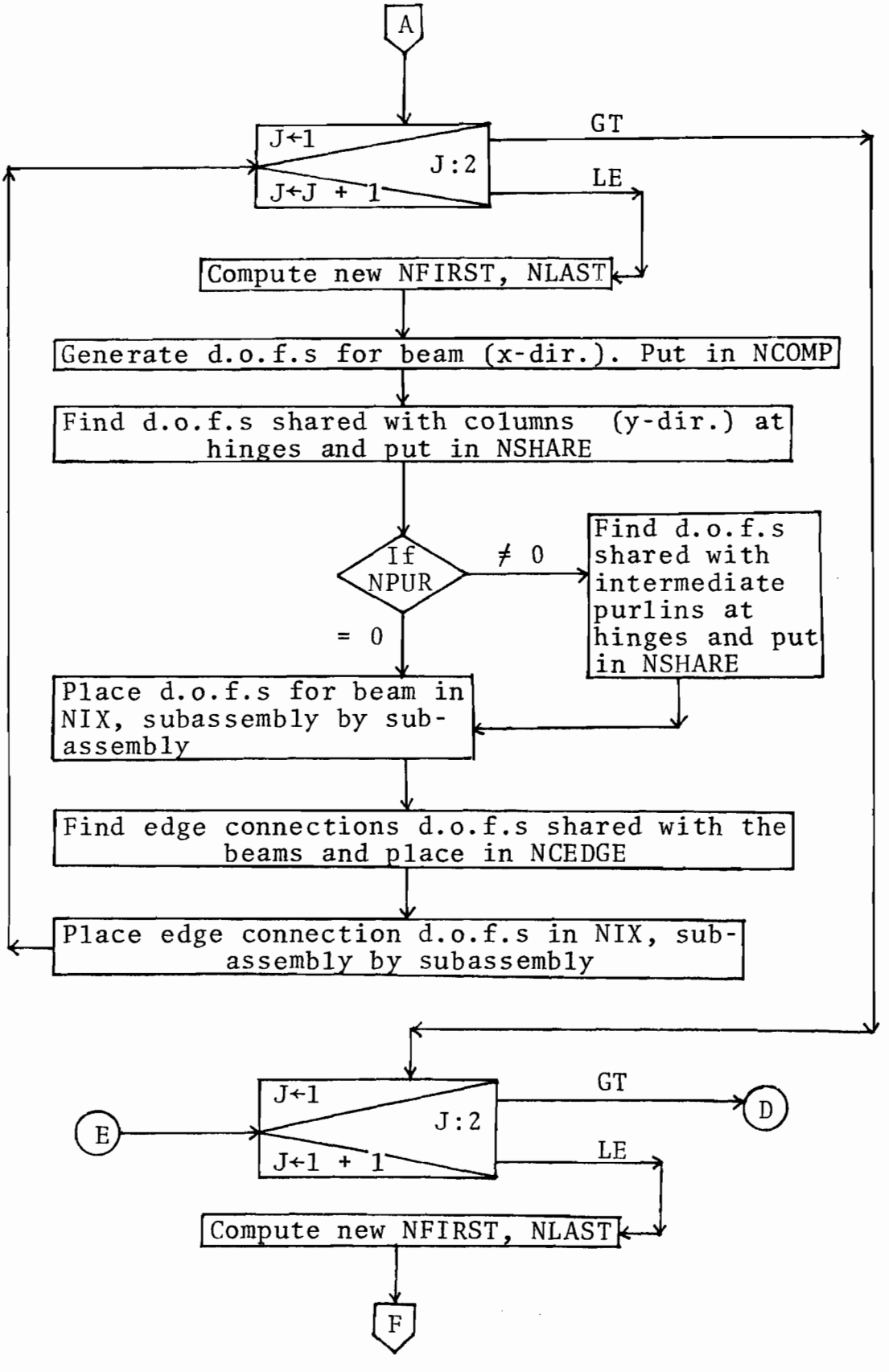

Figure A.4.4 (cont.) Flow chart for subroutine GMESH

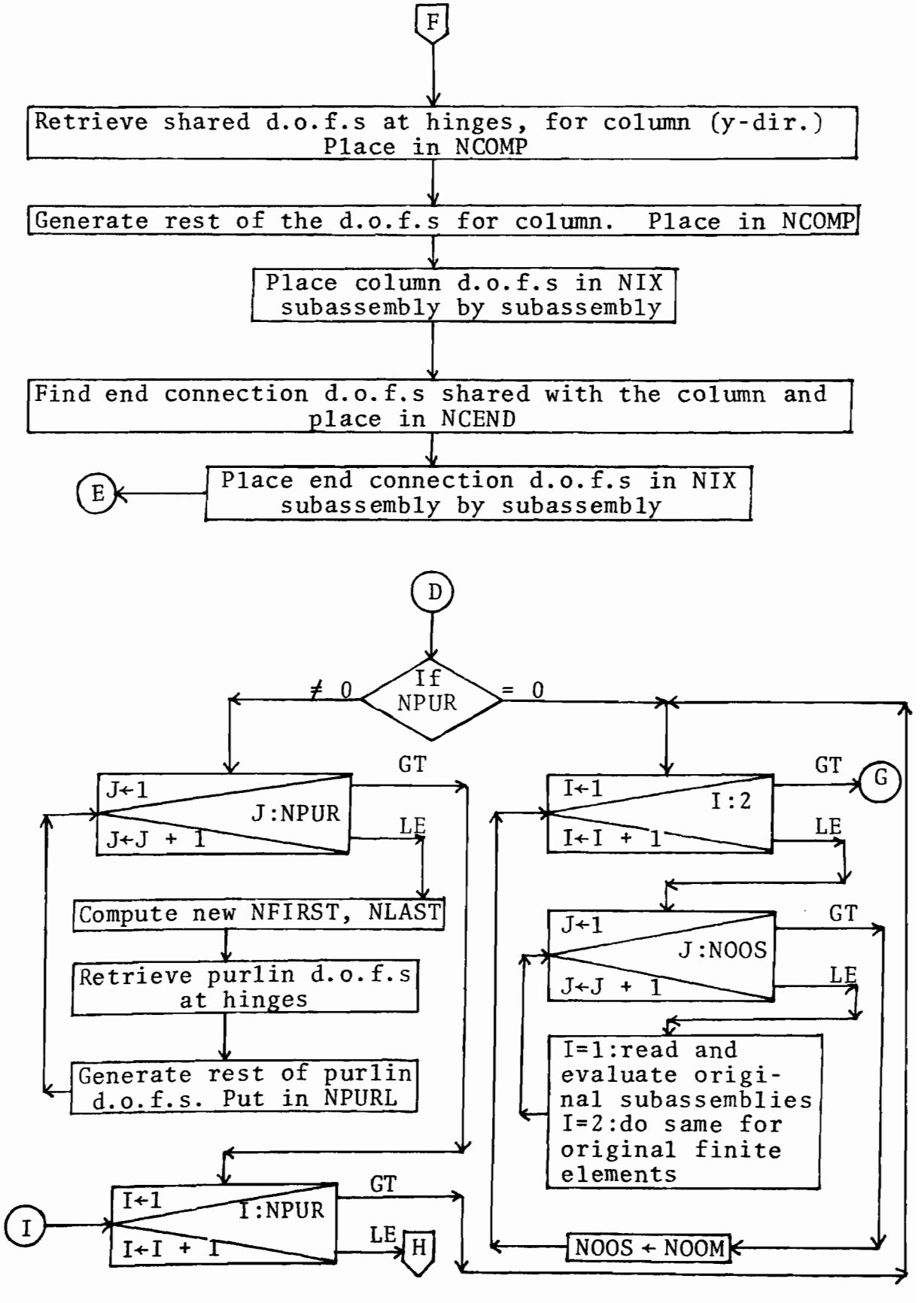

Figure A.4.4 (cont.) Flow chart for subroutine GMESH

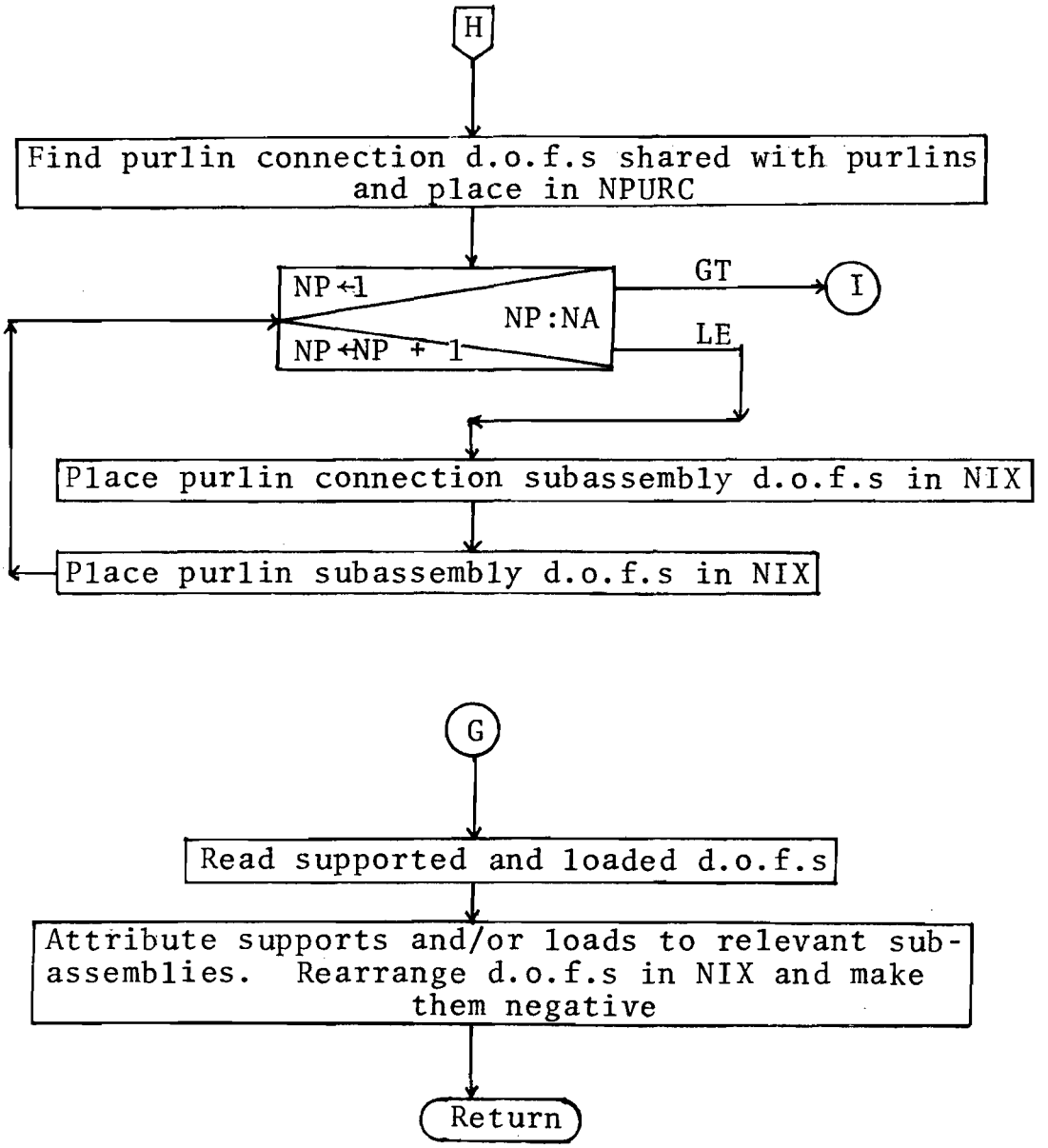

Figure A.4.4 (cont.) Flow chart for subroutine GMESH

1201-408

NON-LINEAR ANALYSIS OF COLD-FORMED STEEL SHEAR DIAPHRAGMS

by

Erdal Atrek and Arthur H. Nilson

ABSTRACT

An efficient method for the analysis of cold-formed steel panel shear diaphragms has been developed which accounts for non-linear behavior. The method is based on residual forces. Diaphragms are modeled by finite elements of three types: the individual panel units, the supporting steel framing, and the connectors. The connectors are considered to be the sole source of non-linear behavior, essentially as indicated by experimental evidence. The computer program is user-oriented, and is equipped with an automatic mesh generator as well as an accelerator to improve convergence rate. Applications of the analysis to diaphragms for which full-scale test results are available show good correlation. The method provides full information on displacements and internal force distributions, as well as overall behavior, and thus provides a sound basis for the development of approximate methods suitable for manual design. It may be directly useful for the design of complex systems such as those including large openings or having unusual proportions, or for the design of innovative stressed-skin structures such as folded plates.

NON-LINEAR ANALYSIS OF COLD-FORMED STEEL SHEAR DIAPHRAGMS

By Erdal Atrek[1] and Arthur H. Nilson,[2] M.ASCE

INTRODUCTION

Use of standard cold-formed steel floor and roof deck panels to resist loads causing shear forces in the plane of their surface is well established engineering practice. While such panels are designed mainly to function as beams to resist gravity loads, it is recognized that complete panel assemblies, together with the supporting steel framework, may be used as shear diaphragms, either in a secondary sense to provide bracing against sway, or in a primary sense in the form of certain types of shell structures such as folded plates. Even the nominal fastening systems (screws or welds) used to prevent accidental displacement of panels or to resist uplift from wind forces, permit development of substantial in-plane shear resistance. Heavier fastening systems may be used to construct very strong and stiff diaphragms where shear loads are large or spans are long.

The design of metal deck diaphragms may proceed based on (a) results of tests on full scale prototype components, (b) approximate analysis by manual calculation, or (c) finite element computer analysis.

In the U.S., since the early 1950's, engineers have relied mainly on prototype tests of full scale components of complete diaphragms. Fig. 1(a) shows a simple three-bay building acted upon by horizontal loading, such as

---

[1]Asst. Prof., Dept. of Civil Engrg., Faculty of Engrg. and Arch., Istanbul Technical Univ., Istanbul, Turkey; formerly graduate research asst., Dept. of Structural Eng., Cornell Univ., Ithaca, N.Y.

[2]Prof. and Chairman, Dept. of Structural Eng., Cornell Univ., Ithaca, N.Y.; M.ASCE.

from wind. The deck is used to provide shear resistance. Conditions in a shear-loaded exterior bay may be duplicated by a cantilever test frame as shown (b). The load-deflection response and strength of the structure may be predicted based on results of testing the cantilever frame. Details of such tests have been standardized by AISI in Ref. (1).

Several approximate methods of analysis have been proposed, notably those by Luttrell (10), Pinkham (14), and Bryan (4). The most generally suitable appears to be that of Bryan, as modified and refined by Davies (5). The essential feature of the analysis by Bryan and Davies is that the properties of individual components of diaphragms, such as connectors or panel elements, are established by test or analysis. An assumed distribution of internal diaphragm forces is made, permitting determination of the displacement component introduced by each part. The flexibility of the entire assembly is the sum of the flexibilities of the parts. The method is suitable for ordinary design-office work using slide rule or electronic calculator, and has been widely used abroad.

For cases where unusual deck geometry, presence of openings, or other complications invalidate the usual assumptions of internal force distributions, or where more refined behavior prediction is necessary, an analysis based on a finite element approach can be used. Such an analysis has also been useful in studying ordinary cases, in order to permit realistic assumptions for internal forces (prerequisite for manual analysis, as described above). The linear elastic finite element analysis of shear diaphragms was first described in a paper by Nilson and Ammar (13).

Diaphragms may exhibit non-linear behavior at relatively low loads, due mainly to stress concentrations at the connectors. In order to trace the load-deflection behavior through the entire range of loading, and to predict failure load accurately, it is necessary that a non-linear analysis be made.

The research described herein extends the work described in Ref. (13) into the non-linear range (2).

BASIS OF FINITE ELEMENT ANALYSIS OF DIAPHRAGMS

The essential features of the linear elastic analysis have been described in Ref. (13), and they will be summarized only briefly here.

According to the finite element method, in general, any continuous body such as a thin plate subject to in-plane loading, may be divided for computational purposes into a large number of discrete elements. Within each of these, the state of stress may be described in simple terms, although stresses may vary in a complex way from element to element. The elements are assumed to be interconnected only at discrete points, usually their corners, where conditions of equilibrium, and in most cases compatibility, are enforced.

The adaptation of such an analysis to metal deck diaphragms is a natural one. Such diaphragms are actually composed of a large number of discrete elements (the individual panels), interconnected only at discrete points to each other or to the supporting framework by welds or screws. With the stiffness properties of the panels, the fasteners, and the supporting members established analytically or experimentally, the ordinary methods of matrix analysis may be used to predict the behavior of the assembly.

(a) Cold-Formed Steel Panels: Standard deck panels used may be placed in one of the two categories shown in Fig. 2. Closed cellular panels (a) are fabricated by spot-welding hat-shaped sections to a flat sheet. The open corrugated or trapezoidal sections, (b) and (c), are more commonly used for sheathing of single-story industrial buildings.

For diaphragm analysis in the case of the cellular panels, the flat sheet is assumed to act in shear independently of the hat sections, as the shear

flexibility of the latter is much greater than the sheeting. The resulting case of plane isotropy is well established and the panel behavior is modeled by use of the material constants for the steel without modification.

Corrugated sheeting, although made of isotropic material, will respond to loading orthotropically due to geometric changes. It is convenient to define an orthotropic flat sheet having the projected planar dimensions of the corrugated sheeting, and behaving in the same manner (Fig. 3). Previous investigators in the field (see Ref. 2) have formulated the material constants for such a case.

Denoting the two principal directions of orthotropy as L (longitudinal) and T (transverse), the following definitions hold:

$$E_L = \frac{p'}{p} E_o \tag{1}$$

where E_L is the effective modulus of elasticity in the L direction, and E_o is the modulus of elasticity of steel.

$$E_T = \frac{J_o}{J} E_o \tag{2}$$

where E_T is the effective modulus of elasticity in the T direction, $J_o = t^3/12$ is the moment of inertia of the panel sheet about its own plane, and J is the moment of inertia of one corrugation about its own mid-plane, defined by:

$$J = \frac{1}{p}\left(\int_o^{p'} z^2 t \, dp' + \int_o^{p'} J_o \cos^2 \alpha \, dp'\right) \tag{3}$$

$$\mu_{LT} = \mu_o \tag{4}$$

where μ_{LT} is the principal Poisson's ratio, and μ_o is the Poisson's ratio for steel.

$$\mu_{TL} = \mu_o \frac{E_T}{E_L} \tag{5}$$

where μ_{TL} is the secondary Poisson's ratio.

For the orthotropic flat sheet, the simple relationship of the shear modulus to μ_o and E_o is no longer valid. If attachment of the corrugated sheet were such that the corrugation geometry is preserved at the ends, but the warping of the end cross-sections is not prohibited, then under a given shear load a uniform shear strain field would be produced in the sheet as shown by shape A of Fig. 4. Thus, the effective shear modulus would be simply:

$$G_{eff} = G_o \frac{p}{p'} \tag{6}$$

where G_o is the shear modulus for steel.

When attachment is made at discrete locations, the end corrugation geometry will not be preserved under shear loading, and Eq. (6) will be deficient. For such cases, Libove (6, 9, 15) and Lawson (8) have made analyses with the recognition that the straight line corrugation generators do not remain straight. Most of this effect is at the ends as shown by shape B of Fig. 4.

Libove has modified Eq. (6) as follows:

$$G_{eff} = G_o \frac{p}{p'} \Omega \tag{7}$$

where Ω is a dimensionless ratio depending on the geometry of the corrugation and its attachment.

Plots of Ω for a great variety of corrugation geometries and sheet dimensions have been prepared with the assumption that discrete attachments exist at least every corrugation pitch. For civil engineering diaphragms, where the attachment interval is in general greater, the added deformation can be accounted for by using a smaller modulus of elasticity in the weak direction (2).

Lawson's expression for G_{eff} depends on a dimensionless parameter $\bar{K}$, and this expression can easily be reduced to the form of Eq. (7).

The expression for G_{eff} by Libove is in an average sense over the entire length of the sheeting (see Fig. 4). There is, in fact, a central region where

the increased flexibility due to discrete attachments is negligible (9). The distance a over which it is not negligible is closely related to the corrugation pitch. If the sheet were to be modeled with different shear moduli in the end and central regions (D and A in Fig. 4), the total tip deflection for an isolated sheet should still be equal to that for the sheet with the average shear modulus. However, since the force distributions in the side connections would be different for the two cases, analysis would yield more accurate results if different shear moduli are used.

The ratio of the tip deflections for the two cases can be written in simplified form as:

$$\left(\frac{L - 2a}{G_{L - 2a}} + \frac{2a}{G_{ae}}\right)\left(\frac{L}{G_{eff}}\right)^{-1} = 1 \tag{8}$$

where $G_{L - 2a}$ for the central region can be obtained by Eq. (6), and G_{ae} is the average effective shear modulus for the end regions. Substituting from Eqns. (6) and (7):

$$G_{ae} = G_o \frac{p}{p'}\left[\left(\frac{1}{\Omega} - 1\right)\frac{L}{2a} + 1\right]^{-1} \tag{9}$$

If the value of a can be estimated reasonably well, then a more accurate analysis with $G_{L - 2a}$ and G_{ae} is possible.

The actual finite element representation of the panels is done by rectangular orthotropic plane stress plate elements with four nodes and, at each node, two degrees of freedom that correspond to translations in the X and Y directions (Fig. 5(a)). The stiffness matrix for this element, based on the preceding analysis, can be found in Ref. (2).

(b) Framing Members: These members are modeled by conventional flexural bar elements with two nodes and, at each node, three degrees of freedom corresponding to translations in the X and Y directions and to rotation around the

Z-axis (Fig. 5(b)). Connections of the framing members to each other are modeled as hinges.

(c) Connections: A diaphragm connection is defined here as the combination of the connector and the small region of attached material in the immediate vicinity of the connector.

The variety and complexity of the shapes and types of connections have led investigators (5, 13) to model these by spring elements in the two orthogonal directions, where the spring stiffness is obtained by a connection shear test (13). In the present analysis, somewhat more sophisticated models of the two spring system have been built according to the locations of the connections (Fig. 6), for reasons detailed in Ref. (2).

Since, from experimental evidence, it is known that excessive deformation or tearing of the sheet material around the connector as well as the tilting of screws or the yielding of welds constitute the only important source of diaphragm non-linearity, only the connections are modeled by non-linear functions, other diaphragm elements being assumed elastic throughout the loading range. Except for seam connections, a connection is considered to behave similarly in all directions on the two-dimensional plane. Thus, the two springs modeling the connection are identical, the behavior curve in the resultant direction being a multi-linear approximation of the connection shear test results (Fig. 7).

COMPUTER PROGRAM

The program originates from a frontal solution routine by Irons (7) and a computer program utilizing this routine for first order clad frame analysis, by Miller (11).

It was found that the residual force method (16) would be the most suitable for the required non-linear analysis. Thus, the frontal solution routine was

coupled with the residual force method, an accelerator for fast convergence, and an efficient mesh generator for reduction of input data, to produce the computer program.

(a) Frontal Solution: Finite element analysis of a structure by the stiffness method involves the matrix equation:

$$[K]\{\delta\} = \{P\} \tag{10}$$

where [K] is the structural stiffness matrix, $\{\delta\}$ is the vector of structural degrees of freedom (the variables), and $\{P\}$ is the vector of external forces and reactions.

When the bandwidth of [K] is large, band solution techniques prove inefficient. Furthermore, proper numbering of the finite element mesh is difficult, especially when changes are made in the design. The frontal technique avoids these difficulties by continually reducing [K] into an upper triangle matrix as each new element is introduced, the variables being kept in high-speed storage only between their first and last appearances. Thus, solution speed depends not on the ordering of the variables, but of the elements, which is a much easier task. Since the numbers assigned to the variables are irrelevant to the solution speed, easy renumbering follows. This property also allows for easy treatment of internal hinges and, in special purpose programs, for efficient mesh generation.

The re-solution facility in Irons' routine requires only that the right hand sides of Eq. (10) be modified for a re-solution, no re-assembly or consequent reduction of [K] being done.

(b) Non-linear Analysis: This re-solution facility suggested the use of the residual force method proposed by Zienkiewicz and co-workers (16). In this method, [K] is not modified with progressive material non-linearity, but the unbalanced forces due to this non-linearity are imposed on the structure as

additional loads. Thus, the process for a given load increment in the non-linear range is iterative, the iterations converging when the effect of the unbalanced (residual) forces becomes negligible. The stiffness matrix [K], once reduced in the first solution, can be used throughout the analysis.

The method depends on the fact that in material non-linearity, a given increment of deflections will uniquely describe the internal force distribution (while the opposite is not necessarily true) and thus, is very easily applied to diaphragm non-linearity, due to the uncomplicated modeling of the connections.

Unless the structure is at collapse condition, the iterations in a given load increment will be convergent, defining, as a result, the equilibrium condition. However, when the degree of non-linearity is high, convergence tends to be rather slow. Therefore a version of the Aitken accelerator as proposed by Boyle and Jennings (3) is employed to speed up convergence (2). High rates of convergence are attained in this manner, and the residual force method becomes very efficient for this problem.

APPLICATIONS

The computer program was applied for the non-linear analysis of four cantilevered diaphragms (2) for which test results are available from earlier investigations at Cornell (10, 12). Non-linear connection behavior was based on tests reported in the Ref. (13).

(a) Open Corrugated Diaphragm 24 in. x 28 in. (61.0 cm. x 69.1 cm.): A specimen of 26 gage standard corrugated sheeting attached to L-section perimeter members, previously tested by Luttrell (10), was analyzed during the development of the program. Only a very rough bi-linear approximation of the connection curve was used, along with an effective shear modulus obtained from research reported in Ref. (13). Still, as described in Ref. (2), the analytical results compare reasonably well with the test results.

(b) Cellular Deck Diaphragm 10 ft. x 12 ft. (3.05 m. x 3.66 m.): A welded cellular metal deck tested by Nilson (12) was analyzed next (Fig. 8). The finite element model is shown on Fig. 9. Detailed descriptions can be found in Ref. (2).

Beyond the proportional limit, in analysis, load increments of five kips (2268 kg.) each were applied. Deflection of the diaphragm in the load direction is compared with the test results on Fig. 10. Excellent agreement was obtained. Redistribution of internal forces due to plastic behavior at the connection produced more uniform distributions compared with the elastic case, before failure was reached (2).

(c) Open Corrugated Diaphragm 10 ft. x 12 ft. (3.05 m. x 3.66 m.): A standard corrugated diaphragm tested by Luttrell (10), is shown in Fig. 11. The test arrangement included three intermediate purlins. Detailed descriptions of the test specimen and the several finite element models developed for this diaphragm can be found in Ref. (2).

Preliminary analysis, utilizing G_{eff} as found for point attachments at corrugation valleys, indicated need to account for the clamping effect of the connector washers on the narrow corrugation valleys. The closest model for which analytical results are available is the case of point attachments at corrugation midheights and valleys described in Ref. (15). G_{eff} for this case is very close to the theoretical upper limit (Eq. 6). Results for the model utilizing the latter are compared against the test results on Fig. 12. It is seen that although the elastic slopes compare very well, the test specimen, overall, is stiffer and stronger than analysis indicated. Several relevant points are detailed in Ref. (2), mainly emphasizing that the connectors for the full scale test and for the connection test (conducted several years later) were different in some respects (e.g. washer size, manufacturer), and that in

the full scale test, tilting of the screws was prevented to a certain degree by the corrugation walls.

Refined models, utilizing different shear moduli for the end and central regions, were also tried. These models produced only about 3% difference in results, but required appreciably greater solution times.

(d) Open Trapezoidal Diaphragm 10 ft. x 12 ft. (3.05 m. x 3.66 m.): The last diaphragm to be analyzed was previously tested by Luttrell (10). It consisted of six sheets connected to WF sections on the perimeter. One intermediate purlin, connected to the sheets by what are termed in Ref. (10) "non-load resisting" connections, ran perpendicular to the seam lines (Fig. 13). The finite element model neglects this purlin.

The deflection of the diaphragm, as obtained from non-linear analysis, is compared with the test results on Fig. 14. The last point on the curve represents an upper bound for the strength of the finite element model.

Since G_{eff} by Eq. (7) was used for non-linear analysis, the model is somewhat stiffer than the test specimen in the lower range of loading. At higher loads the situation is seen to be reversed. This is easily accounted for. As detailed in Ref. (2), the "non-load resisting" connections of the test specimen actually start participating in the load carrying in this loading range.

The force distributions at the connections at different load levels can be found in Ref. (2).

CONCLUSION

(a) Full scale testing of light gage metal diaphragms loaded in shear is time consuming and costly. Computer analysis of proposed design alternatives can be done instead, with less cost and higher efficiency in terms of time spent and information obtained. Furthermore, the volume of data obtained by

computer analyses can be put to good use in developing approximate analyses for hand computation in design offices.

(b) Diaphragm assemblies can be modeled to yield accurate predictions of behavior and strength by non-linear analysis. However, results of connection shear tests are essential to provide the necessary input data.

(c) The accuracy of non-linear analysis for corrugated diaphragms can be increased by using different shear moduli for the end and central regions, but, in most cases, the added expense of the required mesh refinement is not warranted. Recent formulations by other investigators have resulted in accurate values for the effective shear modulus of corrugated sheeting for use in analysis. It does not seem necessary to search for geometric non-linearity effects, as it was seen that diaphragm behavior in the non-linear range is much more dependent on connection non-linearity than on comparable changes in the shear modulus.

(d) The assumption that connections are the only important source of non-linearity has proved satisfactory for the diaphragms analyzed. The connection finite element representations used seems to be well chosen. Further studies may reveal that an orthotropic connection model is feasible for non-linear analysis.

(e) As regards the somewhat unsatisfactory results obtained for the 10' x 12' open corrugated diaphragm, it is believed that the cause has been properly traced to the use of incorrect connection data, based on available information, for the analysis.

APPENDIX A - REFERENCES

1. AISI, Design of Light Gage Steel Diaphragms, 1st ed., American Iron and Steel Institute, New York, N.Y., 1967.

2. Atrek, E. and Nilson, A.H., "Non-linear Finite Element Analysis of Light Gage Steel Shear Diaphragms," Report No. 363, Department of Structural Engineering, Cornell University, Ithaca, N.Y., Sept., 1976.

3. Boyle, E.F. and Jennings, A., "Accelerating the Convergence of Elasto-Plastic Stress Analysis," International Journal for Numerical Methods in Engineering, Vol. 7, 1973, pp. 232-235.

4. Bryan, E.R., Stressed Skin Design of Steel Buildings, 1st ed., Crosby Lockwood Staples, London, England, 1973.

5. Davies, J.M., "The Design of Shear Diaphragms of Corrugated Steel Sheeting," Report No. 74/50, Department of Civil Engineering, University of Salford, Manchester, England, Sept., 1974.

6. Hussain, M.I. and Libove, C., "Stress and Stiffness Data for Discretely Attached Corrugated Shear Webs with Trapezoidal Corrugations," Report No. MAE 5170-T3, Department of Mechanical and Aerospace Engineering, Syracuse University, Syracuse, N.Y., Dec., 1974.

7. Irons, B.M., "A Frontal Solution Program for Finite Element Analysis," International Journal for Numerical Methods in Engineering, Vol. 2, 1970, pp. 5-32.

8. Lawson, R.M., "The Flexibility of Practical Shear Diaphragms," Report No. 75/69, Department of Civil Engineering, University of Salford, Manchester, England, Oct., 1975.

9. Libove, C., "Asymptotic Behavior of Discretely Attached Corrugated Shear Webs," Report No. MAE 5170-T4, Department of Mechanical and Aerospace Engineering, Syracuse University, Syracuse, N.Y., March, 1975.

10. Luttrell, L.D. and Winter, G., "Structural Performance of Light Gage Steel Diaphragms," Research Report No. 319, Department of Structural Engineering, Cornell University, Ithaca, N.Y., Aug., 1965.

11. Miller, C.J. and Sexsmith, R.G., "Analysis of Multistory Frames with Light Gauge Steel Panel Infills," Research Report No. 349, Department of Structural Engineering, Cornell University, Ithaca, N.Y., Aug., 1972.

12. Nilson, A.H., "Report on Tests of Light Gage Steel Floor Diaphragms, 1957 Series," Research Report, Department of Structural Engineering, Cornell University, Ithaca, N.Y., 1957.

13. Nilson, A.H. and Ammar, A.R., "Finite Element Analysis of Metal Deck Shear Diaphragms," Journal of the Structural Division, A.S.C.E., Vol. 100, No. ST4, Proc. Paper 10467, April, 1974, pp. 711-726.

14. "Seismic Design for Buildings," U.S. Army Technical Manual 5-809-10, Department of the Army, Washington, D.C., April 17, 1973.

15. Wu, L-H. and Libove, C., "Stiffness and Stress Analysis of Discretely Attached Corrugated Shear Webs with Quasi-Sinusoidal Corrugations," Report No. MAE 5170-T5, Department of Mechanical and Aerospace Engineering, Syracuse University, N.Y., March, 1975.

16. Zienkiewicz, O.C., Valliappan, S., and King, I.P., "Elasto-Plastic Solutions of Engineering Problems, 'Initial Stress' Finite Element Approach," International Journal for Numerical Methods in Engineering, Vol. 1, 1969, pp. 75-100.

APPENDIX B - NOTATION

The following symbols are used in this paper:

A = cross-sectional area of flexural finite element;

a = distance from corrugated sheet ends where end effects due to discrete attachment becomes negligible;

E_o = modulus of elasticity of steel;

E_L = effective modulus of elasticity in the longitudinal direction;

E_T = effective modulus of elasticity in the transverse direction;

G_o = shear modulus of steel;

G_{ae} = average effective shear modulus for end regions of length a;

G_{eff} = average effective shear modulus for entire length of sheet;

$G_{L - 2a}$ = effective shear modulus for central region of length L - 2a;

I = moment of inertia of flexural finite element;

J = moment of inertia of one corrugation about its own mid-plane;

J_o = moment of inertia of panel sheet about its own plane;

$\overline{K}$ = a dimensionless parameter for stiffness of corrugated sheeting;

$[K]$ = structural stiffness matrix;

L = length of sheet;

$\{p\}$ = vector of external forces and reactions;

p = projected width (pitch) of a single corrugation;

p' = developed width of a single corrugation;

t = thickness of sheet;

z = distance of a given point on the corrugation cross-section from mid-plane;

α = angle with the horizontal of the corrugation at height z;

$\{\delta\}$ = vector of structural degrees of freedom;

μ_o = Poisson's ratio for steel;

μ_{LT} = principal Poisson's ratio;

μ_{TL} = secondary Poisson's ratio; and

Ω = ratio of shear modulus of discretely attached sheeting to that of an identical sheeting attached continuously.

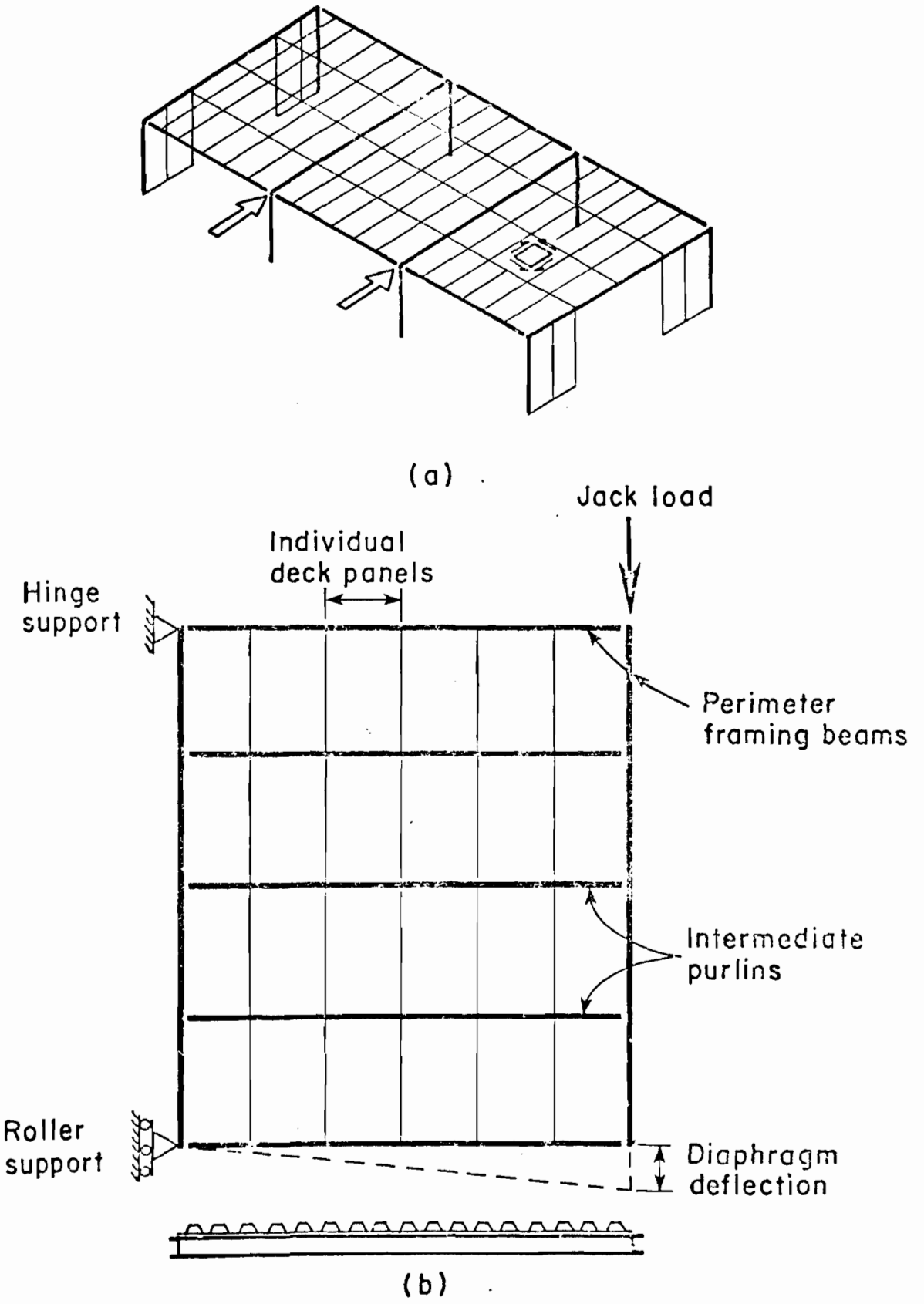

Fig. 1 Shear loading of cold-formed steel diaphragms

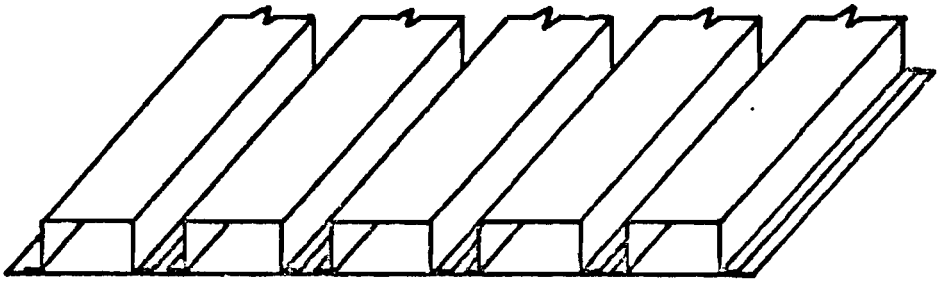

(a)

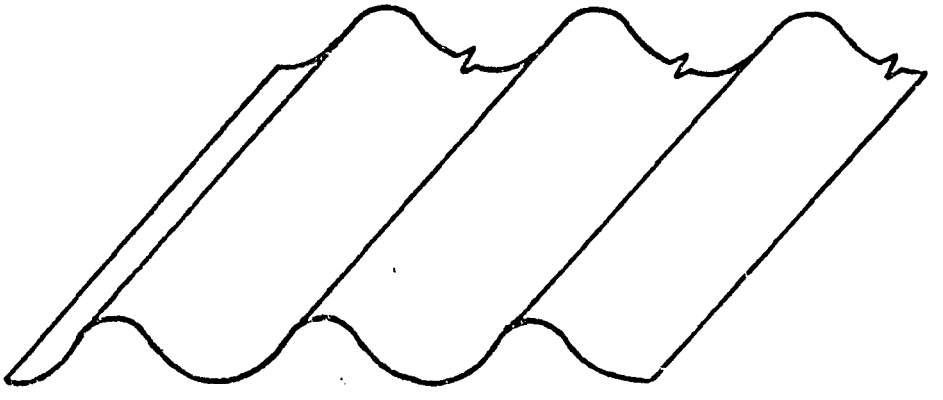

(b)

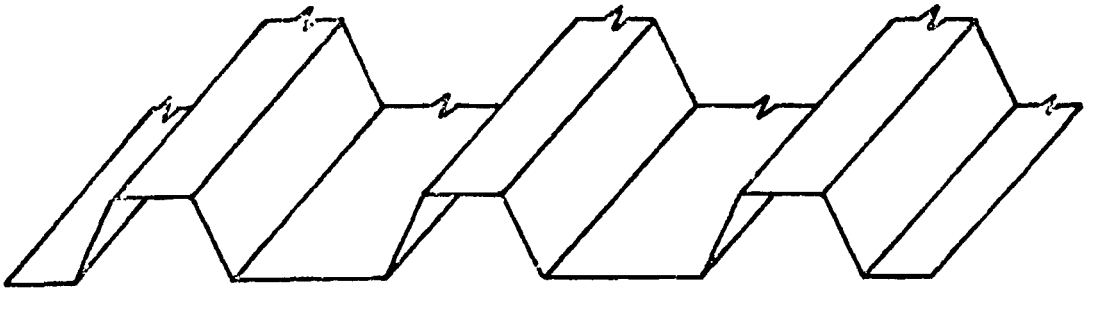

(c)

Fig. 2 Types of deck panels

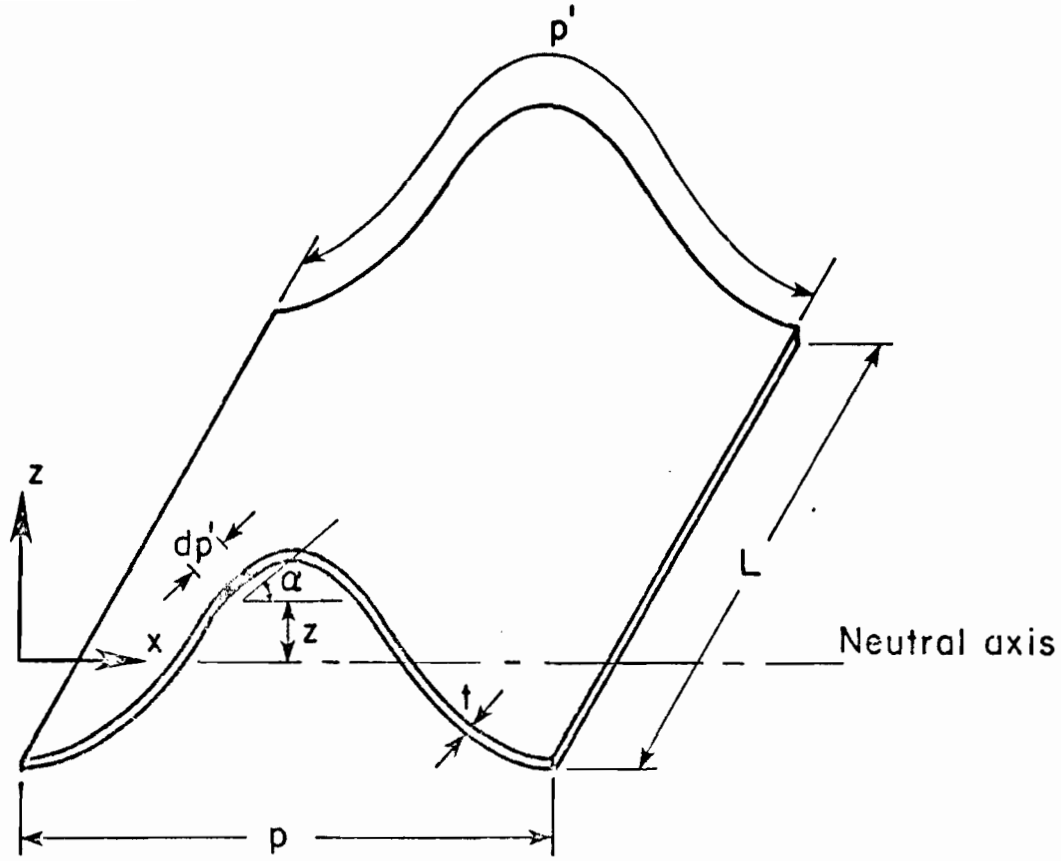

(a)

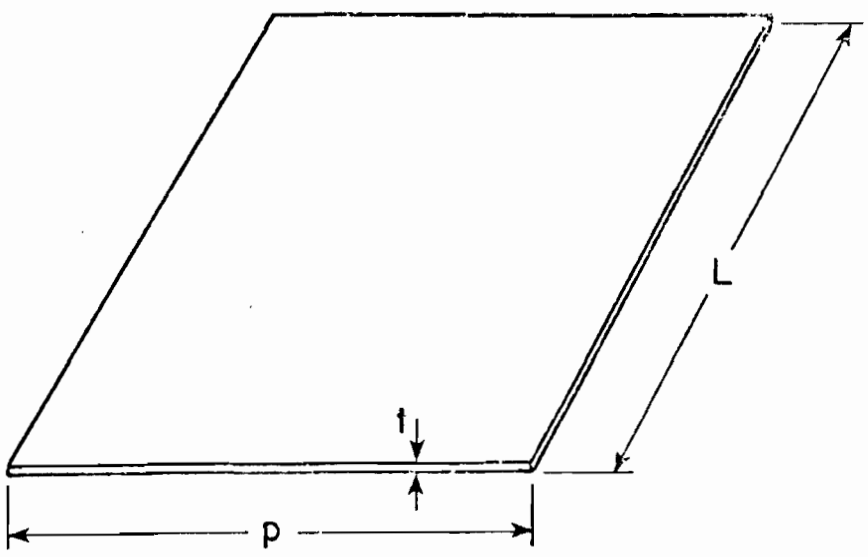

(b)

Fig. 3 Corrugated sheet and equivalent orthotropic flat sheet

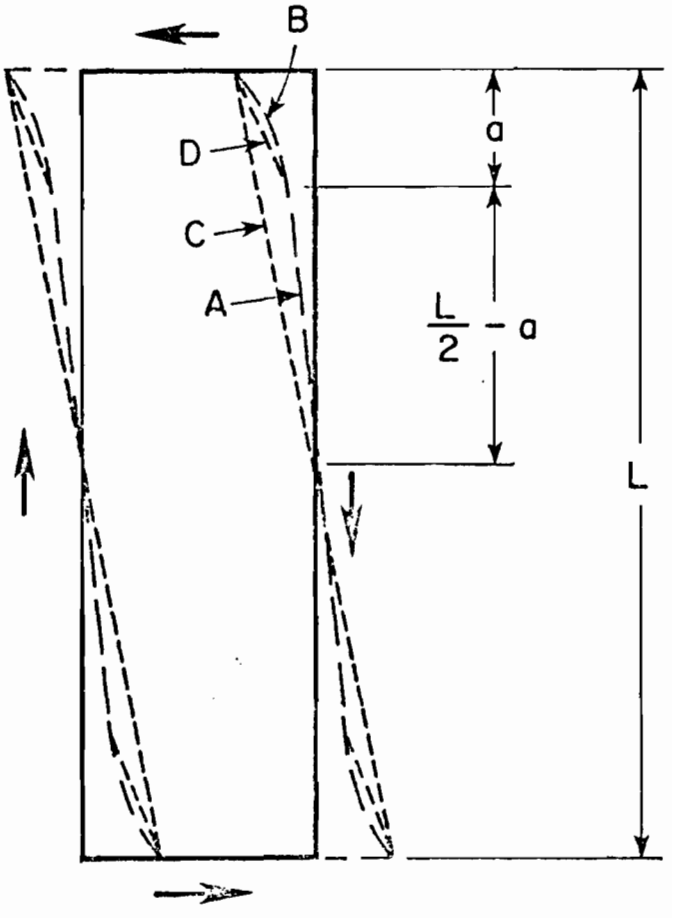

Fig. 4 Deformation of corrugated sheeting

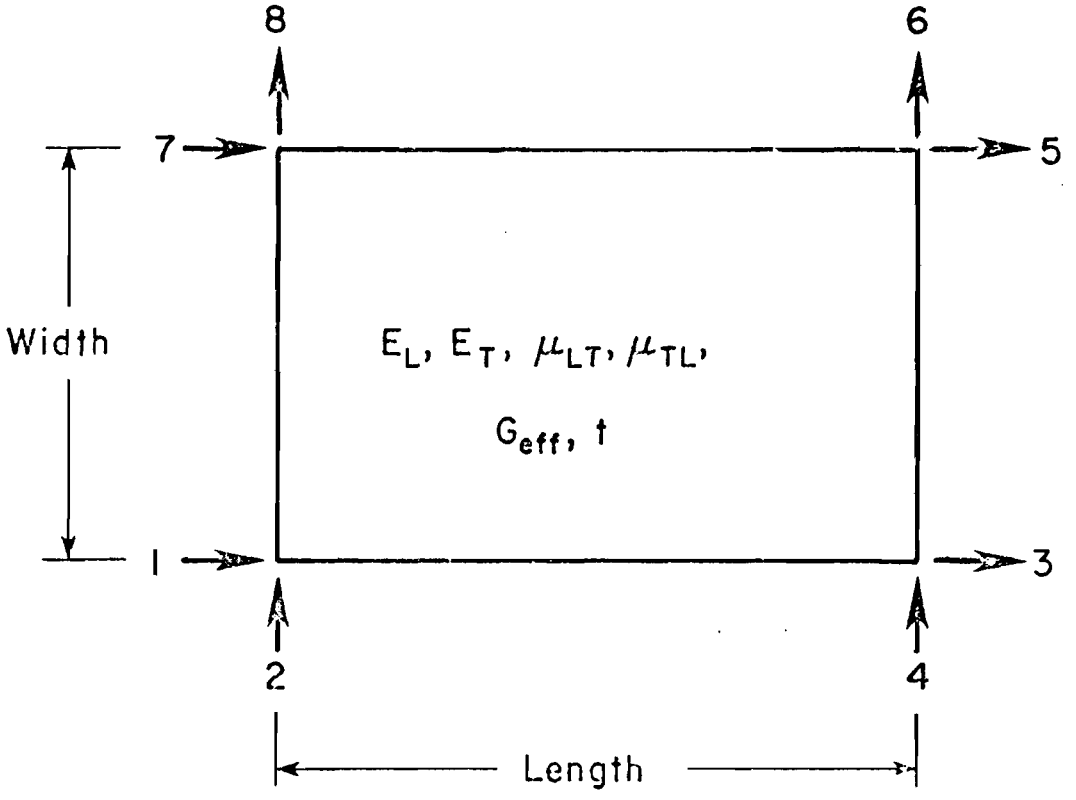

(a)

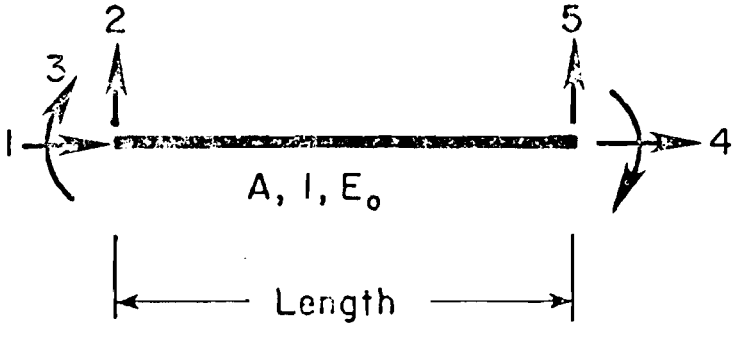

(b)

Fig. 5 (a) Orthotropic plane stress plate element
(b) Flexural bar element

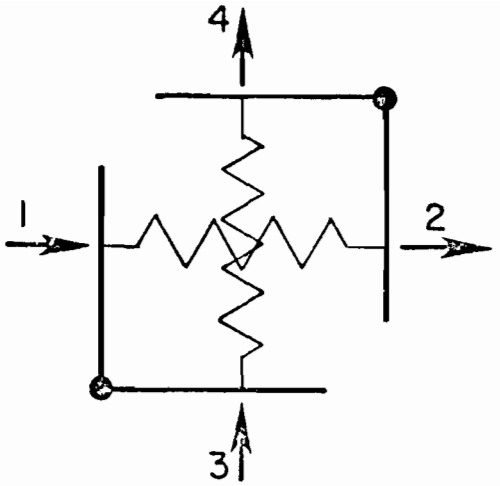

(a) General model

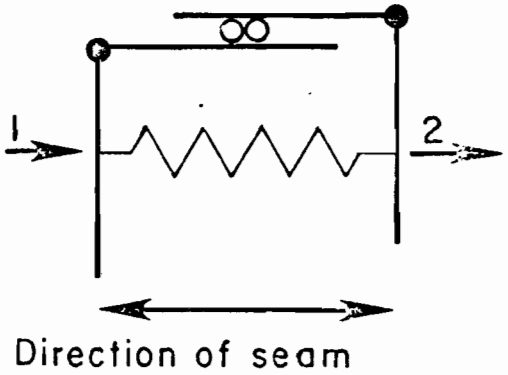

(b) Seam connection

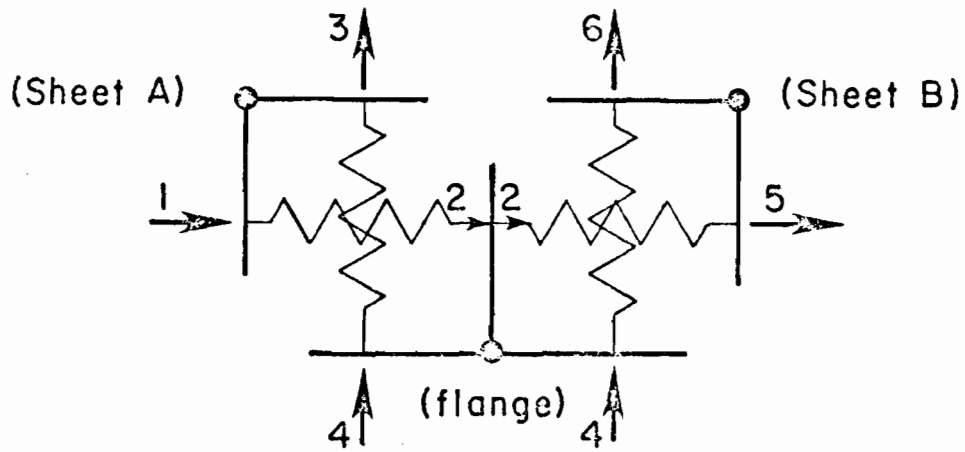

(c) Mechanical end connection at sheet sidelap

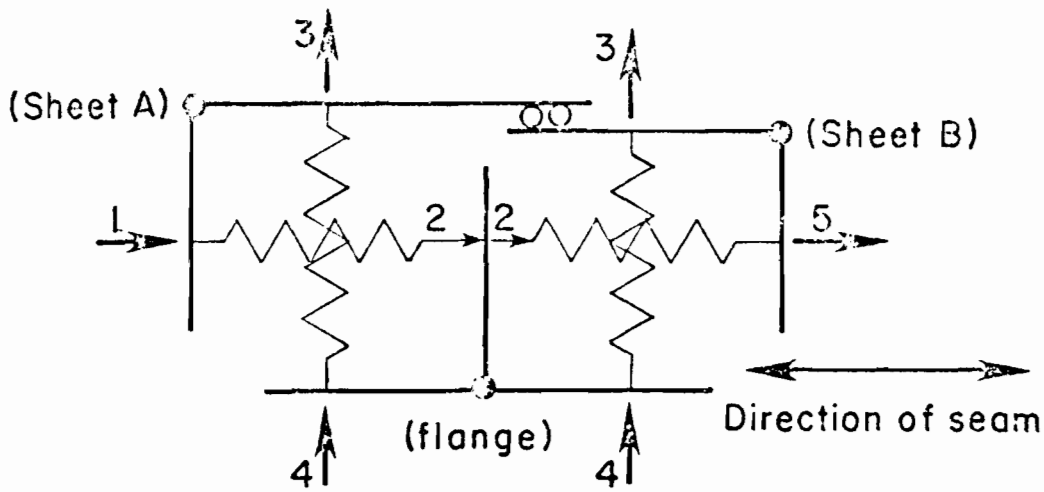

(d) Sheet to purlin connection at sidelap

Fig. 6 Connection elements

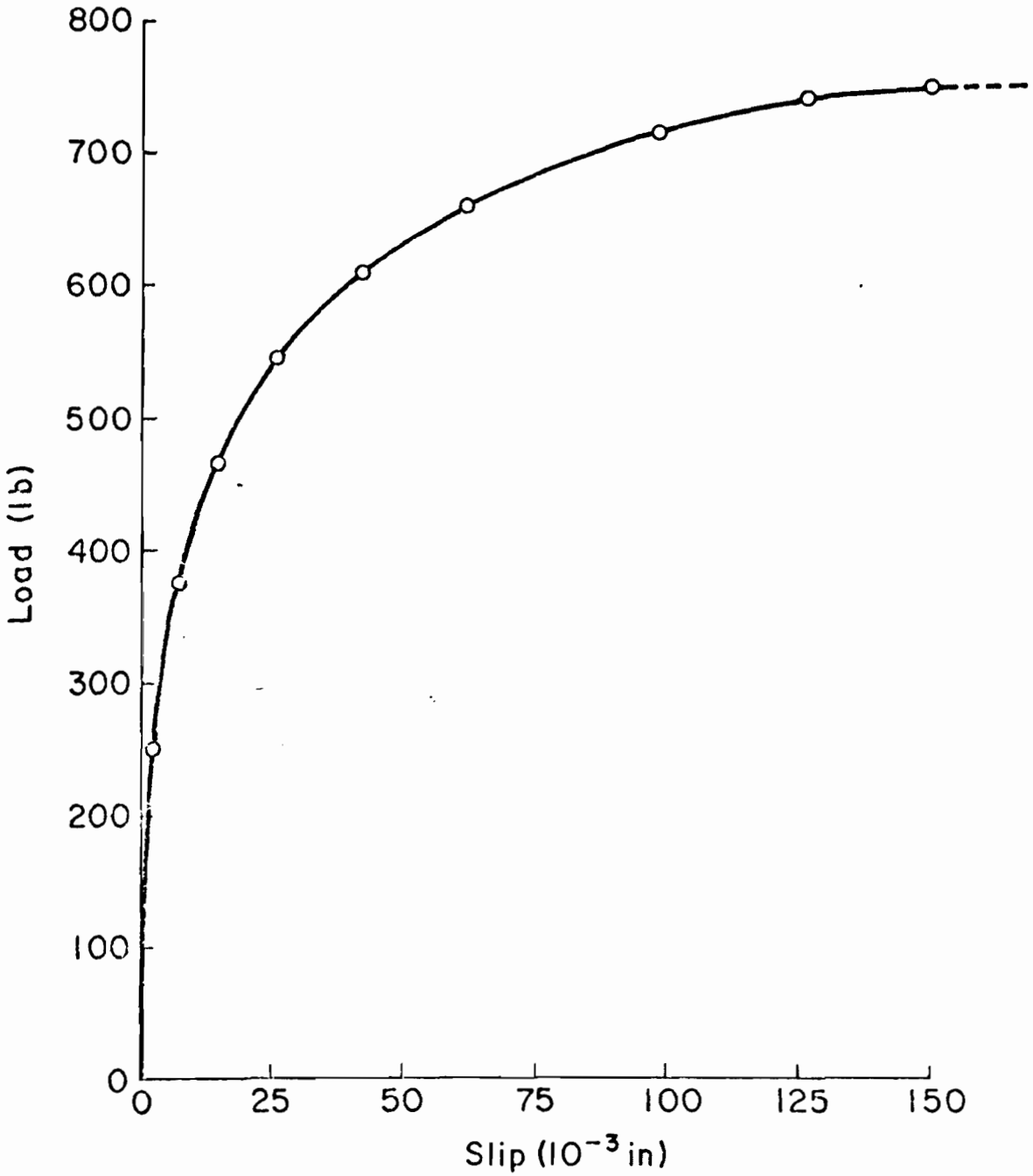

Fig. 7 Typical connection shear test curve

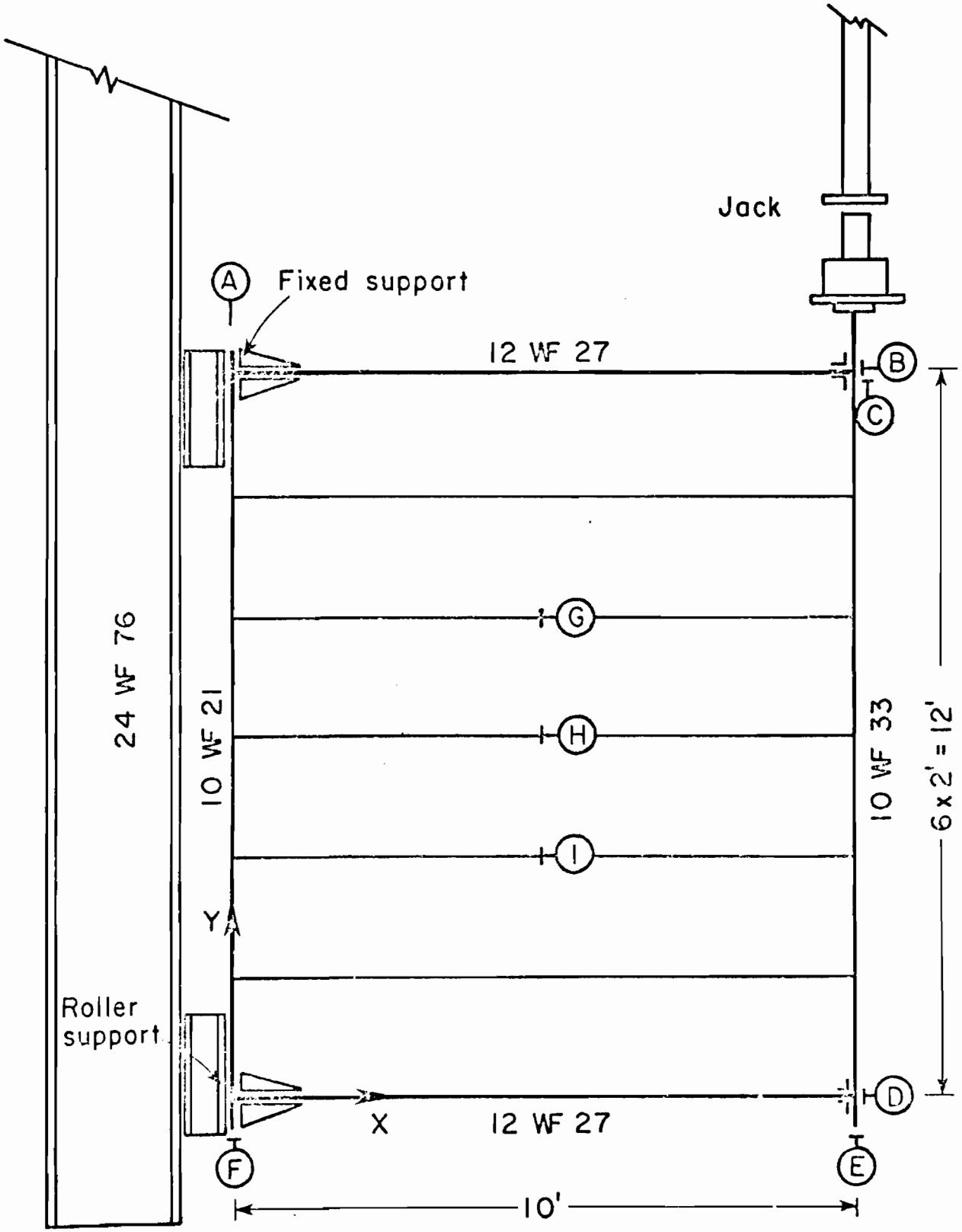

Fig. 8 Test arrangement of the 10' x 12' welded diaphragm

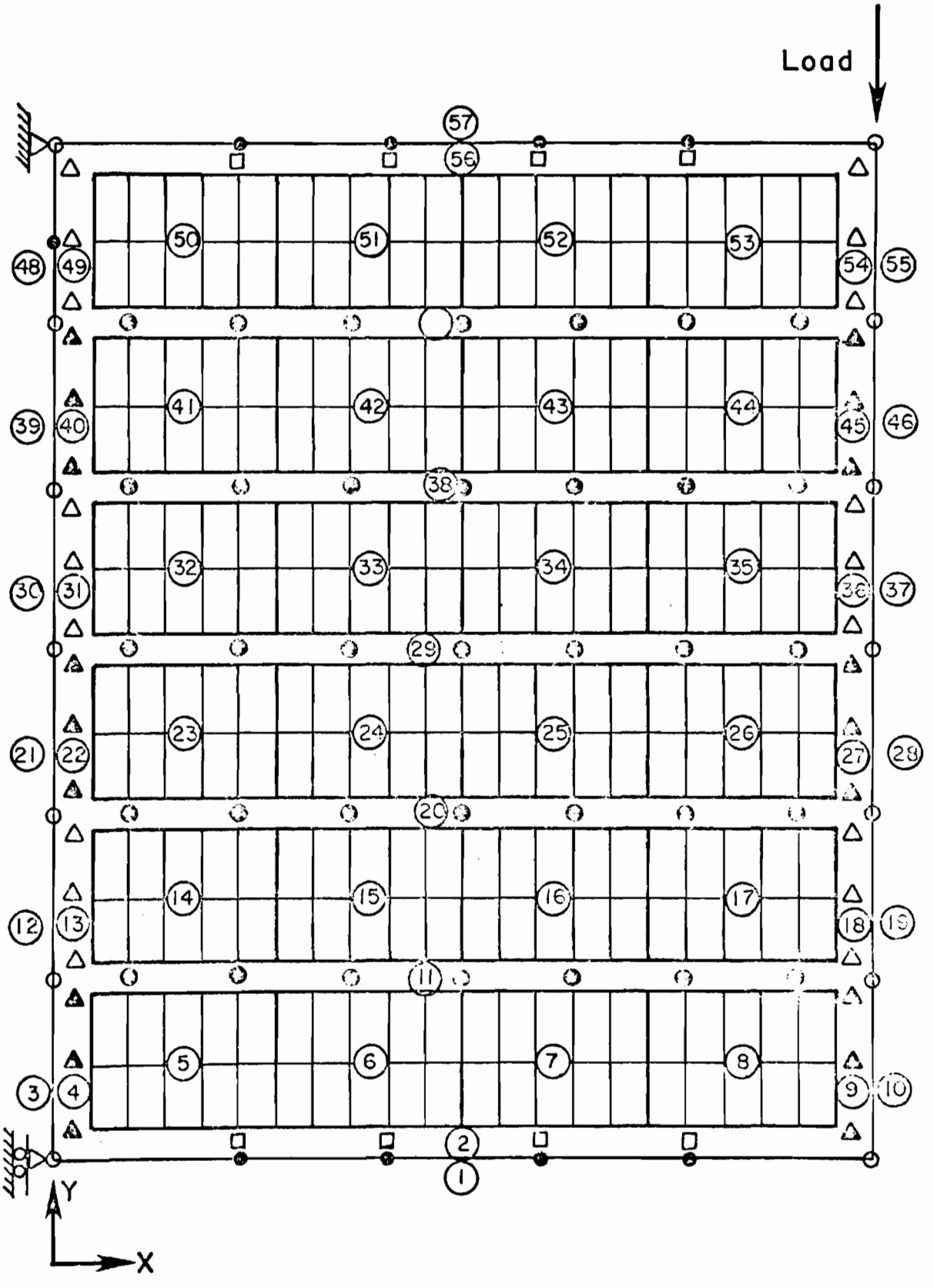

Fig. 9 Finite element mesh and the sequence of sub-assemblies for the 10' x 12' welded diaphragm (unattached geometric shapes indicate connections)

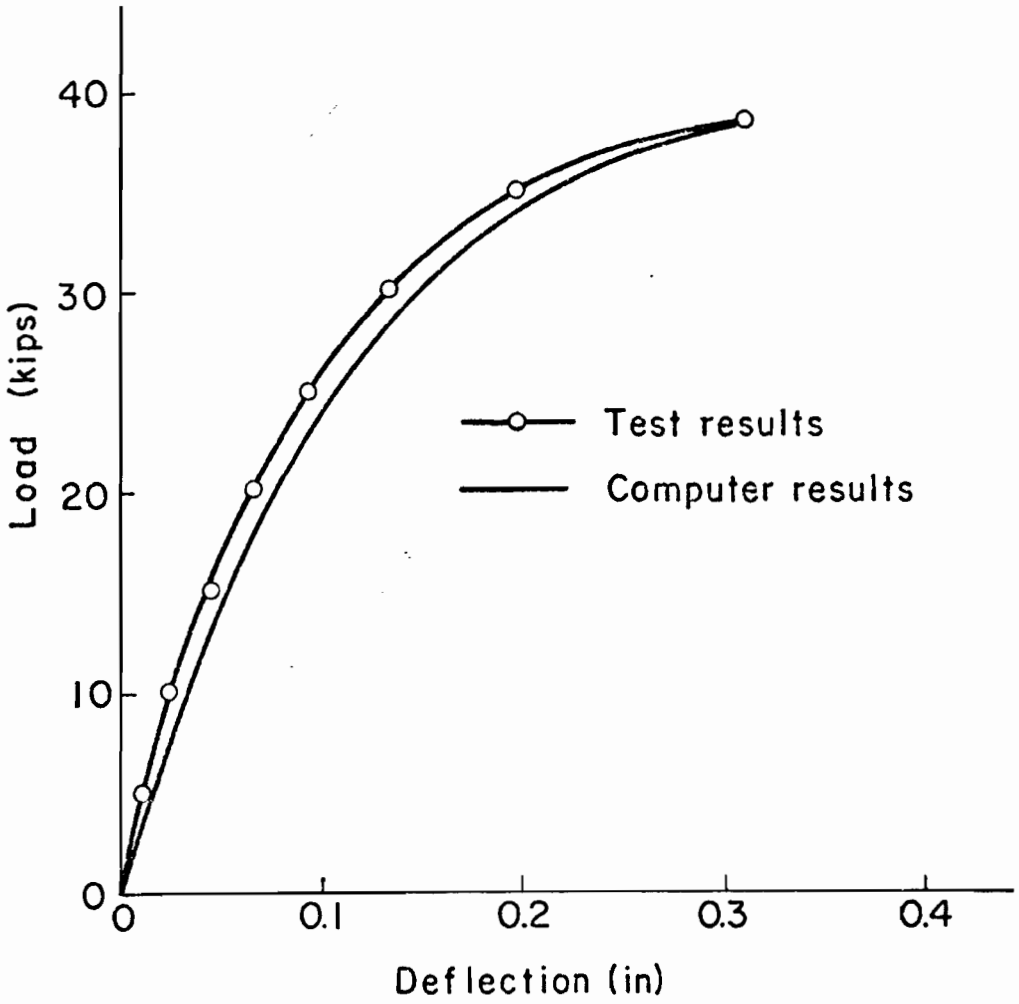

Fig. 10 10' x 12' welded diaphragm. Deflection of representative nodal point

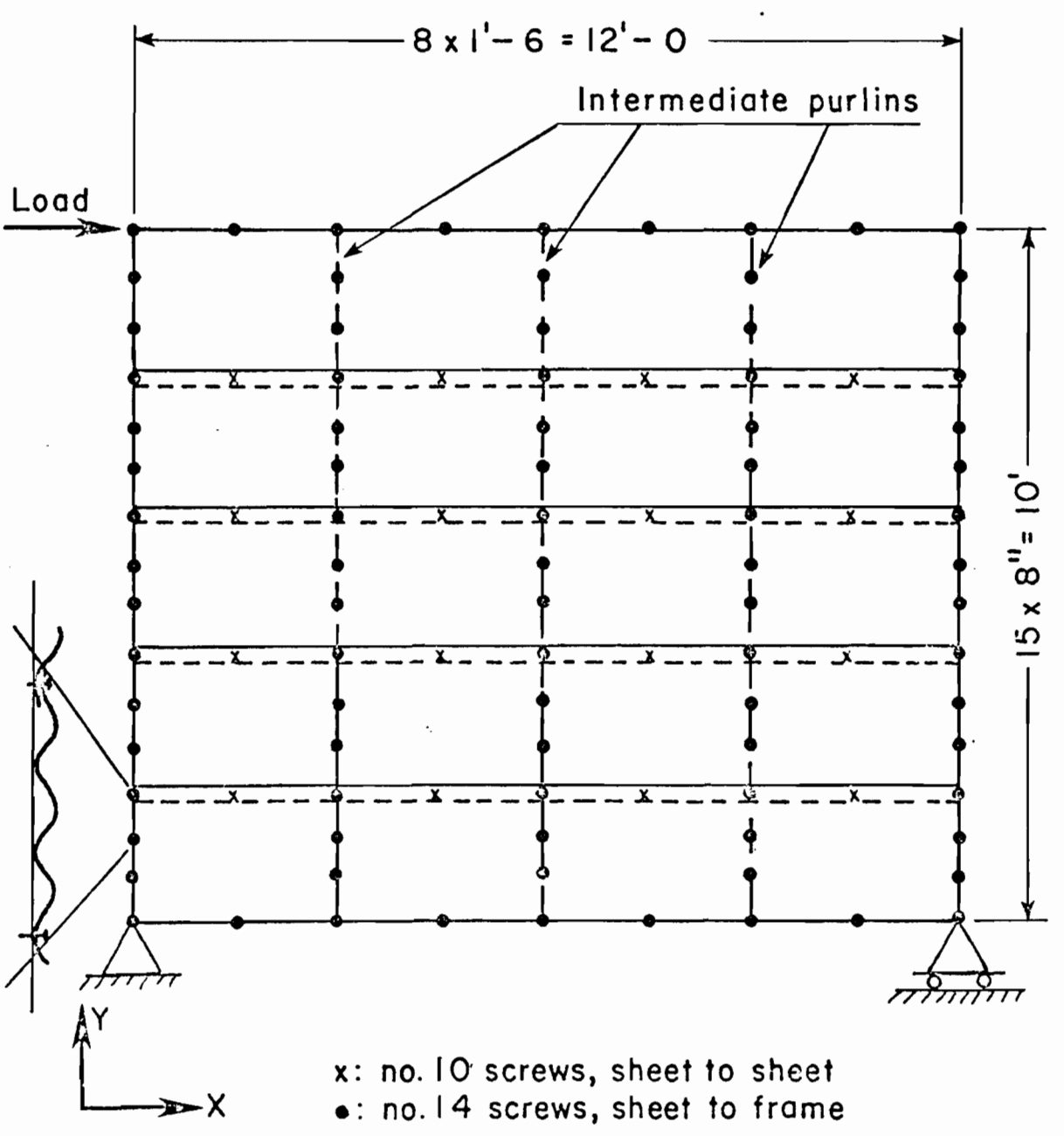

Fig. 11 Test arrangement of the 10' x 12' standard corrugated diaphragm

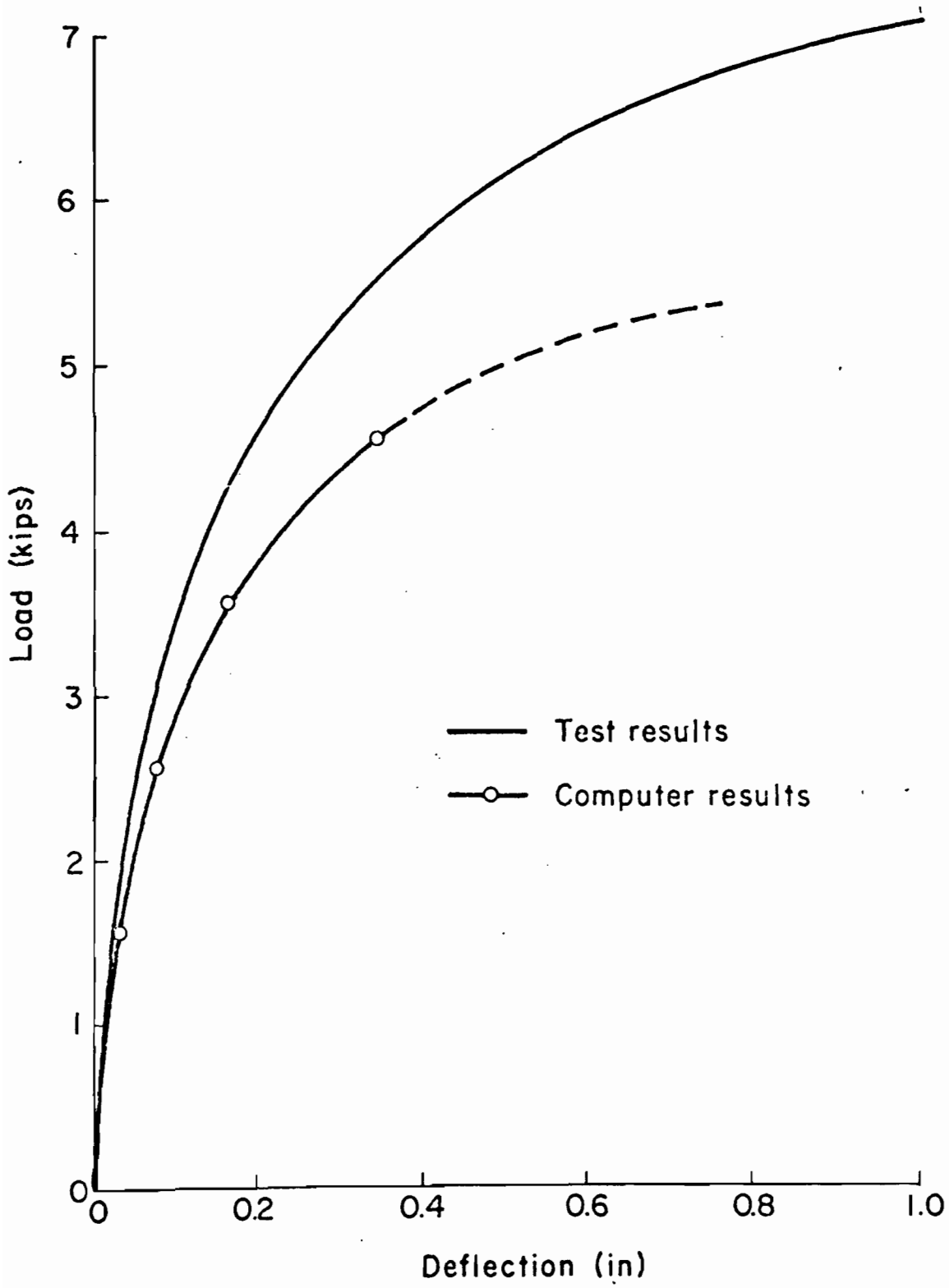

Fig. 12 10' x 12' standard corrugated diaphragm behavior under static load

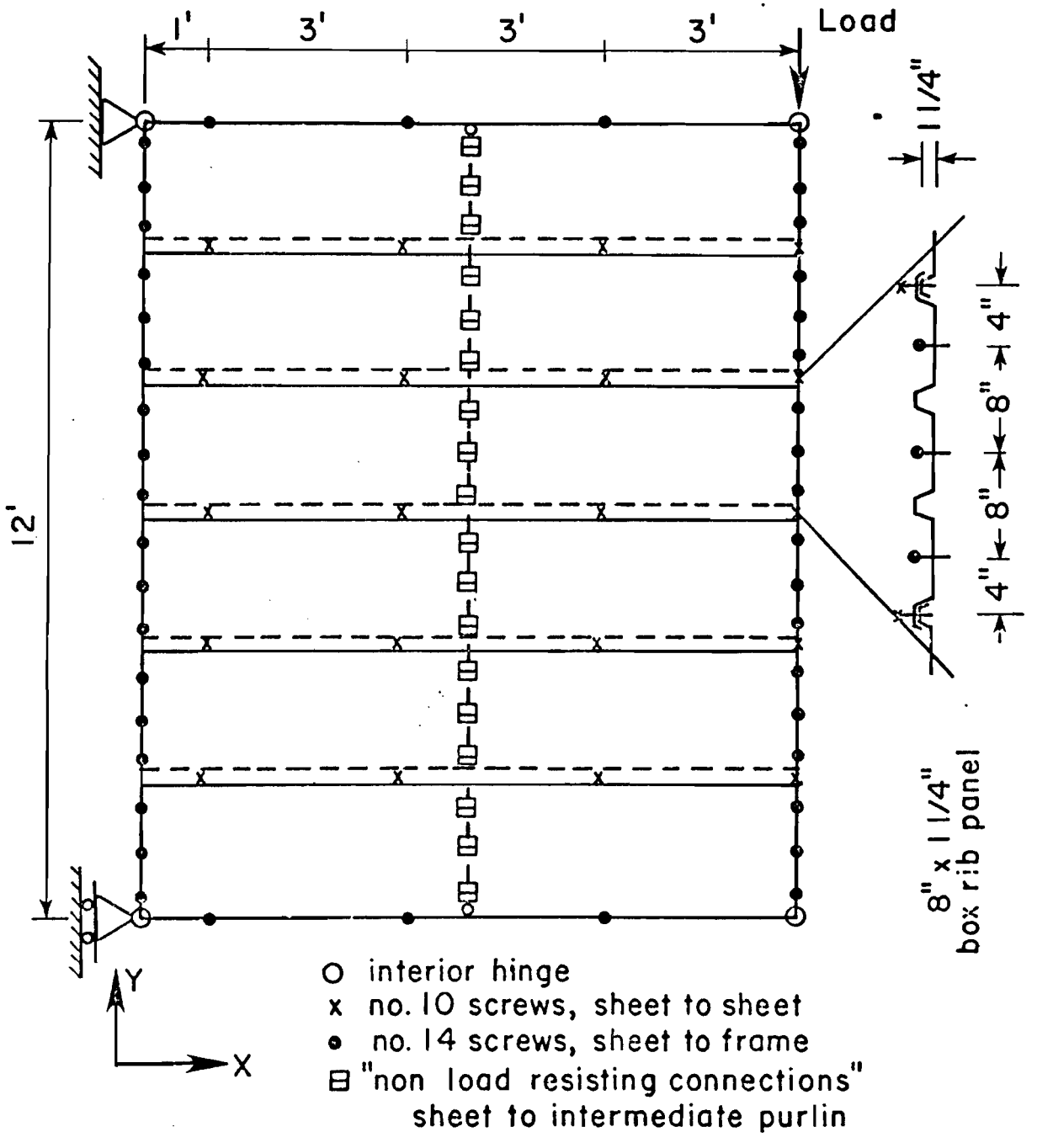

Fig. 13 Test arrangement of the 10' x 12' trapezoidally corrugated diaphragm

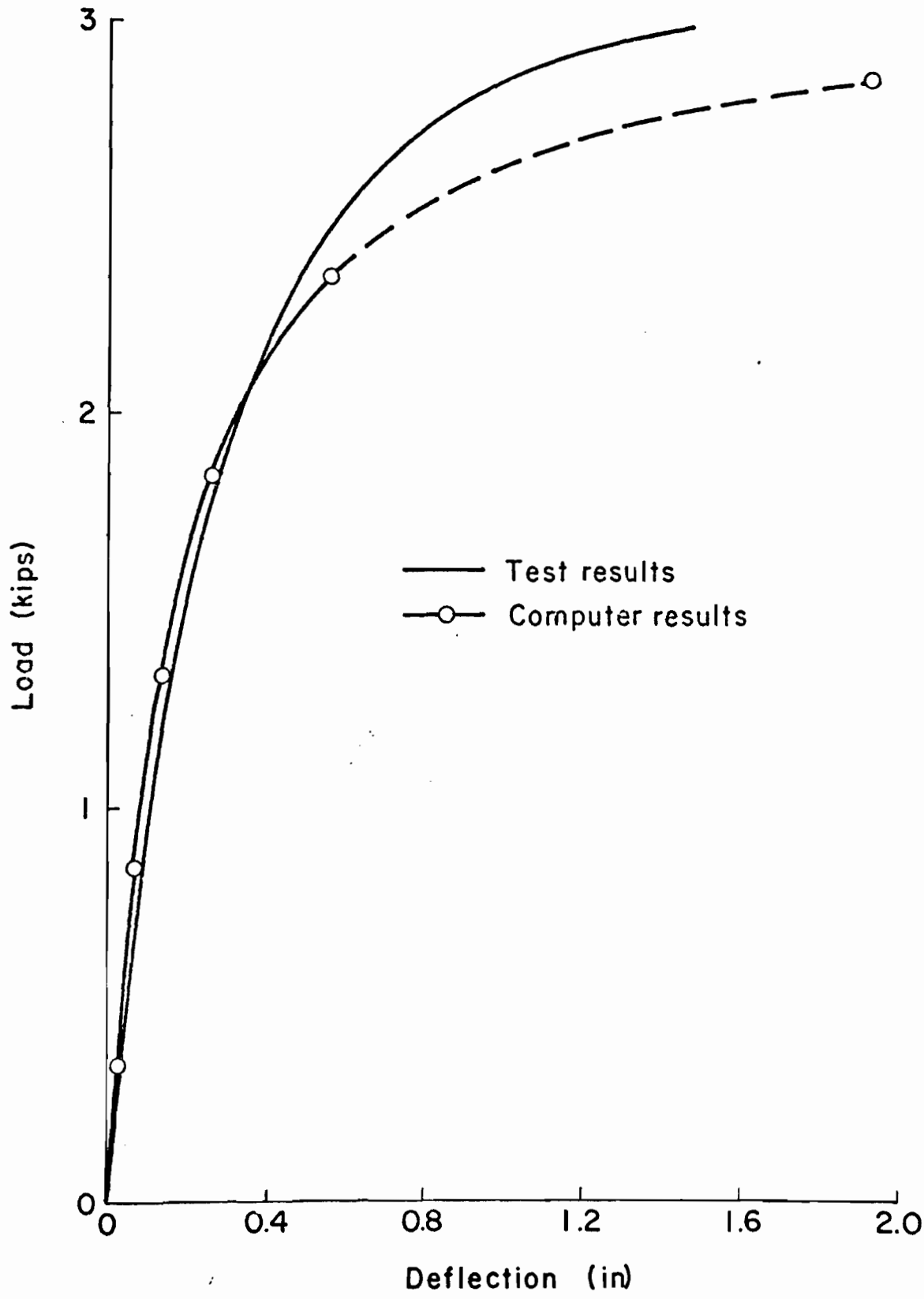

Fig. 14 Trapezoidally corrugated diaphragm.
Deflection of representative d.o.f.